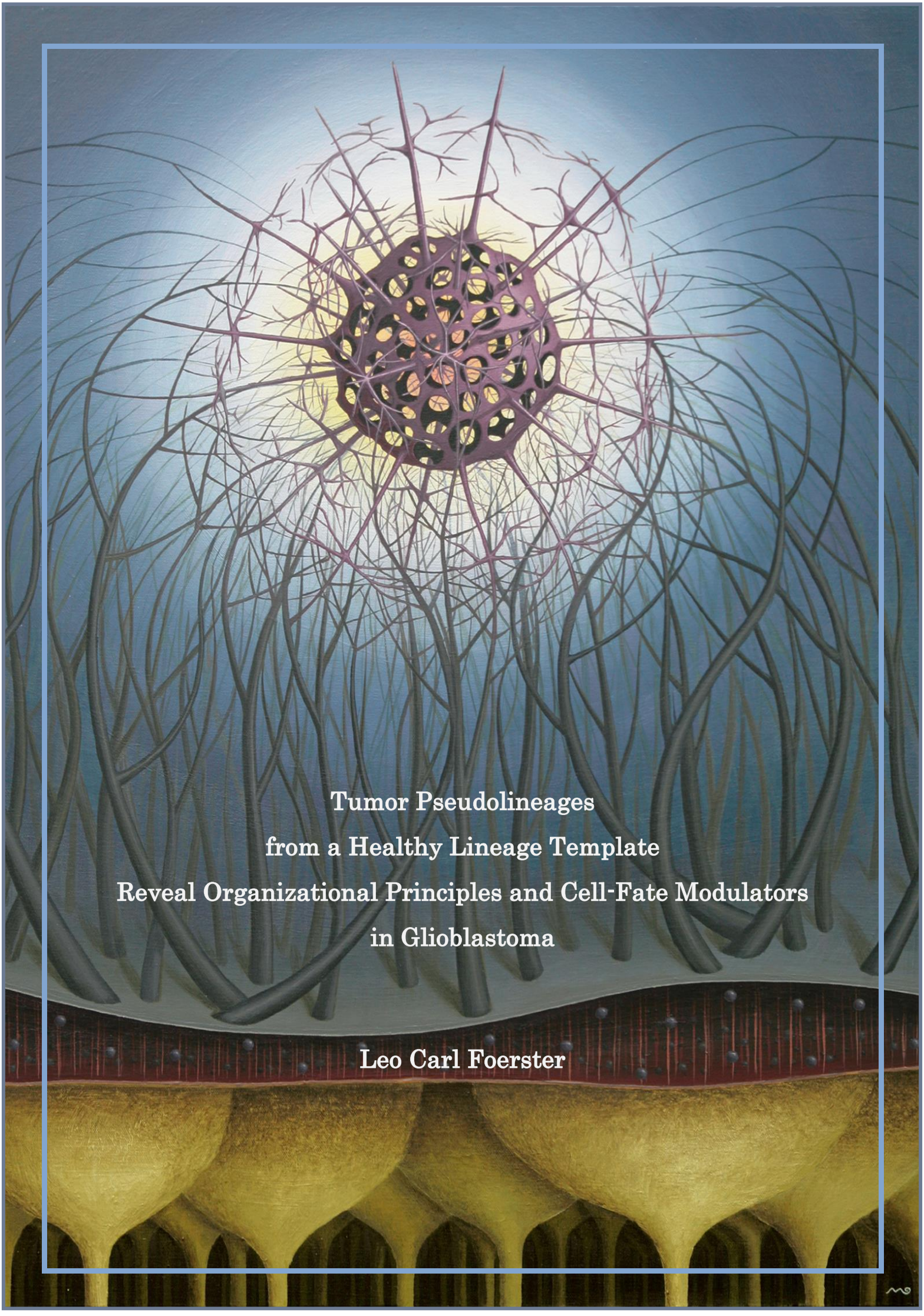

Tumor Pseudolineages from a Healthy Lineage Template Reveal Organizational Principles and Cell-Fate Modulators in Glioblastoma

Leo Carl Foerster

Micah Ofstedahl
2012

R. Trigonacantha
Acrylic on canvas

Reproduced with permission

Inaugural dissertation

for

obtaining the doctoral degree

of the

Combined Faculty of Mathematics, Engineering, and Natural Sciences

of the

Ruprecht – Karls – University

Heidelberg

Presented by

Leo Carl Foerster, M.Sc

Born in Dresden, Germany

Oral Examination: June 13, 2024

Tumor Pseudolineages from a Healthy Lineage Template Reveal Organizational Principles and Cell-Fate Modulators in Glioblastoma

Referees: Prof. Dr. Ana Martin-Villalba

Prof. Dr. Henrik Kaessmann

Summary

Tumors inherit characteristics from their tissue of origin, displaying varied molecular and functional features based on their specific progenitor cells. Leveraging this constraint to isolate similarities between healthy and tumor cells, I developed ptalign as a means to place tumor cells within a fixed healthy lineage trajectory, using healthy stem cell transitions as a template to infer a tumor pseudolineage in the absence of lineage tracing. This approach offers several unique benefits: it facilitates the transfer of vital contextual information from healthy references to clarify tumor processes and enables the comparison of pseudotime expression dynamics across multiple tumors to identify stage- or group-specific tumor vulnerabilities. This view of tumor organization through the lens of healthy lineage transitions provides valuable context for the development of targeted tumor interventions and personalized therapies.

In this thesis, I demonstrate this approach through a systematic study of glioblastoma pseudolineages based in the adult neural stem cell (NSC) lineage. Delineating glioblastoma hierarchies into Quiescence-, Activation-, and Differentiation-stage cells revealed the essential role of the Quiescence-Activation transition in determining patient outcomes. In healthy NSCs, Wnt signaling is a crucial regulator of this transition, and comparing pseudolineage expression dynamics at this transition identified the secreted Wnt antagonists `SFRP1` and `NOTUM` as recurrently dysregulated in glioblastomas. Reintroducing `SFRP1` stalled tumor progression, significantly increasing overall survival of tumor-bearing mice by rewiring tumor cell fate to an astrocytic pseudolineage. This `SFRP1`-induced remodeling was reversed with a small molecule inhibitor, asserting the lineage potential of tumor astrocytes and challenging prevailing assumptions about their plasticity. These findings position `SFRP1` as a potent modulator of cell fate with promising therapeutic potential, highlighting the advantages of a comparative approach to studying tumor cells rooted in the similarities to their healthy counterparts

ptalign pseudolineages provide a novel view of tumor organization through the lens of healthy lineage transitions, uncovering critical vulnerabilities in tumor hierarchies that can be targeted through eg. `SFRP1` or a combination therapy. Overall, expanding pseudolineage inference to additional tumor entities promises to reveal additional vulnerabilities and strategies for their exploitation.

Zusammenfassung

Tumore erben Merkmale der Gewebe aus denen sie entstehen, z.B. charakteristische molekulare und funktionale Ähnlichkeiten zu ihren Vorläuferzellen. Diese Ähnlichkeit zwischen gesunden und Tumorzellen dient als Grundlage für ptalign, welches Tumorzellen innerhalb einer konkreten Hierarchie gesunder Zellen platziert und dabei Übergänge zwischen definierten Zellstadien nutzt um eine Pseudoabstammung (pseudolineage) der Tumorzellen zu erstellen, ohne dafür die genaue Abstammung der einzelnen Zellen mittels genetischer Methoden bestimmen zu müssen. Dieser Ansatz hat mehrere Vorteile, u.A. ermöglicht er die Übertragung von relevanten Informationen des zellulären Kontexts der gesunden Gehirnstamzellen, die der Interpration krebsspezifischer Prozesse dient; so werden auch Vergleiche in der pseudotemporalen (pseudotime) Exprimierungsdynamik unterschiedlicher Gene in und zwischen unterschiedlichen Tumoren ermöglicht, welche die Erfassung von gen- und krebs-spezifischen Prozessen ermöglicht. Diese Sichtweise der Tumororganization, gerichtet an der Verhaltens- und Abstammungsdynamik der zellulären Hierarchie von gesunden Gehirnstamzellen, bietet wertvollen Kontext für die Entwicklung von gezielten Tumorinterventionen und personalisierten Therapien.

In diesem Werk wende ich diese Sichtweise durch eine systematische Untersuchung von Glioblastom pseudolineages, welche auf der zellulären Hierarchie adulter Gehirnstammzellen basieren, an. Durch die Gliederung von Glioblastomhierarchien in Phasen der Quieszenz, Aktivierung, und Differenzierung zeigte sich, dass der Übergang zwischen Quieszenz zu Aktivierung eine bedeutende Rolle für das Überleben von betroffenen Patienten aufweist. In gesunden Gehirnstammzellen ist der Wnt-Signalweg ein entscheidender Faktor in der Regulierung dieses Übergangs. Der weitere Vergleich der pseudotemporalen Exprimierungsdynamik an diesem Übergang zeigte, dass die sezernierten Wnt-Antagonisten `SFRP1` und `NOTUM` in Glioblastomen konsequent dysreguliert waren. Die Wiedereinführung von `SFRP1` blockierte das Fortschreiten des Tumors und verlängerte signifikant das Gesamtüberleben der krebstragenden Mäuse durch das hervorrufen eines astrozytenähnlichen Phänotyps. Dieser Phänotyp konnte durch einen niedermolekularen Inhibitor rückgängig gemacht werden, was, in Widerspruch zu zur Zeit geltenden Annahmen, die Teilungsfähigkeit von Tumorastrozyten bestätigte. Diese Ergebnisse positionieren `SFRP1` als einen potenten Faktor in der Bestimmung von Differenzierungspotenzial und Schicksal von Krebszellen, mit vielversprechendem therapeutischem Potenzial. Zudem werden die Vorteile des Ansatzes, Tumorzellen anhand ihrer Ähnlichkeiten zur Zellhierarchie gesunder Gehirnstammzellen zu betrachten, bestätigt.

Insgesamt bieten ptalign pseudolineages eine neue Sichtweise auf die Organisation von Krebszellhierarchien, welche kritische Schwachstellen in Tumorhierarchien offenbart, die beispielsweise durch `SFRP1` oder eine Kombinationstherapie ausgenutzt werden können. Die weitere Anwendung von ptalign auf diverse Tumortypen verspricht neue Schwachstellen sowie Strategien zu Ihrer therapeutischen Anwendung aufzudecken.

Table of Contents

List of Figures

Introduction:

Results:

ptalign algorithm

States and transitions in the SVZ NSC lineage

Canonical Wnt signaling at NSC lineage transitions

Conserved cell hierarchies in human and mouse neurogenesis

Glioblastoma recapitulates NSC lineage stages

Insights from glioblastoma pseudolineages

Aberrant canonical Wnt signaling in glioblastoma

Directed modulation of tumor pseudolineages by intervention in Wnt signaling

Contribution Statement

This thesis is the result of a close collaboration between the experimental biologist Oguzhan Kaya (defended December 1, 2023) and myself. The results presented here are the product of this collaboration and have been published in a preprint by Oguzhan and I co-authored: (Foerster et al., 2023). In this thesis I have elaborated and contextualized these results, attributing Oguzhan's contributions accordingly. This includes the work of Oguzhan's students Milica Bekavac and Vuslat Akcay, whose contributions are elucidated in Oguzhan's thesis: (Kaya, 2023). Other individuals who made named contributions to the work presented here include Valentin Wüst, who analyzed the spatial transcriptomics datasets generated by Oguzhan, as well as Jooa Hooli, who assisted on technical matters, and also Jocelyn Tang and Jan Brunken, who aided in the experiments carried out after Oguzhan's departure.

I have written the entire text of this thesis in my own voice and will refrain from citing my preprint article going forward. I used ChatGPT 4 to edit and improve text readability in some sections, taking care to always supply my own template. Most figures are adapted from (Foerster et al., 2023), having been prepared by myself and Oguzhan in that work. I received assistance from Irene Lois Bermejo in assembling the figures for this thesis.

NTRODUCTION

1.1 Homeostatic upkeep in the brain: a murine model of neurogenesis

The human brain is a marvel of complexity. It is unfathomable the number of things which have to go just right, the trillions and trillions of interconnected parts which act in seamless cohesion just for you, dear reader, to scan an inked page and internalize my thoughts within the structures of your brain. This act of communication, despite the many caveats associated with it, is made possible due to the similar architecture and processes which govern that most complex organ: our brains. This is no coincidence, as truly one of the miracles of biology is the reproducible *de novo* assembly of the human brain. Not only do the intricate networks of a myriad of functionally distinct cell types have to coordinate all of the complex processes and behaviors that make up the human existence, it has to do so while maintaining a degree of plasticity and capacity to repair. This act, effectively changing the wheels on a moving car – as the saying goes – is unequally preserved between species, with eg. zebrafish able to broadly recover from traumatic brain injury (Kishimoto et al., 2012), while the idea that neurogenesis occurs in the mature mammalian brain was regarded as "somewhat heretical" for many years (Sanes et al., 2019).

The discovery of neurogenic neural stem cells (NSCs) residing in the subventricular zone (SVZ) (Altman & Das, 1965; Lois & Alvarez-Buylla, 1993; Luskin, 1993) and dentate gyrus (Eriksson et al., 1998; Van Praag et al., 2002) of adult rodents, held great promise for their targeted modulation to improve brain regeneration in mammals. Explant and *in vitro* cultures of NSCs were rapidly established (Gritti et al., 1995; Reynolds & Weiss, 1992; L. J. Richards et al., 1992), along with salient markers for their identification (Doetsch et al., 1997, 1999), which cemented their stem properties and ability to give rise to various progeny including neurons, astrocytes, and oligodendrocytes (Kirschenbaum & Goldman, 1995; Levison & Goldman, 1993; Lois & Alvarez-Buylla, 1993). More recently, the reproducible induction of pluripotent stem states in adult cells (Takahashi & Yamanaka, 2006) ushered the development of organoid technologies (Clevers, 2016; Sato et al., 2009) which recapitulate different tissue systems including the human brain (Lancaster & Knoblich, 2014). These technologies provide exciting opportunities to study the development and organization of human brain tissues, mimicking neurological development to reveal the principles underlying neurodegenerative diseases (C. Li et al., 2023) and brain tumor formation (Bian et al., 2018). However, insights from these models of neurogenesis are only relevant insofar as they are applicable to NSCs *in vivo*, and as such it remains important to understand the principles governing the maintenance and dynamics of the healthy murine adult NSC lineage.

1.1.1 Origins and patterning of subventricular zone stem cells

The present state of any complex system, idea, or object is the result of its development over time. To appreciate adult neurogenesis, this means first understanding fetal brain development. The majority of murine brain development takes place in the later stages of gestation and continues into the postnatal period, requiring in the coordinated generation of millions of precisely arranged cells. Neurological tissue generation begins in earnest around gestational day 9 and 10, when neural progenitors diverge from the neuroepithelium and convert into radial glia cells. This conversion is marked by changes in cell morphology, with radial glia characterized by an elongated apical-basal morphology. These cells initially populate the developing neural tube, with an elongated process spanning from the ventricular surface to the outer cellular layers of that organ (Sanes et al., 2019). In this position, radial glia continuously undergo rapid asymmetric divisions which maintain the stem-identity of the mother cell while generating a differentiating daughter (Wilcock et al., 2007). Important for the layered organization of the brain, these daughter cells will migrate along the radial glial process while undergoing additional rounds of symmetric amplifying divisions (Noctor et al., 2002). Thus the brain develops from the inside out, with eg. the various cortical layers characteristic of mammalian brains generated in a temporal order from radial glia which remain at the ventricular surface (Sanes et al., 2019). As is generally the case in development, this process is accompanied by fate-restriction: while radial glia are initially responsible for generating neurons, spatial and temporal cues will redirect them to the generation of astrocytes and oligodendrocytes in a phenomenon known as the gliogenic switch (Malatesta et al., 2008).

The gliogenic switch represents a critical transition in brain development, but nuanced fate restriction is already present in earlier populations. For example, different neuronal subtypes will be generated at different timepoints, with eg. larger neurons often generated before smaller ones (Jacobson, 1977). Regionalization also affects radial glial fates at this stage, with progenitors in the medial ganglionic eminence (MGE) producing tangentially-migrating neurons with different properties than their cortical counterparts (Corbin et al., 2001). As the brain tissues develop, this fate restriction becomes ever more pronounced, with SHH and Wnt signaling already establishing fixed domains within ventral and dorsal domains of the developing SVZ (Fiorelli et al., 2015). These differences extend into the postnatal SVZ (Fig.1a) and likely underlie the regional differences which direct NSC fate toward the generation of specific neuronal subtypes (Lim & Alvarez-Buylla, 2016; Tong et al., 2015) (Fig.1b). The specific cues which guide radial glial and indeed NSC fate choice are particularly relevant to regenerative therapies, but also play a role in eg. organoid patterning.

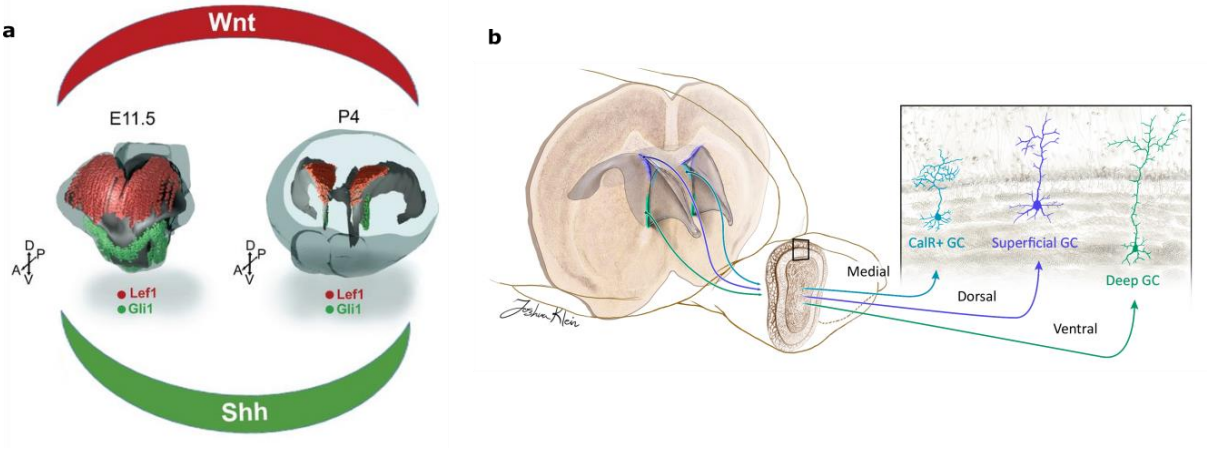

Figure 1: Patterning of SVZ extends into adulthood. a) volumetric reconstruction of E11.5 and P4 mouse forebrains with Lef1-(Wnt) and Gli1-expressing (Shh) progenitors labelled. Image modified from (Fiorelli et al., 2015). b) Distinct neuronal subtypes generated by regionally fated NSCs lining the medial, dorsal, or lateral wall of the SVZ. GC: granule cell. Image modified from (Conover & Todd, 2017).

In the later stages of brain development, radial glia will undergo symmetric differentiating divisions more frequently (Caviness, 2003), leading to the population ultimately exhausting through their transformation into astrocytes (Noctor et al., 2008). However, some radial glia will not complete this transformation and instead enter a dormant state which allows them to persist as NSCs throughout adulthood (Fuentealba et al., 2015; Furutachi et al., 2015). This underscores not only the necessary and important role of cellular quiescence in maintaining stem cell capabilities over long periods, but also highlights the internal and external signals which direct cellular fate in the adult brain. Perhaps unsurprisingly, the transcription factors and niche determinants which regulate these key processes of stem cell identity and fate are commonly dysregulated in brain malignancies (Altmann et al., 2019; Y. Lee et al., 2016; Rajakulendran et al., 2019). Interestingly, the dynamics of fetal neurogenesis which are required to rapidly generate numerous progeny stand in stark contrast to the principles guiding adult neurogenesis.

1.1.2 The neurogenic adult neural stem cell lineage

Stem cell behaviors in some fetal tissues exhibit significant differences to their adult counterparts, for example in the reduced regenerative capabilities of the skin (K. Liu et al., 2014) and heart (Kara et al., 2012). This is also true for NSCs in the postnatal SVZ, which exhibit several key differences to

fetal radial glia. Most notable of these is the prominent role of cellular quiescence among adult SVZ NSCs. While fetal radial glia undergo continuous rapid divisions, adult NSCs remain in a dormant state (where they are often referred to as qNSCs or B-cells) until signaled to activate, for example through local niche signals (Basak et al., 2018; Donega et al., 2022). Once activated, NSCs follow a division hierarchy similar to radial glia, beginning with an asymmetric division and followed by several rounds of transit amplifying divisions (also called the TAP-stage or C-cells) to generate neuroblast progeny (Lim & Alvarez-Buylla, 2016; Ponti et al., 2013). This initial stage of NSC activation can be followed by a return to quiescence, leaving the cell in the G0 phase of cell cycle where it is more likely to reactivate compared to nearby dormant neighbors. This aspect of NSC biology could serve to sustain their long-term existence, as a dedicated quiescent population which activates in short bursts is less likely to accumulate tumorigenic mutations, and maintains a flexible backup pool which can be drawn from eg. in the case of injury (L. Li & Clevers, 2010). This way, fetal and adult stem cell dynamics reflect the different goals of these systems, with rapid expansion being key to the former while long term stability and persistence characterizes the latter. Another important distinction between radial glia and SVZ NSCs is the behavior of their progeny: whereas fetal neuroblasts (also called A-cells) migrate along the radial glial process, adult neuroblasts migrate ventrally toward the so-called rostral migratory stream (RMS) which they follow to the olfactory bulb (OB), where they will ultimately integrate into the existing neuronal circuitry (Sanes et al., 2019) (Fig.2). In ageing, SVZ NSCs become markedly more quiescent (Kalamakis et al., 2019) as the population declines, resulting in an increased in transit amplifying divisions being required to compensate for reduced overall activation levels (Danciu et al., 2023). Thus, while adult NSCs and fetal radial glia cells share astroglial features, they exhibit differing lineage dynamics and progression, with each being characterized by a distinct frequency of activation and the behavior of their progeny.

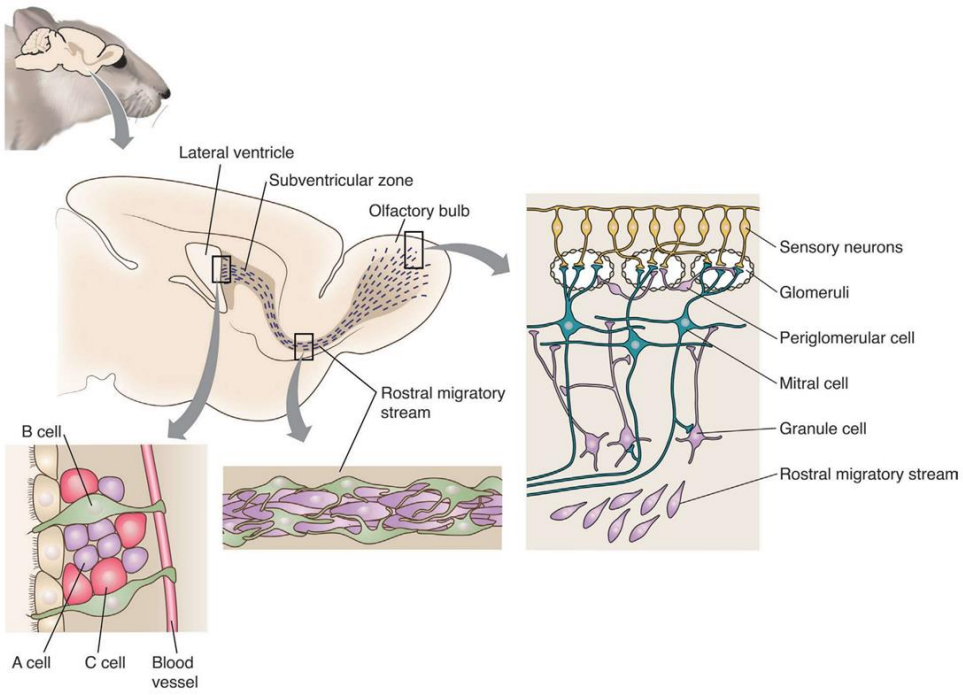

Figure 2: Overview of adult neurogenesis in mice. NSCs line the walls of the lateral ventricle, extending a cilium into the ventricle and contacting the blood stream (B-cell). NSCs activate (C-cell) and generate differentiating neuroblasts (C-cell) that migrate through the Rostral migratory stream to the Olfactory bulb, where they integrate into different interneuron subtypes. Reproduced from (Sanes et al., 2019).

Due to their shared developmental origins as well as morphological and marker features, NSCs are considered specialized astrocytes (Doetsch et al., 1999; Kriegstein & Alvarez-Buylla, 2009). Consistent with the common parenchymal astrocytes which populate the SVZ niche and other areas of the brain, NSCs express classical astrocyte markers such as `GFAP` and `GLAST` (Doetsch et al., 1997) and possess specialized endfeet which contact nearby blood vessels (Mirzadeh et al., 2008). Hinting at their privileged status however, NSCs extend a primary cilium to contract the ventricle, enabling them to communicate via the cerebrospinal fluid (CSF) (Mirzadeh et al., 2008). These two points of contact lend a familiar elongated shape to SVZ NSCs which is reminiscent of radial glia (Fig.2). This way, NSCs can sense and integrate regulatory cues from the CSF, and communicate within the niche or to more distal regions via the blood stream or SVZ-innervating neurons (Freundlieb et al., 2006). NSCs generally organize into a monolayer only a few cell-widths from the ventricular surface, in what is a generally hypoxic environment due to the relatively distant access to the blood stream (Zhu et al., 2005). This lends NSCs particularly adapted to respond in cases of hypoxic injuries such as stroke.

While NSCs exhibit strong intrinsic fating, their ability to adapt and respond to brain injury conditions is not completely understood. Lineage tracing demonstrated that NSCs activate in injury conditions, with several SVZ-derived progeny migrating outside the RMS to the injury site (Llorens-Bobadilla et al., 2015; Yamashita et al., 2006). Whether these cells represent an induced fate-switch upon eg. injury-induced inflammation, or derive from multipotent progenitors which respond to injury cues has important consequences for SVZ-derived tumors such as glioblastomas, though this question remains to be resolved. Indeed, lineage tracing demonstrates that while SVZ NSCs majorly generate neurons, these cells also produce astrocytic and oligodendrocytic progeny (Lim & Alvarez-Buylla, 2016). At the time of writing, no study of NSC lineages at single-cell resolution exists, with the pervading explanation for NSC lineage potential being due to regionalization of the SVZ (Tong et al., 2015). Transplantation experiments showcase the strong intrinsic fating of NSCs (Merkle et al., 2007), suggesting that beyond regional signals alone, NSC fate potential is inscribed in the cellular memory eg. through changes to DNA methylation or accessibility (L. P. Kremer et al., 2022) which drive unique transcription factor programs (Hirabayashi & Gotoh, 2010). While transplanted or *in vitro* cultured NSCs lose their original identity after some time, neuroblasts faithfully persist their specific neuronal fates throughout their migration along the RMS, suggesting that it takes specific external triggers to wipe NSC identity. These features of fate-based regionalization and the identification of eg. specific multipotent NSC populations can be addressed by scRNA-seq, which has seen effective application to SVZ populations.

1.1.3 Neural stem cells at single-cell resolution

Single-cell RNA-sequencing (scRNA-seq) has facilitated many of the major biological advances made during the period of my studies. Compared to bulk sequencing, scRNA-seq enables the precise delineation of different cell types without relying on external markers or selection, thus facilitating the identification of novel or condition-specific reactive transcriptional states. Briefly, the technique builds on the principles established in bulk RNA sequencing, reviewed in (Van Den Berge et al., 2019), with the critical addition of oligonucleotide sequences which enable the assignment of individual sequencing reads to their cell-of-origin. This is usually accomplished through one of two ways: addition of a cell barcode in droplet-based scRNA-seq (Macosko et al., 2015), or physical separation of individual cell libraries in plate-based scRNA-seq (Hagemann-Jensen et al., 2022; Picelli et al., 2014). These methods have different advantages, with droplet-based methods generally trading throughput and speed against the better coverage and higher labor costs of plate-based

methods. The use of unique molecular identifiers (UMIs), which include oligonucleotide labels to facilitate the *in silico* exclusion of PCR duplicates (Islam et al., 2014; Macosko et al., 2015), additionally improves the sensitivity of scRNA-seq data. Overall, scRNA-seq has seen wide adoption and commercialization, and presents a robust view of the transcriptional state of a given tissue or population.

The advent of scRNA-seq required the development of novel analysis techniques to make effective use of the high-throughput and high dimensional data it generates. These have culminated in several established workflows, reviewed in (Amezquita et al., 2020; Heumos et al., 2023; Luecken & Theis, 2019), and software packages to ease their application (Stuart & Satija, 2019; Wolf et al., 2018). These usually comprise various read-quantification (Dobin et al., 2013; Zheng et al., 2017) and normalization steps (Ahlmann-Eltze & Huber, 2023), followed by successive dimension reduction steps aimed at recovering the underlying biological relationships across the expression state of thousands of genes. To this end, uninformative genes are excluded through the selection of highly variable genes (Amezquita et al., 2020), followed by linear decomposition into a defined number of factors using PCA. These are then used to represent high-dimensional cellular neighborhoods in a nearest neighbor graph (KNN) and visualized by embedding eg. in UMAP (McInnes et al., 2020). Downstream analysis strategies include differential gene expression (Soneson & Robinson, 2018), batch-removal via integration (Haghverdi et al., 2018; Lotfollahi et al., 2022; Tran et al., 2020), and trajectory inference via pseudotemporal ordering (Cao et al., 2019; Haghverdi et al., 2016; Setty et al., 2019).

Applied to the adult SVZ, scRNA-seq has revealed the cellular heterogeneity of its constituent populations, enabling the robust and precise delineation of the NSC lineage trajectory (Basak et al., 2018; Carvajal Ibañez et al., 2023; Cebrian-Silla et al., 2021; Kalamakis et al., 2019; L. P. M. Kremer et al., 2021; Llorens-Bobadilla et al., 2015; Mizrak et al., 2019; Zywitza et al., 2018). This has highlighted key differences in ageing (Kalamakis et al., 2019) and injury (Llorens-Bobadilla et al., 2015) compared to homeostasis, revealing the Wnt and interferon signaling pathways as potent modulators of NSC activation. Single-cell analysis reaffirmed the close relationship and transcriptomic similarities between quiescent NSCs and the dormant niche astrocytes (Kalamakis et al., 2019) consistent with their initial designation as B1 and B2-cells, respectively (Doetsch et al., 1999). scRNA-seq furthermore elucidated signatures of NSC regionalization through comparative study of dorsal and ventral domains of the SVZ (Cebrian-Silla et al., 2021). It is likely that greater understanding of the regional determinants of NSC fate can be achieved through multi-omic studies which include eg. assessment of transcriptional and epigenetic states for an individual cell, as was recently

demonstrated for NSCs and niche astrocytes (L. P. Kremer et al., 2022). These advances share a common appreciation for the NSC lineage resolved through state transitions, eg. from dormant astrocytes to quiescent NSCs, which is unique to scRNA-seq and enables the quantitative study of various factors affecting NSC fate choice and lineage dynamics.

1.1.4 Wnt signaling in neural stem cell state transitions

From fetal development to adult neurogenesis, the Wnt signaling pathway plays an important role in regulating the activation state and population dynamics of NSCs. The role of Wnt in development is well established, being conserved across metazoa and intricately linked to fate choice by directing symmetry breaking events (Holstein, 2012). This essential role of Wnt signals stems from their ability to regulate both cellular diversity and spatial form through two sets of partially overlapping cascades known as canonical and non-canonical Wnt signaling, respectively (Loh et al., 2016). Thus Wnt signaling plays a central role in body plan determination and the generation of diverse tissues. While Wnt signaling activity is decreased in adult tissues, it nevertheless plays a crucial role in the maintenance of stem cell pools (Kalamakis et al., 2019; Steinhart & Angers, 2018). Being so intricately linked to organ development, it comes as no surprise that tumors are able to derive significant advantages through aberrant activation of Wnt signals (Y. Lee et al., 2016; Tan & Barker, 2018). Understanding these mechanisms, both in health and disease, is essential for therapeutic interventions in neuro-regeneration and associated malignancies.

In mammals, Wnt signaling is comprised of numerous ligands, receptors and co-receptors (Holstein, 2012) as well as various secreted antagonists. Wnt signals act at short range, generally through a lipid-modified ligand which is produced by a secreting cell and binds to its cognate receptor on a receiving cell to induce a functional response (Loh et al., 2016). Wnts thus establish local diffusion gradients and receiving cells can integrate signals from multiple sources or gradients simultaneously in a kind of Wnt-code (Guder et al., 2006) that encodes eg. positional information. This way, Wnt signals can spatially polarize a cell, for example determining the orientation of asymmetric divisions (Goldstein et al., 2006; Habib et al., 2013), or guiding axon remodeling and synapse formation (Ciani & Salinas, 2005). Though understanding the specifics of the Wnt code and the vast combinatorial complexity of Wnt signals remains an open challenge, existing studies modulating Wnt signals in adult NSCs point to a particular role of secreted Wnt antagonists in regulating cell stage transitions. A `DKK1` knockout, for example, perturbed NSC dynamics and led to an increased number of newborn neurons in aged mice (Seib et al., 2013). A similar effect on hippocampal NSCs was

observed through modulation of SFRP3 (Jang et al., 2013), while neutralizing SFRP5 (Kalamakis et al., 2019) and inhibiting SFRP1 (Donega et al., 2022) in the SVZ both increased NSC activation rates. An equivalent result was observed upon NOTUM inhibition (Mizrak et al., 2020). Together, these studies paint a clear picture of the role of secreted Wnt antagonists in modulating NSC activation. While it appears that NSCs integrate numerous signals to determine their activation, their precise interactions and crosstalk remain to be fully understood. Further exploration of these underlying signaling changes and feedback loops holds potential for their exploitation in modulating the activation state of NSCs in health and disease. Curiously, it is not Wnt but NOTCH signaling which is implicated in the neurogenic gain of stemness, ie. activation, of parenchymal astrocytes.

1.1.5 Emerging evidence on the neurogenic potential of astrocytes

The remarkable variability in brain-regenerative capacity across species starkly contrasts with the considerable conservation of organizational and neurogenic principles shared among them. This is especially true for mammals, for which many organs are unable to regenerate and instead form a dense scar through a process known as fibrosis. In mice, for example, brain injury induces reactive astrogliosis (Escartin et al., 2021) and the formation of a fibrosis-like barrier known as the glial scar which is generally considered detrimental to effective injury repair (Liuzzi & Lasek, 1987). However, other mammals such as the spiny mouse are capable of undergoing scarless regeneration (Gaire et al., 2021) even in nervous tissues, for example in response to spinal cord injury (Streeter et al., 2020). This increased regeneration was linked to the expression of neurogenesis-related genes, suggesting that trading reactive astrogliosis for neurogenic programs could entail improved regenerative outcomes.

Given that NSCs are specialized astrocytes and indeed both populations derive from a common ancestor, the question of the neurogenic potential of parenchymal astrocytes has garnered significant interest. By inhibiting NOTCH1 following brain injury, Magnusson and colleagues found that striatal astrocytes entered a neurogenic program (Magnusson et al., 2014) reminiscent of SVZ NSCs. This was confirmed in a followup study in (Magnusson et al., 2020) where it was determined that neurogenic striatal astrocytes proceed along a differentiation lineage consistent with that of SVZ NSCs outlined above. Another group later employed the same inhibition to demonstrate that striatal astrocyte-derived neurons effectively integrate into the neuronal circuitry (Dorst et al.,

2021). This transformation into neurogenic astrocytes was more frequent in the striatum compared to other brain regions, though recent studies have unveiled a similar regenerative potential for spinal cord astrocytes (Llorens-Bobadilla et al., 2020). While the precise mechanisms and cues which enable of astrocytic neurogenesis will undoubtedly be the subject of further study, these results pave the way for novel therapies aimed at improving local regeneration across various regions of the brain. Together, the ability for common brain astrocytes to enter a stem-like state and contribute to neurogenesis frames this process as an important and underappreciated substrate for the generation of brain tumors.

1.2 When homeostasis goes awry: the origins and pathophysiology of adult human brain tumors

For all the things that have to go right in the organization and population of an adult human brain, it is inevitable that some things go wrong. Given enough time, things begin to change: memories fade, senses blunt, networks atrophy, and stem cells exhaust. For some unfortunate souls, this results in the malignant transformation of certain cells leading to a tumor. This transformation is particularly striking in the adult brain, replacing the highly quiescent homeostatic conditions with a developmental-like setting characterized by rapid and repeated cycles of proliferation. In some ways, tumor cells have merely lost their programming: they are maladapted machines following buggy programs; an infinite while-loop that will consume resources until the system is brought to its knees. But in other ways, tumor cells are more than that: they create structures and environments, adding a spatial component which necessitates fate asymmetry and communication. They present a coordinated front, an organized hierarchy, and follow their programming to develop what is ultimately an organ within an organ – all while displacing the sensitive networks and stratified structures which preceded them: an irreplaceable loss and one which causes intense suffering.

1.2.1 Clinical guidelines for the classification of gliomas

Gliomas are a heterogeneous group of brain malignancies with glial origins. Among these, glioblastoma is the most common and aggressive form, classified according to the World Health Organization of tumors of the CNS (WHO CNS5) as adult-type diffuse glioma (grade IV) that is

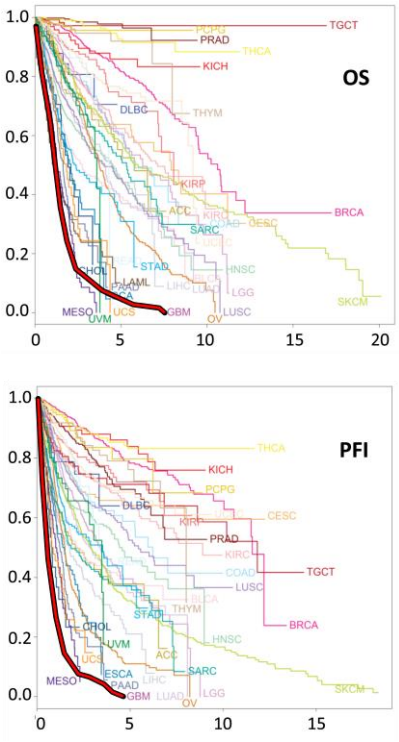

Figure 3: Kaplan-Meier plots of TCGA tumors by cancer type. Survival in years (x-axis) is plotted against the proportion of surviving patients (y-axis). GBM: glioblastoma. Reproduced from (J. Liu et al., 2018). Emphasis added.

isocitrate dehydrogenate (IDH)-wildtype (Louis et al., 2021). In the United States, glioblastoma accounts for 49.1% of all primary malignant CNS tumors and 58.4% of gliomas, making it one of the most frequent brain malignancies. Glioblastoma incidence varies by age, with tumors 3-fold more likely to develop in individuals over 40, and with a median age at diagnosis of 65. Males are also 1.65 times as likely to develop glioblastomas as females, while genetic risk factors have largely failed to materialize (Ostrom et al., 2021). Glioblastomas are uniquely lethal among TCGA tumors (Fig.3) (J. Liu et al., 2018), reflecting their overall poor prognosis with a median overall survival below 15 months and an abysmal 5-year survival rate of 6.8% (Ostrom et al., 2021). This is despite a relatively aggressive standard treatment aimed at maximal safe surgical resection followed by daily radio- and chemotherapy with temozolomide (TMZ) over six weeks, with maintenance TMZ chemotherapy for at least 12 months. Notably, patients whose glioblastomas contact the subventricular zone experience adverse prognosis (Berendsen et al., 2019). Nevertheless, the primary cause of poor survival is tumor recurrence, which occurs in at least 85% of patients (Stupp et al., 2005), and for which no standard treatment regimen exists. Recent years have seen the introduction of monoclonal antibody-based therapies using bevacizumab (Gilbert et al., 2014) or via checkpoint blockade (Cloughesy et al., 2019). However, due to the relative inaccessibility of brain tissues, no targeted therapies are currently available to patients. Collectively, the survival rate of glioblastoma has not significantly improved despite decades of research, and this stagnation will breed tragedy as the rapidly ageing populations of developed countries lead to an inevitable uptick in diagnosis. These observations motivate the development of novel strategies targeting glioblastoma development, for example promoting a molecular view of tumor organization rather than the more traditional histopathological methods.

The heterogeneity of glioblastomas has led to the development diverse tumor classifications which have evolved with the technologies for their measurement. Beginning with microarray-based transcriptomic profiling in conjunction with the TCGA consortium (Phillips et al., 2006; The Cancer Genome Atlas Research Network, 2008; Verhaak et al., 2010), three main transcriptional subtypes

were proposed: proneural, classical, and mesenchymal. These groups are discussed in more detail below. This transcriptomic classification was complemented and reinforced by exome-sequencing (Brennan et al., 2013; Ng et al., 2009) which further underscored the genetic heterogeneity of glioblastomas and the difficulties in its treatment compared to eg. pediatric tumors with clear driver mutations. DNA-methylation-based stratification of glioblastoma patients broadly recapitulated the transcriptional subtypes (Sturm et al., 2012), with novel subtypes only identified for `IDH`-mutant tumors (Ceccarelli et al., 2016; Noushmehr et al., 2010). An integrative transcriptomic and epigenomic study characterized the oligodendrocyte-lineage factor `SOX10` as a master regulator of the proneural tumor type, which additionally catalyzes the switch to a mesenchymal-like type (Wu et al., 2020). A general approach to methylation-based assessment of glioblastoma subtype has since been implemented for aiding clinical diagnosis (Capper et al., 2018), demonstrating the application of molecular methods to support clinical decision making. Approaches in this vein will ultimately pave the way for precision medicine-based interventions which fully utilize the breadth of insights available on the spatial and molecular organization of glioblastomas and other tumors.

1.2.2 Organization and structure of glioblastomas

The resemblance of the glioblastoma molecular subtypes to various populations of glial cells was recognized early on (Phillips et al., 2006; Verhaak et al., 2010). Going from bulk to single-cell profiling of glioblastoma cells confirmed this observation, with an early comprehensive transcriptomic study delineating a four state model of glioblastoma heterogeneity (Neftel et al., 2019) in line with the previous classification into proneural, mesenchymal, and classical subtypes. Consistently, the variable contribution of each of the four AC-, MES-, NPC-, and OPC-like states to individual tumor samples likely determines its assignment to one of the bulk subtypes. Notably, with the exception of the MES-like state the other three cell states are all related to stages of NSC development, suggesting these may share organizational principles. These single-cell studies additionally highlighted the existence of so-called hybrid states (Neftel et al., 2019; Patel et al., 2014), describing cells transitioning between states and providing first evidence for the plasticity of glioblastoma hierarchies. Other studies confirmed this view, eg. identifying a transition from quiescent- to more proliferative states through tumor progression (L. Wang et al., 2019), or through cells residing on different developmentally- (Bhaduri, Di Lullo, et al., 2020; Couturier et al., 2020; Johnson et al., 2021), injury- (L. M. Richards et al., 2021), or metabolically-driven (Garofano et al., 2021) phenotypic axes. Thus, different cell states make up the landscape of any given glioblastoma, and these tumors

are characterized by a high degree of compositional variation overall. Better understanding of the hierarchy and plasticity of these cell states is critical to understand their specific vulnerabilities, and different *ex vivo* organoid (Jacob et al., 2020) and xenograft models (Linkous et al., 2019) provide an opportunity to this end. Alternatively, the development of spatial transcriptomics techniques has enabled the high-throughput identification of diverse tumor cell states in patient tissues.

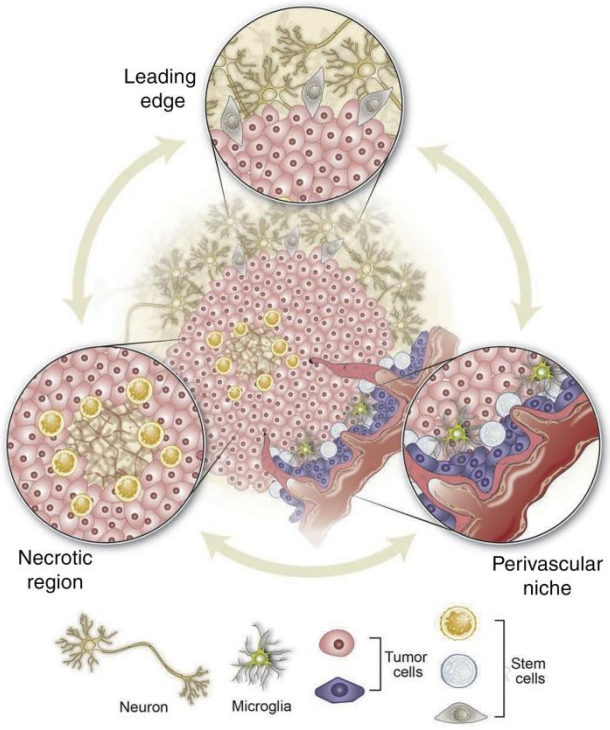

Figure 4: Tumor niches comprising the spatial organization of glioblastomas. Environmental factors lead to the emergence of diverse tumor microenvironments populated by various tumor cell states interacting with local healthy cells. Reproduced from (Prager et al., 2020).

Organized and recurring secondary structures have long been associated with glioblastomas (Scherer, 1938), describing the tumor microenvironment and providing insights into additional factors affecting glioblastoma organization. These tumors tend to converge on three major microenvironmental archetypes: the hypoxic and necrotic tumor core, the perivascular niche, and the invasive edge (Hambardzumyan & Bergers, 2015; Prager et al., 2020) (Fig.4). While morphological and immunohistological studies described the presence of tumor stem cells in each of these environments (Prager et al., 2020), the advent of spatial transcriptomics (Rao et al., 2021) and multiplexed FISH (Goh et al., 2020; Janesick et al., 2023) technologies enables the fine-grained identification of individual cell states *in situ*. These studies consistently identify hypoxia as a driver of

spatial organization with associated enrichment in MES-like and immune-cell populations (Greenwald et al., 2023; Mossi Albiach et al., 2023; Ravi et al., 2022). This is consistent with the SVZ NSC niche, where hypoxia promotes cellular quiescence. Indeed, related studies have (Gangoso et al., 2021; Mossi Albiach et al., 2023) suggested that the MES-like state, the only non-NSC state, in fact represents an AC-like state overlaid with injury-dependent programs reminiscent of reactive astrocytes (Mossi Albiach et al., 2023). Spatial transcriptomics confirms the increased presence of tumor-associated macrophages, which influence glioblastoma progression (Buonfiglioli & Hambardzumyan, 2021), in the perivascular niche (Ruiz-Moreno et al., 2022); while AC-like tumor cells are found in the viscinity of endothelial cells consistent with their affinity for vessel-contact in the healthy brain (Mossi Albiach et al., 2023). Hypoxic gradients also associate with infiltrating cells at the leading edge (Ravi et al., 2022) and negatively affect overall spatial coherence of cell states (Greenwald et al., 2023), an observation that extended to methylation disorder noted for certain environmental stressors (Johnson et al., 2021). Cells at the leading edge which migrate into the healthy tissues exhibit characteristics of migrating CNS-derived cells (Darmanis et al., 2017; Greenwald et al., 2023; Varn et al., 2022) and together present significant obstacle to surgical resection (Comba et al., 2022), being a prime candidate in tumor recurrence. Collectively, these studies demonstrate the complex interplay of cellular states and microenvironmental factors which affect tumor organization, with a notable role of conserved states and characteristics of healthy NSCs among glioblastoma cells.

1.2.3 Experiments elucidating the origins of glioblastomas

The conserved aspects of glioblastoma cell states and organization in relation to SVZ NSCs makes these an attractive candidate tumor cell-of-origin. As human brain tissues are experimentally unavailable, the question of tumor origin is tightly coupled to the characteristics of cancer stem cells, requiring significant histological or maker overlap (Okonechnikov et al., 2021) to support its identification eg. in a mouse model of gliomas. Along this vein, transformation of SVZ NSCs with strong genetic driver mutations (Alcantara Llaguno et al., 2009) was found to induce GBM formation. This central role of the cell-of-origin in determining tumor phenotype was demonstrated in a followup study which induced the same panel of mutations separately in NSCs and OPCs and observed the formation of morphologically and transcriptomically distinct tumor subtypes which persisted through secondary transplantation (Alcantara Llaguno et al., 2009; Z. Wang et al., 2020)

(Fig.5). These results highlight the elevated importance of cell lineage compared to driver mutations, consistent with the genetically heterogenous landscape of glioblastomas. Lineage restriction seems to determine tumorigenicity, as postmitotic neurons were shown to be recalcitrant to malignant transformation (Alcantara Llaguno et al., 2019). However, this study did not assess the ability for astrocytes to undergo malignant transformation, a feat which has only been demonstrated *in vitro* (Friedmann-Morvinski et al., 2012) despite their noted role in the generation of lower grade gliomas (Holland et al., 2000). Using patient samples, SVZ NSCs were found to harbor low-level driver mutations which were found in matched glioblastoma samples (J. H. Lee et al., 2018), an observation which was validated in a mouse model. All of these approaches utilized the targeted mutation of specific populations, while an unbiased PDX barcoding experiment highlighted an invariant stem cell hierarchy rooted in a slow-cycling quiescent population with lineage characteristics consistent with neurogenic NSCs (Lan et al., 2017) and astrocytes (see above). Thus, while a definitive cell-of-origin remains to be identified, existing evidence points to SVZ NSCs as a likely glioblastoma-initiating population. However, it is important to consider the defining role the cell-of-origin has on tumor features in light of the regionalization and diversity of NSC populations, as these may explain some of the intra-tumoral heterogeneity observed in glioblastomas. Additionally, the recent evidence demonstrating the neurogenic capabilities of common brain astrocytes suggests these may have been overlooked as a potential tumor cell-of-origin.

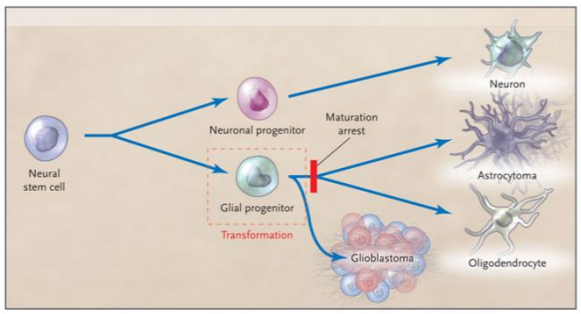

Figure 5: Emergence of gliomas from progenitor cells. Stage-specific transformation and maturation arrest characterize the emergence of various gliomas including glioblastoma, oligodendrocytoma, and astrocytoma. Different cells, such as the neuronal progenitor, likely lead to the emergence of related but distinct glioma subtypes. Modified from (Sanai et al., 2005).

1.2.4 On glioblastoma stem cell plasticity

Cancer stem cells, in the current context referred to as glioma stem cells (GSC), provide a framework for understanding the phenotypic plasticity and structured organization of glioblastoma cells (Gimple et al., 2019; Lathia et al., 2015). GSCs are typically considered to be highly plastic, de-differentiated cells which are able to differentiate into various cellular states depending on external conditions (so-called "GSC-multiplicity") (Prager et al., 2020; Suvà & Tirosh, 2020). In turn, recent publications present a highly plastic view of glioblastoma hierarchies. For example, the study by (Dirkse et al., 2019) enumerates a myriad of cell state transitions measured by FACS markers, though these do not extend to transcriptomic differences. A related *in vitro* barcoding approach identified a quasi-linear GSC hierarchy with diverse state transitions present at low frequency (Larsson et al., 2021). Another study demonstrated that the YAP/TAZ pathway confers stemness properties regardless of the molecular subtype (Castellan et al., 2020), an observation in line with marker-based studies which demonstrate that glioblastoma cells do not become terminally differentiated *in vivo* (Galli et al., 2004). This view presents a deviation from the highly constrained lineages of healthy NSCs and the invariant NSC-like stem cell hierarchy measured in (Lan et al., 2017). Indeed, contemporary single-cell studies of glioma characterize putative GSCs on their cycling activity alone (Couturier et al., 2020; Neftel et al., 2019; Tirosh et al., 2016; Venteicher et al., 2017), overlooking the foundational role of quiescent populations in contributing to tumor growth (Chen et al., 2012; Xie et al., 2022). Consequently, highly cycling populations such as NPC-like cells are given the GSC label, while astrocytes are regarded as terminally differentiated – thus overlooking their latent stem cell potential (see section 1.1.5) and the contribution of eg. radial glia-like populations to tumor hierarchies (Bhaduri, Di Lullo, et al., 2020; R. Wang et al., 2020). Unraveling the division hierarchy of GSCs and resolving the status of proliferating cells as a permanent or transitioning cell state will have important consequences for the targeted eradication of GSCs.

The tumor propagating potential of GSCs suggests a limited view of GSC plasticity. Like SVZ NSCs (see section 1.1.1), GSC-derived tumors exhibit strong intrinsic fating. For example, when cells in a given state are used to grow patient-derived xenograft (PDX) tumors, these will recapitulate the diversity of cell states observed in the primary tumor (Neftel et al., 2019), suggesting that their lineage potential is pre-determined. A similarly constrained plasticity was observed for GSCs isolated *in vitro* (Singh et al., 2004) and mouse models of gliomas with a separate cell-of-origin (Z. Wang et al., 2020). Indeed self-renewing capabilities are not equivalent between glioblastoma cell states, as quiescent cells exhibit a significantly increased ability to generate secondary tumors compared to neuronal, ie. NPC-like, cells (Sabelström et al., 2019). Combined with the reported associations of spatial

determinants of glioblastoma cell state (see above), it remains to be determined whether the consistent features of secondary tumors are due to intrinsic fating of GSCs or a mutational burden which constrains their spatial organization. This question of is also relevant in tumor recurrences which are often accompanied by a switch to a proneural subtype (Varn et al., 2022), suggesting that the underlying fate-potential of tumor GSCs has changed. Regardless of GSC plasticity, it appears that glioblastoma development entails some degree of lineage constraint leading to the clear parallels and conserved characteristics of glioblastoma cell states and organization against the SVZ NSC lineage.

1.3 Lineage constraint exerted by a tumor's memory of its tissue of origin

Biology operates at scales, and especially in evolution, often what is true for the organism is also true for the cell. Here, I want to expound on the notion of lineage constraint which I believe provides a useful perspective on tumor lineages when viewed in the context of developmental fate restriction, ie. the constrained fate potential of cells at different timepoints in development.

A frequent analogy for fate restriction is made through the eponymous Waddington's landscape (Waddington, 1957), where the progression of progenitor to differentiated populations is depicted through the action of marble rolling down a valley toward differentiated fates: the implication obviously being that this represents fate restriction as the marble cannot roll back uphill. However, while cellular transdifferentiation events like with the generation of iPSCs (Takahashi & Yamanaka, 2006) or tumor dedifferentiation (Friedmann-Morvinski & Verma, 2014) refute this model, it remains true in principle. Indeed, the fact that tumors majorly organize by tissue of origin (Hoadley et al., 2018; Schneider et al., 2017) suggests that tumor dedifferentiation is incomplete, and this is where I postulate the action of lineage constraint.

Just like an organism's evolutionary history places constraints on its phenotypic variability, so does a cell's developmental history place constraints on its lineage plasticity. I will contextualize some of the examples from (J. M. Smith et al., 1985) to demonstrate this point. Take for example nautilus or ammonoid shells, which follow a logarithmically coiled shaped (Raup, 1967). The path followed by any point on the growing edge of the shell can be described by the simultaneous solution of two linear differential equations, making it possible to map the distribution of actually occurring morphotypes in the morphospace depicted in (Fig.6). Several caveats apply to this example, but it can be clearly observed that nearly all ammonoids fall on the left side of the curved line. This distinction is biomechanical (rather than through clear developmental constraint, but the example holds), where shells on the right side of the line would be "open" because subsequent coils are not in contact. This is inefficient both structurally and in terms of materials, precluding its emergence by natural selection, which constrains the ammonoid shell morphospace into a limited set of morphotypes.

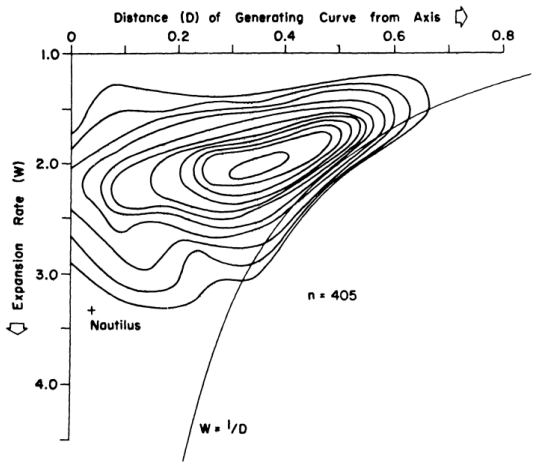

Figure 6: Ammonoid shell-shape selection viewed through a slice of the shell morphospace. 2D density map of shell-shape features measured in 405 extinct ammonoid genera. The W = 1/D line denotes the point where open coiling shells diverge from overlapping coiling. The location of the extant nautilus is indicated. Modified from (Raup, 1967).

A more direct example is given by kangaroos, which travel in a series of leaps. Due to the specialized nature of their limbs, they are unlikely to evolve adaptations to bipedal running. Thus their developmental history of kangaroos places constraints on their future development, preferentially selecting morphological changes that make them better at leap-based locomotion. However it is possible, if incredibly unlikely that extraordinary reconstruction – such as bipedal gait in kangaroos – will take place, and I will revisit this point later. Returning to our metaphor we can, in terms of cellular fate, imagine that the cytosolic content and epigenetic configuration inherited by a given cell acts as a barrier to differentiation processes outside of a narrow window of predetermined fates. Much like kangaroo's limbs, the cell's prior developmental history restricts its future potential.

Tumors too, particularly those arising from adult tissues, inherit the restricted fate potential of their predecessors. So how do they overcome this lineage constraint? Here Maynard Smith's example of the sequence of limb loss in tetrapods is appropriate. Writing contemporaneously to the discovery of Hox genes, Maynard Smith notes that among the numerous lineages of amphibians, reptiles, birds, and mammals which have undergone the evolutionary loss of limbs, this always occurs in a distal to proximal sequence (Lande, 1978): some elements (limbs, digits) are always lost before others. This is true developmental constraint, unknown to Maynard Smith but caused by premature termination of a SHH gradient (Cooper et al., 2014). As loss of the gradient would have consequences for the development of the entire limb, the only available configurations are removal of digits in the reverse order. This limited accessibility of options is the key to lineage constraint experienced during tumor development. As some mutations will not impact the cell, ie. analogous to eg. a NOTCH mutation which will not affect digit patterning, tumor driver mutations can only emerge in a context-specific manner. Different cells vary chiefly according to cell type, and the specific programs active in various cell types determine the context within which lineage constraint

acts, thus resulting in the emergence of tissue specific drivers. In analogy to the key and lock model of enzyme activity: it does not matter which key you are holding if the cell has taken away the lock.

Importantly, this mechanism for lineage constraint does not preclude the random mutation of non-tissue-specific drivers, simply predicting that these will not be able to confer selective advantage. This is consistent with the emergence of low-level driver mutations in healthy tissues (Colom et al., 2020; J. H. Lee et al., 2018; Simpson Ragdale et al., 2023) which can persist for decades before being acted on.

Lineage constraint furthermore predicts that tumors will tend to fix their tissue-of-origin characteristics due to the preference for immediate gains over incremental adaptations. Different tissue's tumors have different proliferation rates (Tubiana, 1989), suggesting that some drivers confer a greater fitness advantage in absolute terms. However, tumors will rarely converge on that fitness optimum, instead maintaining their tissue characteristics through lineage constraint. Here, I find an explanation in Maynard Smith's example of the evolution of mimicry. Major mutations are often involved in the evolution of mimicry (Turner, 1988) because any change to the organism's shape has to trade the potential protective benefits against the cost of disrupted mate recognition and courtship behaviors. Similarly, tumors will not tolerate suboptimal intermediate mutations which might release the constraint on a strong driver, as these need to confer sufficient advantages to not be outcompeted through increased metabolic costs or the risk of immune surveillance. Though there are limitations to this model, for example in the fact that tumors are able to mutate multiple loci simultaneously, it nevertheless appears to hold – perhaps balanced by other factors. This example does, however, reintroduce the notion of extraordinary reconstruction as in the limbs of the tree kangaroo. Here, evolution has found a devious way to get around developmental constraints, bestowing upon the tree kangaroo a bipedal gait and the ability to climb. Similarly, so can tumors overcome lineage constraint in specific cases; and I hypothesize that this means to deviate from the expected tissue characteristics is one factor in the development of cancers of unknown primary (CUPs) (M. S. Lee & Sanoff, 2020).

Putting everything together, I combine this idea of lineage constraint with the shared characteristics of glioblastoma and the NSC lineage outlined above, to use pseudotime-based lineage abstractions to make inferences about glioblastoma hierarchies in the absence of lineage tracing data. These ideas are outlined in the following sections.

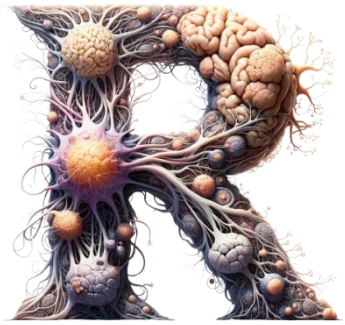

RESULTS

2.1 ptalign facilitates the systematic comparison of tumor pseudolineages

The elucidation of tumor transitions that fuel malignant hierarchies is critical for the identification of targeted interventions that can disrupt malignant progression. Unlike the tight regulation of differentiation observed in healthy lineages, tumors are characterized by a plastic hierarchy of dynamic transitions which are constrained by the memory of their tissue-of-origin (see section 1.3). Knowledge of these dynamics provides a convenient surface to devise tailored interventions, but their inference by conventional lineage tracing is not feasible in human tissues. This limitation led myself and Oguzhan Kaya to conceptualize pseudotime alignment as a means to infer tumor dynamics from a snapshot by studying tumor lineages through the lens of healthy stem-cell transitions. I developed this approach into *ptalign*, which leverages a tumor's memory of its tissue-of-origin to place malignant cells within a reference pseudotime trajectory (Fig.7), thus elucidating tumor dynamics without the need for lineage tracing. ptalign generates what I termed the tumor *pseudolineage*, representing the tumor's underlying dynamics based on states and transitions inferred from the healthy reference. Together, this approach provides a new perspective on tumor organization applicable across various tissues, and enables the study of tumor cells transitioning lineage stages, which reveal an important surface for therapeutic intervention.

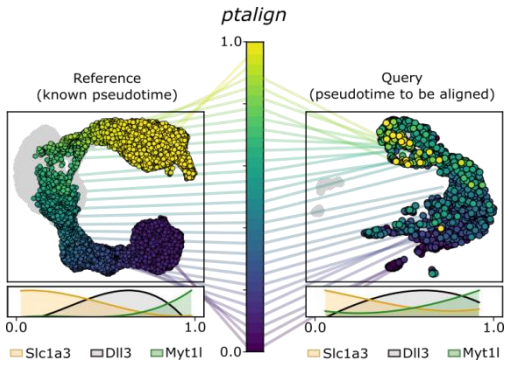

Figure 7: ptalign projects tumor cells onto a reference pseudotime. schematic overview of the projection of cells from a query dataset (right), here a glioblastoma PDX, onto a reference lineage pseudotime, here of SVZ NSCs (left). Pseudotime-binned cells are linked to their average position in the UMAP, and scaled pseudotime expression splines of NSC lineage markers (`SLC1A3`, `DLL3`, and `MYT1L`) highlight conserved dynamics inferred by ptalign.

Tumor pseudolineages can be conceptualized as capturing the compendium of cell states which sustain tumor growth. These states can vary across tumors due to differences in developmental history or physical environment, necessitating organized hierarchies of distinct cell states which sustain the tumor as an organ within an organ. ptalign introduces framework for comparing the dynamics of tumor lineages, not only capturing the relative frequency of cell states – aiding in tumor stratification and the design of targeted interventions – but also standardizing the comparison of cells from diverse tumors by projecting them onto the same reference pseudotime axis. By aligning all tumors on a unified axis, ptalign enables direct comparisons between tumor-tumor and tumor-healthy expression dynamics, which was not previously possible.

This approach, viewing tumor cells through the lens of healthy lineage dynamics, enables the transfer of contextual knowledge from the healthy reference to aid the interpretation of tumor dynamics. Building on this framework to compare different tumor pseudolineages, I use ptalign to identify potent modulators of essential glioblastoma transitions (see section 2.9.2). Unlike conventional pseudotime inference methods, which frequently place cycling cells at the pseudotime root and suggest the existence of an unsupported continuously cycling progenitor, ptalign's methodology is rooted in a healthy reference lineage with known state-ordering. This approach ensures accurate resolution of tumor cell state transitions, unveiling a rich source of clinical insights. The lightweight design, rapid execution, portability, and interpretability of the ptalign algorithm additionally enhance its utility and the valuable insights it can provide. In this work, I demonstrate these advantages of the ptalign algorithm by assessing (section 2.6), evaluating (section 2.7), and modulating (section 2.9) glioblastoma pseudolineages inferred through comparisons to healthy NSCs of the adult mouse brain.

2.1.1 On the use of ptalign in resolving glioblastoma organization visavis SVZ NSC differentiation

In this section, I briefly outline the biological context and motivation for the study of glioblastomas through the lens of healthy NSC transitions as facilitated by ptalign. The data and insights outlined here serve to introduce the datasets necessary to properly document the ptalign algorithm, and are otherwise elucidated in greater detail in subsequent sections.

The ability of ptalign to identify stage transitions is particularly valuable in the study of glioblastomas. These tumors are considerably heterogeneous, displaying a variety of cell states

(Neftel et al., 2019; Varn et al., 2022; Verhaak et al., 2010) that reflect different developmental stages. Few studies have quantified the plasticity of glioblastoma cell hierarchies (Dirkse et al., 2019; Lan et al., 2017; Larsson et al., 2021), and transitional states have remained an underappreciated aspect of tumor organization. Instead, recent developments have focused on the cancer stem-cell hypothesis, identifying and characterizing the so-called gliomas stem-cell (GSC) (Prager et al., 2020) and even employing pseudotime-guided approaches to infer a stem-cell hierarchy with the aim of identifying its root (Bhaduri, Di Lullo, et al., 2020; Castellan et al., 2020; Couturier et al., 2020). However, these studies lend outsized weight to the fact that all cells are born through cell cycle, and frequently identify GSCs by cycling activity (Couturier et al., 2020; Neftel et al., 2019; Tirosh et al., 2016; Venteicher et al., 2017). This perspective overlooks the inherent state plasticity which enables various glioblastoma cells to attain stem-cell properties, lending credence to the idea that it is the transitions to and from proliferating stages which are key to tumor growth and therapy resistance. Thus by employing ptalign to map glioblastomas onto the healthy NSC lineage trajectory, I aim to pivot from GSC-centric analysis to a broader examination of the transitions between multiple cell states and their role in tumor hierarchies.

Glioblastomas in the adult brain are thought to emerge from NSCs of the SVZ (Alcantara Llaguno et al., 2019; J. H. Lee et al., 2018), which develop along highly constrained lineages in the tightly regulated environment of the adult brain (see section 1.1.2) – making them opportune targets for ptalign. In the SVZ, these NSCs line the walls of the ventricle, where they integrate signals from the CSF and bloodstream, communicating across a complicated network to coordinate homeostatic neurogenesis. Most of these NSCs are born in the late embryo and reside in dormant stages, remaining in quiescence (Q) until signaled to enter activation (A), upon which they clonally expand to produce differentiating (D) progeny which integrate as neurons in different areals of the adult brain. Fine-tuning of this process, particularly in injury and aging contexts, remains poorly understood, as do the clonal dynamics of NSCs. These transitions through quiescent, activation, and differentiation (QAD) stages are conserved across different stem cells, demonstrating similar dynamics across brain regions (eg. SGZ), and species (eg. in fetal or organoid models of human brain development, see section 2.5). Thus to study glioblastoma organization through the lens of the healthy NSC lineage, I compiled an SVZ NSC dataset where pseudotime captures differentiation through QAD stages and I could isolate stage-specific genes which enable its transfer between models (section 2.2.2). This dataset forms the lineage reference for the ensuing discussion of the ptalign algorithm.

To facilitate a population-level analysis of glioblastoma organization, I additionally compiled 55 primary glioblastoma scRNA-seq datasets from the literature, which are documented in section 2.7.1. These, together with in-house glioblastoma PDX models created and sequenced by Oguzhan Kaya and his students (as outlined in (Kaya, 2023)), comprise the tumor query in the following sections detailing the ptalign algorithm.

2.1.2 Overview of the ptalign algorithm

Inspired by the principles of sequence alignment, ptalign adapts this methodology to scRNA-seq pseudotime trajectories, aiming to place query (tumor) cells within the best-matching stage of a reference (healthy) lineage pseudotime based on gene expression dynamics. ptalign maps tumor cells to a corresponding point in the healthy lineage pseudotime by means of an anchor gene set which both marks progression through the healthy differentiation trajectory and captures a tumor's memory of its tissue-of-origin (Fig.8). This alignment is achieved by associating the correlation dynamics between a query tumor cell and the healthy reference lineage to a given reference pseudotime (see section 2.1.3). For example, a query cell exhibiting high correlation to early reference pseudotimes will receive a low aligned pseudotime, while a query cell exhibiting high correlations to late reference pseudotimes will receive a high aligned pseudotime. This association is learned by a multi-layer perceptron (MLP) trained to predict pseudotime from reference-reference correlation dynamics. Importantly, multiple tumor samples can be projected into the same reference trajectory, facilitating their comparison in that context. Concretely for glioblastomas aligned to a healthy SVZ NSC lineage reference (see section 2.7.1), ptalign enables the comparative study of the states and transitions which make up tumor pseudolineages.

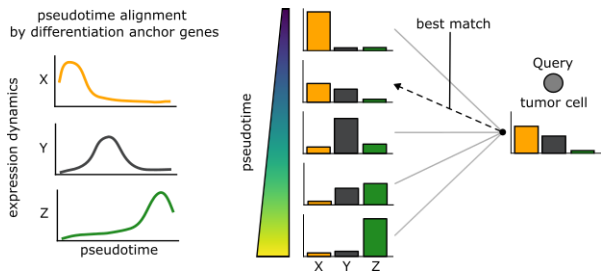

Figure 8: Overview of the ptalign algorithm. Expression dynamics of the anchor genes X, Y, and Z mark progression through a reference lineage pseudotime, and pseudotime is assigned for a query tumor cell by determining the best-matched position in the reference pseudotime according to the expression profile of those anchor genes.

Analogous to the uncertain placement of multimapping reads during sequence alignment, ptalign is currently not able to resolve tumor dynamics across branching pseudotimes. Moreover, as the cell cycle effectively constitutes a branching event in pseudotime, cycling cells are routinely excluded from ptalign analysis. Consequently, the suitability of aligned pseudotimes is assessed by a built-in permutation model which identifies tumors with unexpected or erroneous dynamics, for example having high correlations to both early- and late reference-pseudotimes (see section 2.1.4). This is accomplished through dynamic time warping (DTW) to assess the transcriptional similarity between aligned and permuted pseudotimes, enabling comparison across permutations or tumors. Taken together, this approach presents a fresh perspective on tumor organization, providing a light weight, fast, and interpretable means to fix tumors cells' placement within a reference pseudotime trajectory. Details of the ptalign algorithm are laid out in the following sections.

2.1.3 Query-reference correlation dynamics inform aligned tumor pseudotimes

The path to tumorigenesis is inherently stochastic, altering specific expression programs while leaving others intact. This phenomenon ensures that each tumor retains a memory of its tissue-of-origin, moving uphill in Waddington's landscape yet remaining recognizable based on key characteristics (see section 1.3). To harness these insights, I designed ptalign to leverage these underlying expression programs to map tumor cells to a corresponding point in the healthy lineage pseudotime. This correspondence is determined by matching expression patterns in a curated set of pseudotime-predictive anchor genes from the healthy reference lineage. For this purpose, I isolated 242 QAD genes from the healthy SVZ NSC reference lineage (see section 2.2.2) and used them to conduct ptalign pseudotime alignment of the T6 PDX generated by Oguzhan Kaya (Kaya, 2023).

ptalign employs query-reference correlation dynamics to infer aligned tumor pseudotimes. Expression patterns are quantified by calculating the Pearson correlation of a tumor cell's transcriptome against pseudotime-binned (by default `n_pt_bins=50`) cells from the healthy reference (Fig.9a, upper). This way, tumor cells will tend to exhibit higher correlation to either the early or late parts of the reference lineage, while very few cells correlate with both (Fig.9a, lower). This process generates a query-reference correlation matrix (Fig.9b) which is further processed to isolate correlation dynamics at the expense of correlation strength, since the latter varies with the

tumor's history. By conducting row-wise normalization and scaling correlations to a `[0, 1]` range, I improve the resolution of cells transitioning the edges of high-correlation bands and arrive at a scale-invariant view of the underlying expression dynamics (Fig.9c) that anchor the tumor's memory of its tissue-of-origin. It is by associating these dynamics to a specific reference pseudotime that ptalign makes a prediction for individual tumor cells.

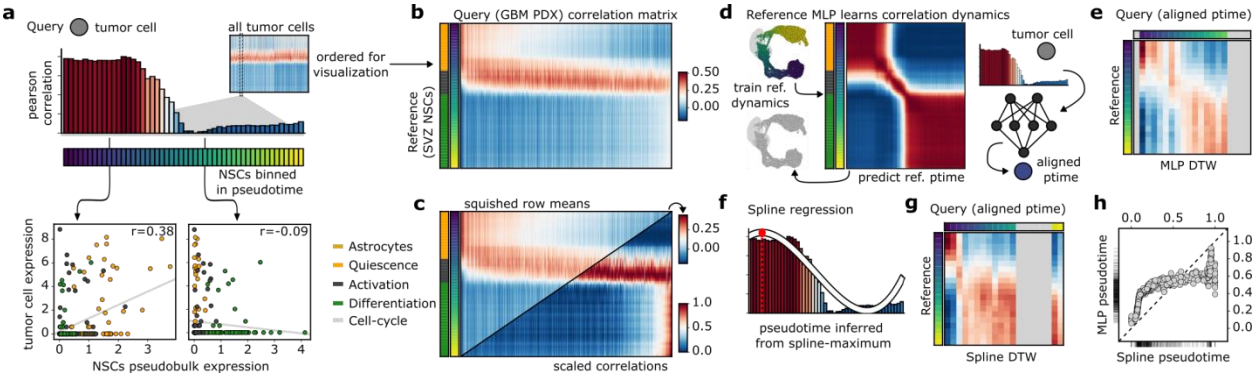

Figure 9: Pseudotime alignment by query-reference correlation dynamics. a) Pearson correlations of a query tumor cell transcriptome with pseudotime-binned cells from the reference SVZ NSC lineage (top). Correlation dynamics for a single cell are depicted, and make up individual columns in the query-reference correlation matrix (inset). Different correlation strength in individual anchor gene expression values for the query tumor cell are depicted for two reference pseudotime bins (bottom). b) The query-reference matrix of raw Pearson correlation values, ordered by aligned pseudotime for visualization purposes, with reference cell states and pseudotimes indicated. c) Matrix from (b) shown with normalization procedure to isolate correlation dynamics by squishing row-means and scaling correlations per cell. d) Reference-reference correlation matrix (left) used to train a MLP to associate correlation dynamics with pseudotimes, which is used to predict aligned pseudotimes based on tumor dynamics (right). e) DTW of aligned pseudotime by MLP-method for query with reference lineage pseudotime. Light gray pseudotime bins contain <5 tumor cells each. f) Pseudotime inference from spline regression, where smoothed correlation dynamics are used to extrapolate an associated reference pseudotime. Note the artefactual increase in the spline curve at late pseudotimes. g) DTW for spline-method aligned pseudotime for query with reference lineage pseudotime. h) Comparison of aligned pseudotimes inferred by MLP- or spline-method, respectively.

To associate query-reference correlation dynamics with reference pseudotimes, I employed a multilayer perceptron (MLP) regressor or spline regression. The MLP proved most effective, learning to predict pseudotimes from the query-reference correlation matrix of the reference dataset alone, where pseudotimes are artificially masked from the 'query' for assessment (Fig.9d). In practice, this network has two internal layers designed around the number of reference pseudotime bins, resulting in a compact model with few trainable parameters. I employ a grid search over regularization parameters to fine-tune the MLP, opting to forego the conventional train-test split and cross-validation. This network robustly and accurately learns to infer pseudotimes from correlation dynamics, producing valid estimates for tumor cell pseudotimes as reflected in the

consistently high correlations along the matrix diagonal (Fig.9e) in the aligned- and reference-pseudotime DTW.

In parallel, I assessed the utility of spline regression to derive aligned pseudotimes, in this case smoothing over correlation dynamics to assign aligned pseudotimes based on spline maxima (Fig.9f). Spline regression is a numerically simpler model without the black-box characteristics inherent to multilayer neural networks such as the MLP, enabling clear association of spline coefficients with aligned pseudotime outcomes. In the case of glioblastomas aligned to the SVZ NSC reference, this approach produced pseudotimes which resulted in a broader spread DTW compared to the MLP-derived DTW (Fig.9g), likely due to the tendency for the underlying polynomial basis splines to skew pseudotime estimates towards the lineage extremities (see Fig.9f). Nevertheless, while spline regression tends to allocate a disproportionate number of cells to extreme early- or late-pseudotimes, it provides a generally accurate pseudotime estimate which correlates well with the MLP-based model (Fig.9h).

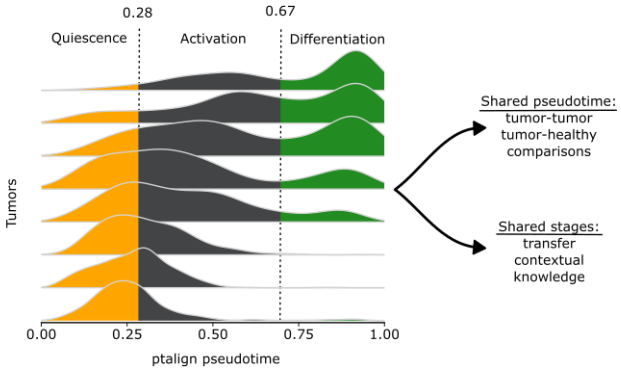

Figure 10: Aligned ptalign pseudotimes inform tumor pseudolineages. KDE plots of cell density over pseudotime for various tumors. QAD-stage boundaries from the reference lineage and extrapolated to the tumors to assign QAD-stage cells, comprising the tumor pseudolineage. Note that different tumors have different pseudolineages, for example QA (truncated) and QAD (complete) pseudolineages. Advantages of projecting tumor cells onto the shared pseudotime axis via ptalign are indicated on the right.

Having generated an aligned pseudotime for a given tumor, its pseudolineage is determined from the relative frequency of cell states in the alignment. This is accomplished by drawing upon the contextual knowledge from the healthy reference lineage, where individual cell states occupy successive pseudotime increments. Consequently, as a tumor's aligned pseudotime places it on the same pseudotime axis as the reference, I employ a simple thresholding approach to assign tumor cell states by transferring the state label from the matched reference pseudotime (Fig.10). Assigning

tumor pseudolineages in this manner, I observed no significant differences between MLP- or spline-based approaches (not shown), instilling confidence in the application of either method to the stratification of patients by pseudolineage in a clinical context.

This way, by capitalizing on the inherent memory of a tumor's tissue-of-origin to isolate correlation dynamics using a pseudotime-predictive anchor gene set from the healthy reference, ptalign maps tumor cells onto the verysame healthy lineage pseudotime. By projecting tumors onto a singular pseudotime axis, this technique not only facilitates the comparative study of tumor-tumor and tumor-healthy expression dynamics, but also enables the transfer of contextual knowledge from the healthy lineage (Fig.10). Overall, ptalign's methodology is both standard and scalable, offering a clear framework for interpreting results. I additionally employ a permutation approach to quantitatively assess the robustness of the dynamics captured by the ptalign pseudotime, which is explored in the following section.

2.1.4 A permutation framework determines consistency of aligned pseudotimes

Given the challenge of interpreting tumor dynamics without access to lineage traced ground truth data, it is crucial to establish metrics for evaluating ptalign's performance on a given dataset. Thus I designed a permutation approach which aims to quantify how well reference lineage dynamics are captured by ptalign pseudotimes by using the shape and strength of correlations in the DTW as a performance metric (Fig.11a). In this approach, as the optimal query-reference pseudotime alignment lies perfectly on the DTW diagonal, I employ the seam carving algorithm to trace and compare the optimal correlation path in the DTW between permutations. This metric assesses the presence of bona-fide reference dynamics, with high-scoring DTWs consistently exhibiting a shorter, narrower matrix traceback. To reduce the influence of gene sets that produce high DTW scores without dynamic patterns, I additionally weighted DTW entries by the variance within each row (called `scale_dtw`). By binning the original anchor gene set into equal-sized expression bins and calculating a DTW traceback score for aligned pseudotimes, and then repeating the process with permuted gene sets (100 times by default) (Fig.11b), I generate an empirical distribution of traceback scores from which I derive a permutation p-value (Fig.11c). This approach identifies aligned pseudotimes that do not significantly outperform those generated from random gene permutations, highlighting instances where the chosen anchor gene set might not effectively capture reference lineage dynamics or when presented tumors without clear cell state stratification. This

permutation strategy offers a straightforward yet robust means to validate the consistency of aligned pseudotimes, employing DTW-based metrics to quantify the reconstructed states and transitions observed in the healthy reference lineage.

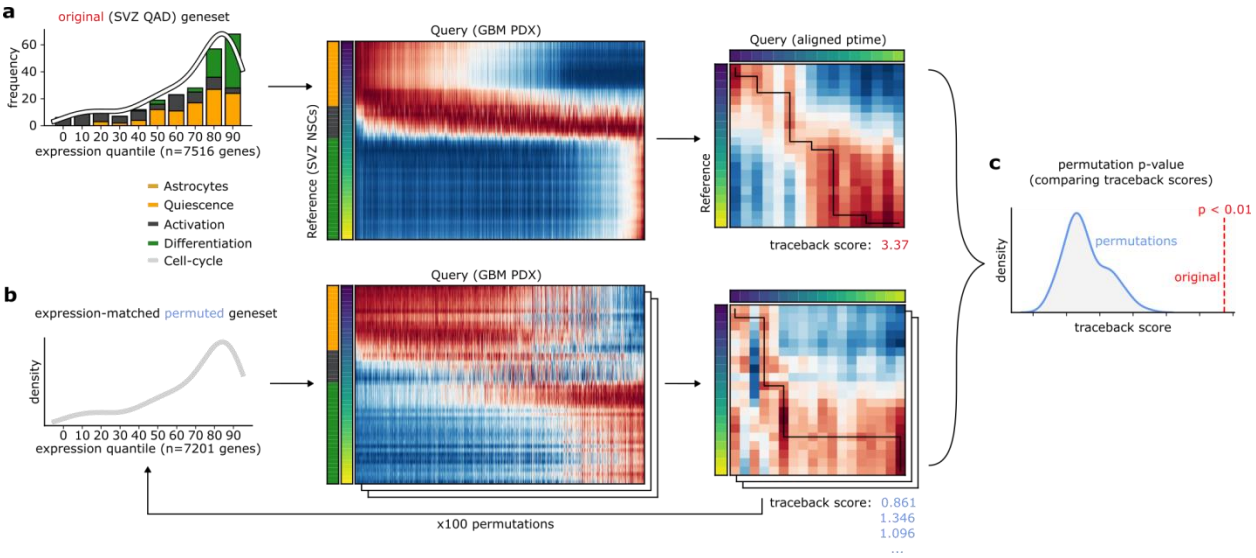

Figure 11: DTW metrics gauge performance in permuted alignments. a) A reference-derived anchor gene set (left) is used to determine query-reference correlation dynamics from which an aligned pseudotime is determined by ptalign (center). DTW of the aligned vs. reference pseudotimes results in a narrow band of high correlations, which is captured by a matrix traceback (right). b) Demonstrating the ptalign permutation strategy through selection of an expression-matched permuted gene set (left), from which an aligned pseudotime is determined by ptalign (center), and the associated DTW evaluated by matrix traceback (right). This procedure is repeated 100 times by default. c) Permutation DTW traceback scores are compared to the original anchor gene DTW traceback to derive an empirical p-value reflecting the consistency of a given ptalign pseudotime.

To validate the permutation strategy's ability to detect defined dynamics, I applied ptalign to a cohort of 55 primary glioblastoma single-cell RNA sequencing datasets retrieved from literature (see section 2.7.1). Comparing ptalign in this cohort using the SVZ NSC reference lineage and QAD gene set with datasets of breast, colon, and lung cancers (Gavish et al., 2023), I observed consistently lower permutation p-values in glioblastomas (Fig.12a). This indicates that QAD dynamics were specifically detected in glioblastomas and not other tissue types, which is consistent with alignment against a reference brain dataset. However, four glioblastomas did not meet the permutation p-value threshold of 0.05 (Fig.12b), prompting further investigation. Analysis using AUCell scoring (Aibar et al., 2017) of QAD gene sets across all 55 glioblastomas showed the four permutation-fail tumors to have higher Q-D gene co-correlations and reduced variation in QAD scores per cell (Fig.12c-d), suggesting permutation-fail tumors are enriched in mixed state cells and a lack clear cell

state stratification. Together, these results demonstrate the efficacy of the ptalign permutation strategy in identifying tumors with bona-fide dynamics and isolating those where the dynamics are absent or atypical.

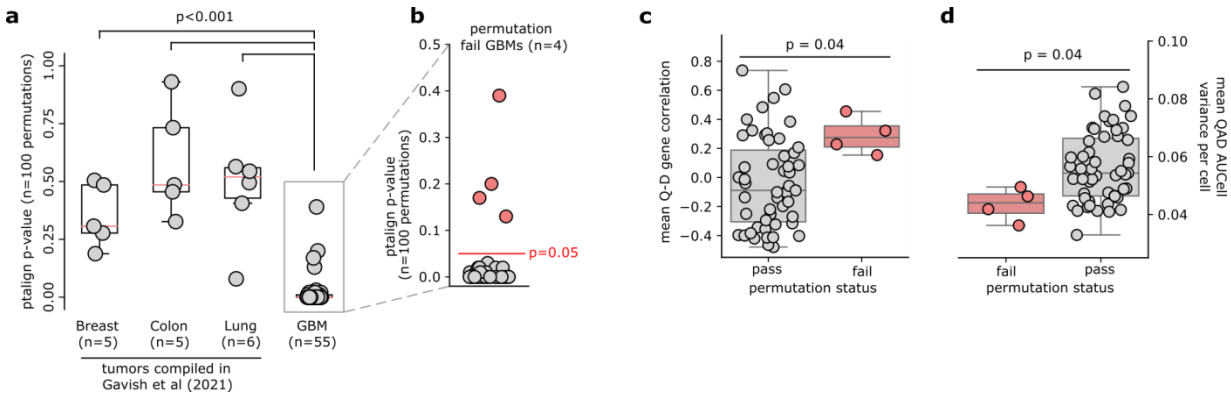

Figure 12: Reference lineage dynamics assessed by the ptalign permutation p-value. a) Comparing ptalign permutation p-values among 55 glioblastoma datasets (see section 2.7.1) and other malignancies from breast, colon, or lung, retrieved from (Gavish et al., 2023). b) Four glioblastoma samples fail to pass the p-value threshold of 0.05. c) Permutation-fail glioblastoma samples are enriched in Q-D-gene co-expression, and exhibit QAD-score variances (d), as measured by AUCell. Significance was assessed by t-test.

These results highlight the effective assessment of lineage dynamics by the ptalign permutation strategy, identifying tumors that exhibit dynamics consistent with their tissue-of-origin and reconstructing their ordering even in the absence of lineage tracing data. This ability to distinguish between tumors exhibiting bona-fide dynamics and those with ambiguous cell states provides interesting avenues to distinguish novel therapeutically relevant glioblastoma subtypes with distinct biological behaviors. Above all, these results emphasize the importance of selecting appropriate gene sets for analysis. With this confirmation of the consistency of ptalign pseudotime alignment, I next endeavored to compare ptalign pseudotimes to conventional trajectory inference methods.

2.1.5 Benchmarking ptalign against conventional methods by pseudotime coherence

Recognizing the need for further validation against other state-of-the-art pseudotime trajectory inference methods, I introduced a comparative metric I call *pseudotime coherence* which quantifies how well different trajectories arrange cells into a cohesive ordering of states and transitions. This

metric was necessitated by the absence of ground truth tumor trajectories to benchmark against. Instead, by assuming that tumor trajectories comprise cells transitioning through ordered states analogous to healthy lineages, pseudotime coherence quantifies the degree to which cells that are similar in gene expression are grouped together in pseudotime. In practice, this is achieved by determining pairwise distances in pseudotime and across the first 10 principal components (PCs) for each cell within a tumor, and evaluating their relationship by Pearson correlation (Fig.13a). The resulting pseudotime coherence scores for individual cells are averaged across a tumor to calculate an overall score for each tumor sample (Fig.13b). This approach quantifies the inherent property of pseudotime to place cells which exhibit similar gene expression profiles in close proximity, thus providing a means to compare different trajectories inferred for individual tumor samples.

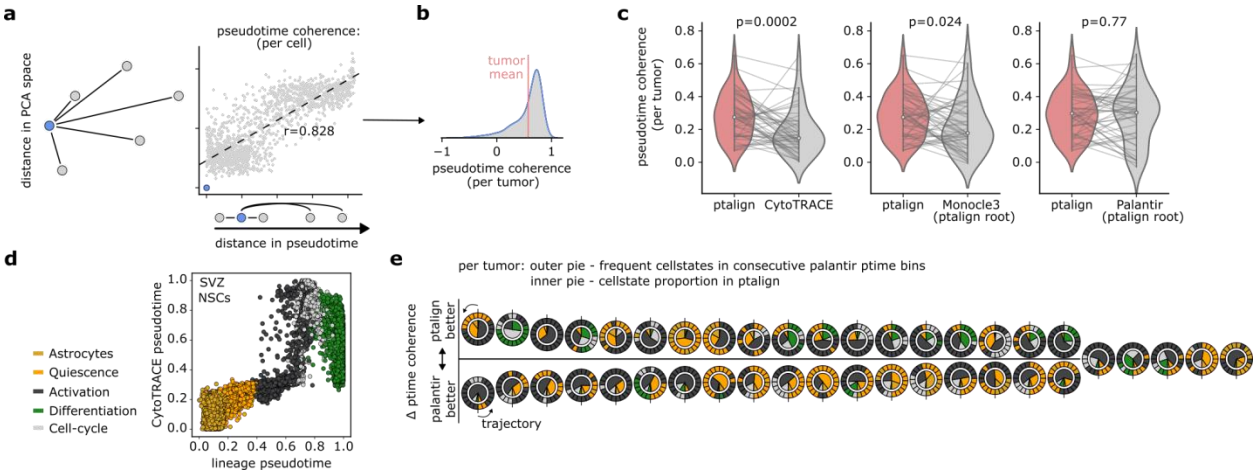

Figure 13: ptalign pseudotimes performance in a coherence benchmark vs. conventional trajectory inference methods. a) Schematic overview of the pseudotime coherence metric. Distances in PCA-space and pseudotime are calculated from each tumor cell (indicated in blue) to all other tumor cells (indicated in gray). Pearson correlation measures the association between these values. b) Per-sample pseudotime coherence is determined by taking the mean of pseudotime coherence values per cell. c) Results of benchmarking ptalign pseudotimes against CytoTRACE (left), monocle3 (center), and palantir (right) pseudotimes by the pseudotime coherence metric. Scores for individual glioblastomas are indicated by a gray line. Statistical significance was assessed by paired t-test. d) CytoTRACE pseudotime compared to the reference pseudotime for the healthy SVZ NSC lineage. e) Contrasting pseudotime coherence values in palantir and ptalign, highlighting cell state ordering in ptalign (inner pie chart) and the most frequent cell state for consecutive palantir pseudotime bins (outer pie chart).

Using the pseudotime coherence metric described above, I benchmarked ptalign pseudotimes against three state-of-the-art pseudotime trajectory inference methods: CytoTRACE (Gulati et al., 2020), monocle3 (Cao et al., 2019), and palantir (Setty et al., 2019). Of these, CytoTRACE employs heuristics over the number of expressed genes to place cells within a differentiation trajectory, monocle3 leverages a reverse graph embedding to infer detailed branching pseudotime trajectories,

and palantir models cell lineage as a probabilistic process to infer branching paths and fate probabilities. For each of these algorithms, I generated tumor pseudotimes for glioblastomas in the 55-tumor cohort (see section 2.7.1) according to the basic usage example in the respective documentation. For monocle3 and palantir, which required a root cell to initiate the trajectory, I used the earliest-pseudotime cell from the ptalign pseudotime for this purpose. No terminal states were set for palantir, allowing the algorithm to automatically determine fate-branches and their ordering. In this comparison, CytoTRACE was significantly outperformed by ptalign, with CytoTRACE producing lower pseudotime coherence scores for virtually every tumor (Fig.13c). I validated this result by examining the distribution of the glioblastoma cell states from (Neftel et al., 2019), which were broadly dispersed in CytoTRACE pseudotimes (not shown), thus confirming the effectiveness of pseudotime coherence in assessing the degree to which similar cell states occupy similar pseudotime increments. Notably, CytoTRACE's heuristic failed in both tumor and healthy brain samples, erroneously placing cycling cells, which express a high number of genes, at the end of healthy pseudotime trajectories (Fig.13d). Compared to monocle3, I observed significantly higher pseudotime coherence for ptalign pseudotimes, with monocle3 occasionally surpassing ptalign in specific samples. Conversely, ptalign and palantir showed no significant differences in pseudotime coherence (Fig.13c). However, the tendency for palantir to place cycling cells at the pseudotime apex and the preponderance of state-switches in successive pseudotime bins (Fig.13e) points to areas of further investigation, addressing how transitions between plastic tumor cell states affects their arrangement into cohesive pseudotimes. These findings highlight the robustness of ptalign, with the permutation module identifying tumors exhibiting the expected dynamics, while the aligned pseudotimes resolve cell state dynamics on par with state-of-the-art algorithms.

In sum, these results underscore the unique applications and benefits which are realized through ptalign’s approach of aligning tumor cells to a healthy reference lineage. I demonstrate these benefits through the assessment (section 2.6), evaluation (section 2.7), and modulation (section 2.9) of tumor pseudolineages in a 55-glioblastoma cohort, leading to the development of actionable clinical insights for glioblastoma. Importantly, these insights are only discernable through systematic assessment of tumor trajectories delineated by ptalign, projecting tumor cells onto the healthy reference and facilitating their interpretation in that context.

2.2 Pseudotime-based characterization of state transitions in the adult SVZ NSC lineage

To demonstrate the utility of pseudotime-based characterization of healthy stem cell lineages, I turn to the adult NSC lineage of the murine SVZ. Neural stem cells in this niche are born during early embryogenesis (Fuentealba et al., 2015; Furutachi et al., 2015) and persist into adulthood, sustained by self-renewal dynamics and complex interactions within the different populations of the niche (Lim & Alvarez-Buylla, 2016). Their organized arrangement near the brain's ventricles, along with known markers that help identify them (Llorens-Bobadilla et al., 2015), makes this population particularly amenable to single-cell RNA-sequencing. I provide a detailed overview of SVZ populations and their lineage dynamics in section 1.1. Here, I summarize the creation and study of a reference scRNA-seq SVZ NSC lineage atlas curated from several published studies. I employ pseudotime-based methods to reveal the states and transitions which characterize this SVZ NSC lineage, and compare these to human NSC dynamics in section 2.5. This atlas is then used in the ptalign study of glioblastoma pseudolineages in section 2.6-2.9.

2.2.1 Assembly and study of a single-cell transcriptomic reference SVZ NSC lineage dataset

Several transcriptomic studies of the SVZ niche at single-cell resolution have been published in recent years, see section 1.1.3. Generally, SVZ cells are isolated and FACS used to exclude non-lineage (eg. oligodendrocyte or microglia) cells, instead enriching NSCs and their progeny (eg. in a GLAST/PROM gate (Llorens-Bobadilla et al., 2015)) for further analysis through 10X genomics or SmartSeq3 (Hagemann-Jensen et al., 2022) sequencing (Fig.14a). In compiling a reference SVZ NSC lineage atlas, I combined three recently-published datasets from the Martin-Villalba lab (our lab) to ensure consistency. I retrieved the published count tables from the SVZ single-cell datasets from (Kalamakis et al., 2019), (L. P. M. Kremer et al., 2021), and (Carvajal Ibañez et al., 2023). Using the available metadata, I retained WT cells from each and used the Seurat (Stuart & Satija, 2019) label transfer pipeline to identify various NSC lineage stages in each replicate. I then integrated these datasets using the Seurat v4.3 workflow[1], revealing NSC lineage stages arranged along a single contiguous component (Fig.14b). This was consistent in integrations with other SVZ NSC scRNA-seq

[1] https://satijalab.org/seurat/articles/seurat5_integration

datasets (eg. from (Cebrian-Silla et al., 2021)) (not shown). The persistence of a single contiguous lineage component suggested the SVZ NSC lineage follows a coherent trajectory, which I isolated using the DBSCAN algorithm to better inspect its constituent stages and transitions.

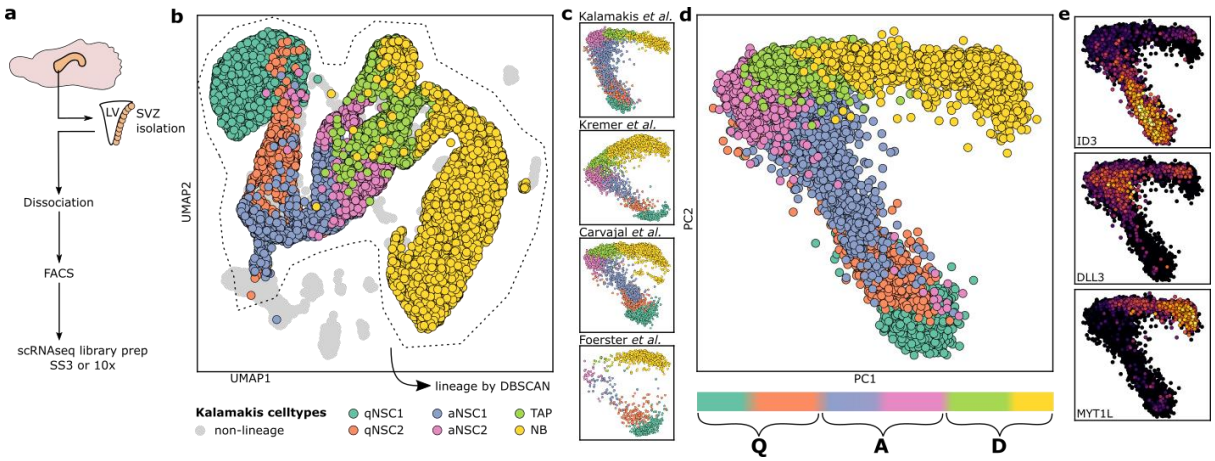

Figure 14: An integrated SVZ reference dataset. a) schematic depicting the general SVZ NSC scRNA-seq pipeline, from SVZ isolation, cellular dissociation, FACS sorting, and resulting library prep. B) integrated UMAP of WT NSCs from three 10X genomics SVZ NSC datasets in (c). Cells are colored by the cell types from (Kalamakis et al., 2019), with non-lineage cells colored gray. DBSCAN was used to isolate the main lineage component. c) PCA plots for SVZ NSCs from four datasets, colored by cell types in (b). d) PCA of the integrated SVZ NSC lineage, with cell types resolved in (Q)uiescence, (A)ctivation, and (D)ifferentiation stages, respectively. e) Expression of SVZ QAD-stage markers in the PCA from (d).

Inspecting the SVZ NSC lineage trajectory, I found that NSC lineage cells from various datasets exhibited a consistent shape when projected into the first two principal components (Fig.14c). Indeed, PCA loadings from the first and second principal components were highly correlated between datasets (not shown). This supports previous observations that the dynamics of SVZ NSCs remain stable across different ages, with variations mainly in the frequencies of cell populations rather than in transcription (Kalamakis et al., 2019). Further analysis of the integrated datasets revealed an ordered arrangement of cell types in the PCA-space, with PC1 capturing differentiation status and PC2 relating cycling activity (Fig.14d). The expression of numerous salient lineage markers such as `ID3`, `DLL3`, and `MYT1L` (Fig.14e) highlighted the semantic and functional similarities between different NSC lineage stages, eg. aNSC1 and aNSC2, supporting a simplified model of NSC lineage dynamics through stages of Quiescence, Activation, and Differentiation.

2.2.2 An NSC lineage pseudotime through Quiescence, Activation, and Differentiation stages

Next I set out to characterize the stages and transitions which comprise SVZ NSC differentiation using pseudotime. To accurately model these dynamics, it was necessary to identify and exclude cells in the cell cycle, both for technical reasons related to ptalign (see section 2.1.2), but also due to the limitations of conventional pseudotime algorithms in capturing cyclical state-dynamics (Lederer et al., 2024; Schwabe et al., 2020). Thus I classified cycling cells by the conventional markers[2] and set a G2M-score cutoff at 0.1 to assign cells' cycling status (Fig.15a), which was consistent with expression of known cell cycle markers including `MKI67`, `TOP2A`, and `UBE2C` (not shown). I then fit a diffusion pseudotime (Haghverdi et al., 2016) from the first two principal components, selecting a root cell from one of the corners of the PCA embedding (Fig.15b). This lineage pseudotime revealed a smooth lineage trajectory in UMAP (Fig.15c), reflecting state transitions evidenced by the expression of `ID3`, `DLL3`, and `MYT1L` (Fig.15d), as above.

Employing a comparative approach without the exclusion of cycling cells, I observed strong agreement in the inferred pseudolineage dynamics (Fig.15e), revealing a consistent and orderly progression of NSC stages with defined transitions regardless of cell-cycle status. Comparison with other pseudotime inference methods, such as Monocle3 and palantir (see section 2.1.5), highlighted similar dynamics (Fig.15f), though Monocle3 predictions deviated for individual datasets. While these results showcase the robust inference of stable cell states and transitions across different pseudotime algorithms, the flexibility and computational efficiency of diffusion pseudotimes made them my preferred method for exploring SVZ NSC lineage dynamics.

[2] https://nbviewer.org/github/theislab/scanpy_usage/blob/master/180209_cell_cycle/cell_cycle.ipynb

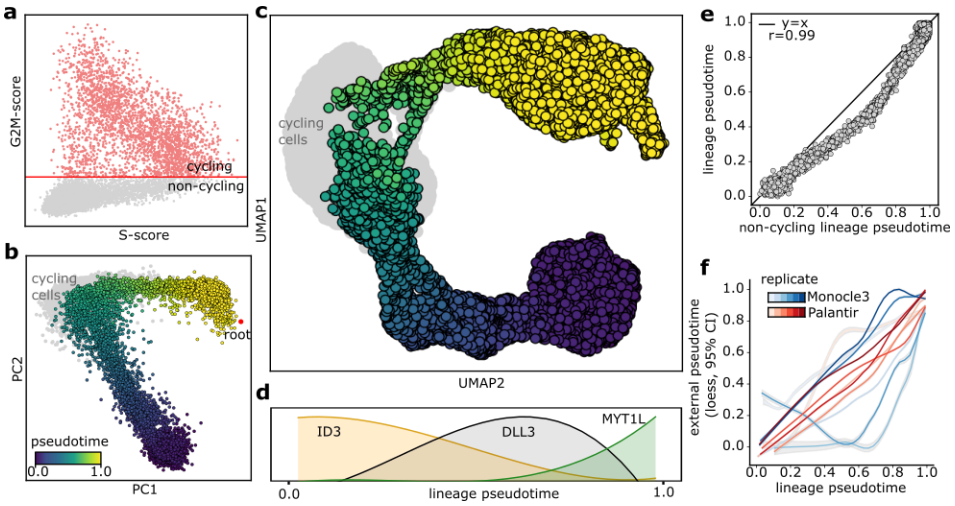

Figure 15: Deriving an SVZ lineage pseudotime. a) scatter plot of cell cycle scoring of SVZ NSC lineage cells. A cycling cell cutoff was set at a G2M-score of 0.1. b) Diffusion pseudotime fit to PCA of SVZ NSC lineage cells. Cycling cells were excluded from pseudotime inference and are colored gray. The pseudotime root cell is indicated. c) Diffusion pseudotime from (b) in the integrated SVZ NSC lineage UMAP. Cycling cells are colored gray. d) Pseudotime expression splines of QAD-stage markers in the SVZ NSC lineage pseudotime from (c). e) Scatterplot of SVZ NSC lineage pseudotime computed with and without the inclusion of cycling cells. f) Comparison of Monocle3 and Palantir pseudotimes for individual SVZ NSC replicates, depicted by loess regression against the SVZ NSC lineage pseudotime from (c).

Assuming even sampling of SVZ NSC lineage cells, the relative frequency of cells in stable lineage stages (eg. Quiescence) and those transitioning between them reflects the time cells spend in each stage. This relationship is captured by pseudotime, which groups transcriptionally similar cells together, allowing for the identification of stable lineage stages from the cell-density along pseudotime. Using this method, I identified three main stages in the NSC differentiation trajectory, termed Quiescence, Activation, and Differentiation, collectively QAD (Fig.16a). This classification simplifies the understanding of SVZ NSC lineage dynamics to the transitions between these three stages. Indeed, this view of stem cell hierarchy, progressing from a dormant stage through activation to differentiation, aligns with how stem cell hierarchies function in various tissue niches (L. Li & Clevers, 2010). Here, I identify these lineage stages from pseudotime alone: an important facet which enables their re-identification in tumor pseudolineages inferred via ptalign (see section 2.1.3). Accordingly, QAD-stage cells arrange neatly in the SVZ NSC lineage UMAP (Fig.16b), consistent with marker gene expression and the detailed cell type labels shown in Fig.14. By delineating Activation-stage and cycling cells in this manner, I reproduce the prior distinction of aNSC1 and aNSC2 stages against TAPs. This also applies to the Quiescence stage, which I subset along qNSC1 and qNSC2 lines to illuminate differences and transitions between quiescent NSCs (Q) and niche astrocytes (astroQ). In sum, the SVZ NSC lineage pseudotime describes NSC differentiation dynamics through the transitions between Quiescence, Activation, and Differentiation stages.

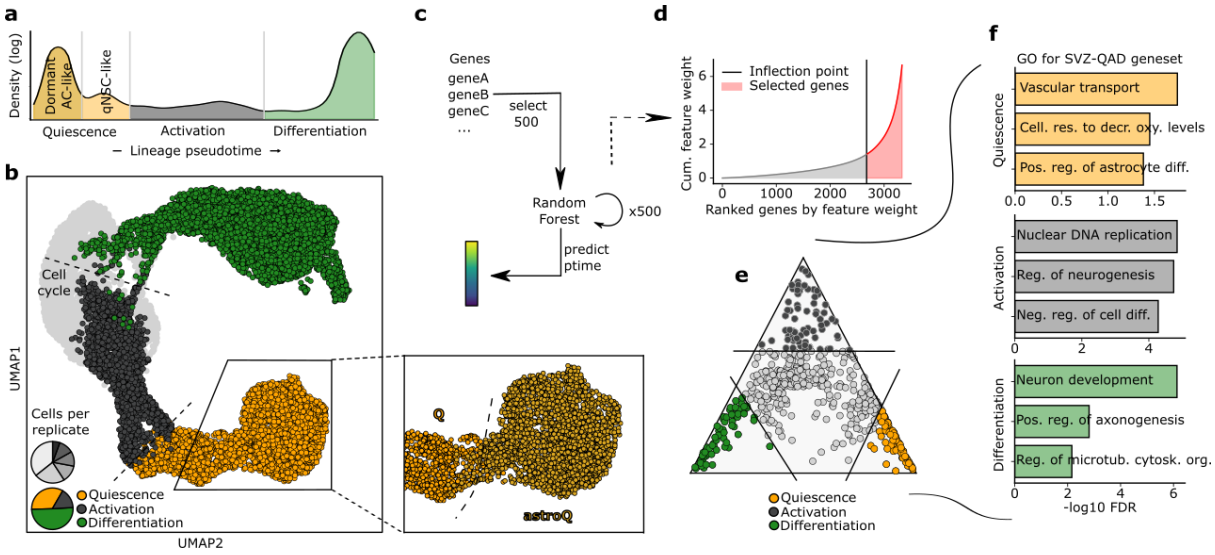

Figure 16: SVZ NSC lineage through QAD stages and transitions. a) KDE of SVZ NSC lineage cell log-density along pseudotime, with QAD-stage increments inferred from cell density-troughs labeled and indicated. b) QAD-stage cells from (a) in the SVZ NSC lineage UMAP. Cycling cells are indicated in gray. Inset pie charts indicate the proportion of cells per replicate and of QAD-stage cells. Zoom of Q-stage cells depicts the separate clustering of the constituent Q-stages from (a): Quiescence and astroQ. c) Schematic depiction of QAD-gene set derivation. A RandomForest model was trained to predict pseudotime using 500 random genes 500 times. Feature weights were tracked and the inflection point in the cumulative feature weight distribution inferred by the kneedle algorithm (d). e) Selected genes from (d) in a ternary plot parameterized by expression level in QAD-stages. Genes which enriched in stage-specific expression were selected and GO-enrichment carried out (f).

I next set out to compile a pseudotime-predictive gene set capturing NSC lineage stages and transitions, for use with ptalign (see section 2.1.3). Comparing expression in QAD-stage cells of the NSC lineage atlas revealed that a significant number of genes are regulated during NSC differentiation, including key developmental pathways such as BMP, SHH and Wnt. Particularly genes involved in the Wnt signaling pathway were differentially regulated during NSC activation, ie. at the transition to and from Quiescence; aligning with previous studies (see section 1.1.4). To derive an anchor gene set for use in ptalign, I selected pseudotime-predictive candidates from a pool of genes exhibiting dynamical expression profiles by repeatedly sampling genes and training a sklearn RandomForest (Pedregosa et al., 2011) classifier to predict cell pseudotime bins (Fig.16c). RandomForest models are able to learn complex non-linear interactions between features, motivating their use over other approaches such as thresholding in DEseq log fold-changes. Importantly, RandomForest models assign weights based on the contributions of individual features to a classification problem, and I tracked the cumulative feature weights of the sampled genes across 500 iterations to select those genes which consistently exhibited high pseudotime predictive

power. This was accomplished by the kneedle algorithm (Satopaa et al., 2011) identifying the inflexion point in the cumulative distribution of feature weights (Fig.16d). As ptalign uses the anchor gene set to infer state-specific dynamics, I additionally subset the predictive genes by their state-specificity in the SVZ NSC lineage atlas (Fig.16e). To facilitate better generalization to disparate tumor datasets, I disallowed the presence of mitochondrial and ribosomal genes in the anchor gene set due to their necessary dysregulation in a tumor context. This way, I arrived at a 242-gene pseudotime-predictive gene set which enriched for relevant functional properties of QAD stages (Fig.16f), paving the way for its use in facilitating the comparison of NSC dynamics in different contexts. This gene set is listed in Table 1 and comprises the anchor gene set used in the examples in section 2.1 and throughout this work. I did not assess the efficacy of other gene sets in capturing NSC lineage dynamics.

In sum, different SVZ NSC scRNA-seq datasets robustly converge on a coherent lineage trajectory, captured here by integration and subset into QAD-stages as depicted above.

2.3 Excursion: Tailored Dash apps for collaborative analysis of scRNA-seq datasets

This section serves to showcase several Dash apps I developed to facilitate the collaborative analysis of scRNA-seq datasets such as the SVZ NSC lineage atlas described above. The information presented in this section departs thematically from the description of NSC lineage dynamics, but having introduced the SVZ NSC lineage atlas, the benefits of employing tailored apps to aide in the assessment of state-linked gene expression and functional studies via gene set scoring are clearly evident. Here, by means of excursion from the main narrative, I introduce two apps I created for the purpose of democratizing insights from single-cell datasets.

High throughput methods such as next-generation sequencing brought with them new developments in computational biology and bioinformatics which have shaped recent developments in the biological sciences. However, these developments simultaneously served to widen the divide between different disciplines. As experimental methods delve deeper into painstakingly molecular processes and computational analysis leverages increasingly abstract mathematical concepts, mastering either discipline requires years of specialized training. This specialization develops skill sets which are not always transferrable, hampering collaborations between experimental and computational researchers. Thus there is a need to bridge the gap between data generation and data analysis to further interdisciplinary understanding and cooperation.

To address this challenge and enhance crosstalk between experimental and computational researchers, I developed several interactive applications using the Dash framework (Plotly Technologies Inc., 2024) to analyze complex datasets such as those generated by single-cell RNA sequencing (scRNA-seq). The first of these serves to facilitate cluster marker discovery and comparison, offering an intuitive interface for identifying and contrasting gene expression profiles across cell clusters. My second app streamlines the process of gene-set scoring, enabling users to easily assess higher-level cellular processes. Together, these apps exemplify how targeted software solutions can mitigate the challenges posed by the interdisciplinary nature of modern biological research.

2.3.1 Cluster marker discovery and cluster comparison

The ability to identify and compare markers across different cell clusters is central to understanding dynamical processes driving cellular diversity and function. This process is streamlined in my Dash app as follows: upon launching the app, users are greeted with a straightforward interface prompting the selection of a dataset from a dropdown menu populated with preprocessed datasets stored on disk. The first point of interaction, the Annotation tab (Fig.17a), enables users to select and annotate relevant cell clusters from a 2D embedding (eg. PCA, UMAP) generated from a user-friendly plotting interface. This plotting interface enables the log-transformation of features for simplified visual interpretation, and enables the simultaneous comparison of up to 9 features plotted in a 3x3 grid. The interactive lasso tool provided by the plotly interface facilitates the precise selection and marking of clusters and cells for further analysis (Fig.17b), allowing annotations such as cell type information to be easily saved and retrieved.

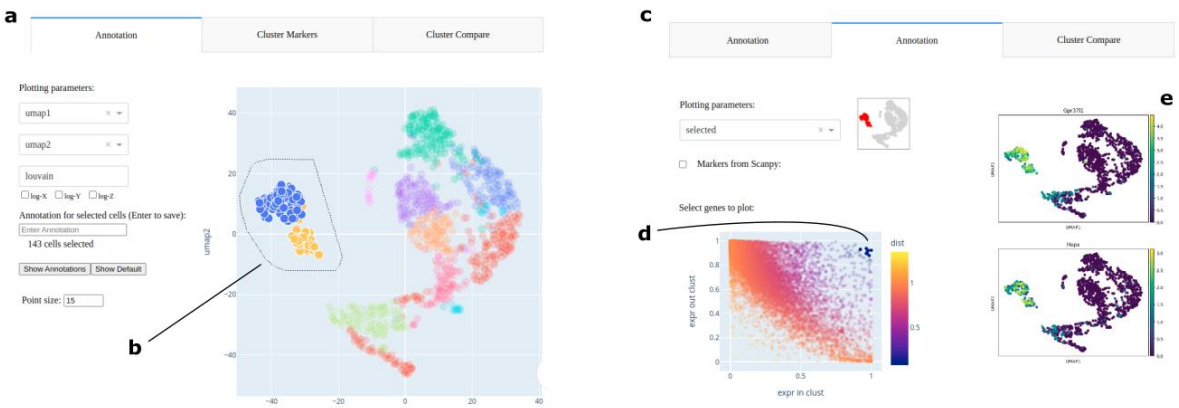

Figure 17: Cluster markers Dash app layout and functionality. Interface is comprised of an Annotation tab (a) which enables flexible creation of scatterplots visualizing various gene- and metadata. By selecting cells in the UMAP using the lasso tool (b), clusters can be selected and annotated, for example in the Cluster Markers tab (c). Genes are scored according to expression inside and outside the selected cluster (d), and repeated use of the lasso tool in this interface will result in the plotting of selected cluster markers (e).

From the clusters selected and annotated in the Annotation tab, the Cluster Markers tab facilitates the discovery of genes enriched within a cluster (Fig.17c). A dropdown menu displays saved annotations, allowing for quick selection of clusters for analysis. By default, this dropdown is populated by the currently selected cells which are indicated in a small UMAP. Selecting cells or a cluster of interest generates an interactive plotly scatterplot showing every gene according to the

proportion of cells which express it inside and outside of the selected cluster (Fig.17d). This operation is kept performant by preprocessing gene expression in a fine grid mesh overlaid in the UMAP which limits the lookup of membership in the selected cells to eg. 100 grid cells compared to thousands of individual cells. In this representation, informative genes will associate with specific quadrants indicating positive or negative markers. Circling genes in this plot with the lasso tool results in rendering their expression UMAPs (Fig.17e), from which salient markers can be extracted.

The Cluster Compare tab allows for the comparison of markers between clusters, utilizing different statistical tests to identify differentially expressed genes. I leverage the scanpy `sc.tl.rank_genes_groups` function to this end, displaying the results in an easily exportable table offering a clear overview of potential markers. Clicking on a gene in the table displays its expression UMAP, providing immediate visual feedback (not shown). The interactive analysis and visualization enabled by this app streamlines the complex process of cluster marker discovery and comparison in scRNA-seq datasets. By simplifying data exploration and marker identification, the app has proved highly effective at stimulating collaborative dialogue and enabling novel insights into the processes being studied.

2.3.2 Geneset scoring and visualization

My second app bridges the gap between raw gene expression data and functional insights by facilitating gene set scoring and visualization in an intuitive manner. Similar to the cluster marker app described above, users are prompted to load one of the available datasets. Users can explore and select gene sets of interest using a keyword search from the msigdb database (Subramanian et al., 2005), which includes collections from Gene Ontology (GO), KEGG, and Reactome, among others (Fig.18a). This feature additionally supports custom user-uploaded gene sets (Fig.18b), offering flexibility for bespoke analyses. The app utilizes AUCell to calculate gene set enrichment scores. AUCell operates on a matrix of ranked gene expressions per cell which are prepared during preprocessing for efficient access. Results are visualized on a UMAP plot of the selected dataset, thus revealing differentially regulated pathways or conditions (Fig.18c). Unique to this app, genes are automatically translated between 1:1 human and mouse orthologs prior to AUCell scoring, facilitating the transfer of functional insights from cross-species annotations. This app provides a common platform for exploring and interpreting scRNA-seq data through a large body of curated gene sets, uncovering the functional dynamics of genes across diverse cellular landscapes.

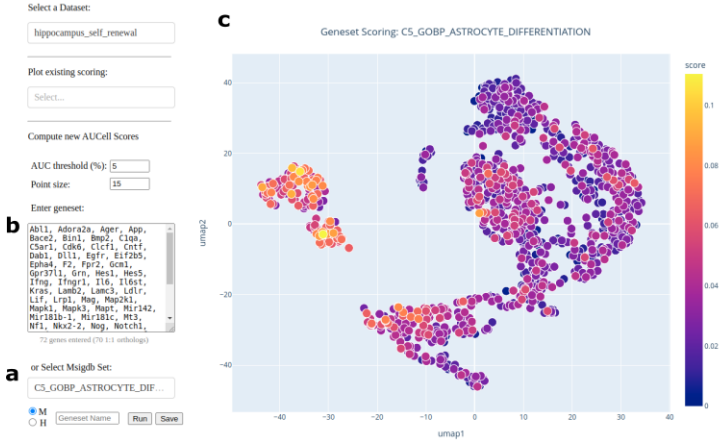

Figure 18: Geneset scoring Dash app layout and functionality. Interface revolves around gene set selection from curated msigdb lists (a) or through manual input of custom gene lists (b). AUCell is used to conduct gene set scoring of the supplied genes, and the results plotted in the UMAP (c).

In sum, interdisciplinary is the necessary way forward in biological studies, but brings with it a large burden of communication. To address this challenge, I developed two Dash apps which bridge the gap between complex computational analyses and the practical needs of experimental biologists, designing an interface to support effective communication of needs and ideas. By making these analyses accessible to researchers without extensive computational backgrounds, my apps serve to reduce the time from data acquisition to insight. This efficiency is crucial in a field where the pace of data generation has eclipsed the capabilities of traditional analysis methods.

Internally, Jooa Hooli and I hosted these apps on institute infrastructure, making them accessible to all colleagues around the clock. This deployment highlighted the Dash framework's challenges with handling large data volumes in HTML elements, a limitation that may be mitigated through client-side optimizations. Similar frameworks are available in Shiny (Chang et al., 2024) and particularly for scRNA-seq datasets through cellxgene (Megill et al., 2021), although I found the latter to not be efficient when balancing multiple datasets as these are generally persisted in memory.

Overall, these apps proved to be invaluable by providing my colleagues a means to gain hands-on experience conducting bespoke analyses, thus building their confidence and reasoning regarding analytical approaches. These skills undoubtedly accelerated the pace of discovery in latter part of my studies.

2.4 Canonical Wnt signaling is tightly regulated at NSC lineage transitions

The high degree of stratification and tight regulation of cell identity in adult brains stands in stark contrast to the scarcity and plasticity of its constituent stem cells. Extensive research into NSC identity and niche maintenance highlights the Wnt signaling pathway as a crucial regulator of stem cell behavior in the adult brain. Particularly NSC transitions to and from the Quiescence-stage are guided by Wnt signaling which influences fate decisions via changes to the methylome and manages NSC activation through localized niche interactions (see section 1.1.4). These properties of Wnt signaling make the pathway particularly interesting in the study of adult tumors, where aberrant signaling dynamics pave the way for sustained activation and likely play a role in tumorigenesis. For these reasons, Oguzhan Kaya and I endeavored to characterize the modulation of Wnt signaling modalities along the NSC differentiation trajectory in greater detail.

2.4.1 The TCF-Lef reporter relates canonical Wnt activity in FACS and immunohistochemistry

In order to investigate the role of canonical Wnt signaling within SVZ NSC lineage populations, Oguzhan used a TCF-Lef reporter transgenic mouse line (`TCF/Lef-H2B::EGFP`) that visually reports canonical Wnt signaling activity via `EGFP` fluorescence (Ferrer-Vaquer et al., 2010) (Fig.19a). To measure reporter activity along the NSC differentiation trajectory, Oguzhan isolated single cells from the striatum, SVZ, RMS, and OB of adult mice via a targeted FACS strategy (Kaya, 2023). These data revealed a high degree of Wnt activation in the SVZ astrocytes and NSCs, which together constitute the Quiescence stage (Fig.19b). Wnt activity levels were lower in nearby striatal astrocytes, highlighting the privileged signaling environment of the SVZ niche. Intriguingly, as cells transitioned to Activation and Differentiation stages, marking their migration towards the OB, there was a strong reduction in Wnt signaling activity. Upon reaching the OB, where cells will ultimately integrate into the existing neuronal circuitry, canonical Wnt activity was restored once more (Fig.19c). This observation led us to hypothesize that a switch from canonical to non-canonical Wnt signaling accompanies NSC differentiation. Indeed, data from *C. elegans* suggests that neuroblast migration is sustained through non-canonical Wnt signaling activity (Rella et al., 2021). Given their propensity to invade distant brain areas, this switch could have significant implications for

glioblastoma cells by suggesting that targeted modulation of the canonical to non-canonical Wnt switch could affect their migratory potential. Further study of this hypothesis was not feasible due to the absence of effective tools for tracking non-canonical Wnt signaling activity *in vivo*.

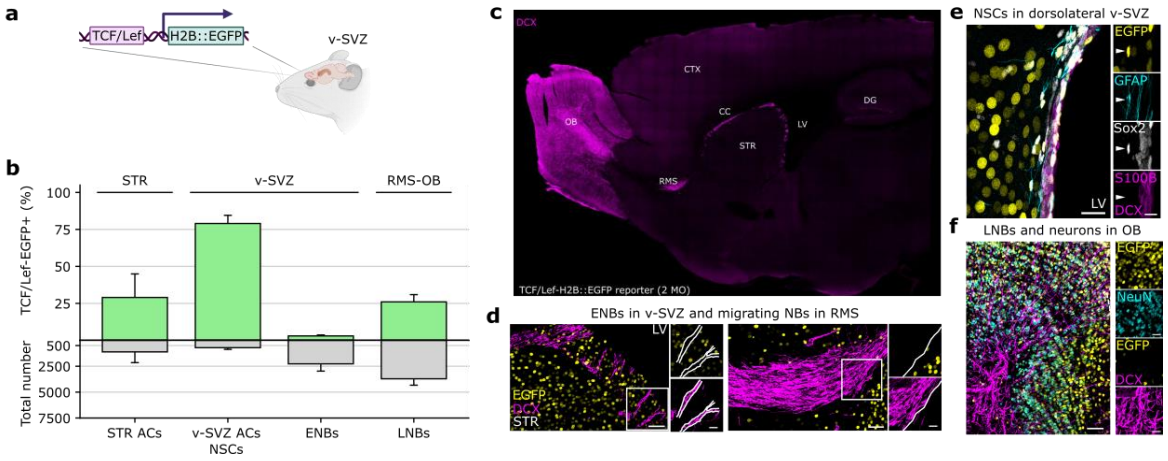

Figure 19: TCF/Lef Wnt reporter quantifications in the SVZ NSC lineage. a) Reporter construct in transgenic mice used to report canonical Wnt signaling activity in the SVZ NSC lineage. b) FACS quantification of TCF/Lef reporter activity in sorted SVZ NSC lineage populations. c) Saggital view of an adult mouse brain including LV, RMS, and OB stained with DCX to highlight neuroblast migration. d) TCF/Lef reporter activity in DCX stained ENBs recently born in the SVZ (left) and migrating along the RMS (right). Note that both populations are EGFP-. e) Highlighting EGFP presence in SOX2+GFAP+ NSCs but absence in S100B+ ACs and DCX+ ENBs lining the lateral ventricle. f) ENBs exiting the RMS gradually gain TCF/Lef reporter activity as they enter the neuronal areals of the OB. AC: astrocyte; STR: striatum; ENB: early neuroblast; LNB: late neuroblast; RMS-OB: rostral migratory stream and olfactory bulb; LV: lateral ventricle; CTX: cortex; CC: corpus callosum; DG: dentate gyrus. Figures adapted from (Kaya, 2023).

In addition to the FACS analysis, Oguzhan explored the role of canonical Wnt signaling in NSC lineage cells by *in vivo* imaging of TCF-Lef reporter activity (Kaya, 2023). These images added important context to the insights gained from the FACS analysis above, revealing the cell type specific functions of canonical Wnt signaling through the generally increased level of Wnt signaling activity in the OB (not shown). Tissue imaging furthermore confirmed the stark drop in reporter activity observed in ENBs (Fig.19d), with migrating neuroblasts being void of canonical Wnt signaling activity (Fig.19e). The resumption of reporter activity in LNBs was also evident (Fig.19f), consistent with their exposure to canonical Wnt signals originating from OB neurons (see section 1.1.4).

The drastic loss and eventual restoration of reporter activity along the NSC differentiation trajectory emphasizes the essential role of canonical Wnt signaling in regulating NSC lineage transitions. Given the complex nature of the Wnt signaling pathway (see section 1.1.4), it is interesting to speculate that related Wnt programs could be involved in the maintenance of the functionally similar long-

term Quiescence of NSCs and terminal differentiation of OB neurons. However, the reduced levels of canonical Wnt activity observed in terminally differentiated striatal astrocytes stand in contrast to this assertion. Clearly, canonical Wnt signaling is preferentially activated in the neuronal SVZ NSC lineage with important roles in functional stem cell identity, while exerting cell type specific functions across other brain areals. Thus, to further elucidate stage-specific determinants of canonical Wnt signaling, Oguzhan and I next endeavored to sequence and analyze the TCF-Lef reporter NSC lineage at single-cell resolution.

2.4.2 Mapping reporter activity in single-cell transcriptomics by plate-based SmartSeq3

Numerous transcription factors involved in Wnt signaling are lowly expressed, limiting their quantification by the usual 10X genomics scRNA-seq approach. Instead, SmartSeq3 (SS3) emerged as an attractive alternative due to the increased recovery of low-abundance genes and the added ability to reconstruct FACS data *in silico* by index sorting. Despite the higher costs associated with plate-based sequencing methods such as SS3, Oguzhan managed to significantly reduce the cost-per-cell by miniaturizing the protocol and automating the process with liquid handling systems and pipetting robots, cutting the cost per cell by about six-fold. These optimizations and the associated protocol are documented in (Cerrizuela et al., 2022; Kaya, 2023). Employing this updated protocol, Oguzhan sequenced 1.564 NSC lineage cell transcriptomes from the SVZ and OB of five replicates of `TCF/Lef-H2B::EGFP` reporter mice (Kaya, 2023).

2.4.2.1 Excursion: umicount quantifies nascent and mature transcript counts from SmartSeq3

Complementing Oguzhan's modifications to the SS3 protocol to increase throughput, I developed a method called *umicount* for quantifying SS3 transcriptomes that accounts for UMIs. This method is rooted in HTSeq-count (Anders et al., 2015) and consists of three steps: extracting UMIs from SS3 FASTQ libraries, aligning the reads post-extraction, and then counting and deduplicating aligned reads and UMIs. Initially, the pysam[3] `FastxFile` module is used to traverse SS3 FASTQs, using regex to identify UMI-containing reads by the presence of the known SS3 template-switching oligo

[3] https://github.com/pysam-developers/pysam

(TSO) sequence. Detected UMIs are appended to the read name and the UMI + TSO sequence trimmed from the read. Reads are then aligned using standard tools like STAR (Dobin et al., 2013). The counting step follows the HTSeq-count implementation[4], with exon- and intron-mapping reads handled separately, thus allowing for precise quantification of spliced and unspliced reads and facilitating RNA-velocity analysis from SS3 data. Additionally, umicount deduplicates UMI counts on the fly and reports duplicated counts, enabling eg. troubleshooting via identification of over-cycled libraries with a high degree of duplication. This way, umicount reports five measures of gene expression, including all combinations of UMI-containing and internal reads at exonic and intronic loci. With built-in multithreading capabilities, umicount presents a competitive tool for read counting in SS3 libraries, which I employed here to quantify gene expression in the aforementioned TCF-Lef reporter transcriptomes.

The umicount tool is available at github.com/leoforster/umicount and was ported to a buildable CLI tool with the help of Jooa Hooli. At the time of publication, the SS3 authors recommend the use of zUMIs (Parekh et al., 2018) for SS3 library quantification. umicount is a lightweight tool which solves a single problem efficiently using established solutions, but benchmarking of umicount against zUMIs remains outstanding largely due to the lack of publically available SS3 datasets to date.

2.4.2.2 Excursion: Populating reconstructed FACS gates with transcriptomic annotations

Using plate-based sequencing methods like SmartSeq3 allows for the mapping of FACS measurements to individual cells based on their position on the plate, in a process called index sorting. This method enables RNA-protein associations to be reconstructed *in silico*, enabling a comparison between identified cell types from single-cell transcriptomics and their original FACS classifications – an innovation I explored here using the TCF-Lef reporter cell transcriptomes sequenced by Oguzhan Kaya. In lieu of cell types I used ptalign to assign QAD-stage cells in this dataset, simultaneously affording the opportunity to benchmark ptalign on an unseen SVZ NSC lineage dataset. Consequently, I fit a NSC lineage pseudotime in the TCF-Lef reporter cells (Fig.20a-b) from the familiarly-shaped PCA embedding as described above. ptalign pseudotime alignment of the TCF-Lef reporter transcriptomes against the reference SVZ NSC lineage atlas produced a correlation matrix clearly stratified by QAD stage cells supported by a highly significant permutation result (Fig.20d). A strong concordance of lineage states was evident from the DTW (Fig.20e), and the

[4] https://htseq.readthedocs.io/en/release_0.11.1/count.html

ptalign pseudotime readily recapitulated the dataset-derived pseudotime (Pearson=0.95, Fig.20f). Thus, ptalign accurately reconstructed the states and transitions of an unseen SVZ NSC lineage dataset, and I next set out to compare the inferred QAD-stage cells in their respective FACS gates using the index sorting information.

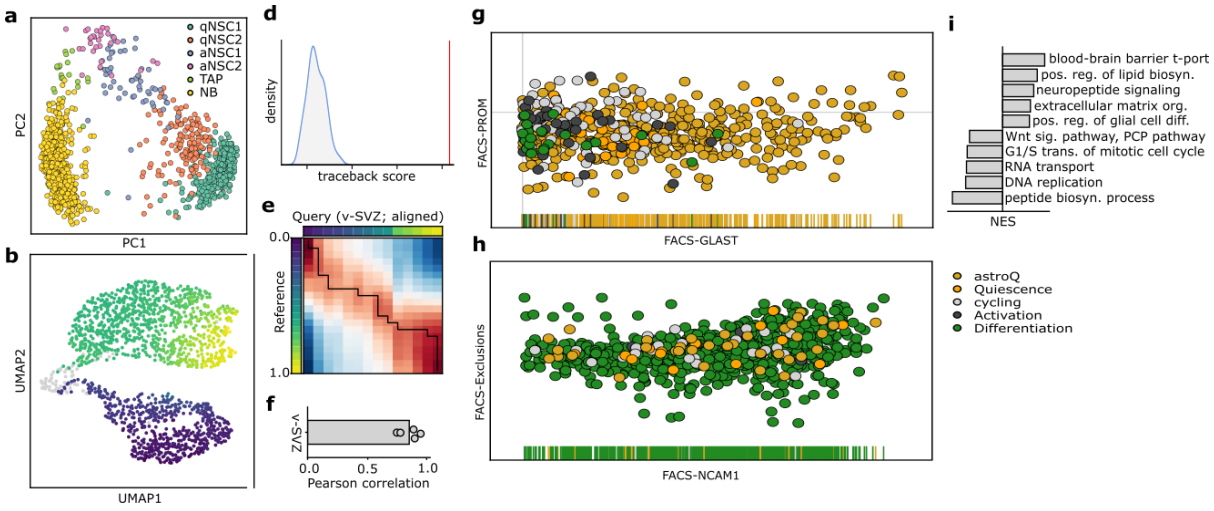

Figure 20: QAD-stage cells in reconstructed FACS gates. a) TCF/Lef SVZ NSC cells from five SS3 plates in PCA with the cell types from (Kalamakis et al., 2019) indicated. The SVZ lineage pseudotime for this dataset was inferred by diffusion pseudotime from this PCA. b) UMAP embedding of cells from (a) with the lineage pseudotime indicated. Cycling cells are excluded from pseudotime inference and are colored in gray. d) ptalign traceback scores from 100 permutations of the TCF/Lef reporter cells from (a) aligned against the SVZ NSC lineage reference. The traceback score for the true QAD-gene ptalign run is indicated in red. e) DTW of the TCF/Lef reporter cells from (a) ptalign pseudotime and the SVZ NSC reference lineage pseudotime. f) Pearson correlation between the ptalign pseudotime and SVZ lineage pseudotime for each of the five replicates of TCF/Lef SVZ SS3 cells. g) FACS GLAST-PROM and NCAM1-exclustions (h) gate reconstructed from SS3 index sorting, ptalign-derived lineage cell types indicated. Gray lines indicate gate thresholds. i) Selected GO terms from GSEA of genes correlated with the GLAST axis from (g).

FACS enables the simultaneous measurement of multiple fluorescent markers to support the sorting of individual cells into different populations based on user-defined gates. For the SVZ NSC lineage (Llorens-Bobadilla et al., 2015), stem cells are traditionally separated from their progeny based on the presence of prominin (PROM1). Similarly, NSC lineage cells are enriched from parenchymal brain cells using GLAST (aka. SLC1A3). In the OB, LNBs can be identified by the presence of NCAM1, though the gold standard for identifying SVZ NSC progeny in the OB remains genetic lineage tracing, eg. in (L. P. M. Kremer et al., 2021). Here, I reconstructed SVZ GLAST-PROM (Fig.20g) and OB NCAM1 (Fig.20h) FACS gates for TCF-Lef reporter cell transcriptomes and populated these with QAD stages inferred by ptalign. These results highlight the preponderance of Differentiation-stage cells in the OB and identified several astrocytes with varying NCAM1 levels, suggesting these were incorrectly

sorted (Fig.20h). In the SVZ, Activation- and cycling-stage cells appear to exhibit slightly increased PROM1 levels while Quiescence-stage cells fall below the PROM1+ gate (horizontal line) (Fig.20g). Differentiation- and Activation-stage cells are evidently GLAST-low, while gating on GLAST-high cells would exclusively enrich for astroQ cells in the SVZ. These results suggest that while GLAST and PROM1 are useful for distinguishing different SVZ NSC lineage populations, careful gating is necessary to ensure accurate selection of the intended populations.

An interesting consequence of the RNA-protein association made possible by index sorting involves the classification of reporter-positive cells to find eg. transcriptional determinants of canonical Wnt signaling activity. Training a classifier to predict eg. TCF-Lef reporter activity from transcriptomic measurements alone would provide a powerful avenue to extrapolate the inference of canonical Wnt activation status across datasets and tissues. This possibility was unfortunately not realized in the context of this study. Nevertheless, transcriptomic associations for FACS GLAST measurements (Fig. 20g) are shown in (Fig.20i), highlighting the otherwise unseen biological signals which are encoded in a given FACS gating.

2.4.2.3 Sustained canonical Wnt activity in Quiescent NSCs

An unequal distribution of reporter-positive cells is evident in the TCF-Lef reporter cell UMAP (Fig.21a), and quantifying the proportion of reporter-positive cells by QAD-stage recapitulates the stark decline in canonical Wnt activity associated with Activation- and Differentiation-stage cells observed previously (see Fig.19). The TCF-Lef reporter is a H2B-EGFP line, meaning EGFP molecules are fused to DNA-bound histones via the highly-stable H2B modification (Kaya, 2023). Their consistently high reporter activity suggests Quiescence-stage cells exhibit sustained canonical Wnt activation (Fig.21b-c), ultimately leading to saturation of available H2B sites which are only diluted by division. This assertion is at odds, however, with the rapid decline in reporter activity observed in Activation-stage cells, as these will, on average, inherit one H2B-saturated set of chromosomes from their (presumably previously quiescent) parent and consequently exhibit EGFP signal. Alternatively, the H2B signal points to the existence of separate populations of rarely- or never-cycling Quiescence-stage cells, an observation plausibly supported by the different levels of reporter-positive cells between the Quiescence and astroQ populations (Fig.21b), which are also visible in the UMAP (Fig.21a). Thus, more than exhibiting a stage-dependent decline in canonical Wnt signaling, investigating reporter activity in scRNA-seq via index sorting reveals that Quiescent cells likely

experience sustained Wnt activation while the sharp decline of these signals in Activation could point to the existence of a distinct Quiescence progenitor population.

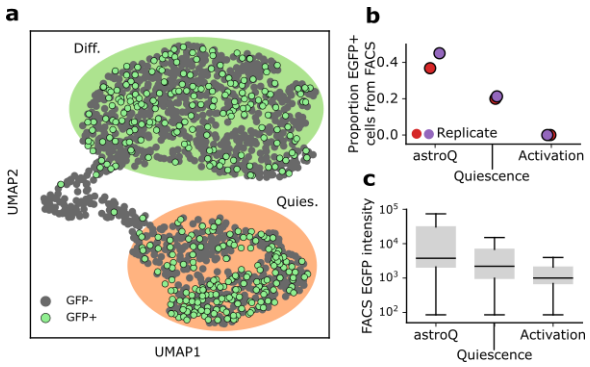

Figure 21: Sustained canonical Wnt activity in Quiescence-stage cells. a) UMAP of TCF/Lef Wnt reporter SVZ NSC lineage, with Quiescence- and Differentiation-stage cells indicated. b) Proportion of EGFP+ cells from FACS by QAD-stage and replicate. Only SVZ replicates were considered. c) Raw FACS intensity by QAD-stage and replicate, indicating enrichment of EGFP activity among astroQ cells.

2.5 Conserved cell hierarchies between human and mouse neurogenesis

Murine neurogenesis is well-documented while understanding of this process has remained elusive in humans. Recent efforts to map human brain development at single-cell resolution (Bhaduri et al., 2021; Cao et al., 2019; Eze et al., 2021; Zhong et al., 2020) and advances in organoid technologies (Bhaduri, Andrews, et al., 2020; C. Li et al., 2023; Velasco et al., 2019) have shed light on the processes governing human neurogenesis. Thus, having characterized the mouse SVZ NSC lineage, I next set out to leverage human fetal and cortical brain organoid datasets to assess the conservation of neurogenic lineage dynamics between humans and mice.

2.5.1 Human brain organoids exhibit a conserved NSC lineage pseudotime

Human brain organoids (HBOs) serve as a practical model of neurogenesis, demonstrating developmental processes *in vitro* (Lancaster & Knoblich, 2014). In this study, they were used to gain molecular insights into neurogenesis and to assess their potential as *in vitro* tumor models. Cortical organoids following the unpatterned cortical specification protocol from (Lancaster & Knoblich, 2014) were obtained from Xiujian Ma and injected with glioblastoma tumor cells by Oguzhan Kaya as patient-derived allograft (PDA) tumors (Kaya, 2023) (Fig.22a). Organoids were harvested two weeks post injection by Oguzhan and labeled with cell hashing (Stoeckius et al., 2018) to perform sequencing of both tumor-infected and healthy cells using the 10X chromium 3' platform. Then I processed cDNA libraries by cellranger and quantified hashtag counts using CITE-seq-count[5].

This organoid dataset was interesting in two respects: providing insights into glioblastoma cell growth *in vitro*, and as a model of human neurogenesis. Thus I set out to isolate the healthy organoid cells and their lineage. Over 90% of cells were confidently assigned a hashtag, enabling reconstruction of individual organoid populations. I separated healthy from malignant cells by transcriptome clustering, detection of the tumor-specific `mCherry` transgene, and through the presence of chromosomal aberrations detected by (*inferCNV of the Trinity CTAT Project.*, 2024) (Fig.22b-d). Analysis of these tumor cells is detailed in section 2.6.3.

[5] https://github.com/Hoohm/CITE-seq-Count

Integrating the healthy cells with a cortical organoid development atlas (Bhaduri, Andrews, et al., 2020), I traced stage transitions through QAD-stages to map a trajectory from astrocyte- and RG-like progenitors to neuronal cell types. Non-lineage cells can arise by chance in some organoids (Pollen et al., 2019; Velasco et al., 2019), and were removed by integration with the SVZ NSC reference from (Cebrian-Silla et al., 2021) in this case (Fig.22e). The organoid atlas identified a panNeuron population which constituted different neuronal subtypes specific to each organoid, eg. with inhibitory or excitatory neuronal lineages marked by `TH` and `POU3F2`, respectively (Fig.22f). This diversity reflects the unpatterned protocol used in organoid generation, contrasting with more recent methods that allow for more fine-grained subtype- and region-specification (Quadrato & Arlotta, 2017). These results illuminate the subtle differences between human and mouse neurogenesis and highlight their organization along QAD stages as identified in mouse SVZ NSCs.

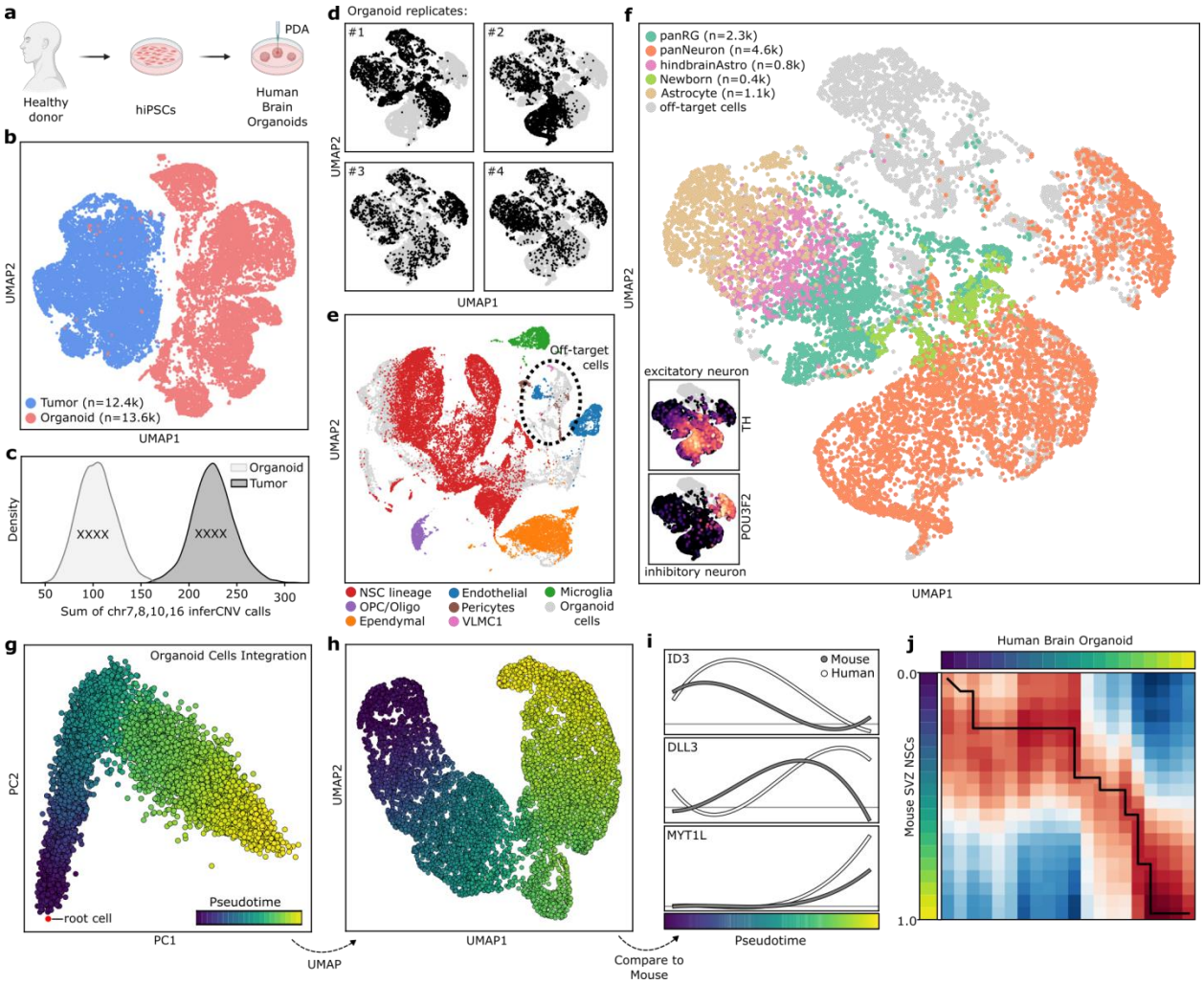

Figure 22: NSC lineage dynamics in human brain organoids. a) Schematic representation of human brain organoid PDA models, cocultured with T6 tumor cells for two weeks. b) UMAP embedding of tumor and organoid cells, colored by source. c) Replicate assignments and copy number variation (CNV) at chromosomes 7,8,10, and 16 were used to distinguish tumor and organoid cells. The latter are revisited in Section 2.6.3. d) UMAP embedding of cells from each of the four organoid replicates highlights cell type diversity between organoids. e) Off-target non-lineage cells identified by integrating organoid cells from (d) with healthy SVZ NSC cells from (Cebrian-Silla et al., 2021). f) UMAP embedding of organoid cells with cell types from (Bhaduri, Andrews, et al., 2020) inferred by label transfer. Note that off-target cells form their own cluster. Insets depict canonical markers for excitatory and inhibitory genes, highlighting the neuronal diversity in this embedding. g) PCA of integrated organoid cells used as a basis for fitting an organoid NSC diffusion pseudotime. The root cell is indicated in red. h) Organoid NSC lineage pseudotime plotted in the integrated organoid cell UMAP. i) Pseudotime expression splines for SVZ NSC lineage QAD-stage markers, highlighting conserved dynamics between mouse (SVZ NSC reference) and human (organoid) NSC lineages. j) DTW of NSC lineage pseudotime in the mouse SVZ NSC lineage reference and the human cortical organoids cells from (d).

The components of the CNS are conserved across vast evolutionary distances (Jékely, 2011, 2021), suggesting a highly conserved sequence of states and transitions likely underlies their development. Thus I used pseudotime analysis to map transitions across QAD stages, providing a basis to compare human cortical organoid NSC lineage dynamics to mouse SVZ NSCs. Due to the noted variability of neuronal subtypes among organoids, I first combined organoid replicates by integration.

Encouragingly, this integrated lineage followed the same V-like shape observed along PC1 and 2 of the mouse SVZ NSC datasets (see Fig.14). This suggested that the two models share a common differentiation trajectory, and I fit a NSC lineage pseudotime to capture its progression (Fig.22g-h). Comparing pseudotime-expression between organoid and mouse NSC lineages revealed conserved dynamics throughout Quiescence-, Activation-, and Differentiation-stages as marked by `ID1`, `DLL3`, and `MYT1L`, respectively (Fig.22i). Further comparison by DTW (see section 2.1.2) confirmed these conserved dynamics (Fig.22j), with the deviation at Quiescence- and Activation-stages likely reflecting the different environments in the highly quiescent adult brain and the highly active developing organoid. This comparison showcases pseudotime as an effective tool for capturing and quantitatively comparing lineage dynamics, validating the use of human cortical organoids as neurogenesis models showing remarkable conservation to the mouse NSC lineage hierarchy.

2.5.2 Quiescent cells emerge at low frequency during human fetal brain development

The observation of conserved NSC lineage dynamics in the mouse brain and human cortical organoids suggests that fundamental mechanisms governing NSC behavior are shared across species. However, the definitive test of these findings lies in comparing *in vivo* dynamics between species. Fortunately, a large volume of single-cell transcriptomes from human cortical brain development has been published in recent years (Bhaduri et al., 2021; Cao et al., 2019; Eze et al., 2021): many of which were curated into a meta-atlas by (Nano et al., 2023). Encompassing around 600,000 cells across various cortical regions and developmental stages from Carnegie stage 12 to gestational week 26, this dataset provides a comprehensive view of human cortical development. Thus I set out to evaluate the extent of conservation in NSC lineage dynamics between adult mouse SVZ NSCs and human cortical brain development.

As with cortical organoids above, UMAP indicated the presence of a clear lineage trajectory in the cortical development dataset with transitions through astrocyte, RG, and neuronal stages corresponding to QAD (Fig.23a). Subgroups of inhibitory and excitatory neurons were readily discernible, though their separation by region or individual was not as pronounced as in cortical organoids (not shown). Given the strong batch effect across datasets in the meta-atlas, I focused on the largest cohort from (Bhaduri et al., 2021) for pseudotime analysis (Fig.23b). PCA embeddings of cells from individual developmental timepoints exhibited the familiar V-shape (see above) and diffusion pseudotimes fit in this way captured clear transitions between QAD-stages (Fig.23c).

Intriguingly, mouse-human pseudotime expression dynamics were clearly conserved for MYT1L and, to a lesser extent, for ID3, whereas DLL3 expression was widely promiscuous in the fetal context (Fig.23d). This variability might stem from the concurrent presence of different maturation stages across brain regions, which were not accounted for in this analysis; or, as DLL3 marks activation-stage cells, could be a consequence of the incredible rate of growth in the developing brain. These observations highlight the conservation of neurodevelopmental states amidst context-dependent transcriptional variability, illuminating the careful balance between genes and environment in shaping neurogenesis.

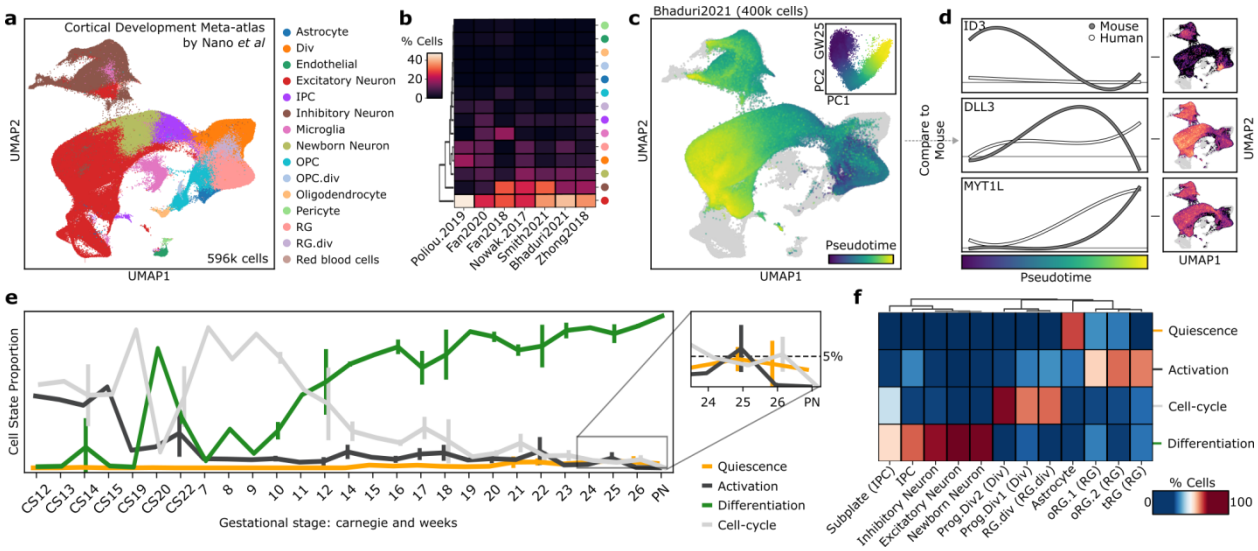

Figure 23: QAD-stage cell frequencies in human fetal brain development. a) UMAP and cell types of the human cortical development meta-atlas from (Nano et al., 2023). b) Proportion of cells from (a) assigned to each cell type from each batch. c) Cells from (Bhaduri et al., 2021) highlighted in the UMAP from (a) based on the fetal NSC lineage pseudotime inferred from the inset PCA embedding, shown here with GW25 as an example. d) The fetal NSC lineage pseudotime captures shared dynamics in the QAD-stage marker genes compared to the SVZ NSC reference lineage, measured here by spline regression. UMAP plots of individual gene expression trends are indicated. e) Proportion of QAD-stage assigned cells across fetal brain development, from Carnegie stage (CS) 12 to gestational week (GW) 26 and a single postnatal (PN) timepoint. Lines represent mean and standard deviation, where available, in QAD-stage cell proportion, as indicated. f) Overlap between QAD-stage labels and selected cell types from (a).

QAD-stage cells were clearly present in fetal brains, prompting a quantification of their frequency across developmental time. Consequently, I assigned cycling and QAD-stage labels by AUCell-scoring of the SVZ-QAD gene set (see section 2.2.2) and observed the expected correspondence with the annotated cell types, with Quiescence-stage cells predominantly found in astrocytes and to a lesser extent in outer radial-glia (oRG) cells (Fig.23f). This is consistent with the developmental origins of cortical astrocytes from oRGs at the gliogenic switch (Sanes et al., 2019), and raises questions about

the coupling of state and fate in this population (Weinreb et al., 2020). Notably, Activation- and Differentiation-stage cells constituted the majority of the developing cortex, with Quiescence-stage cells consistently below 5% across all timepoints (Fig.23e). This is in stark contrast to the pervasive presence of Quiescent-stage cells in the adult brain, where astrocytes play particularly important roles (see section 1.1.5). These observations underscore the dynamic nature of neurogenesis, where the balance between quiescence and activation shifts markedly as the brain matures (Sanes et al., 2019). Thus while NSC lineage dynamics are conserved across development and adulthood, the underlying regulatory mechanisms limit their functional contributions in important ways. As we will see (section 2.7.3), these distinctions are pivotal when considering the pathology adult cancers, suggesting that comparisons to fetal development could fail to resolve important aspects of glioblastoma biology.

2.6 Glioblastoma recapitulates NSC lineage stages

Arising in the highly sensitive and privileged tissues of the adult brain, glioblastomas are one of the most lethal adult tumors. For generations, researchers have drawn parallels between glioblastoma cells and those of the healthy brain, initially through morphological similarities (Scherer, 1938), and later in bulk (Phillips et al., 2006; Verhaak et al., 2010) and eventually single-cell (Couturier et al., 2020; Johnson et al., 2021; Neftel et al., 2019; Patel et al., 2014; L. M. Richards et al., 2021) transcriptomics. However, these comparisons, which often centered on the developmental stages of the brain, failed to account for key properties of adult brain stem cells (see section 2.5), for example the lack Quiescence-stage cells which are otherwise abundantly present in adult brains. Only through the recent availability of cell type resolved transcriptomes of glioblastoma cells and healthy adult NSCs in mice, has a deeper examination of the similarities between these two entities become feasible. Within this framework, the unbiased barcoding-based experiment (Lan et al., 2017), which identifies an invariant glioblastoma hierarchy – characterized by a slow-cycling stem cell which gives rise to a rapidly cycling progenitor that ultimately generates differentiated progeny – presents a view of glioblastoma organization which is highly consistent with the QAD dynamics I previously described for healthy neural stem cells (see section 1.1.2). Against this backdrop, I set out to use ptalign to map glioblastoma pseudolineages by direct comparison to the healthy adult mouse NSC lineage curated in section 2.2. This analysis highlights the recapitulation of NSC lineage stages by the human glioblastoma pseudonymously referred to as T6. This tumor, an `IDH`-wt glioblastoma from an elderly male treated at Universitätsklinikum Ulm, clearly recapitulates NSC lineage dynamics and serves as an excellent example of how a tumor retains the memory of its tissue-of-origin.

Glioblastoma cells *in vitro* often fail to accurately reproduce the organization and dynamics which are characteristic of human glioblastomas *in vivo* (Prager et al., 2020). To overcome this and facilitate the study of diverse glioblastoma cells *in vivo*, Oguzhan Kaya generated patient derived xenograft (PDX) T6 tumors by orthotopic transplantation of glioblastoma cells into the striatum of immunocompromised mice (Kaya, 2023). PDX tumors were variably generated from T6 cells in untransduced (‘naïve’) or lentivirally transduced (‘reporter’; employing a `TCF/Lef-EGFP` reporter of canonical Wnt activity, see section 2.4.1) conditions. Details of the reporter and insights into tumor Wnt-signaling dynamics are detailed in section 2.8 below. On average, mice bearing T6 tumors reached the humane endpoint around five mpi, upon which Oguzhan isolated tumor cells by FACS and produced single-cell transcriptomes by the modified SmartSeq3 (SS3) protocol (Kaya, 2023).

2.6.1 Patient-derived xenograft tumors organize into distinct transcriptional states

In total, Oguzhan processed cells from six separate T6 PDX tumor samples, sequencing a full 384-well plate of cells from each sample. These included two naïve and two reporter tumors profiled with the modified SS2 protocol, as well as two additional reporter tumors which were profiled by the modified SS3 protocol. The improvements brought by the SS3 protocol were readily evident, with notably higher gene counts in SS3 cells at a fraction of the sequencing depth (Fig.24a-b). Despite rigorous gating in FACS, mouse cells were invariably sequenced with each tumor and had to be separated based on their alignment properties (Fig.24c). The remaining tumor cells exhibited correlated gene expression among SS3 replicates (Pearson=0.98), with slightly reduced consistency observed between SS2 reporter and naïve conditions (Pearson=0.86) (Fig.24d). This could be due to PCR biases which are negated by the use of UMIs in SS3, or relates to cell composition bias introduced by the `HLA-I` FACS gating strategy employed for naïve cells (Kaya, 2023) (not shown). For these reasons, I focused downstream analyses on the reporter populations alone.

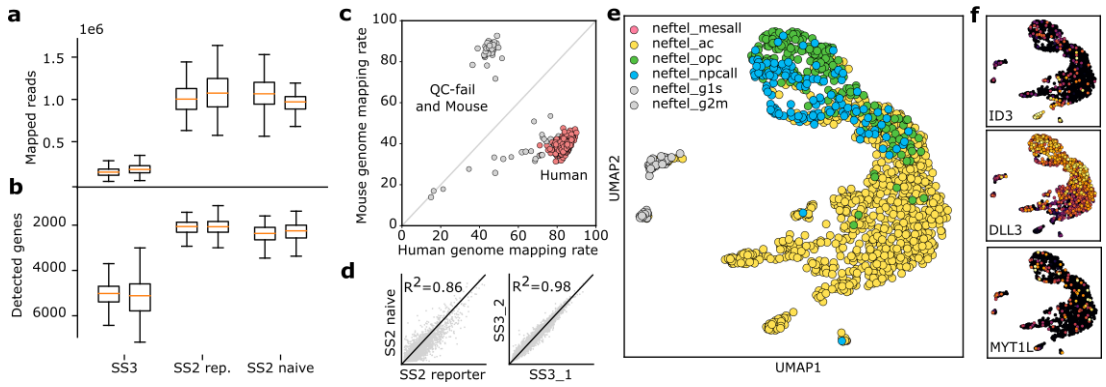

Figure 24: Distinct transcriptional states in T6 glioblastoma PDX. a) Mapped reads and detected genes (b) between T6 PDX replicates from SS3 TCF/Lef reporter as well as SS2 reporter- and naïve conditions. c) FACS sorting of TCF/Lef reporters by endogenous mCherry fluorescence (Kaya, 2023) includes low-quality and mouse cells, as indicated here through mouse- and human-genome mapping rates per cell. d) High transcriptional congruence in PDX cells isolated from different mice. e) UMAP embedding of integrated SS2 and SS3 TCF/Lef reporter cells from T6 PDXs, colored by cell states from (Neftel et al., 2019) assigned by gene set scoring. f) QAD-stage marker expression in the UMAP from (e).

Applying the meta-module scoring method from (Neftel et al., 2019) on T6 PDXs, I observed tumor cells enriched in astrocytic (AC-like) and neuronal progenitor cell (NPC-like) states (Fig.24e), among

others. Leveraging SS3 index sorting (see section 2.6.2.1) I noticed a correlation between these transcriptional states and physical cell characteristics from FACS: with NPC-like cells generally being smaller and AC-like cells larger (not shown), consistent with (Sabelström et al., 2019). The presence of these meta-module states echo the NSC lineage progression through QAD stages. An important distinction however arises in the view of Neftel and colleagues that NPC-like cells comprise tumor stem cells while AC-like cells represent a differentiated population (see section 1.1.5). This view mirrors the dynamics of fetal brain development but inverts the roles typically observed in adult brain tissues. Notably being one of few *in vivo* glioblastoma lineage tracing studies, the work by Lan and colleagues identified a tumor stem cell hierarchy which closely resembles the QAD stages of the adult NSC lineage (Lan et al., 2017). Encouragingly, the QAD-stage markers `ID3`, `DLL3`, and `MYT1L` (see Fig.14) distinguish different transcriptional states within glioblastoma (Fig.24f), reinforcing the notion that these tumors can be characterized according to the QAD-stages of the healthy adult SVZ NSC lineage.

2.6.2 Glioblastoma cells resemble QAD-stages of the NSC lineage hierarchy

Encouraged by the structured arrangement of QAD-stage markers in T6 cells, I conducted a Seurat integration of these cells with the TCF-Lef SVZ NSC lineage (Fig.25a-b) from Fig.20. The resulting UMAP reaffirmed the conservation of NSC lineage stages and transitions in this glioblastoma: revealing tumor cells intermingled with healthy astroQ and Differentiation-stage cells, and otherwise connected by a distinct but consistent lineage trajectory in each case (Fig.25c). My attempt to use RNA-velocity to resolve tumor dynamics was inconclusive. Instead, I fit a diffusion pseudotime to capture the tumor lineage progression (Fig.25d, inset) as I had done previously for the SVZ datasets (see Fig.15). This approach, along with AUCell scoring of the QAD gene set from section 2.2.2, revealed a clear transition through Quiescence-, Activation-, and Differentiation-stages in the tumor UMAP (Fig.25d) which mimicked the integration trajectory. Indeed, by comparing expression levels of `GLAST` and `NCAM1` along pseudotime, a clear lineage hierarchy was visible (Fig.25e). These results confirm that glioblastomas harbor transcriptionally distinct cells which follow a structured lineage trajectory similar to healthy cells. In accordance with the stem cell hierarchy identified by Lan and colleagues (Lan et al., 2017), I next cemented NSC lineage dynamics though QAD stages in this glioblastoma using ptalign.

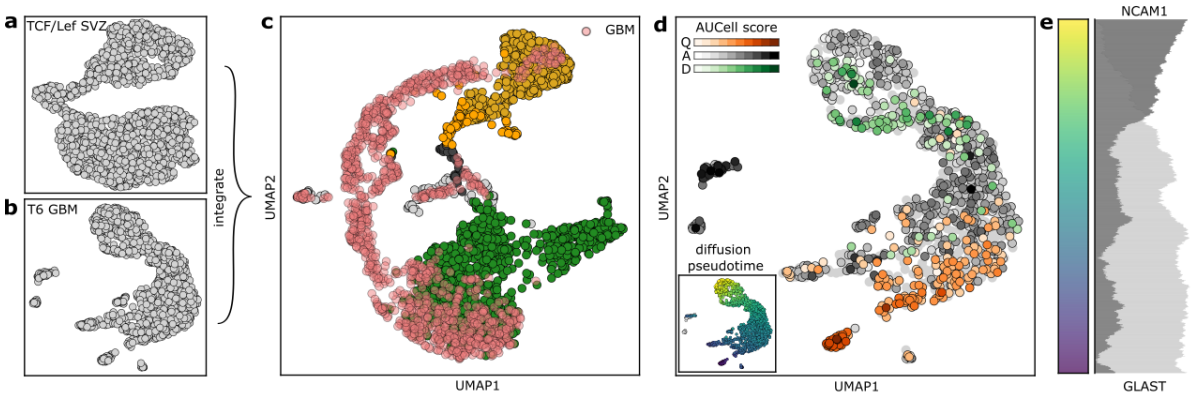

Figure 25: QAD-stage cells in T6 glioblastoma PDX. a) TCF/Lef SVZ NSC SS3 lineage and T6 glioblastoma cells (b) UMAP, combined through integration and visualized in (c) to reveal overlapping cell states. d) T6 glioblastoma UMAP from (b) colored by AUCell scoring of QAD-stage genes, with cells colored by their maximum stage-score, where intensity relates the difference to the second-highest score. Inset depicts the dataset-derived T6 lineage diffusion pseudotime. e) **GLAST** and **NCAM1** UMIs in a rolling window over the T6 lineage diffusion pseudotime from (d).

2.6.2.1 Tumor QAD pseudolineage reconstructed by ptalign

I inferred a T6 pseudolineage[6] by projecting cells into the SVZ NSC lineage atlas, revealing the presence of cells across QAD stages (Fig.26a) supported by a highly significant permutation result (Fig.26b) and a narrow DTW (Fig.26c) comparable to that of the SVZ datasets (see Fig.9). ptalign pseudotimes for individual PDX replicates were consistent with the dataset-derived diffusion pseudotime (Fig.26d), suggesting that glioblastomas converge on an optimal pseudolineage configuration to support their growth. QAD-stage cells in the T6 pseudolineage (Fig.26e) closely match those inferred by gene set scoring above. The QAD-stage markers `ID3`, `DLL3`, and `MYT1L` – which are not part of the ptalign QAD gene set – exhibit similar pseudotime expression dynamics (Fig.26f) as the reference SVZ NSC lineage atlas (see Fig.20). These results highlight the strong and reproducible detection of NSC-like lineage dynamics in this glioblastoma. Compared to conventional methods, ptalign demonstrably simplified the detection of lineage dynamics and enabled their comparison by resolving stable and transitioning cell stages.

[6] Note that these data were used previously to document the ptalign algorithm in section 2.1.

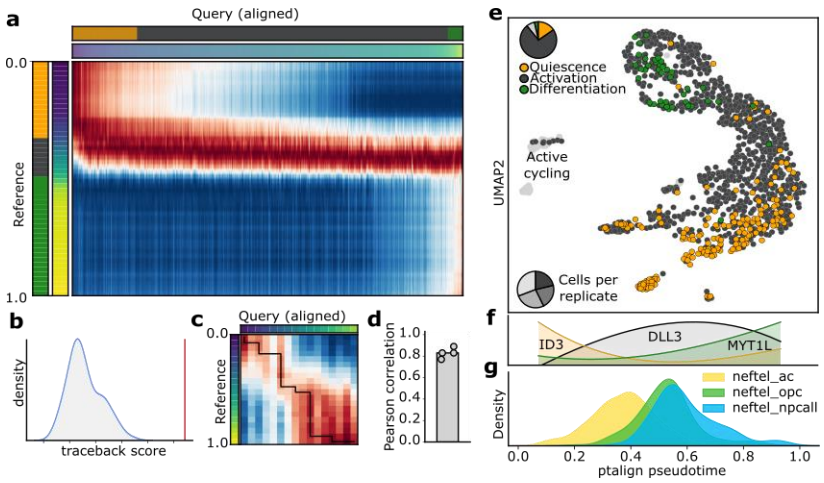

Figure 26: QAD-stage cells by ptalign in T6 glioblastoma PDX. a) ptalign correlation heatmap for T6 glioblastoma PDX cells (Query) and the SVZ NSC reference lineage (Reference). The aligned pseudotime and QAD-stages are indicated. b) Traceback scores for 100 permutations of the pseudotime alignment in (a). The true QAD-gene ptalign traceback score is indicated in red. c) DTW of the pseudotime alignment from (a). d) Pearson correlation between dataset-derived T6 lineage pseudotime and the ptalign pseudotime from (a) for each of the PDX replicates. e) QAD stages in the SVZ NSC reference lineage. f) ptalign pseudotime from (a) in the T6 UMAP. g) UMAP embedding of T6 glioblastoma cells colored by QAD-stage. Inset pie charts depict proportion of QAD-stage cells and cells per replicate. Cycling cells are excluded from ptalign and colored in gray. h) Pseudotime expression dynamics of QAD-stage markers captured by spline regression. i) KDE density plot of (Neftel et al., 2019) cell stats from gene set scoring, arranged in pseudotime.

Pseudolineage analysis of the T6 PDXs demonstrates the utility of the study of glioblastoma organization through the lens of healthy NSC lineage stages and transitions. However, the placement of oligodendrocytic tumor cells, which are absent from the SVZ NSC lineage atlas (see section 2.2), remains an open challenge. Based on comparisons to the Neftel meta-modules, ptalign assigns higher pseudotimes to OPC-like cells but these are not consistently placed in the Differentiated stage (Fig.26g). It is likely that inclusion of additional oligodendrocyte marker genes, for example from the OPC-like meta-module, could guide ptalign inference in this case. Nevertheless, the arrangement of PDX cells into consistent pseudolineages reveals their inherent organization into defined hierarchies which are dissected by ptalign.

2.6.3 Patient-derived allografts highlight intrinsic fating of glioblastoma cells

Tumor pseudolineages in T6 PDXs were highly consistent despite SS2 and SS3 replicates being generated years apart. This suggests that the consistent arrangement of cells into distinct pseudolineages may be a fundamental characteristic intrinsic to each tumor cell, rather than being a

product of the physical environment of the tumor. To explore this hypothesis, I analyzed T6 pseudolineages in diverse environments on the basis of the human cortical organoids Oguzhan injected with T6 glioblastoma cells, ie. the patient-derived allografts (PDAs) from section 2.5.1.

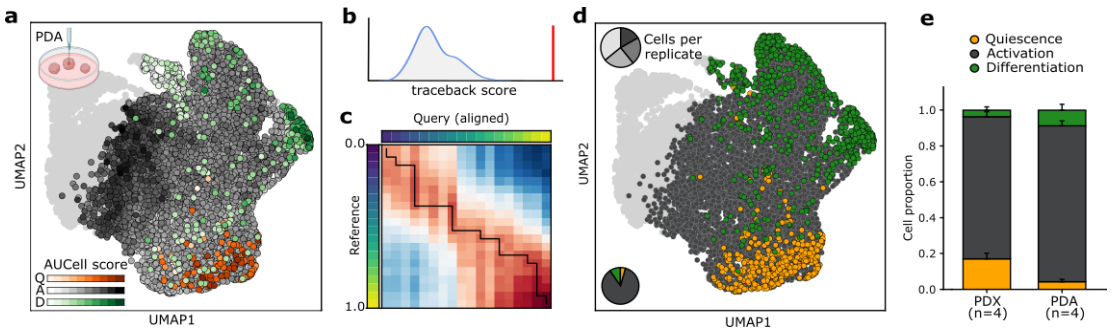

Figure 27: Consistent pseudolineages in T6 PDX and PDA glioblastomas. a) T6 glioblastoma cells cocultured with healthy cortical organoids from section 2.5.1 in an integrated UMAP and colored by enrichment of AUCell QAD-gene scores. Cycling cells are colored gray. b) Traceback score for 100 permutations of pseudotime alignment between T6 PDA cells and the SVZ NSC lineage reference. The true QAD-gene traceback score is colored red. c) DTW of the T6 PDA ptalign pseudotime and the SVZ NSC lineage reference. d) UMAP embedding of T6 PDA cells colored by ptalign-derived QAD-stage. Inset piecharts depict proportion of QAD-stage cells and cells per organoid. e) Barchart of QAD-stage cell proportions in T6 PDX and PDA replicates, with standard deviation between replicates indicated.

The precise patterning of human brain organoids is difficult to control, and these often develop into tissues resembling disparate brain regions (Pollen et al., 2019; Velasco et al., 2019). Previously, I showed that the PDA organoids profiled by Oguzhan in section 2.5.1 exhibit diverse NSC lineage as well as non-lineage cell types at different frequencies (see Fig.22). Hence these organoids constitute varied environments which could influence tumor growth. Tumor cells from these four PDA replicates however reproduced the transcriptomic stages observed in the PDX (see Fig.25), with AUCell scoring separating these into QAD-stages (Fig.27a) which were reconstructed by ptalign (Fig.27d). The PDA pseudolineages exhibited a clearly significant permutation result and an ideal DTW (Fig.27b-c) closely resembling the SVZ lineage comparisons (see Fig.9). Comparing pseudolineages inferred for T6 PDA and PDX samples (Fig.27e), these largely agreed except for an increased proportion of Activation-stage cells in the PDA which appears to have come at the expense of Quiescence-stage cells. This could be explained by the presence of growth factors and other chemicals necessary for organoid development which are not present in the adult brain. Taken together, this suggests that while external factors can influence the proportion of cells in different stages, their fundamental organization into pseudolineages remains consistent, hinting at an intrinsic capability of glioblastoma cells to organize into a distinct hierarchy.

These results support the idea that a tumor's developmental history fixes its lineage potential through genetic or epigenetic mechanisms which are intrinsically imprinted in every tumor cell. Thus, tumor cells invariably establish fixed lineages fated much like healthy stem cells to ultimately grow what is functionally an organ within an organ. Consistent with lineage constraint limiting the extent to which a tumor can deviate from the memory of its tissue-of-origin (see section 1.3), this investigation into the T6 glioblastoma strongly supports the existence of a QAD-stage hierarchy mirroring the adult SVZ NSC lineage. This PDA experiment in particular establishes organoid models as an effective means to study tumor organization, setting the stage for high throughput screens of factors involved in modulating tumor lineages.

In sum, I have demonstrated the efficacy of ptalign pseudolineage analysis on a single human glioblastoma, highlighting the conserved stages and transitions to the healthy SVZ. This approach enables the transcriptomic profiling of eg. the tumor stem cell hierarchy identified in (Lan et al., 2017) even in the absence of a genetic lineage tracing. However, the key advantage enabled by ptalign remains the projection of tumor samples onto a unified pseudotime axis, enabling the comparison of different lineage stages or transitions in that context. I demonstrate this procedure in the coming sections, characterizing glioblastoma pseudolineages in a large cohort and conducting a comparative study of the functional, clinical, and transcriptional differences which underlie the heterogeneity of these tumors.

2.7 Insights from pseudolineage inference on published primary glioblastoma datasets

Tumor heterogeneity is a central concept in oncology. This heterogeneity is fixed through a tumor's unique developmental history, leading to a spectrum of intra-tumoral heterogeneity which frequently presents a barrier to effective treatment. Glioblastomas in particular are recognized for their notable inter-tumoral heterogeneity, with different cell state configurations underlying disease progression and patient outcomes. To better understand these complexities, researchers have used extensive single-cell and spatial transcriptomics studies to dissect the distinct characteristics of individual tumor cells in glioblastomas (see section 1.2). However, these studies rarely reflect on the organizational principles which determine how these diverse cell states arise or how they contribute to tumor growth.

These questions are addressed through ptalign, which leverages the tumor's memory of its tissue-of-origin to place tumor cells in a reference lineage trajectory. This approach enables the transfer of contextual knowledge from healthy cell lineages to better understand the organizational principles of tumor cells, including how different cell states emerge and support tumor growth. By applying ptalign to place glioblastoma cells within a reference NSC lineage (section 2.1.2), I demonstrated the intrinsic fating of glioblastoma cells (section 2.6.3) and identified incompatibilities in their comparison to fetal over adult NSC lineages (section 2.5.2). Here, I extend this approach to a larger cohort of published glioblastoma scRNA-seq datasets, leveraging the shared pseudotime axis unique to ptalign to quantitatively study various features underlying glioblastoma heterogeneity. This approach illuminated the essential role of Quiescence-stage cells in glioblastoma organization, identifying a distinct set of tumor pseudolineages characterized by diverse patient outcomes. I further profiled salient biomarkers for these groups from a conventional methylation assay, demonstrating the transfer of insights from ptalign into a clinical setting. Crucially, ptalign facilitates the comparison of pseudotime expression dynamics across different tumors or between tumor and healthy tissues at scale, illuminating fundamental principles of glioblastoma organization through the discovery of potent fate-modulating factors (see section 2.9). These findings are elucidated below, and collectively demonstrate the unique advantages of ptalign for understanding and targeting heterogeneous tumor entities.

2.7.1 ptalign unveils tumor pseudolineages in a primary glioblastoma scRNA-seq cohort

Building on the observations around pseudolineage characterization in a glioblastoma PDX (see section 2.6), I next compiled a cohort of 260.399 cells from 86 primary glioblastoma single-cell and single-nucleus transcriptomic datasets across 9 studies. These datasets and their sources are summarized in (Foerster et al., 2023) (and Fig.28). I applied quality control of mitochondrial content and UMI counts, revealing highly reduced numbers of MKI67+ cells in single-nucleus RNA-seq samples (Fig.28a-b). This suggests that cycling cells may be lost during snRNA-seq library preparation, and I excluded all 19 snRNA-seq samples from downstream analysis such as not to bias pseudolineage inference. Following the approach outlined in (Neftel et al., 2019), I excluded non-malignant clusters by marker expression, then used CNVs from inferCNV to call malignant cells by their correlation to the mean malignant cell per sample (Fig.28c), resulting in 136.443 putative malignant cells. Finally, I filtered tumors with fewer than 400 cells leaving 55 tumor samples. Metadata (Fig.28d) identified most tumors as IDH-wildtype Grade IV glioblastomas, while eg. reporting of MGMT methylation status varied (Louis et al., 2021). Tumor samples originated from a wide range of brain regions, and though reporting was sparse, appeared to contain more male than female samples, consistent with glioblastoma epidemiology (Ostrom et al., 2021). These 55 samples comprise a glioblastoma cohort which I used to characterize different aspects of intra-tumoral heterogeneity according to their ptalign pseudolineage.

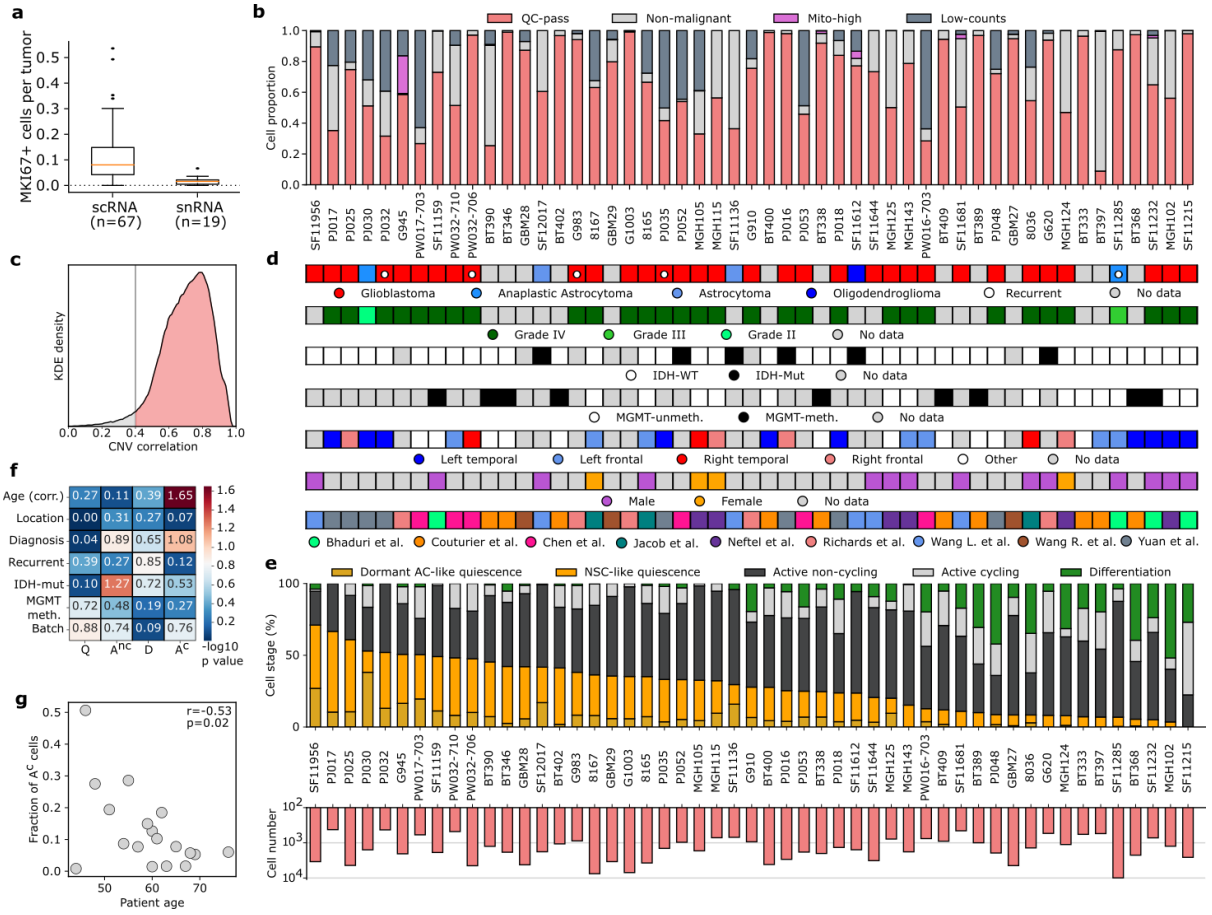

Figure 28: External glioblastoma scRNA-seq datasets metadata and QAD-stages. a) MKI67+ cells were detected in snRNA-seq glioblastomas at much lower frequency that in scRNA-seq glioblastomas, motivating their exclusion. b) Quality-control metrics for 51 primary glioblastoma samples. Non-malignant denotes healthy cells, while Mito-high contain elevated levels of mitochondrial transcripts and Low-counts denotes cells with low numbers of detected UMIs. c) KDE density of tumor cells CNV correlation to an average healthy cell, as described in (Neftel et al., 2019). d) Collated patient metadata across studies for tumor diagnosis, IDH mutation status, MGMT-methylation status, location, and sex. e) Top: stacked barcharts depicting the proportion of cells assigned to QAD stages and dormant astrocyte (AC)-like cells from ptalign pseudotimes, as well as cycling cells (gray), for (n=51) primary GBM scRNA-seq tumors. Bottom: number of cells assigned a ptalign pseudotime for each tumor. f) Heatmap of log-transformed p-values from one-way ANOVA test for association between named feature and QAD-stage cell proportion. g) Fraction of cycling cells detected in a patient tumor decreases with patient age.

I conducted ptalign pseudotime alignment of the 55 glioblastoma cohort with the SVZ NSC reference lineage from section 2.2. I note that previous analyses of PDX and PDA pseudolineages (section 2.6.3) indicated that tumors exhibit fixed lineage potential, suggesting that pseudolineages inferred from the glioblastoma cohort should generally be representative of each tumor as a whole. Encouragingly, most tumors expressed the majority of SVZ QAD genes (from section 2.2.2), suggesting the presence of QAD-stage cells, which were positively identified in the various tumor pseudolineages (Fig.28e). Overall, four tumors failed to pass the ptalign permutation threshold (discussed in section 2.1.5), likely due to their co-expression of Quiescence- and Differentiation-

genes which limited the resolution of QAD dynamics. The remaining 109.101 cells from 51 tumors exhibited a broad range of pseudolineage modalities prominently featuring Quiescence- and Activation-stage cells with Differentiation-stage cells absent from some tumors. Using ANOVA to test for associations between tumor metadata and QAD-stages (Fig.28f) revealed that the few `IDH`-mutant samples were enriched in Activation-stage cells (not shown). Patient age was furthermore negatively correlated with the proportion of Activation-stage cells (Fig.28g, Pearson=-0.53), consistent with tumor lineage constraint acting in the highly quiescent environments of aging brains (Kalamakis et al., 2019). Thus, ptalign identifies diverse pseudolineages in glioblastomas that recapitulate epidemiological factors which underlie their organization and growth.

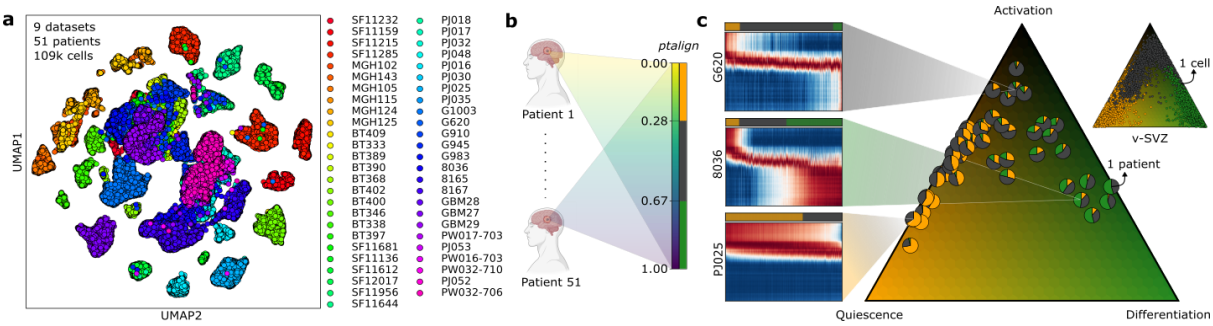

Figure 29: Glioblastoma organization revealed through 51 tumor pseudolineages. a) UMAP embedding of primary glioblastoma cells colored by patient origin. b) Schematic depiction of arbitrary patient samples projected onto the SVZ NSC reference pseudotime by ptalign, enabling pseudolineage inference and QAD-stage assignment. c) Ternary plot of 51 primary glioblastoma datasets from (a) arranged by relative QAD-stage proportions. Inset heatmaps show correlation matrices for representative Q, A or D-enriched tumors. Inset ternary depicts QAD geneset scores for SVZ NSC lineage cells with associated QAD state labels. Figure panels and legend were adapted from (Foerster et al., 2023).

The utility of ptalign is demonstrated in the above figure, where embedding large cohorts in UMAP will invariably cluster cells by their patient origin, thus masking any potential shared biology (Fig.29a). Instead, ptalign highlights commonalities between tumors by leveraging the memory of their tissue-of-origin to view them through the lens of healthy lineage transitions. Projecting individual tumors onto a common cell trajectory in this way (Fig.29b) highlights the differences in their underlying biology which contribute to intra-tumoral heterogeneity of glioblastomas. Here, the 55 glioblastoma pseudolineages reveal a clear progression of Quiescence-, Activation-, and Differentiation-stage cells (Fig.29c) which closely follows the SVZ NSC lineage continuum. These results support the existence of preferred pseudolineage configurations which are capable of sustaining the progression and growth of glioblastomas. Perhaps these pseudolineages exhibit survivorship bias over other configurations such as purely Q-D tumors – though such tumors may be

rarer and were not sampled in my glioblastoma cohort. Together, these data support the development of pseudolineage-based patient stratification approaches with promising prospects for the systematic comparison of gene expression dynamics between tumor groups and against the healthy lineage.

2.7.2 QAD stage association with tumor clones by CNV

Tumors are born by competition, acting as a clonal entity to outcompete their neighbors and acquire malignant traits (Colom et al., 2020). Every tumor, however, contains multiple subclones which compete for dominance and play a role in stage-progression and metastasis. Thus, to test whether tumor pseudolineages arise by a complex hierarchy of tumor cell differentiation or through the competition of individual state-biased clones, I investigated state-mixing in individual tumor clones.

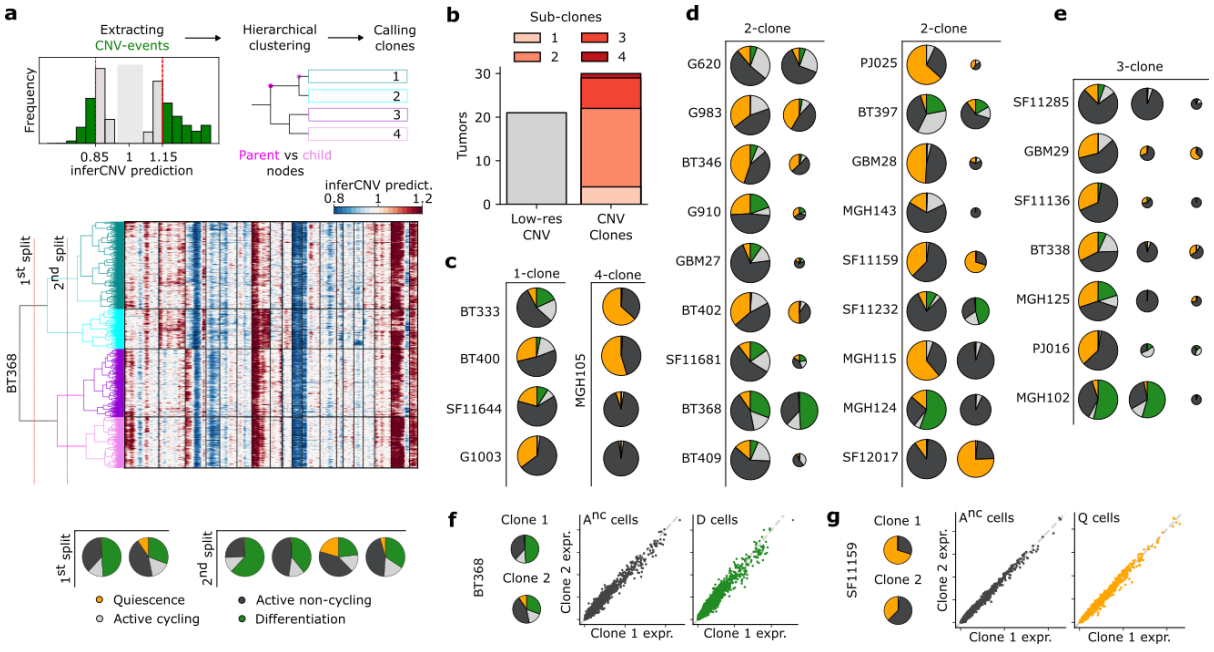

Figure 30: Limited QAD-stage variability in glioblastoma CNV clones. a) Schematic representation of clone assignment for BT368. CNV-events are determined by thresholding inferCNV predictions and used to compare parent vs. child nodes in the 1st and 2nd split of a CNV-based hierarchical clustering. b) Barchart depicting CNV-clones assigned per tumor. c) Proportion of QAD-stage and cycling cells per clone for tumors with 1 and 4 (c), 2 (d), or 3 (e) clones. Piechart size relates relative clone size. f) Gene expression in QAD-stage cells from two clones in BT368 (f) and SF11159 (g) as denoted by piecharts. Scatterplots depict mean log-normalized expression of pseudobulk QAD-stage cells per clone, for all expressed genes. A^{nc}: Activation-stage (non-cycling). Figure panels and legend were adapted from (Foerster et al., 2023).

Single-cell transcriptomics does not directly measure mutation information, yet in aggregate can provide an accurate view of copy-number variations (CNV) present in different cells (Serin Harmanci et al., 2020). Here, I used (*inferCNV of the Trinity CTAT Project.*, 2024) to identify tumor clones within my glioblastoma cohort, with the aim of comparing QAD-stage bias between clones and assessing inter-clonal expression differences which might reveal their origin from different tumor microenvironments. CNV calls across tumors exhibited the characteristic gain of chromosome 7 and loss of chromosome 10 frequently found in glioblastomas (Louis et al., 2021). To identify macroscopic tumor clones, I compared the incidence of high-confidence CNV-events in a hierarchical clustering of tumor cells' inferCNV profiles (Fig.30a). I applied heuristics over the frequency and direction of CNV events between parent or child nodes at the first and second split of the hierarchical clustering to assign between one and four clones per tumor (Fig.30b). In my glioblastoma cohort, I observed multiple QAD stages present in most tumors' clones (Fig.30c-e). This suggests that rather than the competition of individual state-biased clones, glioblastoma organization is driven by a hierarchy of differentiating cell states which is maintained even when CNV events occur. Clonal evolution is nevertheless necessary for tumor development and progression, and might lead to lineage plasticity over time as demonstrated in relapse and metastasis (Varn et al., 2022). This notion is consistent with the arguments for lineage constraint determining tumor plasticity as laid out in section 1.3.

To test whether individual tumor clones reflect distinct parts of the tumor environment, reflecting eg. infiltrating cells or cells in the tumor core (see section 1.2.2), I compared state-matched gene expression profiles among clones individual tumor clones. I observed no significant expression differences between QAD-stage cells in different tumor clones (Fig.30f-g), with no clear enrichment for genes ranked by expression difference (not shown). Taken together, and in accordance with several prior studies (Bhaduri, Di Lullo, et al., 2020; Chaligne et al., 2021; Tirosh et al., 2016; Venteicher et al., 2017), these results suggest that CNV is not a major source of intra-tumor pseudolineage heterogeneity.

2.7.3 Quiescent and not Differentiated cells are ubiquitous across glioblastomas

Tumor pseudolineages in the glioblastoma cohort were consistently dominated by Activation-stage cells, while Differentiation-stage cells appeared only in a subset of tumors (see Fig.28), suggesting these are not essential to sustain glioblastoma growth. Quiescence-stage cells, on the other hand,

were present in virtually every tumor (Fig.31a), suggesting that, in analogy to the healthy SVZ NSC lineage, it is the Quiescence-Activation and not the Activation-Differentiation transition which sustains glioblastoma growth. This observation supports the glioblastoma stem cell hierarchy proposed in (Lan et al., 2017) and is consistent with the noted role of quiescent cells in repopulating tumors upon treatment (Chen et al., 2012; Xie et al., 2022). This view of the glioblastoma lineage hierarchy challenges the conventional belief that Differentiation-stage cells constitute tumor stem cells while Quiescence-stage cells such as tumor astrocytes constitute a terminally differentiated population (Couturier et al., 2020; Neftel et al., 2019; Tirosh et al., 2016; Venteicher et al., 2017). These beliefs align with a developmental view of the glioblastoma hierarchy and stem from historic associations of stem-like populations with cycling cells (Singh et al., 2004; Verhaak et al., 2010) (Fig.31b). However, mounting evidence including the neurogenic potential of common brain astrocytes (Magnusson et al., 2014, 2020) as well as tumor cell barcoding (Lan et al., 2017; Larsson et al., 2021), phylogenetic reconstruction (Muskovic et al, personal communication), and my own analysis of healthy (section 2.2.2) and tumor (section 2.6) transcriptomics, support an adult view of the glioblastoma lineage hierarchy.

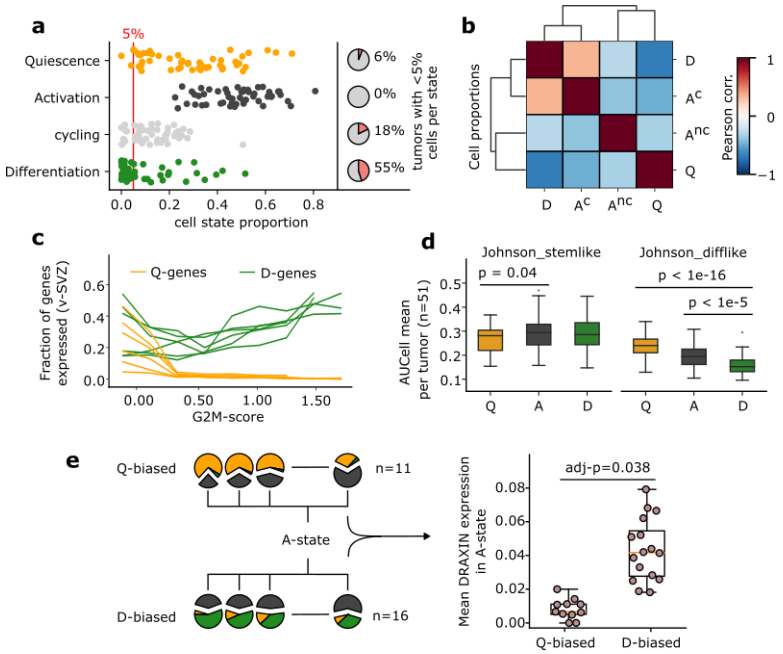

Figure 31: Stem- and Differentiated-cell nomenclature in QAD- and published glioblastoma gene signatures. a) Proportion of QAD-stage cells in 51 primary glioblastomas. Piecharts denote proportion of tumors with <5% cells in each cell stage. b) Correlation heatmap of QAD-stage cell proportions across 51 primary glioblastomas. c) Fraction of expressed genes from Q- and D-stages plotted against G2M score for the six individual replicates of the SVZ NSC reference lineage. d) Mean AUCell score per tumor of the stem- and diff-like signatures from (Johnson et al., 2021) subset by QAD-stage. Boxplots depict interquartile-range with outliers. e) Comparison of expression levels in Activation-stage cells of Quiescence- and Differentiation-biased tumors indicates that DRAXIN is significantly enriched in D-biased tumors.

Viewing glioblastoma hierarchy as paralleling the adult NSC lineage clarifies that Differentiation-stage cells are coupled to cell cycle because they are its product rather than its catalyst. In the SVZ NSC lineage, Differentiation genes manifest during cell cycle while Quiescence-stage expression programs (Fig.31c), which constitute the stem cell population in this case (Lim & Alvarez-Buylla, 2016), are shut off prior to cell cycle entry. This notion is supported in glioblastomas by orthogonal experiments in (Sabelström et al., 2019) which demonstrate that unlike Quiescence-stage cells, Differentiation-stage cells are unable to induce growth of secondary tumors. Taken together, these data challenge prevailing assumptions in the gliomas field which assign stem-like status to Differentiation-stage cells, exemplified here through gene set scoring of the pan-glioma signatures from (Johnson et al., 2021) (Fig.31d). Thus, an updated view of glioblastomas rooted in Quiescence-stage cells places these cells at the forefront of tumor organization, unveiling novel treatment opportunities. This is a prime example of how the direct comparison of GBM and NSC cellular hierarchies via ptalign can enhance our understanding of tumor processes by leveraging the wealth of contextual knowledge available from NSCs.

The incomplete presence of Differentiation-stage cells in glioblastomas also presents an opportunity for tumor stratification. I used the ubiquitous presence of Activation-stage cells across glioblastomas as a means to assess lineage potential by comparing Activation-stage transcriptomic determinants of Quiescence- or Differentiation-stage-biased tumor pseudolineages. This revealed the secreted Wnt antagonist `DRAXIN` (Hutchins & Bronner, 2018) as a reliable predictor of tumor pseudolineage (Fig.31e), highlighting the pivotal role Wnt signaling plays in regulating tumor cell plasticity and supporting its use as a pseudolineage-predictive biomarker.

2.7.4 Patient stratification by glioblastoma pseudolineage informs clinical outcomes

A major axis of variation between glioblastoma pseudolineages exists in the relative frequencies of Quiescence- and Differentiation-stage cells. I determined that this distinction is marked by the presence of `DRAXIN` in Activation-stage cells, and next set out to assess its impact on individual patient outcomes. Unfortunately, clinical metadata are not frequently published together with single-cell datasets, and I instead turned to the clinically annotated cohorts of `IDH`-wildtype

glioblastomas from The Cancer Genome Atlas (TCGA) (Verhaak et al., 2010) and published in (Wu et al., 2020) (Fig.32a).

In total, I compiled 399 glioblastoma samples: 343 from TCGA sequenced by microarray and RNA-seq (compiled by Ahmed Sadik), and 56 RNA-seq samples from (Wu et al., 2020). To identify clinical correlates of tumor pseudolineage, I aimed to use bulk deconvolution to quantify the contribution of QAD-stage cells in each sample. In previous work with bulk samples, Verhaak and colleagues had introduced the so-called mesenchymal (Quiescence) and proneural (Differentiation) tumor types but failed to identify a significant link to patient survival (Verhaak et al., 2010). I reasoned that this could be improved by using the collective single-cell transcriptomes of glioblastoma QAD-stages to direct bulk sample deconvolution. Thus I derived a GBM-QAD gene set analogous to the SVZ-QAD gene set (section 2.2.2). I selected genes with stage-specific expression among glioblastoma cells and screened their stage-specificity in the SVZ NSC lineage atlas (Fig.32b), finally establishing a 271-gene GBM-QAD gene set (Table 2) by thresholding in QAD-stage log fold-changes from DEseq. I similarly derived a 92-gene cell-cycle gene set. Around one third of the GBM-QAD genes were contained in the SVZ-QAD gene set (Fig.32b). Consistently, GBM-QAD stage genes were enriched for functionally relevant categories (not shown), supporting their use in the deconvolution of bulk glioblastoma samples.

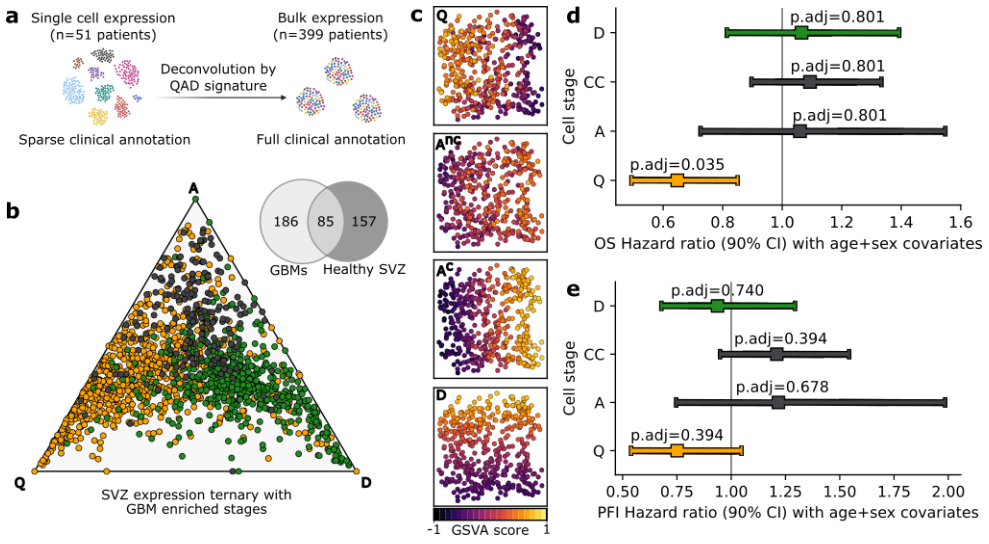

Figure 32: Glioblastoma Quiescence signature is predictive of positive patient outcomes. a) Schematic depiction of extrapolating scRNA-seq data to fully annotated bulk TCGA samples using a GBM-QAD signature. b) Selected QAD-stage enriched genes from glioblastoma samples plotted in a ternary based on their enrichment in QAD-stages of the reference SVZ NSC lineage. Inset Venn diagram depicts quantitative overlap between GBM-QAD and SVZ-QAD gene sets. c) Bulk glioblastomas nonparametric GBM-QAD scoring by GSVA in 2D-PCA scatterplots of QAD-stage scores, respectively. d) Predicted hazards and 90% confidence intervals from a Cox proportional hazards model with age and sex covariates of overall survival by bulk GBM-QAD signature score from (b) for overall survival (d) and progression free interval (e), with

associated model p-values. A^{nc}: Activation-stage (non-cycling); CC, A^{c}: cell cycle. Figure panels and legend were adapted from (Foerster et al., 2023).

Deconvolution of bulk samples has gained attention since the advent of single-cell RNA-sequencing, with numerous methods introduced (reviewed in (Avila Cobos et al., 2020; X. Wang et al., 2019)) to enable their retroactive study. However, many of these methods are unable to generalize to the multi-modal RNA and microarray glioblastoma samples I compiled from TCGA and (Wu et al., 2020). Instead, I leveraged the non-parametric and unsupervised approach implemented in GSVA (Hänzelmann et al., 2013) to score tumor samples by GBM-QAD and cycling genes and estimate their cell state composition. I compiled GSVA scores for pseudobulk scRNA-seq datasets from my glioblastoma cohort and bulk samples that remained after excluding recurrent, treated, or otherwise low quality samples. These scores were projected into two dimensions by PCA (Fig.32c) which arranged samples according to QAD-stage composition, with a Quiescence-Activation axis in PC1 and PC2 capturing Differentiation. Encouragingly, scRNA-seq samples were organized in accordance with their ground-truth pseudolineages in this embedding, suggesting that nearby bulk samples would similarly cluster by pseudolineage. This approach to bulk deconvolution using non-parametric gene set scoring by GSVA presents an effective way to infer pseudolineages from multi-modal tumor samples.

Leveraging the clinical data available from the deconvoluted bulk sample QAD-stage composition in a Cox model accounting for patient sex and age revealed a significant association between higher Quiescence scores and increased patient survival (Fig.32d). Notably, the protective effects of increased Quiescence surpassed the detrimental effects of Activation and cycling, which was also evident for progression-free intervals (Fig.32e). Taken together, these data support the stem-like properties of Quiescence-stage cells in glioblastoma, highlighting the increased importance of the Quiescence-Activation over the Activation-Differentiation transition in sustaining glioblastoma growth. Consistently, patients whose tumors comprise a Quiescence-enriched pseudolineage are likely to have different disease progression and survival outcomes than patients with a Differentiation-enriched tumor, supporting the use of `DRAXIN` as an actionable biomarker.

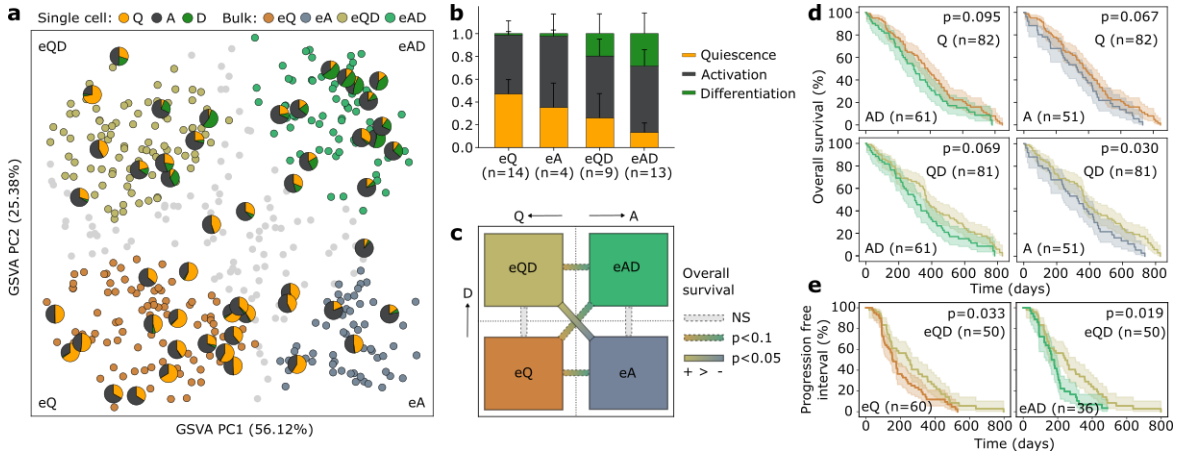

Figure 33: The Quiescence-Activation transition plays a central role in determining patient outcome. a) GBM-QAD signature scores in GSVA PCA overlaid with ptalign QAD-stage piecharts for 51 primary glioblastomas. Four groups of glioblastomas enriched (e-) by stage are colored, making up eQ, eA, eQD, and eQD classes. b) Mean proportion of QAD-stage cells per glioblastoma class among scRNA-seq samples. Error bars denote standard deviation. c) Pairwise overall survival for eQ,eA, eQD, and eQD glioblastomas. Comparison color gradients indicate better (+) and worse (-) survival quadrants, respectively. d) Pairwise overall survival for eQ,eA, eQD, and eQD bulk glioblastomas. e) Kaplan Meier curves depicting progression-free interval for eQD compared to eQ (left) and eAD (right) GBMs. Kaplan Meier significance was assessed by log-rank test with patients up to 95th survival percentile included. Figure panels and legend were adapted from (Foerster et al., 2023).

I next used the positions of the ground-truth scRNA-seq samples in the GSVA PCA to define four reference pseudolineages from which to guide the stratification of bulk patient samples. I assigned bulk samples to the nearest reference point using heuristics over the Euclidean distances between individual tumors. This way, I delineated four tumor classes each enriched (e-) in the predominant stages of their pseudolineage: eQ, eA, eQD, and eAD (Fig.33a). This labeling was supported by cell frequencies in scRNA-seq samples (Fig.33b). Consistent with the Cox regression above, evaluating patient survival by tumor class revealed that only those comparisons which span the PC1 Quiescence-Activation axis exhibited significantly different outcomes (Fig.33c), underscoring the significance of targeting the Quiescence-Activation transition to achieve positive patient outcomes. Indeed, pairwise comparisons of patient survival between tumor classes consistently indicated improved outcomes for eQD and eQ tumors (Fig.33d). Intriguingly, while eQD and eQ tumors exhibited similar survival outcomes, eQD tumors had significantly improved progression-free intervals over eQ tumors (Fig.33e). Thus while a Quiescence-biased pseudolineage generally improves prognosis, differentiating between a truncated (eQ) and complete (eQD) tumor pseudolineage additionally factors into clinical outcomes. In the case of eQD and eQ tumors, these outcomes could relate to functional differences between astrocytic and mesenchymal (MES-like) tumor cells which are commonly associated with immune-infiltration (Greenwald et al., 2023; Mossi Albiach et al., 2023; Ruiz-Moreno et al., 2022); both of which are considered among Quiescence-

stage cells in ptalign. Overall, these results demonstrate the utility of pseudolineage inference on a cohort of bulk glioblastoma samples, revealing principles of tumor organization which delineate patient outcomes and providing a contextual framework for their stratification.

2.7.5 Excursion: Comparison of published glioblastoma gene set classifications

Transcriptomic classification of glioblastoma subtypes has evolved with the technologies for its quantification, from initial bulk cohorts measured in (Phillips et al., 2006; Verhaak et al., 2010), to methylation subtypes characterized in (Ceccarelli et al., 2016; Noushmehr et al., 2010) and the multitude of tumor cell states revealed through single-cell approaches (Garofano et al., 2021; Johnson et al., 2021; Neftel et al., 2019; L. M. Richards et al., 2021). Yet many of these studies arrive at similar conceptions of glioblastoma archetypes. In my own orthogonal approach, studying glioblastoma organization through the lens of the SVZ NSC lineage, I identified a major variation in glioblastoma subtypes through the presence of Quiescence- or Differentiation-stage cells (see Fig.28). Delineating glioblastoma organization along this axis has clear parallels to the mesenchymal and proneural tumors from (Verhaak et al., 2010), while the underlying cell stages are clearly related to AC- and NPC-like states from (Neftel et al., 2019) (see section 1.2.2). Thus, to investigate to what extent these different views of glioblastoma converge on a coherent set of underlying factors, I conducted AUCell scoring of glioblastoma transcriptomic signatures from (Johnson et al., 2021; Neftel et al., 2019; L. M. Richards et al., 2021; Verhaak et al., 2010) on the 55 tumors in my glioblastoma cohort.

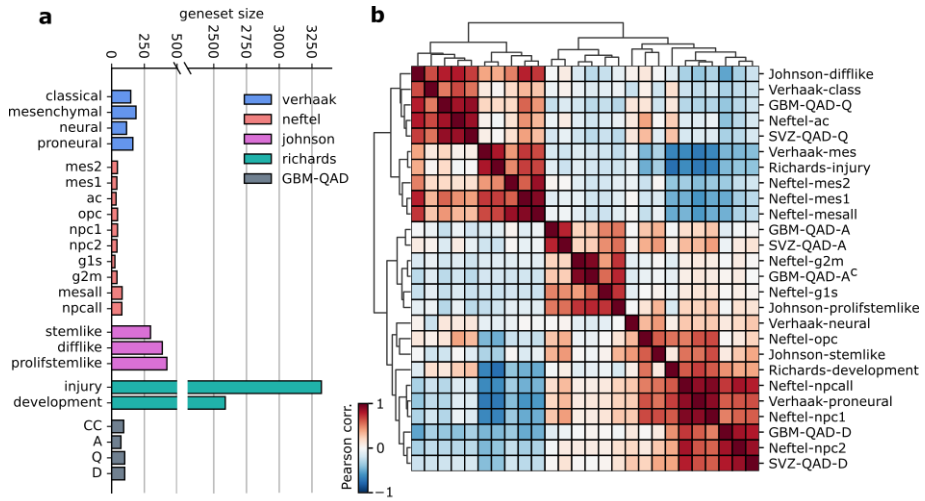

Figure 34: Comparison of published glioblastoma gene sets. a) Published glioblastoma gene sets by publication (color) arranged by gene set size. b) Correlation heatmap of published glioblastoma gene sets AUCell scores across 51 primary glioblastoma scRNA-seq datasets. CC, A^c: cell cycle.

In addition to the above mentioned signatures from (Verhaak et al., 2010) and (Neftel et al., 2019), I analyzed the so-called pan-glioma stem-like, diff-like, and prolifstem-like states from (Johnson et al., 2021) and the injury- and development-axis from (L. M. Richards et al., 2021). These signatures exhibited striking differences in gene set size, going from as few as 50 genes to thousands (Fig.34a). Though at this latter end I must question the utility of signatures which encompass a significant portion of the human proteome. Nevertheless, correlating AUCell scores across all 109.101 cells from my glioblastoma cohort resulted in a broad clustering of three cell state groups corresponding to QAD-stages (Fig.34b). This clustering highlighted shared similarities in astrocytic and mesenchymal signatures within a combined Quiescence cluster, consistent with the description of mesenchymal tumor cells as astrocytic cells affected by the presence of immune cells in their immediate environment (Mossi Albiach et al., 2023). Inspecting the Differentiation cluster, I noticed that the GBM-QAD Differentiation-stage signature exhibits lower correlation to the oligodendrocytic (OPC-like) signature from (Neftel et al., 2019) than Activation-stage signature, suggesting that oligodendrocytic tumor cells may be misclassified as Activation-stage cells in ptalign (see section 2.6.2.1). However, the classification of oligodendrocytic tumor cells may not be accurate, as these are only explicitly identified in (Neftel et al., 2019) and their functional or molecular properties not fully validated. This is supported by the OPC-like signature otherwise exhibiting broad correlation to neuronal signatures and the stem-like signature from (Johnson et al., 2021). This analysis furthermore highlights the semantic difficulties associated with the stem-like properties of neuronal (Differentiation-stage) cells (see Fig.31), as evidenced by the pan-glioma signatures from (Johnson et

al., 2021). Particularly the stem-like signature from (Johnson et al., 2021) correlates with neuronal and oligodendrocytic signatures as well as the Activation- and Quiescence-stage signatures, undermining the proliferative hierarchy outlined in that study. Taken together, these results highlight the convergence of transcriptomic signatures of glioblastoma cell states in three groups broadly corresponding to QAD-stages of the SVZ NSC lineage, further supporting the view of glioblastoma hierarchies through the lens of healthy lineage transitions as set forth in ptalign.

2.7.6 Methylome-based inference of glioblastoma pseudolineages using EPIC array

Pseudolineage inference on bulk transcriptomic glioblastoma samples from TCGA and (Wu et al., 2020) guided their separation into four tumor groups stratified by patient outcome. However, this approach contrasts with the clinical practice of using methylation arrays for the WHO classification of brain tumors (Capper et al., 2018), highlighting a gap between RNA-based patient stratification and its clinical implementation. Toward bridging this gap, a related study recently resolved the methylome profiles of SVZ lineage (eg. QAD) stages at single-cell resolution (L. P. M. Kremer et al., 2022) to reveal that various NSC lineage stages exhibit distinct methylation profiles, for example between SVZ astrocytes and qNSCs (see section 1.1.5). Combining this result with the noted overlap between glioblastomas and the healthy SVZ NSC lineage which is central to this work, I hypothesized that differences in QAD-stage proportions could be evident in bulk tumor methylomes. Thus, to enable efficient patient stratification and to facilitate the application of tumor pseudolineages in a clinical setting, I used 83 glioblastoma samples with matched RNA-seq and methylation data from the TCGA and (Wu et al., 2020) cohorts to demonstrate the feasibility of pseudolineage inference from tumor methylomes (Fig.35a).

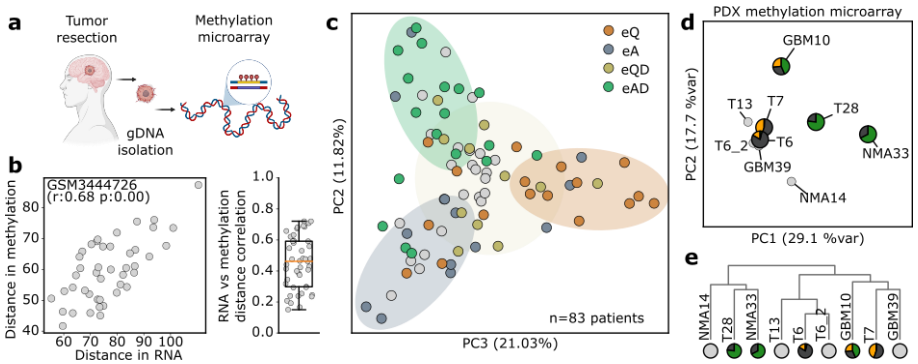

Figure 35: Bulk glioblastoma methylomes recapitulate tumor pseudolineages. a) Schematic depiction of gDNA isolation and bulk methylation quantification by Illumina 450k and EPIC 850k methylation microarrays. b) Inter-tumoral euclidean distances in methylation- and RNA-modalities for selected tumor (left) vs. other tumors; and correlation per tumor (right). c) PCA embedding of variable methylation sites in (n=83) glioblastomas with matched methylation and RNA profiling from. QAD-stage enrichments are underscored with transparent ellipses. d) PCA of methylation values from in-house PDX samples with matched QAD-stage proportions from scRNA-seq depicted in pie charts. e) Hierarchical clustering of variable methylation sites recapitulates pseudolineage structure from scRNA-seq depicted in pie charts.

Clustering all 83 methylome- and RNA-matched tumors by their methylation profiles revealed robust segregation by tumor pseudolineage. Consistently, comparing pairwise inter-tumoral distances in methylation and expression revealed these to be correlated between tumors (Fig.35b). PCA embedding of variable methylation sites separated alive and deceased patients on PC1 (not shown), while tumors segregated into QAD-stages along PC2-3 (Fig.35c). I additionally observed correspondence between bulk methylation profiles and tumor pseudolineage in nine in-house glioblastoma samples Oguzhan Kaya processed with the same methylation array technology (Fig.35d). Several of these tumors were used to generate PDXs and sequenced by Oguzhan and Milica Bekavac (Bekavac, 2022), and are elucidated further in section 2.8.5. Here, hierarchical clustering of these tumor methylomes highlighted the close correspondence between bulk methylomes and pseudolineages inferred from single-cell transcriptomics (Fig.35e). Together, these results reveal methylation as a conserved aspect of tumor biology which exerts a memory of its tissue-of-origin and is maintained despite malignant transformation. As methylation classically precedes and underlies transcription, the concordance of these modalities is consistent with the notion of lineage constraint directing the organization of tumor hierarchies. Further study of the methylome differences in developing and adult NSC lineages could provide valuable evidence to support a view of glioblastoma organization through adult NSC lineage dynamics. Similarly, the analysis of single-cell methylomes from QAD-stage glioblastoma cells is likely to reveal additional loci with variable methylation status across the tumor pseudolineage, which could lead to better patient stratification and could further illuminate fate-modulating factors which are active in tumor cells.

2.7.7 Pseudolineage prediction from bulk methylomes

Emboldened by the correlation between methylation and expression distances between tumors as well as their robust clustering by tumor pseudolineage, I next set out to quantitatively relate tumor methylomes to their transcriptomic pseudolineage stratification. Leveraging the 83 bulk glioblastoma samples with matched methylome and RNA-seq data, I identified several CpGs which clearly correlated with RNA GSVA scores (Fig.36a), and combined these with highly variable CpGs to train an sklearn ElasticNet model (Pedregosa et al., 2011) to predict GSVA scores on a 66/33 train-test split in a grid-search paradigm. An ElasticNet model was selected due to its feature selection capabilities, the interpretability associated with a linear model, and the robust performance of ElasticNet models in the face of large discrepancies in feature number (here >10.000) over sample count. Assessing the performance of the best grid-search model on the test data revealed a mean Pearson correlation of 0.70 across QAD- and cycling-stages (Fig.36b). Surprisingly, predictions of cycling scores had the lowest accuracy, while the most accurate predictions were made for Differentiation- and Activation-scores. This is in contrast to RNA-seq, where signal from cell cycle activity consistently dominates the weaker Activation-stage identity (see Fig.32). These results nevertheless demonstrate that tumor pseudolineages can be assessed from bulk methylomes, opening avenues for their application in patient stratification and disease monitoring.

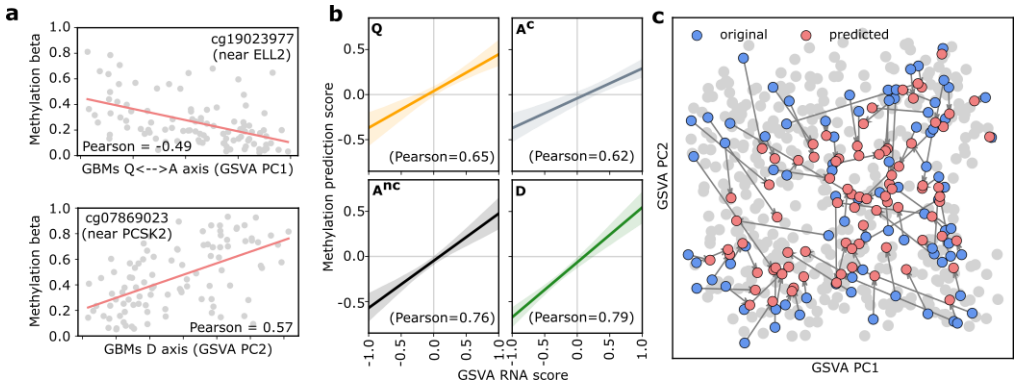

Figure 36: Pseudolineage prediction from bulk methylomes. a) Individual methylation CpGs exhibiting correlation to PC1 (left) and PC2 (right) of the GBM-QAD GSVA embedding. b) Regression and 90% CI on a (n=28) holdout set for ElasticNet predictions on methylation data, compared to RNA-based value from GSVA for GBM-QAD gene sets. Models were trained on a (n=55) tumor training cohort. Pearson correlations between truth and prediction are indicated. d) GSVA PCA of original GBM-QAD scores and predicted scores from ElasticNet regression in (c). Grey lines connect each original point with the position its predicted counterpart lands in the PCA. A^{nc}: Activation-stage (non-cycling); A^{c}: cell cycle.

Transforming ElasticNet GSVA score predictions back into the PCA-space used to stratify glioblastomas by tumor class (see Fig.33) highlighted the feasibility of predicting tumor pseudolineage from methylation, though predicted and true GSVA scores distributed unevenly in the resulting embedding (Fig.36c). I did not assess the classification performance of an ElasticNet aimed at predicting tumor class over RNA GSVA score. Nevertheless, this supports the application of an additional model to predict tumor class from the ElasticNet output in order to demonstrate clinical viability of this approach. This additional model could also access underlying methylome information to improve performance. Other interpretable models which could be used in this context include RandomForest or nearest-neighbor-based approaches. The use of the methylation-based PCA coordinate or weighting by PCA loading to improve predictions presents an interesting avenue for further study. Together with the robust clustering of glioblastoma methylomes by pseudolineage, these results indicate that tumor methylomes contain clear and sufficient signal for pseudolineage inference. The use of ElasticNets to predict RNA GSVA scores in this case serves to demonstrate the feasibility of this approach, paving the way for the clinical application of the insights into glioblastoma organization which are described in this work.

In sum, glioblastoma pseudolineages represent an effective means to assess heterogenous features which contribute to tumor organization and progression. Unlike naïve clustering techniques, a pseudolineage-based perspective of glioblastoma heterogeneity places tumors on a shared axis, faithfully recapitulating the underlying organizational principles and facilitating their comparison in that context. This includes the diversity of pseudolineage stages in CNV clones, the ubiquity of Quiescence-stage cells in glioblastomas, and the clinical significance of the Quiescence-Activation transition. Through pseudolineage inference on bulk tumor methylomes, I furthermore demonstrated the possibility to transfer these insights into the clinics for patient stratification and disease monitoring. Together and in light of the noted role of Wnt signaling in regulating it, the role of the Quiescence-Activation bears additional scrutiny in order to derive stage-specific interventions which can achieve improved patient outcomes.

2.8 Aberrant canonical Wnt signaling activity in glioblastoma pseudolineages

The Wnt signaling pathway plays a crucial role in regulating adult neurogenesis (Donega et al., 2022; Kalamakis et al., 2019; Seib et al., 2013), and is commonly disrupted in various tumors (Y. Lee et al., 2016; Steinhart & Angers, 2018), including glioblastomas. This pathway is closely linked to stem cell identity in the adult and developing brain, and my own investigation into the dynamics of a canonical Wnt reporter in the adult SVZ NSC lineage (see section 2.4) revealed that Wnt signaling is tightly regulated at Quiescence-Activation transition *in vivo*. Remarkably, precisely this Quiescence-Activation transition was critical for predicting patient outcomes from glioblastoma pseudolineages (see section 2.7.4). Considering the otherwise striking parallels between the adult NSC lineage and glioblastoma hierarchies, this suggests two possibilities: either Wnt signaling is conserved and contributes to the organization of glioblastoma cells into NSC-like hierarchies, or Wnt signaling pathways are disrupted and license the extended stem cell identity which fuels glioblastoma growth. To explore this hypothesis, Oguzhan Kaya and I turned to the `TCF/Lef::EGFP` canonical Wnt reporter described in section 2.4.1. As the following sections demonstrate, the latter hypothesis rings true, with canonical Wnt signaling notably disrupted at the Quiescence-Activation transition in glioblastoma pseudolineages. As we will see (in section 2.9), this observation reveals an important vulnerability in glioblastoma organization which Oguzhan and I exploited via the targeted modulation of Wnt signaling components. This divergence between glioblastoma biology and normal neurogenesis is evident already in an *in vitro* setting.

2.8.1 Glioblastoma cells do not display canonical Wnt activity in vitro

Prior to their use as patient-derived models of glioblastoma organization, Oguzhan cultivated T6 glioblastoma cells isolated from surgical resection under *in vitro* conditions (Kaya, 2023). Under these conditions, glioblastoma cells form spheres as they self-renew, resembling primary NSCs *in vitro* (Kaya, 2023). However, by transducing T6 cells with the `TCF/Lef::EGFP` genetic reporter of canonical Wnt signaling (Fig.37a), Oguzhan observed that these cells do not display canonical Wnt activity *in vitro* (Kaya, 2023) despite expressing various components of the Wnt signaling pathway (not shown). This was true in 2D spheroids (Fig.37b, left) as well as 3D cultures in a collagen matrix

(Fig.37b, right). While cells in the former are limited in their differentiation potential, collagen-embedded cultures exhibit distinct behaviors characteristic of different pseudolineage stages (Kaya, 2023), suggesting that the observed absence of canonical Wnt signaling activity does not affect the emergence of various tumor cell states. However, `Wnt3a` ligand, a strong simulator of canonical Wnt signaling activity (Kaya, 2023), was able to elicit reporter activity (Fig.37b, lower), indicating that T6 cells are able to respond to Wnt-dependent stimuli. Interestingly, stimulation by `Wnt3a` induced a migratory phenotype in some collagen-embedded T6 cells (not shown), suggesting that rescuing Wnt signaling activity could present a means to elicit coordinated functional changes in glioblastoma cells.

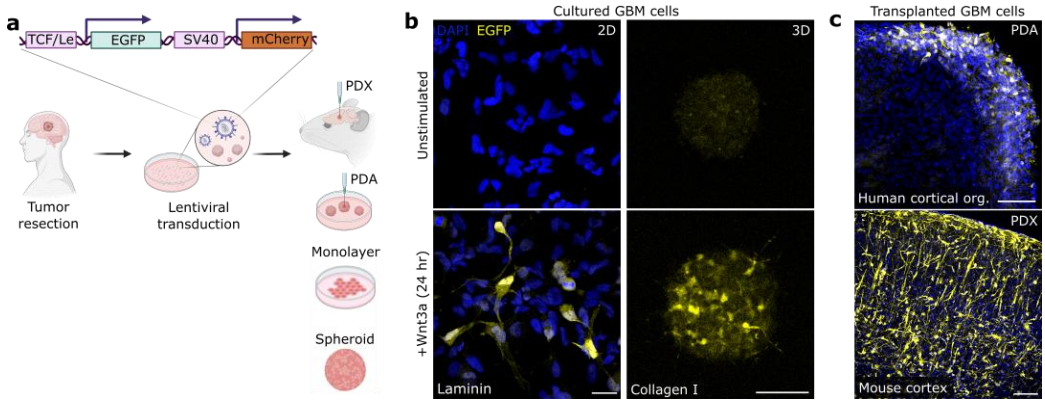

Figure 37: Glioblastoma cells do not display canonical Wnt activity *in vitro*. a) Schematic representation of conditions of T6 Wnt reporter measurements carried out by Oguzhan (Kaya, 2023). b) Wnt-reporter glioblastoma cells were cultured on laminin coated chambers (left; fixed, stained; scale bar, 25µm) or as 3D spheroids in collagen matrix (right; live, unstained). Images were acquired 24h post recombinant-Wnt3a treatment. Scale bar, 100µm. C) Wnt-reporter glioblastoma cells transplanted into HBOs (left, 10dpi) or mouse brains (right, 5mpi). Scale bars, 100µm. Figure panels and legend were adapted from (Foerster et al., 2023).

Contrary to their *in vitro* counterparts, T6 cells embedded in healthy tissues in PDX and PDA models exhibited consistently high levels of Wnt reporter activity (Fig.37c). Considering their diverse pseudolineages, this observation supports the notion that Wnt signaling may be involved in directing glioblastoma cell fates as in the SVZ NSC lineage. Extending this conclusion to T6 cells *in vitro*, where the ubiquitous presence of growth factors maintains most cells in the Activation stage, would explain their lack of canonical Wnt signaling activity in analogy to SVZ Activation-stage cells (see section 2.4.1). In this scenario, treating *in vitro* cultures of glioblastoma cells with Wnt ligands to stimulate canonical Wnt activity could phenocopy their transition to Quiescence or Differentiation stages where Wnt activity is high in SVZ NSCs (see Fig.19). This hypothesis remains unexplored as Wnt-stimulated *in vitro* cultures of T6 cells were not sequenced in this study. While the targeted

modulation of glioblastoma cell fates in this manner presents interesting therapeutic possibilities by eg. inducing Quiescence to elicit positive patient outcomes (see section 2.7.4), it does not explain the origin of the ligands which induce activation of the pathway *in vivo*.

2.8.2 Neuronal contacts promote Wnt activity in glioblastoma cells

The diverse environments of human cortical organoids present a unique opportunity to study the interactions between healthy and malignant cells which lead to the induction of canonical Wnt signaling activity in tumor cells. As described in section 2.5.1, Oguzhan transduced four human cortical organoids with T6 Wnt reporter glioblastoma cells, which he then sorted and sequenced by 10X genomics two weeks post injection. Leveraging Oguzhan's cell hashing strategy and his separation of reporter-positive and negative cells by sequencing lane (Kaya, 2023), I was able to reconstruct the fraction of reporter-positive tumor cells in each host organoid. This highlighted a high degree of inter-organoid variability in reporter-positive cells, ranging from 10% to 80% across replicates (Fig.38a-b). Comparing reporter-positivity to organoid cell type composition revealed a clear correlation between Wnt-active tumor cells and the number of neurons present in each organoid (Fig.38c). Conversely, I found a negative correlation between Wnt-active tumor cells and organoid radial-glia. Repeating this analysis for excitatory and inhibitor neurons only revealed a clear association between Wnt-active tumor cells and excitatory neurons, which was inverted for inhibitory neurons (Kaya, 2023) (not shown). Intriguingly, Oguzhan noticed that inhibitory neurons express several secreted Wnt antagonists including `SFRP1` (Fig.38d), suggesting that these cells might actively inhibit Wnt activation in nearby tumor cells. Individual PDA tumors exhibited consistent Wnt activity levels throughout QAD-stage pseudolineage cells, highlighting their failure to regulate Wnt signals at the Quiescence-Activation transition as healthy SVZ NSCs do (Fig.38e). These tumors did, however, exhibit small differences in Quiescence-stage cell proportions which anti-correlated with Wnt activity levels (Fig.38f), suggesting these could be related to Wnt modulation from inhibitory neurons. I also noted enriched proportions of reporter-positive cells in the Quiescence stage (Fig.38g), recapitulating the link between Wnt and Quiescence observed in SVZ NSCs (see Fig.21). Taken together, these results clearly demonstrate a neuronal origin for the induction of canonical Wnt signaling activity in glioblastoma cells.

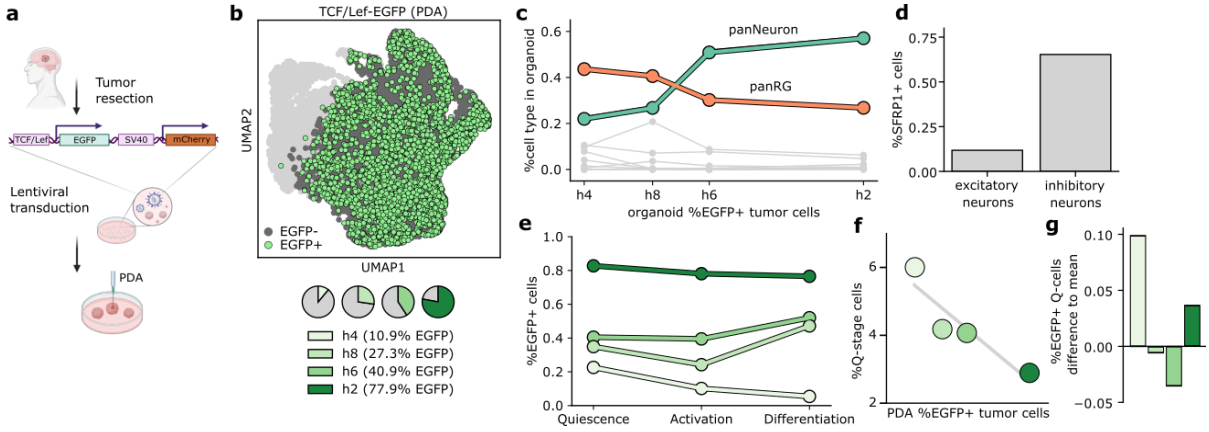

Figure 38: Glioblastoma Wnt activity levels depend on the composition and type of nearby healthy cells. a) Schematic representation of T6 PDA experiment, injecting T6 TCF/Lef Wnt reporter glioblastoma cells into human cortical organoids as described in Section 2.6.3. b) UMAP embedding of T6 PDA cells from `EGFP`+ and `EGFP`- conditions as resolved *in silico* by hashtag and sequencing lane. Total proportion of reporter-positive cells per replicate is given by the piecharts below. c) Type distribution among healthy organoids cells plotted against proportion of reporter-positive cells in T6 PDA replicates. The two major panNeuron and panRG cell types are indicated, the rest are colored gray. d) Proportion of `SFRP1`-expressing cells by empirical expression threshold in excitatory and inhibitory neurons from pooled organoids. e) Proportion of reporter-positive cells in QAD-stage cells of T6 PDA replicates. f) Relationship between proportion of Quiescence-stage cells and T6 PDA replicate reporter-activity. g) Enrichment of Quiescence-stage cell proportion compared to the average of QAD-stage reporter-positive cells per T6 PDA replicate.

To elucidate the spatial crosstalk between glioblastoma cells and those of a healthy mouse brain, Oguzhan processed several slices of a T6 PDX tumor for spatially resolved transcriptomics (SRT) by Resolve Biosciences. A detailed methodology for these experiments is outlined in (Kaya, 2023). This technology measures the spatial arrangement of a panel of QAD-stage and mouse cell type specific transcripts on the basis of RNA hybridization, which can then be overlaid with fluorescence images to extract additional insights (Fig.39a). For a more detailed overview, see (Foerster et al., 2023; Kaya, 2023). Here, computational analysis of SRT experiments was performed by Valentin Wüst, who provided data on segmented and transcript-assigned cells which I used for the subsequent analyses presented here and in section 2.9.

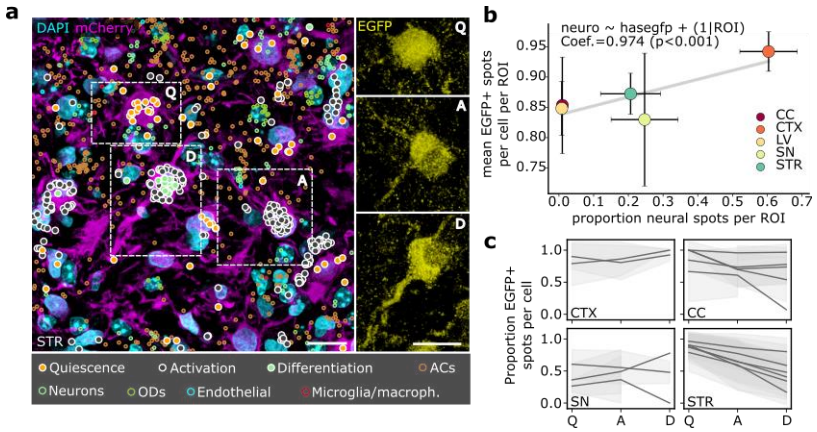

Figure 39: Spatial transcriptomics confirms pervasive Wnt activation in the presence of healthy neurons. a) Spatial transcriptomics (Resolve biosciences) ROI of QAD-stage cells in a T6 PDX brain. Left: striatal section of clustered cells from QAD-stages overlaid with DAPI and mCherry immunofluorescence. Tumor transcripts are colored by QAD-stage with a white outline; mouse transcripts are colored by cell type. Right: QAD-stage cells' EGFP fluorescence. Scale bars, 10µm. b) Proportion of mouse neuronal transcripts detected from n=6 ROIs for different brain regions, plotted against proportion of EGFP+ spots for cells in that same ROI. Errorbars in x- and y- axis denote the standard deviation in the measured quantity over (n=6) replicates, though not every region appears in every ROI. A linear model fit to determine the slope coefficient between proportion of neural spots and tumor cell EGFP+ spot proportion finds a highly significant positive association. c) Proportion of EGFP+ spots by QAD-stage for individual regions with >20 cells among spatial ROIs. Figure panels and legend were adapted from (Foerster et al., 2023).

By overlaying the pixel coordinates of transcript spots from the SRT experiment with their EGFP fluorescence intensity, I was able to clearly distinguish between reporter-positive T6 cells and the healthy mouse cell background (not shown). I assigned segmented tumor cells to QAD-stages based on transcript counts in a process similar to the AUCell assignments in section 2.6.2 (see Fig.25). This revealed Wnt-active tumor cells distributed across QAD-stages (Fig.39a) and brain regions. Comparing the incidence of neuronal transcripts with reporter-positive tumor cells in different brain regions confirmed my prior observation (see Fig.38) that tumor cell in proximity to healthy neurons engage in canonical Wnt signaling activity (Fig.39b). Due to the limited number of mouse genes included in the SRT transcript panel, I was unable to distinguish between excitatory and inhibitory neurons in this analysis. Nevertheless, these results highlight the cell type specific interactions which are present in different tumor environments. It remains to be explored whether the Wnt signaling activity induced by neuronal proximity affects QAD-stage transitions in tumor cells. However, the organization of T6 tumors into consistent pseudolineages in PDA and PDX models despite a high degree of variation in environment (see Fig.38) and Wnt signaling activity (Fig.39c) suggests that Wnt is not essential for stage transitions in glioblastoma.

2.8.3 Ventricular outgrowths do not exhibit Wnt activity in patient derived xenografts

The diffuse and infiltrative growth which is characteristic of glioblastomas (Louis et al., 2021) means that tumor cells will colonize disparate regions of the brain even in a PDX model. The T6 tumor, for example, rarely forms a monolithic tumor core, instead generating tumor cells which migrate eg. along the corpus callosum to invade distal regions of the brain (not shown). Thus the local environment of individual tumor cells is largely dependent on nearby healthy cells, with one notable exception: ventricular growths.

Infiltrating T6 cells will occasionally reach the ventricle and extravasate to colonize the ventricular cavity itself. This process brings with it two important advantages: uninhibited 3D expansion upon fleeing the crowded brain parenchyma, and escape from Wnt-inducing signals secreted eg. by neuronal cells as demonstrated above (see Fig.38). This leads to large ventricular growths comprised solely of tumor cells, which are completely void of canonical Wnt signaling activity (Fig.40a). Both of these features of ventricular growths parallel the characteristics of *in vitro* cultured glioblastoma cells (see Fig.37), plausibly explaining the poor prognosis associated with patients bearing ventricular tumors (Berendsen et al., 2019).

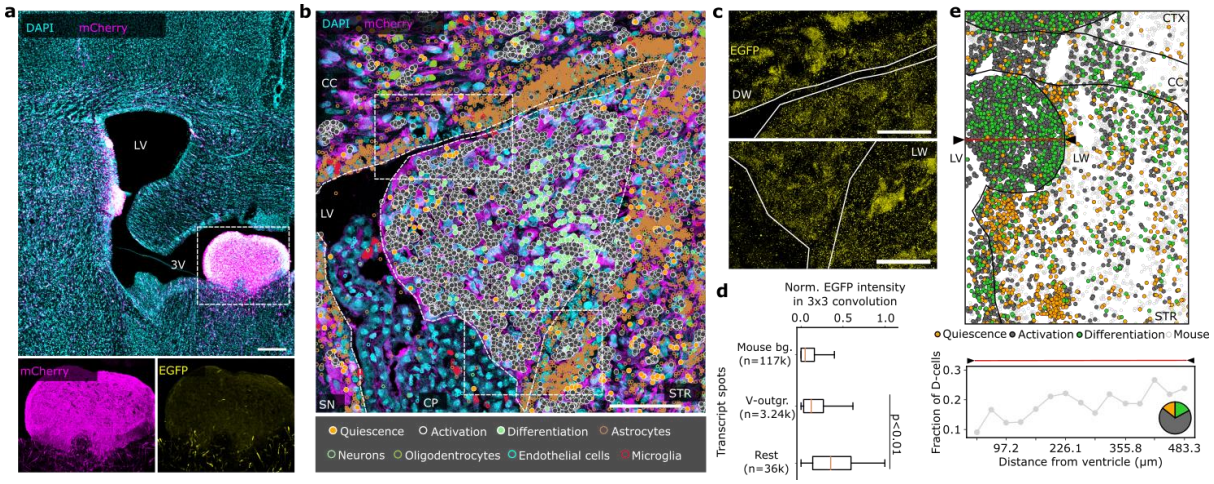

Figure 40: Ventricular growths are void of canonical Wnt signals and enrich in Activation-stage tumor cells. a) Immunofluorescence image of a T6 PDX tumor glioblastoma cells (`mCherry`) as a large ventricular growth in the third ventricle. Scale bar, 250µm. Insets highlight tumor cells devoid of Wnt activity, which is regained upon entry to the brain parenchyma.b) Wnt-reporter spatial transcriptomics ROI of a ventricular outgrowth. Transcriptomic markers are overlaid with DAPI and `mCherry` immunofluorescence. Tumor transcripts are colored by QAD-stage with a white outline, mouse transcripts are colored by cell type. Scale bar, 50µm. c) Contrasting `EGFP` fluorescence at dorsal- , and lateral-walls of the ventricle from (b). Scale bars, 25µm. d) Normalized `EGFP`-intensity for mouse background (bg.) and tumor cells within (V-outgr.) and outside (rest) the ventricular growth from (b). Significance was assessed by permutation test. e) Top: large ventricular growth in a non-Wnt-reporter spatial transcriptomics ROI with transcripts associated to segmented nuclei to assign species and QAD-stage. Red line traces largest extent from LW to LV. Bottom: increasing Differentiation-stage cell fraction with distance from ventricle. ENB: early neuroblast; LNB: late neuroblast; STR: striatum; RMS: rostral migratory stream; OB: olfactory bulb; AC: astrocyte; CC: corpus callosum; CTX: cortex; SN: septal nuclei; LV: lateral ventricle; CP: choroid plexus; DW: dorsal-wall; SW: septal-wall; LW: lateral-wall. Figure panels and legend were adapted from (Kaya, 2023).

Oguzhan's SRT experiments included a single Wnt-reporter ventricular growth which provided a means to study the organization of this unique tumor environment. I reconstructed QAD-lineage stages for cells in this sample (Fig.40b), noting the preference for Quiescence-stage cells to associate near the edges of the ventricle, while the ventricular growth itself was comprised of reporter-negative Activation- and Differentiation-stage cells (Fig.40c-d). This reflects the *in vitro*–like characteristics of the growth, where the high proliferation rate is reminiscent of a developing brain (Sanes et al., 2019), highlighting the semantic discrepancies between stem cell nomenclature in glioblastomas (see section 2.7.3). As pertains to the adult view of glioblastoma hierarchies, the Differentiation-stage cells in the ventricular growth are plausibly related to migrating neuroblasts of the SVZ NSC lineage, representing recently-born tumor cells which will exit the growth and invade into nearby brain regions. This view is consistent with the migrating tumor cells infiltrating the healthy brain parenchyma until their environment instructs their differentiation through canonical

Wnt signals, which is likely the case for healthy neuroblasts which migrate to colonize the OB (Rella et al., 2021). A second ventricular growth from a non-reporter T6 PDX confirmed these observations by organizing along an Activation-Differentiation gradient in the absence of canonical Wnt signaling activity (Fig.40e). These results support the notion that Wnt signaling is dispensable for glioblastoma organization, with the *in vitro*-like characteristics of ventricular growths suggesting that aberrant Wnt signaling licenses sustained tumor activation and growth.

2.8.4 Tight regulation of Wnt signaling at healthy stage transitions is lost in glioblastoma

Finally, to illuminate the mechanisms of aberrant Wnt signaling in glioblastomas, I compared TCF/Lef readouts of canonical Wnt activity in single-cell transcriptomes of T6 PDX and PDA tumors. Leveraging the index sorted PDX transcriptomes (see section 2.8.4), I observed reporter-positive cells distributed throughout the tumor UMAP, contrary to the clear stage-stratified canonical Wnt signaling activity observed in the healthy SVZ NSC lineage (see section 2.4.1). This was confirmed through the proportion of reporter-positive cells among individual QAD-stages in PDX and PDA tumors (Fig.41a-b), which revealed that the tight regulation of canonical Wnt signaling at the Quiescence-Activation transition *in vivo* was lost in glioblastoma. A similar result was achieved in the SRT data, highlighting extensive reporter-activity in Quiescence-, Activation-, and Differentiation-stage cells (Fig.41c) in contrast to their healthy counterparts (see Fig.19). Indeed, stratified by pseudolineage stage, a consistent enrichment of tumor transcripts in reporter-positive cells emerged across QAD-stages (Fig.41d) and brain regions (Fig.41e). Thus, T6 glioblastoma is characterized by aberrant Wnt signaling at the crucial Quiescence-Activation transition which plays a significant role in determining patient outcomes (see section 2.7.4).

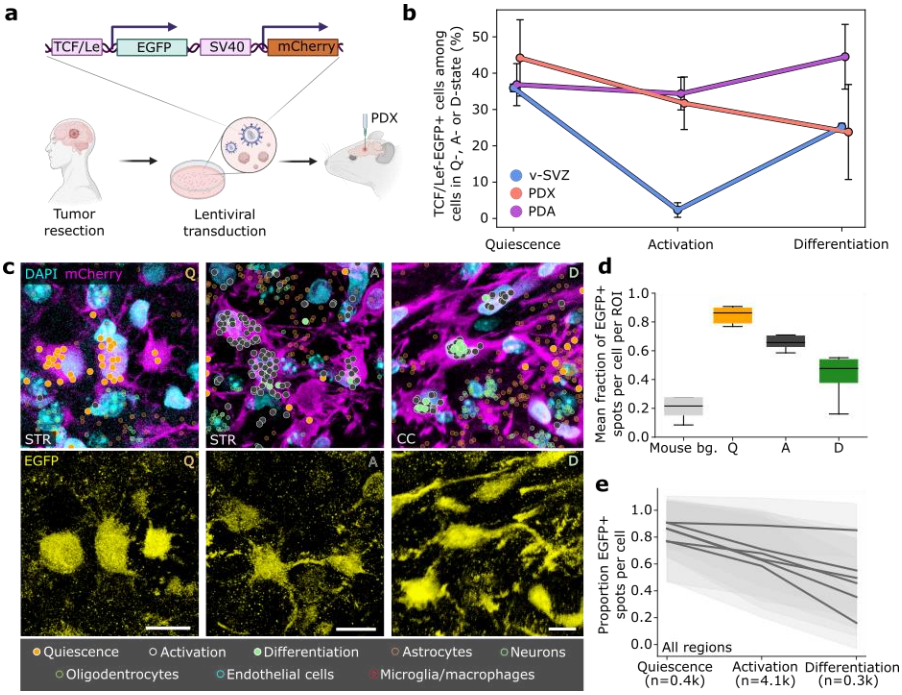

Figure 41: T6 glioblastoma cells fail to regulate canonical Wnt signaling at the Quiescence-Activation transition. a) Schematic depiction of the TCF/Lef reporter constructs used to measure canonical Wnt activity in SVZ NSCs as well as in PDX and PDA tumors. Note that the SVZ reporter was H2B-EGFP. `mCherry` ubiquitously labels tumor cells. b) TCF/Lef reporter activity quantified in QAD-stage SVZ NSCs (n=5 replicates of SS3, see Section 2.4.2) and T6 PDX (n=4 replicates of SS3, see Section 2.6) and PDA (n=4 replicates of 10X, see Section 2.6.3) cells. Reporter activity was quantified by FACS and QAD-stage by scRNA-seq. Errorbars represent standard deviation in the normalized Wnt active cell-proportion. c) Selected Q (left), A (center), and D (right) cells in spatial transcriptomics with transcripts overlaid with DAPI and `mCherry` (top) or `EGFP` (bottom) immunofluorescence. Scale bars, 10µm. d) Mean fraction of EGFP+ spots for mouse and QAD-stage cells in n=6 spatial transcriptomics ROIs. e) Proportion of `EGFP`+ spots by QAD-stage for all regions with >20 cells among spatial ROIs. STR: striatum; CC: corpus callosum. Figure panels and legend were adapted from (Kaya, 2023).

The mechanisms which enable glioblastoma cells transitioning the Quiescence-Activation stages to retain high levels of canonical Wnt signaling activity, when this same transition is so tightly regulated in the healthy lineage, remain to be explored. Closer study of the Wnt-low Activation-stage cells from ventricular growths could inform the functional differences which underlie this transition in the presence or absence of Wnt signals, however these cells are currently not identifiable from single-cell transcriptomes alone. This could be remedied in future datasets through targeted surgical resection of glioblastoma cells from ventricular growths, or by labeling and sorting these populations from a PDX model. Together, these results reinforce the notion that Wnt signaling is tightly related to stem cell identity *in vivo*, while this regulation is lost in order to license the sustained stem cell properties which support the growth of brain tumors. Intriguingly, T6 cells exposed to varying environments responded with different levels of canonical Wnt signaling activity (see Fig.38) without affecting their pseudolineage, suggesting that while cells are capable of responding to external Wnt stimuli, they have lost the ability to translate such signals into functional cellular behaviors. Thus,

whether Wnt signaling remains a promising target for modulating tumor fate, ie. consistent with the induction of migratory phenotypes upon Wnt stimulation *in vitro*, depends on the prevalence of aberrant Wnt signaling dynamics across glioblastoma patients – an endeavor currently limited by the time-consuming process of generating Wnt-reporter cell lines.

2.8.5 Excursion: Wnt reporter quantification in diverse patient PDXs

Concurrent to the T6 PDXs, Oguzhan and his student Milica Bekavac generated three additional Wnt-reporter lines from in-house patient lines: GBM10, T28, and NMA33. Experimental details from the generation and sequencing of these lines as well as associated metadata are available in (Bekavac, 2022). Through imaging xenografted brains from these tumors, Milica identified three distinct organizational patterns characterized by infiltrative, cystic, or compact growth (Fig.42a). Each of these tumors in turn exhibited reporter-positive cells (Fig.42b, lower), and cells from each were sequenced by SS3. Upon their ptalign pseudotime alignment with the SVZ NSC lineage reference from section 2.2, I found that two of the three tumors (T28 and NMA33) failed to pass the ptalign permutation thresholds (Fig.42c). This may suggest that these samples constitute other brain-invading entities such as metastases from an as-of-yet undiscovered primary (M. S. Lee & Sanoff, 2020). These tumors were characterized by low and high levels of reporter activity, respectively, pointing to the dynamic role of Wnt signaling in different contexts. Despite their presumed origins outside of the brain, these tumors remain a useful cohort against which to contrast insights into glioblastoma organization and the disparate roles of Wnt signaling in health and disease.

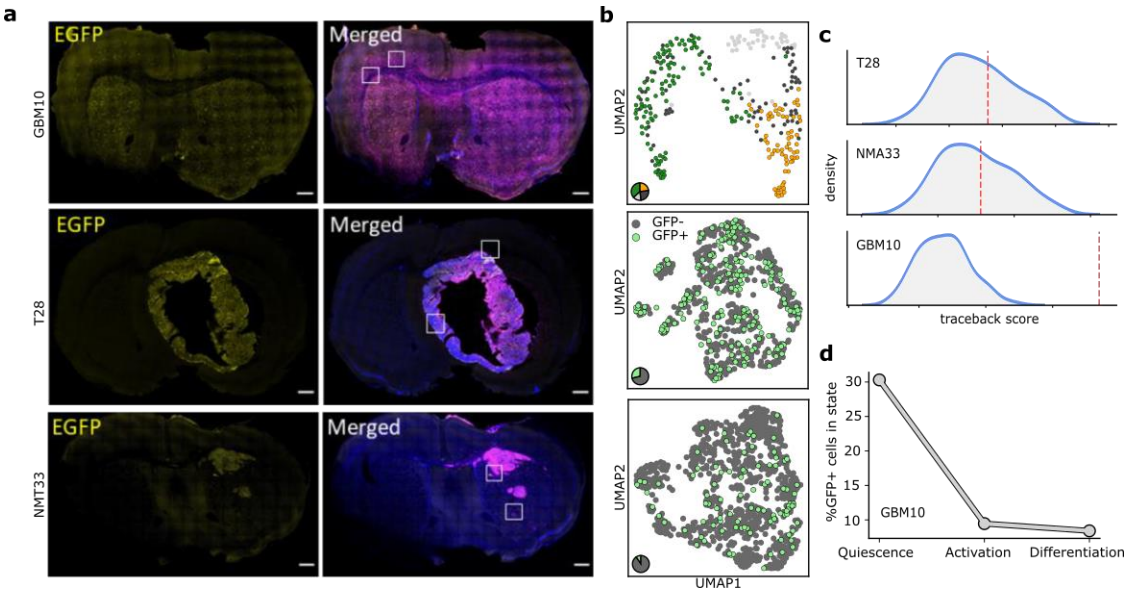

Figure 42: Wnt reporter activity in the growth of three additional glioblastoma PDXs. a) Representative immunohistochemistry images of xenograft tumors from (Bekavac, 2022). Coronal sections were taken and stained for mCherry, EGFP, and DAPI. b) UMAP embedding of QAD-stage cells in GBM10 (top) and reporter-active cells sorted from FACS (lower two). Inset pie charts denote proportion of QAD-stage and reporter-positive cells, respectively. c) Traceback scores from 100 permuted ptalign pseudotimes, true QAD-gene traceback score is shown in red. d) Proportion of reporter-positive cells among QAD-stage cells in (n=1) replicate of the GBM10 tumor.

The GBM10 tumor, however, which had a presentation and morphology very similar to the T6 tumor, was assigned a significant pseudolineage with clear separation of QAD-stage cells (Fig.42c). The GBM10 UMAP contained a particularly clear lineage trajectory through QAD stages, motivating its further study to resolve their ordering, for example through RNA velocity. As in T6, GBM10 Quiescence-stage cells were frequently Wnt-active (Fig.42d), an observation consistent with SVZ NSCs (see Fig.21); however, unlike T6, the GBM10 pseudolineage exhibited a drastic reduction in reporter-activity at the Quiescence-Activation transition consistent with the healthy SVZ NSC lineage. This suggests that Wnt signaling dynamics may be intact in GBM10, however whether and how this tumor responds to Wnt stimulation was not assessed in this study. These results underscore the heterogeneous nature of glioblastomas, revealing the diverse paths to malignancy despite their similar features as determined by lineage constraint.

In sum, glioblastomas tend to be insensitive to canonical Wnt signals, an observation contrary to the tight regulation of Wnt signals at the Quiescence-Activation transition in SVZ NSCs. This suggests that aberrant Wnt regulation could be one way glioblastomas license the extended stem cell identity which fuels their growth. Curiously, tumor cells did respond to stimulation by Wnt signals *in vitro*,

and there is a consistent association between canonical Wnt signals and cellular Quiescence. Indeed, tumor cells demonstrate upregulated reporter levels when in the viscinity of healthy neurons, though this did not affect their pseudolineage except the relatively minor effect of SFRP1-secreting inhibitory neurons on increased Quiescence in one of the T6 PDA replicates. Ventricular growths appear to confirm this association between Wnt and Quiescence, though from the opposite end: as these growths exhibit neither Wnt signals nor Quiescence-stage cells. The regulatory environment and cellular processes which govern the growth and migration within this exceptional organ remains to be elucidated. Taken together, contrasting the central role of Wnt signals in regulating stem cell identity *in vivo*, and the loss of associated regulation in the T6 glioblastoma, motivates the targeted modulation of Wnt signaling to direct tumor fates, consistent with the external determinants of tumor Wnt signals described above.

2.9 Directed modulation of glioblastoma pseudolineages by intervention in the Wnt signaling pathway

Viewing tumors as cellular hierarchies recapitulating the development of an organ within an organ provides important context for understanding the organization and dynamics that drive tumor growth and regeneration. In the present case, my pseudolineage-based study of glioblastoma hierarchies through the lens of healthy SVZ stem cells revealed the essential role of the Quiescence-Activation transition in fueling tumor lineages and affecting patient outcomes (see section 2.7.4). Building from the healthy SVZ lineage context where Wnt signaling is tightly regulated at this transition (see section 2.4), I found its regulation to be disrupted in glioblastomas (see section 2.8.4). Despite evidence suggesting that Wnt is dispensable for stage transitions in tumors (see Fig.38), lineage constraint maintains that tumors will be able to respond to specific Wnt stimuli regardless if parts of the pathway have been compromised. Thus, to disrupt tumor organization and progression, Oguzhan Kaya and I leveraged our unique perspective of tumor dynamics to achieve targeted modulation tumor pseudolineages by intervening in the Wnt signaling pathway. This approach highlights the advantages of understanding tumor organization through the lens of healthy transitions, enabling the systematic identification of tumor vulnerabilities and the design of treatments targeting them.

2.9.1 Excursion: Consistent tumor pseudolineages despite systemic Wnt inhibition by LGK974

Employing a genetic reporter of canonical Wnt signaling activity in various glioblastoma models (see section 2.8), Oguzhan and I repeatedly observed an association between Quiescence-stage tumor cells and increased canonical Wnt signaling activity. These cells play an essential role in fueling tumor growth and frequently evade targeting by conventional therapies, leading to inevitable recurrence (Chen et al., 2012; Xie et al., 2022). Consequently, targeting this population, for example by inducing their activation and making them amenable to eradication through conventional alkylating agents like temozolomide (TMZ) (Stupp et al., 2005), could lead to more effective and lasting treatments. Particularly the T6 tumor exhibited dysregulated signaling by maintaining high levels of canonical Wnt activity at the Quiescence exit, in contrast to healthy cells (see section 2.8.4).

Thus, Oguzhan and I hypothesized that by inducing a reduction in Wnt signaling activity analogous to the strong downregulation observed in healthy cells, these cells might respond by transitioning to the Activation-stage. For the T6 tumor, this approach held the added benefit of phenocopying the lack of Wnt activity observed in *in vitro* cultured cells (see Fig.37) and ventricular growths (see Fig.40), both of which were composed of Activation-stage cells. To this end, Oguzhan orally administered the PORCN inhibitor LGK974, which inactivates Wnt ligands by inhibiting their palmitoylation (J. Liu et al., 2013), in T6 PDX mice (Fig.43a). This was followed by sorting and sequencing T6 as described previously (see section 2.6).

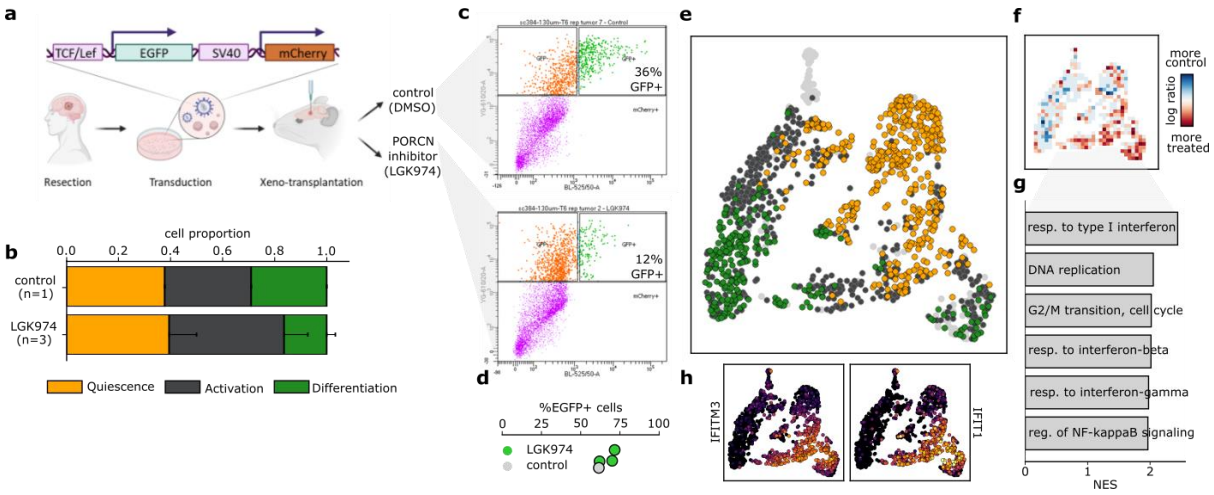

Figure 43: Canonical Wnt inhibition by LGK974 fails to modulate tumor pseudolineages. a) Schematic depiction of the T6 Wnt reporter PDX experiment with two treatment groups: control and inhibitor. b) Proportion of QAD-stage cells measured in three replicates of LGK974-treated and one replicate of control PDXs. Error bars denote standard deviation. c) Proportion of EGFP+ cells measured in FACS gating by Oguzhan for a control (top) and inhibitor (bottom) treated sample. d) Proportion of EGFP+ cells in sequenced PDXs from (b). These plates may have been gated on GFP activity, invalidating this panel. e) UMAP embedding of integrated PDXs from (b), colored by QAD-stage. Cycling cells are depicted in gray. f) Cell frequencies by condition measured in a grid mesh overlaid on the UMAP from (e), with the log ratio of control or inhibitor-treated cells depicted. g) Selected GO-terms from GSEA of genes ranked by enrichment in the inhibitor-specific cluster from (f). h) Expression levels of two interferon-related marker genes in the UMAP embedding from (e).

As with previous PDXs, Oguzhan sequenced one plate each of cells from three replicates of inhibitor-treated and one replicate of Wnt-reporter tumors. These tumor's pseudolineages were replicated between treatments, with the largest difference in Differentiation-stage cells (Fig.43b). While Oguzhan observed a reduction in reporter activity in treated animals in FACS (Fig.43c), reconstructing FACS measurements in the sequenced cells by index sorting revealed these to have consistent levels of reporter activity between conditions (Fig.43d). Thus the reduced frequency of Differentiation-stage cells in treated PDXs is not explained by varying levels of Wnt activation.

Integrating cells between replicates revealed the existence of a treatment-specific cluster (Fig.43e-f) which indicated that Wnt inhibition induced an interferon-dependent response in tumor cells (Fig.43g-h). These results underline my previous conclusions regarding the insensitivity of T6 cells to varying levels of Wnt activity, as these will consistently produce identical pseudolineages as seen here. While a treatment-specific cluster did emerge, the cells within arranged by QAD-stage and did not affect the overall tumor pseudolineage. This could be due to the limited penetrance of the LGK974 inhibitor into brain tissues when given orally, leading only to transient or incomplete Wnt inhibition at the target site. Overall, these results highlight the inefficiencies associated with broad spectrum approach, while the targeted modulation of tumor pseudolineages requires a more precise understanding of the state of Wnt signaling in human glioblastomas.

2.9.2 Identification of dysregulated Wnt signaling components in ptalign pseudotimes

Transitioning from macro-level investigations of Wnt reporter activity to a detailed view of individual pathway elements, I turned to the systematic comparison of expression dynamics in ptalign pseudotimes of my 55-glioblastoma cohort (see section 2.7.1) to identify recurrently dysregulated Wnt signaling components. This approach leverages the fact that ptalign pseudotimes, being based in the reference lineage pseudotime, reproduce the same underlying dynamics for each aligned tumor sample (see section 2.1.3). Consequently, for a given pseudotime, eg. 0.1, reflecting a Quiescence-stage cell, different tumor and healthy cells bearing the same pseudotime will exhibit similar functional properties and expression. This provides a means to conduct controlled comparisons of expression dynamics between individual tumors (tumor-tumor) and to the healthy reference (tumor-healthy), which is a unique advantage of ptalign. Here, I employ this approach to single out recurrently dysregulated Wnt pathway components by comparing the expression profiles of 37 Wnt-pathway genes from the SVZ NSC lineage to the 55-glioblastoma cohort.

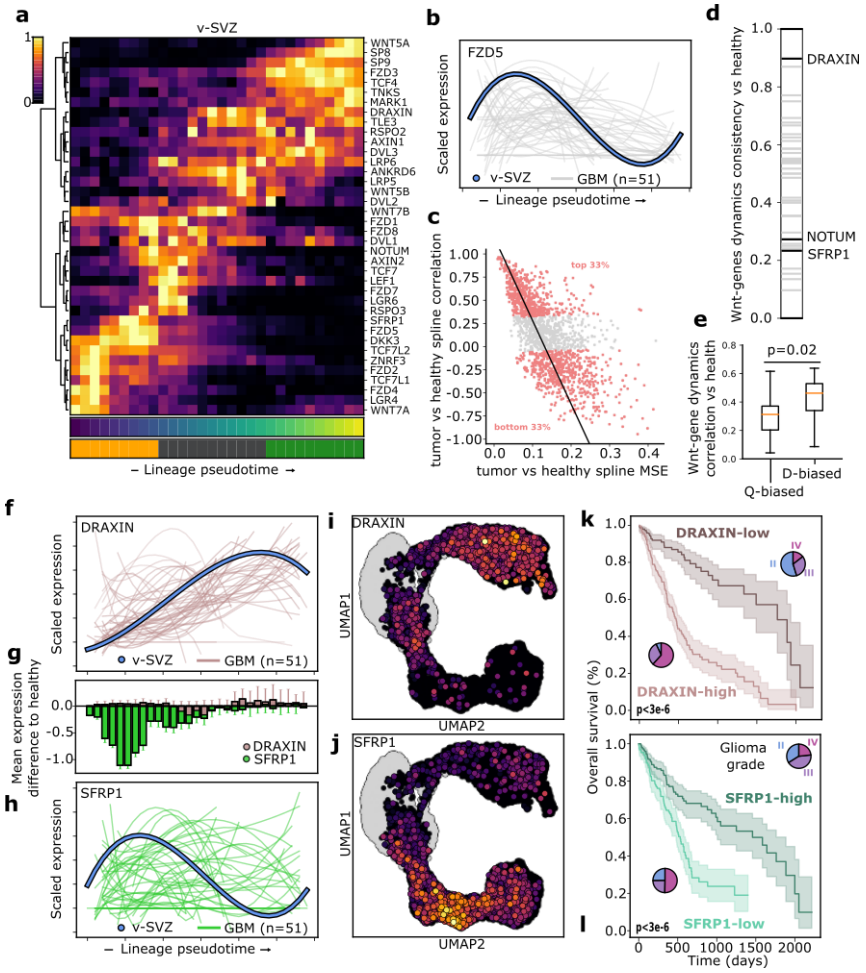

Figure 44: Differential pseudotime expression dynamics between glioblastomas and SVZ NSCs reveals recurrent dysregulation of secreted Wnt antagonists. a) Wnt-signaling genes expressed in SVZ NSCs clustered by their scaled expression along pseudotime. b) Splines of scaled FZD5 expression in glioblastoma pseudolineages, with SVZ NSC reference expression dynamics in blue. c) MSE and correlation scores for pairs of gene (n=37) and tumor (n=51) compared to the SVZ NSC reference expression dynamics for that gene. The top and bottom third of gene pairs, colored in red, was used to determine the Wnt dynamics signaling consistency score in (d). e) Boxplot depicting the correlation coefficient for Wnt-genes in Quiescence- and Differentiation-biased tumors, respectively. f) Splines of scaled DRAXIN and SFRP1 (h) expression in glioblastoma pseudolineages, with SVZ NSC expression dynamics in blue. g). Mean tumor deviation from SVZ NSC reference for SFRP1 and DRAXIN expression. Errorbars represent standard deviation. i). Log-normalized expression of DRAXIN and SFRP1 (j) in the SVZ NSC lineage UMAP, with cycling cells in gray. k) Kaplan Meier curves depicting overall survival for DRAXIN and SFRP1 (l) –low and –high expressing tumors from TCGA GBM and LGG cohorts. Kaplan Meier significance was assessed by log-rank test but I noted the wrong p-value. Inset pie charts depict the proportion of tumors by glioma grade for each of the high- and low-curves.

Wnt signaling is tightly regulated at SVZ NSC lineage transitions *in vivo* (see section 2.4.1). Consistently, individual Wnt signaling components also exhibit precise regulation, as revealed by the cascading landscape of expression (Fig.44a) in the pseudotime-dependent clustering of 37 Wnt-related genes from the SVZ NSC lineage. I used spline regression to capture pseudotime expression dynamics in healthy and tumor cells, demonstrated here with FZD5 (Fig.44b). Then, I fixed the

spline-smoothed healthy dynamics and quantified their divergence across the 55 glioblastoma samples. Using the correlation distance to quantify difference in direction and the mean squared error (MSE) to quantify difference in scale, I compared the frequency of a given gene in the top and bottom third of all pairwise divergence estimates (Fig.44c) to compile a pan-tumor Wnt-gene dynamics consistency score (Fig.44d). From this analysis, I noticed that Wnt-gene expression dynamics in Differentiation-biased tumors were generally better correlated to the healthy reference than those of Quiescence-biased tumors (Fig.44e). As every gene disrupted in a truncated (QA) pseudolineage is also present in a complete (QAD) pseudolineage, this is unlikely to be due to a biased divergence metric. Instead, this result suggests that Wnt signaling is more consistently disrupted in Quiescence-biased tumors, perhaps due to the loss of its tight regulation at the SVZ NSC Quiescence-Activation transition (see Fig.19). Consistently, the secreted Wnt antagonists SFRP1 and NOTUM, which both peak at this transition, exhibited the worst-conserved expression dynamics; while DRAXIN, another Wnt antagonist which peaks at the Differentiation-stage, scored among the best (Fig.44f-j). These results highlight the selective dysregulation of Wnt antagonists at the Quiescence-Activation transition in glioblastomas and identify it as a salient target for therapeutic intervention. Supporting this distinction, both SFRP1 and DRAXIN exhibited highly grade-specific expression trends, with SFRP1-expression present in LGGs and lost in glioblastomas, while DRAXIN was absent in LGGs and present in glioblastomas (Fig.44k-l).

This unique approach, identifying recurrently dysregulated genes in a cohort of tumors by comparing their ptalign expression dynamics to the healthy reference, emerges as a powerful means to identify and target specific tumor vulnerabilities. Though currently implemented only in the ad-hoc method described above, I will generalize this approach in future work to arrive at statistically sound quantitative estimates of expression divergence. Extended to tumor-tumor comparisons this approach can unveil differential dynamics which highlight functional properties of the underlying tumors, eg. revealing adaptation to hypoxic conditions or drivers of complete vs. truncated tumor pseudolineages. Particularly comparing expression dynamics at stage transitions can identify key modulators of tumor cell fate, as evidenced by the following experiments of SFRP1-overexpression.

2.9.3 Forced expression of secreted Wnt antagonists stalls malignant lineage progression

The Secreted frizzled related protein 1 (SFRP1), which competes to bind and sequester free Wnt ligands in the extracellular space, acts as an inhibitor of Wnt signal transmission (Lopez-Rios et al., 2008). This has several important advantages which make it an attractive candidate for the targeted modulation of tumor pseudolineages. Most prominent is the contrast between the relatively high expression and precise peak of SFRP1 levels in the Quiescence-Activation transition of healthy SVZ NSCs, compared to its very low or entirely absent expression in the 55-glioblastoma cohort (see Fig.44h). This is supported by numerous studies across multiple cancer entities (Caldwell et al., 2004; Dahl et al., 2007; Joesting et al., 2005; Qu et al., 2013; Shi et al., 2007; Veeck et al., 2006), suggesting that loss of SFRP1 – particularly through epigenetic silencing (Baharudin et al., 2020) – is a potent factor in the malignant transformation of tumor cells (Yu et al., 2019). Moreover, SFRP1 expression levels are closely linked to overall survival in the TCGA cohort (Fig.44l), exhibiting a negative correlation with tumor grade. This is consistent with the action of SFRP1 at the crucial Quiescence-Activation transition which determines patient prognosis (see section 2.7.4). Indeed, inhibition of SFRP1 in human (Donega et al., 2022) or neutralization of its nearest paralog SFRP5 in mouse (Kalamakis et al., 2019) brains resulted in an Activation-stage shift in affected cells. SFRP1 is also related to stem cell identity by its cell type specific demethylation in SVZ NSCs compared nearby parenchymal astrocytes (L. P. M. Kremer et al., 2022), suggesting that losing SFRP1 plays a role in licensing sustained stem cell identity in tumor cells. This is consistent with my interpretation of the dysregulated Wnt-signaling at the Quiescence-Activation transition previously (see section 2.8.4), supporting its use as a targeted intervention over eg. LGK974, as SFRP1 acts at a precise transition which is regulated by Wnt signaling. Previous data (see section 2.8.2) relating the increased proportion of Quiescence-stage cells associated with tumor cells in proximity with SFRP1-expressing inhibitory neurons moreover suggests that SFRP1 has the capacity to influence tumor pseudolineages. For these reasons, Oguzhan and I decided to re-introduce SFRP1 expression at the Quiescence-Activation transition by inducing its expression in a Wnt-dependent manner in T6 glioblastoma cells.

2.9.4 SFRP1 overexpression directs tumors to a quiescent, astrocyte-like phenotype

In Wnt-reporter experiments on SVZ NSCs (see section 2.4) and T6 glioblastomas (see section 2.8), Quiescence-stage cells consistently exhibited high levels of reporter activity. Consequently, Oguzhan and his student Milica generated a TCF/Lef::SFRP1-P2A-EGFP T6 cell line as outlined in (Bekavac, 2022; Kaya, 2023) (Fig.45a). Modifying T6 cells in this way did not affect their propagation, as they do not exhibit reporter activity *in vitro* (see section 2.8.1). Oguzhan, with his students Nina Stinchcombe and Vuslat Akcay (Kaya, 2023), validated the sensitivity of this construct by Wnt-stimulation in an ELIZA assay (Fig.45b), demonstrating a ~20-fold increase in SFRP1 levels upon Wnt3a treatment. In a PDX model, Wnt-reporter mice began to reach the human endpoint around five months post injection (mpi), while SFRP1-OE mice remained symptom free. This continued until six mpi, when Oguzhan terminated the experiment solely to maintain comparable groups. By then, SFRP1-OE mice had survived significantly longer than their Wnt-reporter counterparts (Fig.45c). To investigate the determinants of this improved survival, Oguzhan sorted and sequenced three replicates of T6 SFRP1-OE PDX tumors by SS3 (Kaya, 2023).

Cells from SFRP1-OE tumors were stalled in a dormant astrocyte-like (astroQ) stage. Comparing SFRP1-OE to Wnt-reporter tumors revealed a strong shift to the Quiescence stage (Fig.45d), with a significant enrichment of astroQ cells in SFRP1-OE tumors (Fig.45e). Consequently, it appeared that SFRP1-overexpression had acted on the Quiescence-Activation transition to promote cells' entry into the Quiescence-stage, explaining the improved survival outcomes of the SFRP1-OE mice. I observed an increased fraction of cycling cells in the SFRP1-OE tumors, though this could be attributed to the slower, smaller SFRP1-OE tumors having a similar number of cycling cells as the Wnt-reporter tumors. Comparing between genotypes with DEseq2 highlighted a large number of differentially expressed genes which persisted into stage-matched comparisons (not shown). GSEA over these genes revealed that induction of SFRP1-induced astrocytic phenotypes was associated with IFN-g and IL10 production, as well as other astrocyte-related processes. Consistently, downregulated terms included Activation-related processes such as spindle assembly and translation (Fig.45f). These results underscore the utility of a perspective informed by lineage constraint, where despite T6 tumors exhibiting broad insensitivity to external canonical Wnt signals (see section 2.8.2), evidently enough of the Wnt transduction machinery remains present to receive and implement the molecular functions of SFRP1. Together, these results demonstrate the fate-modulating potential of a single overexpressed protein, shifting the presentation and organization of an entire tumor and stalling its constituent cells in the Quiescence-stage.

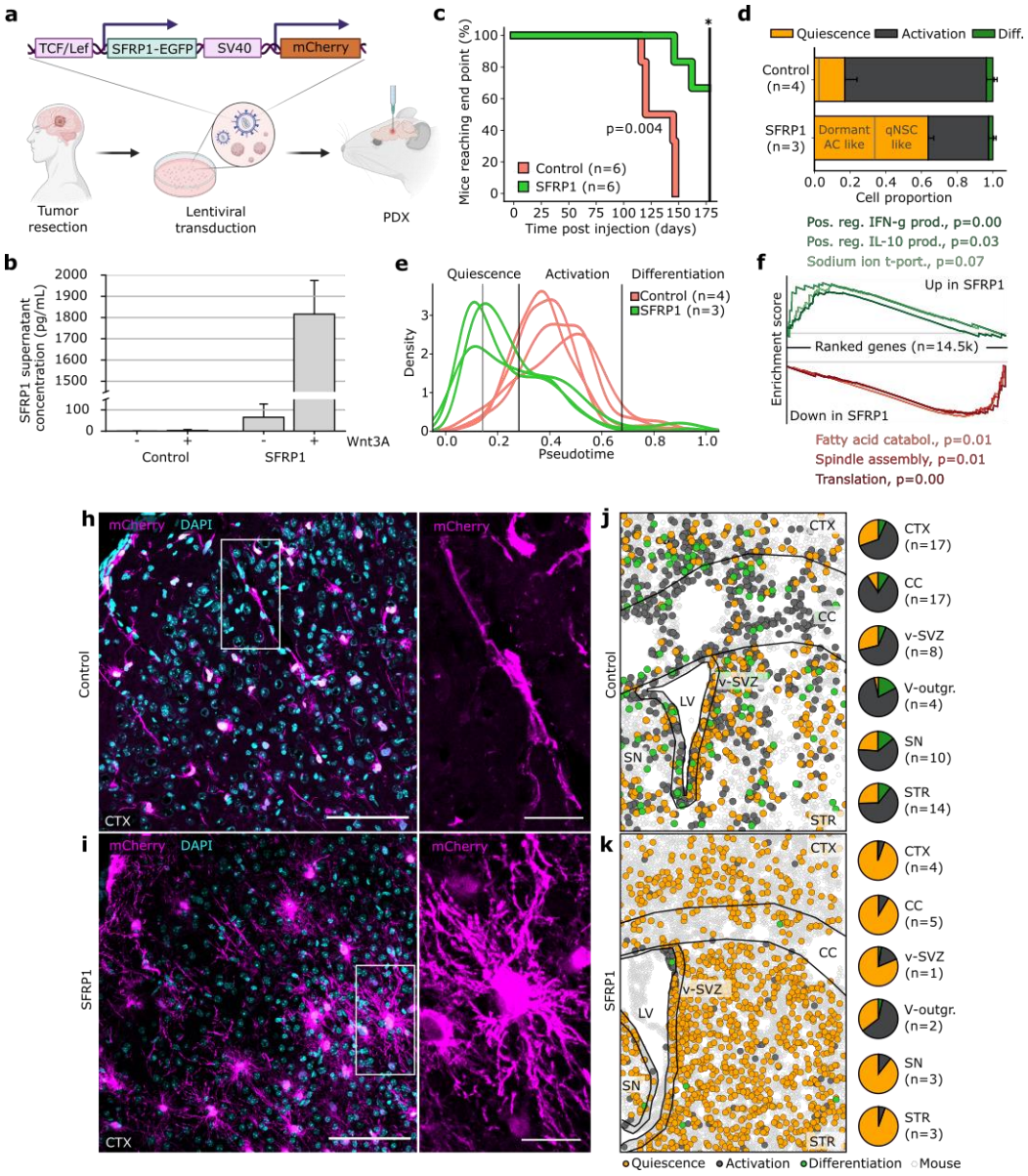

Figure 45: SFRP1 overexpression induces the generation of astrocytic glioblastoma cells. a) Schematic depiction of SFRP1overexpressing (OE) construct. `mCherry` ubiquitously labels tumor cells. b) `SFRP1` concentration by ELISA in supernatant of cells stimulated with/without `WNT3A`. Errorbars represent standard deviation in n=3 replicates. c) Kaplan-Meier curve of mice reaching end point post injection for n=6 mice in control and `SFRP1` cohorts. Significance was assessed by log-rank test. (*) denotes termination of experiment. d) Proportion of QAD-stage cells identified by ptalign in SFRP1-OE cells (n=3 replicates) and control (n=4 replicates). Errorbars represent standard deviation. e) Cell densities along ptalign pseudotime by Gaussian KDE. SVZ QAD-stage boundaries are highlighted. f) Selected GSEA enrichments from genes ranked by DEseq2 Log fold-change between pseudobulked SFRP1-OE and control. h) Representative immunofluorescence images of T6 cells in a control and SFRP1-OE (i) PDX cortex. Scale bars 100µm, in insets 25µm. j) Entire spatial transcriptomics ROI depicting similar regions in control and SFRP1-OE (k) PDX brains. Transcripts were associated to segmented nuclei to assign species and QAD-stage. Piecharts indicate sum of QAD-stage cells by brain region across ROIs. CTX: cortex; CC: corpus callosum; LV: lateral ventricle; V-outgr.: ventricular outgrowth; SN: septal nuclei; STR: striatum. Figure panels and legend were adapted from (Foerster et al., 2023).

The transcriptomic shift of SFRP1-OE cells was accompanied by simultaneous changes in morphological and spatial organization of the tumor. Oguzhan conducted immunohistochemistry staining of tumor section to reveal highly penetrant and significantly changed morphologies of SFRP1-OE cells, from Wnt-reporter neuron-like cells with isolated processes to large, extensively branched, astrocyte-like cells with extensive connections to its neighbors (Fig.45h-i). These results were complemented by an additional spatially resolved transcriptomics experiment carried out on SFRP1-OE tumors by Oguzhan and processed by Valentin Wüst as previously described (see section 2.8.2). This revealed Quiescence-stage cells extending to every brain region in SFRP1-OE tumors, with the exception of ventricular growths (Fig.45j-k). Taken together, these results present `SFRP1` as a potent modulator of tumor pseudolineages, promoting a sustained and pervasive transformation of tumor cells into the Quiescence stage by targeting an essential transition in the glioblastoma lineage hierarchy. The therapeutic benefits of such a treatment are evident and complement my previous result linking increased Quiescence to positive patient outcomes in glioblastoma (see section 2.7.4). However, before speculating about the therapeutic benefits of `SFRP1`, there are two important issues to resolve: whether other tumors respond to SFRP1-OE in a consistent manner, and to what extent the secreted nature of `SFRP1` affects healthy cells in the tumor periphery.

2.9.5 SFRP1 overexpression does not affect healthy cells in an allograft model

Patient-derived allograft models of T6 cells injected into human cortical organoids (see section 2.6.3) had proved an effective means to study the effect of tumor environment on its organization. As in PDX models, T6 PDA tumors faithfully recapitulated Wnt signaling dynamics which were not present under *in vitro* conditions (see section 2.8.2). Thus, to assess the impact of `SFRP1`-overexpressing tumor cells on the healthy environment, Oguzhan generated SFRP1-OE T6 PDA tumors (Fig.46a) and sequenced four replicates of healthy and malignant cell populations two weeks post injection as outlined previously (see section 2.5.1).

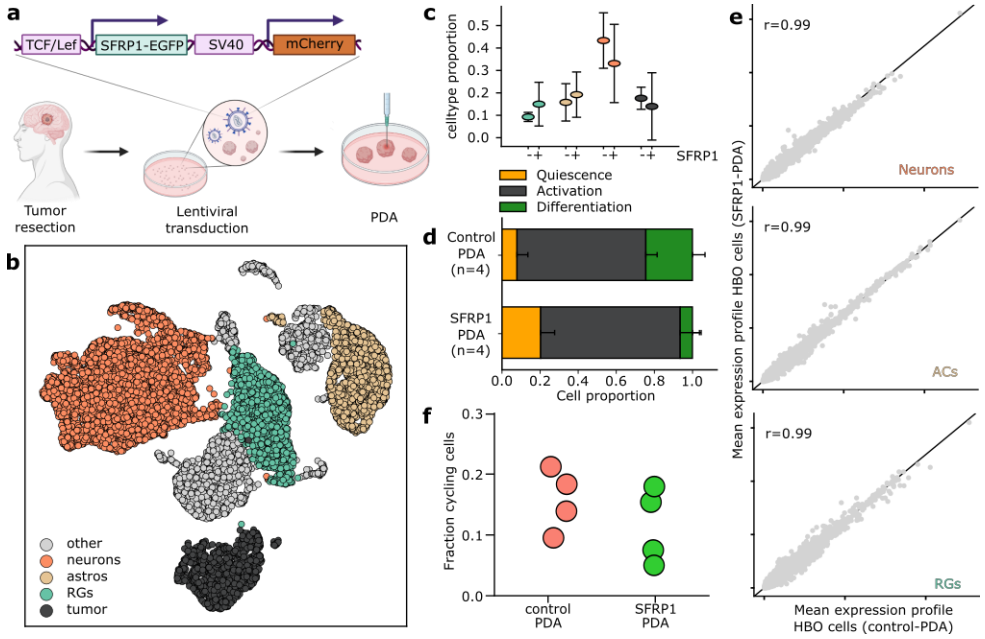

Figure 46: SFRP1 overexpression does not affect healthy cell transcription. a) Schematic representation of T6 PDA SFRP1-OE experiment, injecting SFRP1-OE cells into human cortical organoids and harvesting 2wpi. b) UMAP embedding of n=8 replicates of SFRP1-OE T6 PDA cells and healthy organoid cells. Tumor cells as well as major cell types comprising neurons, astrocytes, and radial glia (RGs) are indicated. Unknown or uncharacterized cell types are colored gray. c) Proportion of organoid cells by cell type for each PDA replicate, with `SFRP1` presence indicated. Dots are colored according to the cell type colors in (b). d) Proportion of QAD-stage cells from ptalign in n=4 replicates each of control and SFRP1-OE T6 PDA cells. Error bars denote standard deviation. e) Mean log-normalized expression for n=4 replicates each of control and SFRP1-OE PDA neurons (top), astrocytes (center) and radial glia (bottom), with Pearson correlation between genotypes. f) Proportion of cycling cells observed in SFRP1-OE and control replicates each.

UMAP embedding of SFRP1-OE PDA cells revealed the presence of a malignant cell cluster as well as multiple cell type clusters (Fig.46b). Healthy Neuronal, Astrocytic, and Radial Glia-like organoid cells were detected at similar frequencies between conditions (Fig.46c). As in the T6 PDXs, SFRP1-OE PDA tumor pseudolineages were shifted toward the Quiescence-stage (Fig.46d). Though this transformation was not as prominent as in the T6 PDXs (see Fig.45), it is nevertheless encouraging to see increased numbers of Quiescence-stage cells only two weeks post-treatment. The fact that T6 PDA pseudolineages per default contained lower numbers of Quiescence-stage cells compared to PDXs (see section 2.6.3) further underscores the potency of the SFRP1-OE treatment. However, despite its clear effect on tumor cells, I observed no expression differences in healthy cells from Wnt-reporter or SFRP1-OE conditions (Fig.46e). This suggests that `SFRP1` is only able to execute its molecular function in the presence of Wnt signals unique to stem- and stem-like tumor cells. Interestingly, while SFRP1-OE PDXs exhibited an increased proportion of cycling cells over their Wnt-reporter counterparts, I failed to observe this difference in PDA tumors (Fig.46f). As human cortical organoids only rarely provide the conditions for tumors to generate ventricular growths, this

suggests that the increased cycling cell fraction in SFRP1-OE PDXs could be due to cells from the highly proliferative conditions of the ventricular growths.

2.9.6 Ventricular growths enable escape from Wnt-based interventions

Previously documented in section 2.8.3, ventricular growths represent a unique environment in glioblastomas: void of Wnt-inducing signals and with the opportunity for 3D expansion inhibited only by the fluid pressure of the CSF. These features revealed a significant weakness of Wnt-based interventions such as the Wnt-dependent SFRP1-overexpression described above (see section 2.9.3).

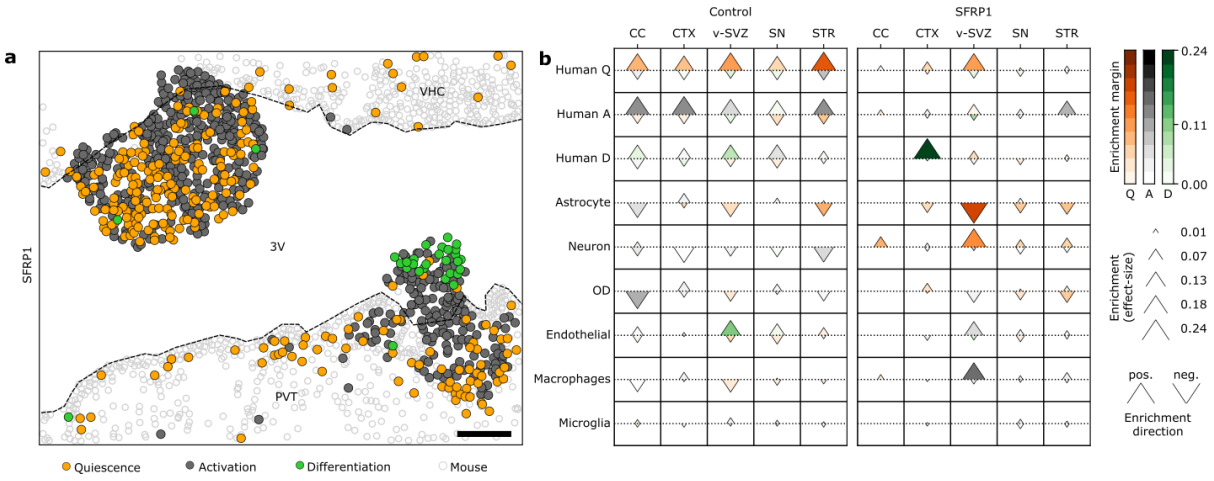

Figure 47: Spatial transcriptomic assessment of SFRP1-overexpressing PDX brains. a) Zoomed SFRP1-OE spatial transcriptomics ROI with QAD-stage cells in two ventricular outgrowths. Transcripts were associated to segmented nuclei to assign species and QAD-stage. Scale bar, 10µm. b) Neighborhood enrichment by permutation for segmented cells in n=17 Wnt-reporter and n=6 SFRP1-OE spatial transcriptomics ROIs. Cell type enrichments are reported for QAD-stage cells with other cell types (rows), with enrichment direction by shape and strength by size while color relates the enrichment margin between the largest and second-largest enrichments. 3V: third ventricle; VHC: ventral hippocampal commissure; PVT: periventricular nuclei of the thalamus. Figure panels and legend were adapted from (Foerster et al., 2023).

Similar to their counterparts in Wnt-reporter PDXs (see section 2.8.3), ventricular growths in SFRP1-OE brains organized along distinct pseudolineages even in the absence of canonical Wnt signals (Fig.47a). This is consistent with the stable generation of T6 PDA pseudolineages despite varying levels of Wnt signaling activity (see section 2.8.2), supporting the notion that tumor organization is driven by the population dynamics of tumor cells and depends less on the effects of healthy brain

cells in the local microenvironment. This was confirmed through a neighborhood enrichment statistic computed by Valentin which indicated there was no significant preference of QAD-stage tumor cells to the neighborhoods of various mouse cell types across different brain regions (Fig.47b).

2.9.7 NOTUM overexpression phenocopies the effects of SFRP1

Parallel to the SFRP1-OE experiments outlined above, Oguzhan and I investigated the role of NOTUM in modulating tumor pseudolineages due to its recurrent dysregulation in the 55-glioblastoma cohort (Fig.48a). Similar to SFRP1, NOTUM is a secreted Wnt antagonist which deacylates free Wnt ligands and inhibits their ability to bind their cognate receptor (Kakugawa et al., 2015). Extending these functional similarities, like SFRP1, NOTUM has been described as negative regulator of cell proliferation (Mizrak et al., 2020), consistent with its expression at the Quiescence-Activation transition in SVZ NSCs *in vivo* (not shown). Thus, Oguzhan generated five and sequenced a single replicate of T6 TCF/Lef::NOTUM-P2A-EGFP, so-called NOTUM-OE, tumor cells (Fig.48b).

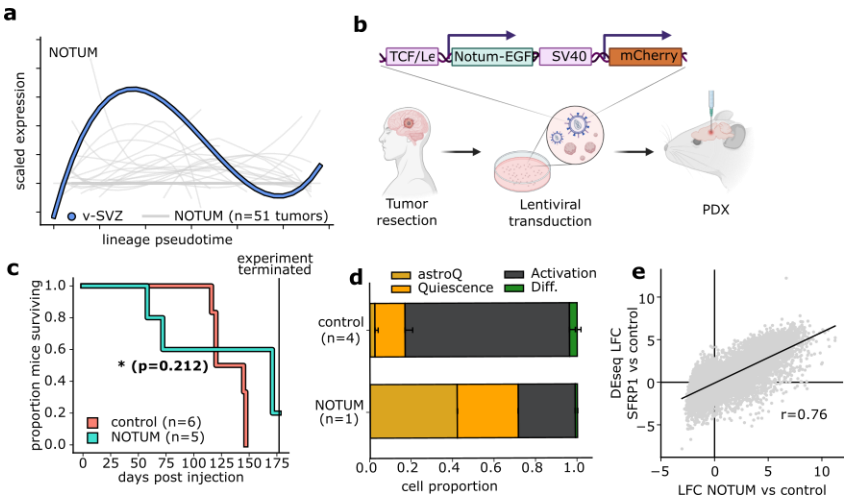

Figure 48: NOTUM overexpression phenocopies the effects of SFRP1. a) Splines of scaled NOTUM expression in glioblastoma pseudolineages, with SVZ NSC reference expression dynamics in blue. b) Schematic representation of NOTUM-OE PDX construct. c) Kaplan-Meier curve of mice reaching end point post injection for n=6 mice in control and n=5 in the NOTUM-OE cohort. Significance was assessed by log-rank test. (*) denotes termination of experiment. d) Proportion of QAD-stage cells identified by ptalign in NOTUM-OE cells (n=1 replicate) and control (n=4 replicates). Errorbars represent standard deviation. e) Mean NOTUM-OE log fold-change against SFRP1-OE DEseq2 log fold-change. Black line indicates best fit. Pearson correlation is indicated.

NOTUM overexpressing tumors phenocopied the effects of SFRP1 overexpression outlined above. Perhaps unsurprisingly, NOTUM-OE mice exhibited extended overall survival compared to Wnt-reporter PDXs (Fig.48c). This increase in survival did not endure as long as in SFRP1-OE mice, which could be due to the leaky expression of the NOTUM overexpression construct (not shown). Assigning a NOTUM-OE pseudolineage revealed a substantial increase in Quiescence-stage cells (Fig.48d), reflecting their transition to astroQ stages as in SFRP1-OE. Here, NOTUM-OE diverged from SFRP1-OE tumors, with Differentiation-stage cells entirely absent from the single NOTUM-OE pseudolineage. Consistently, comparing differentially expressed genes in SFRP1-OE to those in NOTUM-OE PDX revealed that transcriptional changes to Wnt-reporter PDXs were largely conserved (Pearson=0.76) (Fig.48e), suggesting that overlapping downstream effectors direct the generation of astrocytic tumor cells. Overall, the results from SFRP1- and NOTUM-OE demonstrate that the forced expression of Wnt antagonists elucidates strong and lasting disruption of tumor pseudolineages by stalling their progression out of the Quiescence stage. This result is particularly striking given the insensitivity of T6 pseudolineages to canonical Wnt signals (see section 2.8.2), highlighting that despite degenerating parts of the pathway, T6 cells remain sensitive to its targeted modulation by individual effectors. To better understand these mechanisms, Oguzhan and I next turned to whole-genome bisulfite sequencing to assess SFRP1-OE-induced methylation changes.

2.9.8 Astrocytic mouse DMRs are demethylated in SFRP1 overexpressing glioblastoma cells

Previously, comparing bulk tumor methylomes from TCGA revealed that the different QAD-stage proportions of various tumor pseudolineages were measurable from the methylation status of a subset of CpGs (see section 2.7.6). This result was motivated by a parallel study which revealed that cell types of the adult SVZ, most prominently astrocytes and NSCs, exhibited divergent methylation profiles (L. P. M. Kremer et al., 2022) (see section 1.1.3). As SFRP1-OE resulted in a strong shift to Quiescence-biased tumor pseudolineages, Oguzhan and I set out to investigate the methylation changes underlying this transition. To this end, three technical replicates of control and SFRP1-OE PDX tumors were subjected whole-genome bisulfite sequencing (WGBS) by Oguzhan and his student Vuslat Akcay (Akçay, 2023). By mapping these libraries to the human and mouse reference genomes using the Bismark pipeline (Krueger & Andrews, 2011), I isolated human-specific reads which I used to estimate mean CpG methylation. However, conventional DMR-discovery methods failed to identify relevant DMRs in this dataset (not shown), likely due to its sparsity and associated low

statistical power. These challenges led me to instead compare T6 cells by their methylation status at the published SVZ cell type-resolved DMRs from (L. P. M. Kremer et al., 2022), which I transferred to the human genome using liftOver[7].

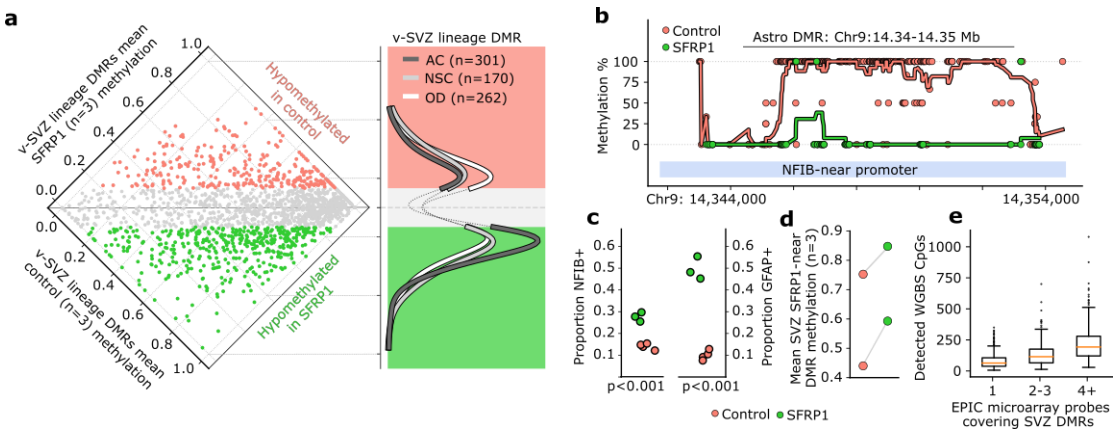

Figure 49: SFRP1-OE induces demethylation at specific SVZ astrocyte DMRs. a) Left: scatterplot of mean methylation of SVZ cell type DMRs from (L. P. M. Kremer et al., 2022) in SFRP1-OE and control WGBS (n=3 technical replicates each). Differentially methylated regions are highlighted by genotype. Right: SVZ cell type DMRs in a Gaussian KDE over the vertical axis of the scatterplot. b) Selected SVZ DMR overlapping an NFIB-promotor in SFRP1-OE and control. Points correspond to CpG mean methylation between replicates. Lines comprise a 10-CpG methylation moving average. c) Proportion of NFIB+ (left) and GFAP+ (right) Quiescence-stage cells among PDXs. Significance was assessed by t-test. d) Mean methylation at SFRP1-overlapping DMRs for n=3 technical replicates of control and SFRP1-OE WGBS. e) Number of CpGs detected in WGBS for DMRs grouped into those covered by 1, 2-3, or 4+ probes in Illumina EPIC 850k methylation microarray. AC: astrocyte; OD: oligodendrocyte. Figure panels and legend were adapted from (Foerster et al., 2023).

SFRP1-OE tumors demonstrated preferential demethylation of astrocytic SVZ DMRs, lending additional support to Quiescence-stage shift induced by SFRP1 overexpression. The SVZ lineage DMRs from (L. P. M. Kremer et al., 2022) are delineated by cell type and comprise astrocyte-, NSC, and oligodendrocyte-specific DMRs, which I had to map to syntenic positions in the human genome to enable their assessment in glioblastoma samples. In comparing DMR methylation differences between SFRP1-OE and Wnt-reporter WGBS samples, I identified those loci with a methylation distance exceeding one standard deviation as hyper- or hypomethylated depending on their direction. This revealed a large number of differentially methylated DMRs in SFRP1-OE (Fig.49a, left), among which astrocytic SVZ DMRs were enriched among those hypomethylated upon SFRP1-OE (Fig.9a, right). Demethylation of these regions classically associates with increased expression of nearby genes, providing a clear link to the Quiescence-inducing effects of SFRP1. Consistently, I observed that one of the most divergently methylated DMRs overlapped an NFIB promotor

[7] https://genome.ucsc.edu/cgi-bin/hgLiftOver

(Fig.49b). NFIB is the primary transcriptional activator of the astrocyte marker GFAP (Doetsch et al., 1999) and is one of the factors used in reprogramming iPSCs into astrocytes (Steele-Perkins et al., 2005). Expectedly, demethylation of this NFIB promotor was accompanied by an increase in NFIB+ and GFAP+ cells in SFRP1-OE tumors (Fig.49c). These results highlight the complete transformation of tumor cells towards an astrocytic differentiation status, rewiring transcriptional state and remodeling spatial interactions through altered morphology, all while cementing these changes by directed demethylation at specific functionally relevant loci. In this vein, I noticed that SFRP1-OE induced methylation of the endogenous SFRP1 locus (Fig.49d), suggesting that expression of the protein is typically regulated through a feedback loop which was disrupted through the sustained transcription of SFRP1 from the synthetic locus. Further study of the effectors of this loop may provide valuable insights into the mechanisms of SFRP1 leading to the induction of astrocytic traits in tumor cells. Of note, the methylation differences documented here were only visible in WGBS, and few SVZ DMRs are measured by more than a handful of sites on the conventional methylation array used eg. in TCGA glioblastomas (see section 2.7.6) (Fig.49e). Taken together, the litany of cellular changes demonstrated here through the overexpression of a single protein are striking; however, lasting elimination of glioblastoma cells will ultimately require their Activation, motivating a means to release SFRP1-induced Quiescence.

2.9.9 Treating glioblastoma cells with an SFRP1 inhibitor induces their activation

While increased Quiescence among glioblastoma cells is desirable to achieve increased patient survival (see section 2.7.4), eradication of the disease requires their effective elimination. Quiescence-stage cells are classically resistant to conventional glioblastoma therapies (Chen et al., 2012; Xie et al., 2022), which instead target cycling and Activation-stage cells through alkylating agents like temozolomide (TMZ). Given these circumstances, a combined therapy employing SFRP1 overexpression to stall cells in the Quiescence stage, and their coordinated release by SFRP1-antagonizing signals – thus providing an increased surface for the action of TMZ – presents a promising avenue to simultaneously improve patient survival and decrease the remission rate of glioblastomas. Short of identifying an Activation-promoting molecule expressed at the Quiescence-Activation transition in glioblastoma pseudolineages, I endeavored to release cells from the effects of SFRP1 by means of the small molecule inhibitor WAY-316606 (WAY) (Bodine et al., 2009). To this

end, I teamed up with Jocelyn Tang who generated human cortical organoids and measured the response of organoid-injected T6 SFRP1-OE cells to treatment with the WAY inhibitor (Fig.50a).

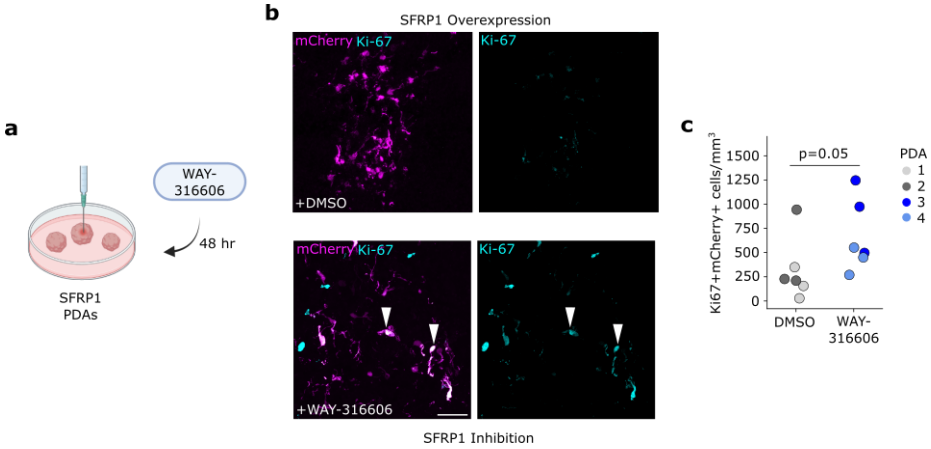

Figure 50: SFRP1 inhibition induces proliferation in an organoid model. a) Schematic representation of the SFRP1 inhibition experiment, with T6 SFRP1-OE cells injected in organoids in a PDA model as described previously. 2wpi, treatment and control cells were subjected to SFRP1-inhibition by WAY-316606. b) Representative immunohistochemistry images of proliferating (KI67+) tumor cells (mCherry+) in SFRP1-OE and SFRP1-OE inhibition conditions. c) Estimated KI67+mCherry+ cells per mm^3 from segmented cells in three technical replicates of two treated and untreated organoids each. A linear model was used to assess the difference in treatment groups while accounting for the pseudoreplication introduced by the technical replicates, achieving a significant difference between SFRP1-inhibition and untreated groups.

To measure the response of SFRP1-OE cells to inhibitor treatment, Jocelyn stained fixed PDA organoids for MKI67 as a proxy for cycling activity (Fig.50b). As T6 cells endogenously express mCherry (see section 2.8.1), Jan Brunken was able to segment tumor cells using Cellpose (Stringer et al., 2021) in these images, extrapolating the ratio of MKI67+/mCherry+ double-positive cells among tumor cells to estimate a density metric representing cycling tumor cells in both WAY inhibitor and control samples. Jocelyn generated three technical replicates each from two PDA organoids in treatment and control conditions, and I compared the cycling density metric between these conditions by testing for a significant slope in a linear model accounting for variation between technical replicates. This model detected a significant effect of the treatment on the density of cycling cells (Fig.50c), highlighting that inhibition of SFRP1 induced the simultaneous release of tumor cells from the Quiescence-stage. While this experiment confirms the lineage potential of astroQ tumor cells, consolidating their role at the base of the tumor hierarchy, their precise lineage potential remains to be assessed. Overall, these results pave the way for the future development of potent tumor therapies employing the pervasive transformation of tumor cells into the Quiescence

stage in combination with their induced shift towards the Activation stage, priming their elimination by conventional agents such as TMZ.

In sum, contrary to the insensitivity of T6 cells to broad changes in canonical Wnt signals, for example the PDA replicates from section 2.8.2 and the LGK974 experiment above, the SFRP1- and NOTUM-overexpression experiments demonstrate that these cells respond in turn to targeted modulation of specific parts of the canonical Wnt cascade. This has encouraging consequences for therapeutic interventions based on these proteins, as beyond targeting a broad cascade to which the tumor has evolved an insensitivity, precision interventions can affect intact parts of the pathway and elicit a targeted response. In some lucky scenarios, I might speculate that prior events inducing eg. aberrant Wnt signals in glioblastoma cells would sensitize them further to the sustained presence of SFRP1, for example if the prior mutations remove a critical feedback loop that tampers the effects of SFRP1 under homeostatic conditions. In this vein it is very encouraging to see consistent transcriptional changes induced by NOTUM overexpression, suggesting these proteins do indeed converge on a shared downstream pathway and paving the way for other or shared effectors which might elucidate the mechanisms of their action further. Intriguingly, these effects of the secreted Wnt antagonists SFRP1 and NOTUM do not exist in isolation, and indeed similar effects were reported in association with SFRP5 and SFRP3 (see section 1.1.4), among others. If these proteins do exhibit such a degree of redundancy they will provide a wide therapeutic surface for additional Wnt-based interventions of this nature.

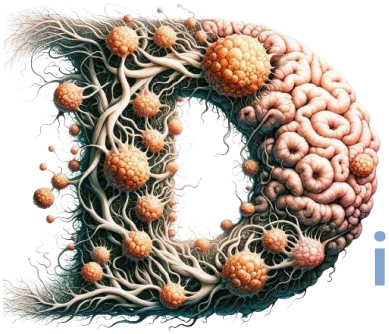

iscussion

Above all, cancers are heterogeneous: with every tumor effectively its own disease, it is no surprise that this heterogeneity poses significant challenges for treatment and contributes to cancer's status as a leading cause of death worldwide (Ostrom et al., 2021). However, despite their differences, all cancers share their relentless drive for growth, which is reflected in the convergent mutation of a number of pathways (Futreal et al., 2004). Yet when comparing mutation frequencies across cancers, this shared growth imperative comes secondary to their fundamental organization by tissue of origin (Hoadley et al., 2018; Schneider et al., 2017). This reveals an essential principle of tumor organization, as tumors do not arise in isolation but from pre-existing tissues. Consequently, a simplistic interpretation of tumor development solely predicated on fitness maximizing processes fails to account for critical aspects of their development. For example, while lung tumors proliferate faster than brain tumors, brain tumors mutate different pathways than lung tumors even if these mutations would unlock the greater proliferation rate of lung tumor cells. Consequently, other forces during tumor development must drive the emergence of tissue-specific mutational profiles.

The concept of lineage constraint explains these differences (see section 1.3). During development, cellular fates are restricted through the subsequent activation and repression of fate-determining factors (eg. PAX6, which establishes progenitor domains during brain development (Kikkawa et al., 2019)), some of which re-emerge at later timepoints to direct subsequent behaviors (eg. PAX6, which regulates the survival of adult neurons (Ninkovic et al., 2010)). In this case, rather than developing a new factor to direct each cascading fate decision, the cell has cleverly modified other parts of the pathway to restrict the action of such factors in a kind of specificity by dependence. Hence there's no use for glioblastomas to mutate eg. KRAS (S. Wang et al., 2022), since the substrates targeted by KRAS are not present in a glioblastoma cell. Importantly, this specificity stems from the developmental lineage constraints inherent to the tissue from which a given tumor originates. The healthy NSCs which develop into glioblastomas do not express relevant parts of the KRAS pathway, and so there is nothing to be gained by modifying this pathway for brain tumors. This example could be reversed in the case of lung tumors. Thus, tumor heterogeneity is driven by lineage constraint, which ensures that tumors inherit and propagate the characteristics of the cells they develop from.

One consequence of this view is that tumors fix their tissue-of-origin characteristics through a preference for incremental adaptations. Much like elected politicians, tumors do not have the benefit of long-term planning, and while eg. compounding different mutational effects could make a KRAS mutation attractive for glioblastoma cells in the long term, the clone which acts this way is going to be outcompeted by its neighbors which simply mutate the nearest low hanging fruit. This

way, the eternal rat-race of clonal red queen dynamics ensures that incremental fitness advantages will be prioritized over long-term transcriptional rewiring, guaranteeing that tumors retain the characteristics of their tissue-of-origin. This explains why tumors are classified according to their tissue-of-origin, but also highlights the potential of studying tumors to unravel the processes and interactions which govern the dynamics of healthy stem cells.

My contribution to this field lies in the development of *ptalign*, a pseudotime-alignment approach which derives a tumor pseudolineage by projecting tumor cells onto a fixed healthy stem cell lineage reference. This method leverages the ideas from lineage constraint to interpret tumor processes through the lens of healthy lineage transitions, enabling the study of tumor hierarchies in the absence of lineage tracing, and facilitating the comparative study of tumor-tumor and tumor-healthy expression dynamics. Here, I employ ptalign to dissect glioblastoma hierarchies into Quiescence, Activation, and Differentiation stages inferred from the SVZ NSC lineage hierarchy, ultimately conducting a population-level study of the organizational principles governing glioblastoma from a 55-patient cohort. Comparing between patient pseudolineages, I provide evidence for the placement of Quiescence-stage tumor cells at the base of the tumor hierarchy, and reveal the Quiescence-Activation transition as a critical modulator of tumor pseudolineages. These insights unveil novel therapeutic strategies and I delineate salient biomarkers for their application. Extending pseudolineage analysis to the molecular level, I identify critical features of the Wnt signaling pathway which are lost in glioblastomas, ultimately revealing the secreted Wnt antagonists `SFRP1` and `NOTUM` as recurrently dysregulated factors in glioblastoma. By reintroducing these factors I achieved a targeted modulation of tumor pseudolineages towards the Quiescence stage, demonstrating how specific tumor vulnerabilities are revealed by this approach. Beyond glioma, I envision the application of ptalign in a pan-cancer context to reveal therapeutic targets in various solid tumors and uncover shared principles underlying stem cell activation which are exploited across cancers.

3.1 ptalign enables the systematic comparison of malignant and healthy lineages

ptalign exploits the persistent likeness of tumor cells to their healthy tissue-of-origin to place cells within a reference lineage hierarchy. This approach, assigning tumor pseudotimes by fixing a reference trajectory topology and determining the optimal placement of query cells within its

bounds, presents a novel perspective on tumor lineages. This approach differs from conventional pseudotime inference methods which aim at deriving a trajectory that minimizes expression differences between neighboring cells (Saelens et al., 2019). These trajectories are ultimately unique to each sample and not comparable between tumors, as different populations might be placed at the pseudotime root, while trajectories which do capture similar hierarchies might find these variably stratified. These issues are resolved in ptalign, as all aligned cells are placed within the same reference pseudotime axis while specific pseudotimes in the reference and query trajectories represent similar functional cell stages with similar transcriptional profiles. Additionally, while conventional pseudotime algorithms are forced to assign every cell a pseudotime value, often leading to distinct populations of eg. low-quality or doublet cells in pseudotime, ptalign is able to identify out-of-distribution cells and exclude these from the pseudotime alignment. Detecting these non-lineage cells is currently accomplished by thresholding on the minimum correlation value in the reference-correlations for that cell, a comparison which is not possible in the framework of conventional pseudotime inference algorithms. However, both ptalign and conventional methods can likely benefit from improved detection of out-of-distribution cells by cluster-aware or gene-based methods.

By matching cells in a tumor sample to their counterparts in a healthy reference, ptalign is more similar to other pseudotime alignment approaches like tuMap (Alpert et al., 2022). This method builds on the idea set forth in cellAlign (Alpert et al., 2018), leveraging a dynamic programming-based approach to determine the optimal arrangement of pseudo-nodes in a healthy and tumor pseudotime to match their pseudotime progression. This idea of 'matching' pseudotimes highlights the key difference to ptalign, as both cellAlign and tuMap operate on the assumption that an optimal tumor pseudotime already exists. Indeed, tuMap itself suggests the use of a tumor pseudotime exhibiting an underlying developmental (ie. healthy) structure, motivating the use of ptalign to identify such a pseudotime which can be refined through tuMap. In its alignment approach, tuMap weights genes by their conservation between healthy and tumor samples – a strategy which could be extended to ptalign to improve the selection and generalization of the pseudotime anchor gene set. Whereas tuMap will always report an alignment while leaving the user to interpret its efficacy through a complicated mapping error, one advantage of ptalign is that through the simple statement of its aims of placing tumor cells within a reference lineage hierarchy, quantification of the alignment performance is kept simple, straightforward, and interpretable through the use of DTW. Moreover, the built-in ptalign permutation module provides a sensitive and tractable overview of the method's performance without requiring the user to understand complex transformation functions and dissimilarity landscapes, as in tuMap.

One limitation of the ptalign algorithm is its incompatibility with branching pseudotimes. Most conventional pseudotime algorithms support the inference of branching pseudotimes (Saelens et al., 2019), and indeed these capture valuable dynamical processes in complex datasets such as fetal development (Cao et al., 2019). However, applied to tumor samples where ground truth lineage dynamics are unknown, pseudotime branches can be a means to overcluster the data or introduce spurious hierarchies. This is the case in self-contained branching events such as cell cycle, which provides a convenient branch-point to erroneously separate the progression prior to and after the cell cycle. Given an appropriate reference, ptalign will accurately resolve this progression, however the cycling cells themselves are excluded in the analysis. This is consistent with other pseudotime alignment methods such as tuMap, which do not support branching pseudotimes. A recently proposed method for the alignment of single-cell trajectory trees (Sugihara et al., 2022) tackles the branch-matching problem by matching minimum spanning trees using linear alignment, though this approach cannot resolve cyclical trajectories. As the problem solved by ptalign can essentially be phrased in terms of point matching, distance-based heuristics can likely be applied to extend the method to enable the placement of tumor cells in a branched reference trajectory. However, in this case problems would arise in the quantification of aligned pseudotimes due to limitations of DTW-based methods. This limitation could be overcome, however, through the recently described application of arboreal matching to compare complex branching trajectories (Do et al., 2019), leaving the incorporation of branched pseudotimes in ptalign alignments a possibility for future development.

ptalign uses information from a healthy lineage to fix the tumor topology, but tumor cells are often known to be more plastic than their healthy counterparts. For example, in glioblastomas this plasticity remains unresolved (Prager et al., 2020), largely speculated from *in vitro* experiments (Castellan et al., 2020; Dirkse et al., 2019; Larsson et al., 2021) and without the benefit of empirical lineage traced ground truth datasets. Directed lineage transitions can be inferred using methods like RNA-velocity (La Manno et al., 2018) and CytoTRACE (Gulati et al., 2020), providing a means to quantitatively address tumor plasticity. However, CytoTRACE was ineffective in adult tissues, succumbing to the erroneous placement of cycling cells mentioned above, while recent studies have cast doubt on the data processing and modeling assumptions in RNA velocity (Barile et al., 2021; Marot-Lassauzaie et al., 2022). One study did identify velocity fields resolving progenitor-to-differentiated trajectories in glioblastomas (Couturier et al., 2020), though they did not consider stage transitions. Actual lineage tracing will be the ultimate test of tumor stem cell plasticity, but until then the reference-based approach employed by ptalign at minimum adds the ability to resolve and compare ordered stage transitions between tumors, which did not exist previously.

Discovering tumor vulnerabilities through pseudotime expression dynamics remains one of the key advantages of ptalign. By comparing expression divergence between the 55 glioblastoma cohort and the healthy SVZ NSC lineage I was able to identify `SFRP1` and `NOTUM` as recurrently dysregulated Wnt signaling modulators, leading to the discovery of their potent ability to arrest pseudolineage progression. However, in this analysis I quantified their divergent expression by a tailored ad hoc method which is unlikely to scale to large numbers of genes. The challenge with identifying recurrently dysregulated genes lies in detecting robust differences in pseudotime expression dynamics between groups of tumors (eg. tumor-tumor) or to a healthy reference (eg. tumor-healthy). I previously explored the use of multiple mixed linear models to provide a grounded means to test for differential dynamics between populations, though this approach did not generalize well to variable pseudotime expression dynamics. One interesting question for future developments is the automatic clustering of genes and samples by expression dynamics. This way, clustering samples by their dynamics can reveal group-specific vulnerabilities, while grouping genes by their pseudotime-expression likely enables the discovery of upstream regulators analogous to the regulon approach in SCENIC (Aibar et al., 2017). Both of these approaches remain broadly unexplored in the current study. Perhaps one avenue could leverage a previous generation of methods developed to resolve expression dynamics in time-series microarray datasets (Conesa et al., 2006; Ernst et al., 2005; Paparrizos & Gravano, 2017), though many of these programs have become inaccessible in the intermittent years. Overall, how to best characterize pseudotime-dependent expression changes at a population level remains an open question (Song & Li, 2021), and future developments in this space will have direct application to ptalign. Developing high-fidelity time-series based clustering approaches to compare tumor-tumor and tumor-healthy pseudotime expression dynamics remains a key area of focus toward realizing the full potential of ptalign.

Overall, ptalign opens interesting prospects of resolving pseudolineages in a pan-cancer context. With the advent of scRNA-seq, studies identifying parallels between healthy and diseased samples have multiplied (Couturier et al., 2020; Good et al., 2018; K. S. Smith et al., 2022; Van Galen et al., 2019), supporting the general action of lineage constraint and providing a basis for their comparison by ptalign. Indeed, different tissue tumors could be used to compare the different paths to tumorigenesis, for example contrasting Wnt dynamics in colon tumors with the present study of glioblastomas. Such an approach provides exciting prospects for the discovery of tissue-specific vulnerabilities and gives the added bonus of illuminating organizational principles underlying the regulation of diverse tissue stem cell programs. This will require curation of specific domain knowledge of various healthy stem cell lineages; however, less curation is required for tumors, with the recently published meta atlas of 1000 tumors (Gavish et al., 2023) providing an attractive

resource to probe the existence of shared principles of stem cell activation which are exploited across tumor entities.

3.2 Glioblastoma organization viewed through an astrocytic NSC hierarchy

My survey of NSC lineage scRNA-seq datasets revealed a remarkable conservation of neurogenesis dynamics regardless of species or ontogeny. This is consistent with the ancient origins of CNS specification (Jékely, 2021), as NSC lineage cells from the adult murine SVZ, human fetal brain, or cortical organoids uniformly progress through a series of common lineage stages. Indeed, the ubiquitous presence of quiescent astrocytes in adults (Kalamakis et al., 2019) compared to their late emergence and low frequency during fetal development highlights the key differences between developing and mature brains. Combined with the recent evidence that injury conditions can induce the activation and subsequent generation of neurons from common parenchymal astrocytes (L. P. M. Kremer et al., 2022; Magnusson et al., 2014), glioblastoma origins through a failed attempt at regeneration, ie. from transformed neurogenic astrocytes (Mossi Albiach et al., 2023), holds significant potential in shaping our understanding of the disease.

Several key observations motivate the astrocytic origins of glioblastomas. Unlike pediatric tumors with defined progenitors (Okonechnikov et al., 2021; K. S. Smith et al., 2022), glioblastomas occur throughout the brain (Ostrom et al., 2021). While this is in line with the strong migratory phenotype frequently associated with glioblastoma cells, it is also plausibly explained through their local origin from common parenchymal astrocytes. Previous studies on mouse models of glioblastoma determined SVZ NSCs to be the tumor cell-of-origin (Alcantara Llaguno et al., 2019; J. H. Lee et al., 2018), and these do likely do contribute to the formation of numerous tumors. However, in the drastic conditions introduced in such a tumor model, the first tumors will tend to emerge in the most-susceptible population. In the sensitive tissues of the brain, however, the first tumors are usually the only tumors which will be observed, suggesting that slow-growing astrocyte-derived tumors may be overlooked in this context. Moreover, activated astrocytes produce a neurogenic lineage that is similar to SVZ NSCs (Magnusson et al., 2020), but SVZ NSCS, which are more frequently cycling than terminally differentiated astrocytes, may accumulate fewer mutations as these are cleared through transcription coupled repair mechanisms (Hanawalt & Spivak, 2008; Hendriks et al., 2008). As a terminally differentiated astrocyte can persist for decades without

activating, this provides substrate for the random degeneration of numerous loci through clock-like mutational processes (Alexandrov et al., 2015), which are not cleared through cycling activity. This is consistent with the ideas of lineage constraint laid out above, as astrocytes can accumulate mutations in key tumorigenic pathways which do not affect their homeostatic function but which have devastating consequences when these cells are eventually stimulated to activate. This persistence of tumor driver mutations for decades until their transformation upon external stimuli supports the emerging view of inflammatory origins of tumorigenesis (Simpson Ragdale et al., 2023).

Studying glioblastoma organization using ptalign further strengthened these tumor's origins in adult neurogenic lineages. Analysis of tumor pseudolineages in the 55 glioblastoma cohort revealed the frequency of Quiescence- and Differentiation-stage cells as a major axis of variation in glioblastomas. Only through the contextual knowledge provided by the NSC reference and made available in ptalign was I able to subset these tumors into two groups of truncated (QA) and complete (QAD) pseudolineages. In analogy to the healthy NSC lineage, these groups reflect the self-renewing or differentiating modes of division available to Quiescence-stage NSCs (Obernier et al., 2018), thus more closely resembling adult neurogenic lineages compared to their fetal counterparts. Given that SVZ NSCs display strong intrinsic fating (Merkle et al., 2007), these different pseudolineages might additionally suggest an origin in distinctly-fated NSC populations. Extending this view to astrocytes, whose activation potential differs across brain regions (Magnusson et al., 2014), provides an interesting avenue to explore glioblastoma heterogeneity; however, whether activated astrocytes are able to engage in self-renewing divisions remains to be seen. The noted role of Wnt signaling in regulating cellular polarity and division asymmetry (Goldstein et al., 2006; Habib et al., 2013) makes it an interesting candidate in the specification of eg. truncated glioblastoma pseudolineages – providing additional support for the disrupted pseudolineage hierarchy achieved by `SFRP1`-overexpression. Overall, understanding glioblastomas is heavily linked to the study of their healthy counterpart, highlighting the potential for ptalign to generate testable hypotheses related to tumor organization and hierarchy.

The ubiquity of Quiescence-stage cells among glioblastoma pseudolineages motivates their targeting to disrupt tumor progression. Particularly in their ability to propagate tumors *in vivo*, Quiescence-stage cells emerge as ideal GSC candidates (Suvà & Tirosh, 2020), making all the more surprising that the field has focused on the stem properties of Differentiation-stage cells and considers Quiescence-stage cells as a differentiated population (Neftel et al., 2019; Tirosh et al., 2016; Venteicher et al., 2017). This is a matter of glioblastoma organization viewed through adult vs. developmental NSC hierarchies. In the former, Quiescence-stage cells represent the stem population, while in the latter

this role is assumed by Differentiation-stage cells. As GSCs ought to be present in every tumor, the presence of Differentiation-stage cells in only half of the glioblastoma pseudolineages suggests that Quiescence-stage cells, which are ubiquitous across glioblastomas, play an essential role in the tumor hierarchy. This notion is reinforced by considering lower grade gliomas (LGGs), which are generally agreed to have astrocytic origins (Louis et al., 2021). Given the highly conserved NSC dynamics regardless of ontogeny or species outlined above, I find it unlikely that glioblastomas developed a separate stem population compared to LGGs. Instead, rather than representing a novel stem population, it is likely that the unique ability for glioblastomas to generate neuronal Differentiation-stage cells contributes to their poor prognosis through the propensity of these cells to infiltrate (Comba et al., 2022) and form connections (Jung et al., 2019; Osswald et al., 2015) in the healthy brain tissue. This view of glioblastoma hierarchy is confirmed by the unbiased barcoding study in (Lan et al., 2017) which revealed an invariant GSC hierarchy driven by a quiescent progenitor, as in adult neurogenesis. Indeed, the cycling-based identification of GSCs is questionable when viewed through the lens of the SVZ NSC lineage, where Differentiation genes are upregulated during cell cycle although these are clearly the product of the division and not its catalyst. Taken together, numerous evidences point to glioblastoma hierarchies recapitulating those of adult neurogenesis and reinforce the notion that Quiescence-stage cells make up the GSC population. This challenges a view of glioblastoma hierarchy held in the field and underscores the need for novel therapeutic strategies which target this population. Importantly, these insights would not have been available without the framework of ptalign enabling the functional interpretation of glioblastoma pseudolineage stages based on their origins in the healthy SVZ NSC lineage.

By overexpressing SFRP1 in glioblastoma cells, Oguzhan and I elicited a ubiquitous and robust modulation of tumor pseudolineage which effectively arrested cells in the Quiescence-stage. This protein was identified by comparing expression dynamics in ptalign pseudotimes of the 55 glioblastoma cohort, identifying it as a recurrently dysregulated factor in glioblastoma. This is consistent with previous literature characterizing epigenetic silencing of SFRP1 in various tumors (Baharudin et al., 2020; Yu et al., 2019). Notably, all of these observations are equally relevant for NOTUM overexpression. It is surprising that despite the recurrent loss of SFRP1 across glioblastomas, cells preserve the ability to respond to SFRP1 stimulation in a manner consistent with prior inhibition experiments (Donega et al., 2022) and its expression at the Quiescence-Activation transition *in vivo*. This has positive implications for therapeutic interventions targeted at stage transitions over individual stages themselves, which are discussed below. Importantly, both the fact that SFRP1-overexpressing tumors are able to grow and colonize the entire brain despite their Quiescence-stage bias, along with the SFRP1 inhibitor experiment, demonstrate that

astrocytic tumor cells can re-enter and populate the tumor hierarchy, supporting their placement as the glioma stem cell. Intriguingly, the SFRP1-dependent switch from a complete (QAD) to truncated (QA) tumor pseudolineage could be due to a switch from mixed asymmetric and symmetric modes of division to a strong bias toward symmetrically self-renewing divisions. The role of Wnt in regulating this division behavior through SFRP1 would be consistent with the concomitant increase in self-renewing divisions (Bast et al., 2018) and canonical Wnt activity (Kalamakis et al., 2019) in aged brains. Better understanding of the mechanisms driving such a switch in facultative stem cell behavior could greatly improve the therapeutic surface for targeted modulation of tumor plasticity. Likewise, regenerative therapies in the healthy brain can also benefit from these insights. In general, employing tumor systems to study healthy stem cell dynamics remains an underappreciated aspect of oncology. Particularly due to the lineage constraint active in tumor cells, these can provide a detailed picture of essential stem cell processes and the consequences of their aberration (Pertesi et al., 2019). Additional lineage tracing experiments will be necessary to elucidate the mechanism of the SFRP1-induced shift to Quiescence-biased pseudolineages. Overall, it is enticing to speculate an Activation- or Differentiation-inducing effect resulting from the inhibition of DRAXIN, the best conserved of the Wnt-modulators assayed by ptalign.

3.3 The interplay of intrinsic and environmental Wnt signals directs tumor pseudolineages

Improved cell type resolution obtained from scRNA-seq motivates deeper understanding of the factors contributing to cell fate. Building on previous studies implicating the Wnt signaling pathway in the activation of SVZ NSCs (Donega et al., 2022; Mizrak et al., 2020), Oguzhan employed a fluorescent TCF/Lef Wnt reporter to study Wnt signaling dynamics in health and disease at single-cell resolution (Kaya, 2023); the first study of this kind. This revealed tight regulation of canonical Wnt signaling at the Quiescence-Activation transition *in vivo*, combined with a clear enrichment of reporter activity in the Quiescence-stage. Glioblastomas, meanwhile, required external cues to initiate canonical Wnt signaling activity and did not alter their pseudolineage characteristics in response to reporter levels. This suggests that these tumors have developed an overall insensitivity to Wnt signals, a development perhaps necessary to maintain a persistent stem cell state. However, tumor cells' selective and robust response to targeted Wnt modulation via SFRP1 or NOTUM

revealed that these had degenerated specific parts of the pathway while leaving others intact, providing opportunity for therapeutic exploitation.

While numerous Wnt-related genes have been documented (Boonekamp et al., 2021), many of which exhibit coordinated expression dynamics along the SVZ lineage, the landscape of Wnt-related gene expression is much less clear in glioblastomas. This is best exemplified through tumor ventricular growths. In Oguzhan's PDXs, tumor cells are injected into the striatum and eventually disperse to colonize the entire mouse brain. This includes cells which hone to the SVZ and extravasate to occupy the ventricular cavity, where the absence of nearby healthy cells means their lateral expansion in 3D is uninhibited – likely resulting in the poor survival of patients with ventricular tumors (Berendsen et al., 2019). As contact with healthy brain cells was the leading driver of canonical Wnt signaling activity in glioblastoma cells, the lack of Wnt signals in ventricular growths means these most closely resemble the *in vitro* tumor conditions. This is contrast to Quiescence-stage cells, which consistently exhibited increased levels of canonical Wnt signaling activity across all measured modalities, suggesting that maintaining cells in a Quiescence-stage requires specific Wnt signals. Surprisingly, the contents of the CSF are not sufficient to elicit canonical Wnt activity in tumor cells. While it is enticing to speculate that Wnt ligands are absent from the CSF, it could as well bias cells towards non-canonical modes of Wnt signaling. Alternatively, the CSF is known to contain SHH (Huang et al., 2010), a signaling protein which frequently acts in competition to Wnts (Joksimovic et al., 2009; Ouspenskaia et al., 2016), suggesting that ventricular growths may be the result of hedgehog-directed pseudolineages. In either case, ventricular growths were consistently dominated by Activation-stage cells, recapitulating the morphologies and behavior of *in vitro* cultured glioblastoma cells. In this context, their organization along Activation-Differentiation gradients might point to ventricular growths as the birth place of glioblastoma cells, which then assume a migratory phenotype consistent with Differentiation-stage cells (Rella et al., 2021). These growths have flown under the radar of recent systematics attempts to characterize glioblastoma organization (Bast et al., 2018; Greenwald et al., 2023; Mossi Albiach et al., 2023), motivating their further study. Thus, ventricular growths represent a peculiar case of spatially-constrained tumor pseudolineages which organize along Activation- and Differentiation-stage gradients in the absence of canonical Wnt signals.

Notably, tumor cells responded to endogenous SFRP1 released by healthy neurons. Why they retain this ability when SFRP1 was lost in virtually all studied glioblastomas remains a mystery, as it leaves tumor cells at the mercy of nearby SFRP1-expressing cells. Perhaps this is an adaptive trait, guaranteeing the presence, at low frequency, of Quiescence-stage tumor stem cells. Though why

these cells are not simply outcompeted by SFRP1-insensitive clones prior to chemotherapy, when they finally become essential (Chen et al., 2012), remains to be elucidated. This tradeoff between the insensitivity of tumor cells to broad fluctuations in pathway activity and their sensitive response to targeted interventions motivates the detailed study of pseudolineage modulating factors to achieve positive patient outcomes.

3.4 Clinical innovations from glioblastoma pseudolineages

I extended pseudolineage inference from single-cell to bulk glioblastoma datasets using GSVA to reveal four major tumor groups which affected distinct patient outcomes. These groups were characterized by enrichment (e-) in different pseudolineage stages: eQ, eA, eQD, eAD. Here, Quiescence-biased (eQ, eQD) groups exhibited better survival outcomes, consistent with their slower growth. This is in contrast to the classification by (Verhaak et al., 2010) where proneural tumors tended to have the best outcomes. Curiously, proneural tumors in that paper broadly correspond to eAD tumors in the present study, which exhibited consistently bad survival outcomes. Though the inclusion of LGGs and the reclassification of glioblastomas as solely IDH-wildtype (Louis et al., 2021) may explain this discrepancy, it is likely that deconvolution through a single-cell reference also improves the detection of distinct glioblastoma signatures. Given the developmental view of glioblastoma hierarchies in (Verhaak et al., 2010) and the adult view expounded in the current study, it is intriguing to note that in both cases, enrichment in what the authors consider the tumor stem cell results in improved patient survival.

Survival outcomes in the various tumor classes could be related back to functional differences in their pseudolineages. While eQ and eQD tumors exhibited the best overall survival with no significant difference between the two, the eQD group had a significantly better PFI. It is enticing to postulate that this could be due to more dormant astrocytes being present in the eQD group, but I did not follow this hypothesis. It is also interesting to note that eQ and eQD tumors comprise the prototypical truncated and complete tumor pseudolineage, suggesting that the associated differences in stem cell division mode described above could relate to the variations in PFI. Overall, survival comparisons between tumor classes revealed the Quiescence-Activation transition as a crucial determinant of patient outcomes, highlighting the relevance of Wnt-based interventions to disrupt tumor progression.

Clustering samples with matched methylation- and RNA-measurements revealed that pseudolineage stages are inscribed in tumor methylomes. This was consistent with the stage-specific methylation of SVZ NSCs (L. P. M. Kremer et al., 2022) and the broad overlap to the (Verhaak et al., 2010) tumors which were observed in (Ceccarelli et al., 2016; Noushmehr et al., 2010). Consistently, the increased incidence of Quiescence-stage cells in SFRP1-overexpressing tumors was visible in WGBS tumor methylomes, with a clear signal delineated by the SVZ NSC- and astrocyte-DMRs from (L. P. M. Kremer et al., 2022). Set against the single-cell methylomes in (Johnson et al., 2021) for which "methylation disorder" became the dominant signal over any underlying biology, the approach outlined here highlights the importance of contextual knowledge in driving insights into tumor processes. Thus, as methylation information is already routinely assessed in the clinic (Capper et al., 2018) the inference of RNA-based pseudolineages from tumor methylomes demonstrated in this study provide a valuable basis for disease monitoring, the design of targeted therapies, or to identify patients who are likely to benefit from existing therapies such as SFRP1-induced pseudolineage arrest.

The SFRP1 and NOTUM overexpression experiments demonstrate the efficacy of targeted interventions to disrupt tumor pseudolineages. In both cases, tumor cells were arrested in the Quiescence-stage and particularly SFRP1-overexpressing mice exhibited a significantly increased survival. Encouragingly, SFRP1-overexpression did not elicit transcriptional changes in nearby healthy cells, suggesting that the action of SFRP1 may require a particular Wnt signaling conformation such as the one characteristic of SVZ stem cells and their malignant counterparts. As loss of SFRP1 was characteristic of glioblastomas, it remains to be seen whether SFRP1-overexpression is effective in LGGs. Similarly, the consistently high expression levels of DRAXIN might suggest that its overexpression in LGGs could elicit a similarly potent pseudolineage transformation. Regardless how it is used, an effective means of delivering the payload to patient tumors, such as through the use of AAVs (L. P. M. Kremer et al., 2021), will have to be devised.

Using a small molecule inhibitor of SFRP1 highlighted opportunities for transition-targeting combination therapies which can improve glioblastoma cell clearing. Quiescence-stage cells present a problem for conventional glioblastoma therapy through temozolomide (TMZ) or similar alkylating agents which primarily eliminate cycling or Activation-stage cells (Xie et al., 2022). As such, SFRP1-overexpression alone, while conducive to extending patient lifespan, does not represent an efficient means to eliminate the underlying disease. Instead, by first synchronizing cells in the Quiescence-stage through SFRP1-overexpression and then orchestrating their simultaneous activation through SFRP1-inhibition, a much greater killing effect can be achieved through TMZ. Thus by targeting a

transition over a concrete cell stage many more cells are cleared by the resulting therapy, hopefully leading to improved or lasting remission. The SFRP1 inhibitor experiment however raises additional questions about the persistence of the SFRP1-overexpression phenotype. As application of the inhibitor is sufficient to induce the activation of tumor cells, this suggests that the effects of SFRP1 are transient and require persistent presence of the protein to maintain the phenotype. This also raises the question of how permanent the astrocyte-like methylation identity of SFRP1-overexpressing cells is: as methylation changes are generally associated with long-term fate choice, these changes might present a barrier to activation through SFRP1 inhibition. These phenomena will require additional study into the mechanisms driving SFRP-induced pseudolineage arrest. Taken together, this result supports an astrocytic origin for glioblastoma hierarchies by demonstrating the stem cell potential of these cells. Overall, the combined application of the robust and specific pseudolineage-arresting effects of SFRP1-overexpression with a coordinated activation through its inhibition, presents a promising means to affect improved killing via TMZ, ultimately extending disease-free survival in patients.

Conclusion

"The ships hung in the sky in much the same way that bricks don't"

Douglas Adams, The Hitchhiker's Guide to the Galaxy

Through its clever phrasing, the above quote forces the reader to give pause and consider how two things are similar despite that they quite emphatically are not. Observing how things are similar has led to remarkable leaps in biology, from Darwin's observations to Linnaeus' systematics and Mendel's careful counting. Now, in the molecular age and with the combined efforts of billions of transistors at our fingertips, we are more equipped than ever to identify how different any two things are. But all of life is remarkably similar, a product of the central dogma and the various behaviors it begets. Cancers are no different, and I render Adams' quote to frame a comparison between cancer cells and their healthy counterparts: viewing the two much in the same way they aren't different.

We classify tumors according to their tissue of origin because they exhibit strong tissue-specific characteristics. I posit that this is due to the relatively restricted fate potential of adult cells which is faithfully inherited by tumor cells leading to their lineage constraint. Leveraging this constraint to isolate similarities between healthy and tumor cells, I developed *ptalign* as a means to place tumor cells within a fixed healthy lineage trajectory, using healthy stem cell transitions to infer a tumor *pseudolineage* in the absence of lineage tracing. By fixing the tumor lineage topology in this way, ptalign provides a framework to study tumor processes through contextual knowledge from the healthy reference. Notably, placing multiple tumors in the same reference trajectory facilitates the comparative study of tumor-tumor and tumor-healthy expression dynamics, providing a novel view of tumor organization which proved effective in elucidating tumor vulnerabilities through the targeting of lineage transitions.

In this work, I demonstrated the assessment, evaluation, and modulation of tumor pseudolineages in a cohort of 55 primary glioblastoma datasets. This revealed that glioblastomas develop into truncated or complete pseudolineages, plausibly reflecting the division characteristics of the cells

they derive from. Transferring contextual knowledge from the NSC lineage onto glioblastoma pseudolineages provided evidence of tumor organization rooted in adult NSC lineages, challenging the commonly held developmental view of their hierarchy. Wnt signaling was identified as a crucial regulator of NSCs transitioning from a Quiescent to an Activation state, a transition which also played a significant role in glioblastoma prognosis. Comparing pseudotime expression dynamics at this transition identified the secreted Wnt antagonist SFRP1 as recurrently dysregulated in glioblastomas, motivating its use in the targeted modulation of tumor pseudolineages. Reintroduction of SFRP1 directed tumors to a truncated pseudolineage dominated by astrocytic tumor cells, significantly improving the survival of tumor-bearing mice. This demonstrates SFRP1 as a potent fate-modulating factor in glioblastoma with exciting prospects for its therapeutic application, highlighting the advantages of a comparative approach to studying tumor cells rooted in the similarities to their healthy counterparts.

Several key lessons motivate the further development of ptalign and related technologies. Most prominently, ptalign demonstrated the efficacy of targeting a lineage transition over conventional strategies which prioritize individual cell states. This provides several therapeutically relevant benefits, as modulating a transition effectively targets at least two cell states at once and can lead to the subsequent restriction of other cell fates in a linear model of tumor hierarchy. Combination therapies which utilize this approach to synchronize cell states will synergize well with existing therapies targeting individual states, boosting patient outcomes without rendering existing strategies obsolete.

The real strength of ptalign lies in the adaptability of the method to different situations, paving the way for a pan-cancer approach to mine countless existing atlas datasets for specific tumor vulnerabilities. The unique perspective of tumor organization enabled in ptalign provides a rich source of testable hypotheses to interrogate functional aspects of tumor biology. These insights serve to elucidate the underlying principles driving tumor organization, laying the groundwork for novel treatment strategies and the development of personalized therapies. All told, this approach leverages the similarities between cancers and healthy cells to provide important context for understanding where they are different: these roles could just as well be reversed, illuminating principles of healthy development by learning from cancer.

Supplementary Tables

SVZ QAD Geneset

Table 1(i): Quiescence-stage genes derived from the SVZ NSC lineage. These genes are enriched in expression in the Quiescence-stage of the SVZ NSC lineage, comprising both qNSCs and niche astrocytes. Together with the SVZ-QAD Activation-stage and Differentiation-stage genes, these genes were used to conduct ptalign pseudotime alignment of various single-cell glioblastoma datasets.

ABHD3	ENSG00000158201	FJX1	ENSG00000179431	PCDH7	ENSG00000169851
ACAA2	ENSG00000167315	FXYD1	ENSG00000266964	PLA2G7	ENSG00000146070
ACSBG1	ENSG00000103740	GABBR2	ENSG00000136928	PREX2	ENSG00000046889
ACSL3	ENSG00000123983	GABRB1	ENSG00000163288	RAMP1	ENSG00000132329
ALDH1L1	ENSG00000144908	GABRG1	ENSG00000163285	RGCC	ENSG00000102760
ALDOC	ENSG00000109107	GJB6	ENSG00000121742	S100A1	ENSG00000160678
APPL2	ENSG00000136044	GPC5	ENSG00000179399	S1PR1	ENSG00000170989
AQP4	ENSG00000171885	GPR37L1	ENSG00000170075	SCRG1	ENSG00000164106
ASS1	ENSG00000130707	GRIN2C	ENSG00000161509	SDC4	ENSG00000124145
ATP1B2	ENSG00000129244	GRM3	ENSG00000198822	SERPINE2	ENSG00000135919
BAALC	ENSG00000164929	HAPLN1	ENSG00000145681	SFXN5	ENSG00000144040
BCAN	ENSG00000132692	HEPACAM	ENSG00000165478	SLC38A3	ENSG00000188338
CA2	ENSG00000104267	HOPX	ENSG00000171476	SLC39A12	ENSG00000148482
CAMK2N1	ENSG00000162545	HSPA2	ENSG00000126803	SLC4A4	ENSG00000080493
CHCHD10	ENSG00000250479	HTRA1	ENSG00000166033	SLC6A11	ENSG00000132164
CHST1	ENSG00000175264	ID2	ENSG00000115738	SLC7A10	ENSG00000130876
CHST2	ENSG00000175040	IL33	ENSG00000137033	SLC9A3R1	ENSG00000109062
CLDN10	ENSG00000134873	KCNK1	ENSG00000135750	SLCO1C1	ENSG00000139155
CLMN	ENSG00000165959	LIMCH1	ENSG00000064042	SLITRK2	ENSG00000185985
CLU	ENSG00000120885	MERTK	ENSG00000153208	SMPDL3A	ENSG00000172594
CMTM5	ENSG00000166091	MGLL	ENSG00000074416	SPARC	ENSG00000113140
CRYM	ENSG00000103316	MGST1	ENSG00000008394	SPARCL1	ENSG00000152583
CXCL14	ENSG00000145824	MLC1	ENSG00000100427	SREBF1	ENSG00000072310
DAAM2	ENSG00000146122	MT3	ENSG00000087250	TCF7L2	ENSG00000148737
DHRS3	ENSG00000162496	MYORG	ENSG00000164976	THBS4	ENSG00000113296
DKK3	ENSG00000050165	NAAA	ENSG00000138744	TLCD1	ENSG00000160606
EDNRB	ENSG00000136160	NIM1K	ENSG00000177453	TMEM176A	ENSG00000002933
EPHX2	ENSG00000120915	NKAIN4	ENSG00000101198	TMEM229A	ENSG00000234224
EPS8	ENSG00000151491	NTM	ENSG00000182667	TRIL	ENSG00000255690
EVA1A	ENSG00000115363	NTSR2	ENSG00000169006	TST	ENSG00000128311
F3	ENSG00000117525	OAF	ENSG00000184232	TTYH1	ENSG00000167614
FAM107A	ENSG00000168309	PAQR7	ENSG00000182749	VCAM1	ENSG00000162692
FBXO2	ENSG00000116661	PBXIP1	ENSG00000163346	VEGFA	ENSG00000112715
FGFR3	ENSG00000068078				

Table 1(ii): Activation-stage genes derived from the SVZ NSC lineage

ADGRV1	ENSG00000164199	GSX1	ENSG00000169840	NOTCH1	ENSG00000148400
ANP32B	ENSG00000136938	HAT1	ENSG00000128708	NOTUM	ENSG00000185269
ARL4C	ENSG00000188042	HELLS	ENSG00000119969	NPTX2	ENSG00000106236
ASCL1	ENSG00000139352	HELT	ENSG00000187821	NR4A1	ENSG00000123358
BTG2	ENSG00000159388	HES6	ENSG00000144485	ODC1	ENSG00000115758
CCND1	ENSG00000110092	HMGB2	ENSG00000164104	OLIG2	ENSG00000205927
CDK6	ENSG00000105810	HMGN5	ENSG00000198157	PCNA	ENSG00000132646
CENPM	ENSG00000100162	IER2	ENSG00000160888	PPP1R15A	ENSG00000087074
CORO1C	ENSG00000110880	JUNB	ENSG00000171223	RBM3	ENSG00000102317
CRLF1	ENSG00000006016	KCNE5	ENSG00000176076	RRM2	ENSG00000171848
DCTPP1	ENSG00000179958	KLF4	ENSG00000136826	SERF2	ENSG00000140264
DLL1	ENSG00000198719	LIMA1	ENSG00000050405	SIVA1	ENSG00000184990
DLL3	ENSG00000090932	LRRFIP1	ENSG00000124831	SLBP	ENSG00000163950
DTL	ENSG00000143476	LSM2	ENSG00000204392	SOCS3	ENSG00000184557
DTYMK	ENSG00000168393	LYAR	ENSG00000145220	SUMO2	ENSG00000188612
DUT	ENSG00000128951	MCM2	ENSG00000073111	TEAD2	ENSG00000074219
E2F1	ENSG00000101412	MCM3	ENSG00000112118	TIPIN	ENSG00000075131
EGFR	ENSG00000146648	MCM5	ENSG00000100297	TMEM132B	ENSG00000139364
EGR1	ENSG00000120738	MCM6	ENSG00000076003	TNFRSF19	ENSG00000127863
FABP7	ENSG00000164434	MFNG	ENSG00000100060	TPM4	ENSG00000167460
FOS	ENSG00000170345	NBL1	ENSG00000158747	UHRF1	ENSG00000276043
FOSB	ENSG00000125740	NCALD	ENSG00000104490	UNG	ENSG00000076248
GADD45G	ENSG00000130222	NHP2	ENSG00000145912	WDR89	ENSG00000140006
GMNN	ENSG00000112312	NKD1	ENSG00000140807	ZFP36	ENSG00000128016
GNL3	ENSG00000163938	NOLC1	ENSG00000166197		

Table 1(iii): Differentiation-stage genes derived from the SVZ NSC lineage

ABRACL	ENSG00000146386	FXYD6	ENSG00000137726	PCDH9	ENSG00000184226
ADARB2	ENSG00000185736	GAD1	ENSG00000128683	PLCL1	ENSG00000115896
ANKS1B	ENSG00000185046	GAD2	ENSG00000136750	PLXNA4	ENSG00000221866
APP	ENSG00000142192	GNG2	ENSG00000186469	PODXL2	ENSG00000114631
ARX	ENSG00000004848	IGFBPL1	ENSG00000137142	RUNX1T1	ENSG00000079102
BASP1	ENSG00000176788	KIF5C	ENSG00000168280	S100A10	ENSG00000197747
BCL11B	ENSG00000127152	LMO3	ENSG00000048540	SCRT1	ENSG00000261678
C11orf96	ENSG00000187479	LRRC7	ENSG00000033122	SHTN1	ENSG00000187164
CDK5R1	ENSG00000176749	LY6H	ENSG00000176956	SNRPN	ENSG00000128739
CELF4	ENSG00000101489	MAP1B	ENSG00000131711	SP8	ENSG00000164651
CITED2	ENSG00000164442	MEX3A	ENSG00000254726	SP9	ENSG00000217236
CTXN1	ENSG00000178531	MLLT11	ENSG00000213190	SRRM4	ENSG00000139767
DBN1	ENSG00000113758	MPPED2	ENSG00000066382	ST18	ENSG00000147488
DCBLD1	ENSG00000164465	MTSS1	ENSG00000170873	STMN2	ENSG00000104435
DCX	ENSG00000077279	MYT1L	ENSG00000186487	STMN3	ENSG00000197457
DLX2	ENSG00000115844	NAV3	ENSG00000067798	STMN4	ENSG00000015592
DLX5	ENSG00000105880	NOL4	ENSG00000101746	TIAM2	ENSG00000146426
DPYSL3	ENSG00000113657	NREP	ENSG00000134986	TMEFF1	ENSG00000241697
ELAVL3	ENSG00000196361	NRXN3	ENSG00000021645	TOX3	ENSG00000103460
ELAVL4	ENSG00000162374	NSG1	ENSG00000168824	TTC9B	ENSG00000174521
ENOX1	ENSG00000120658	NSG2	ENSG00000170091	UCHL1	ENSG00000154277
FNBP1L	ENSG00000137942	PAFAH1B3	ENSG00000079462	ZNF704	ENSG00000164684
FSCN1	ENSG00000075618	PBX3	ENSG00000167081		

GBM QAD Geneset

Table 2(i): Quiescence-stage genes derived from glioblastomas. These genes are enriched in expression in the Quiescence-stage of glioblastomas and the SVZ NSC lineage, and were used in conjunction with the GBM-QAD Activation-stage and Differentiation-stage gene sets to enable pseudolineage inference by bulk decomposition of TCGA and Wu et al samples

ACSS3	ENSG00000111058	GFAP	ENSG00000131095	PLA2G5	ENSG00000127472
ADCYAP1R1	ENSG00000078549	GLIS3	ENSG00000107249	PLCD3	ENSG00000161714
AGT	ENSG00000135744	GPR37	ENSG00000170775	PLTP	ENSG00000100979
AHNAK	ENSG00000124942	HEPACAM	ENSG00000165478	PON2	ENSG00000105854
ALDH1L1	ENSG00000144908	HIF3A	ENSG00000124440	PROS1	ENSG00000184500
ALDOC	ENSG00000109107	HNMT	ENSG00000150540	RAMP1	ENSG00000132329
AQP4	ENSG00000171885	HOPX	ENSG00000171476	RFX4	ENSG00000111783
ARAP2	ENSG00000047365	HRH1	ENSG00000196639	RGMA	ENSG00000182175
ATP1A2	ENSG00000018625	HSPB8	ENSG00000152137	RHPN1	ENSG00000158106
ATP1B2	ENSG00000129244	HTRA1	ENSG00000166033	ROM1	ENSG00000149489
BAALC	ENSG00000164929	ID3	ENSG00000117318	SCARA3	ENSG00000168077
BBOX1	ENSG00000129151	ID4	ENSG00000172201	SDC4	ENSG00000124145
BDH2	ENSG00000164039	IL33	ENSG00000137033	SFXN5	ENSG00000144040
C21orf62	ENSG00000205929	ITGA6	ENSG00000091409	SLC1A2	ENSG00000110436
C3	ENSG00000125730	ITM2C	ENSG00000135916	SLC1A3	ENSG00000079215
CA2	ENSG00000104267	ITPKB	ENSG00000143772	SLC25A18	ENSG00000182902
CCDC80	ENSG00000091986	KCNN3	ENSG00000143603	SLC4A4	ENSG00000080493
CHI3L1	ENSG00000133048	LAMB2	ENSG00000172037	SMOX	ENSG00000088826
CLU	ENSG00000120885	LFNG	ENSG00000106003	SPARC	ENSG00000113140
CRB2	ENSG00000148204	LIFR	ENSG00000113594	SPARCL1	ENSG00000152583
CRYAB	ENSG00000109846	LIMCH1	ENSG00000064042	SPOCD1	ENSG00000134668
CSF1	ENSG00000184371	LRIG1	ENSG00000144749	SSPN	ENSG00000123096
CXCL14	ENSG00000145824	MAOB	ENSG00000069535	TGFB2	ENSG00000092969
DHRS3	ENSG00000162496	MGST1	ENSG00000008394	TIMP3	ENSG00000100234
DKK3	ENSG00000050165	MLC1	ENSG00000100427	TIMP4	ENSG00000157150
EDNRB	ENSG00000136160	MT3	ENSG00000087250	TMEM176A	ENSG00000002933
EFEMP1	ENSG00000115380	NDP	ENSG00000124479	TMEM47	ENSG00000147027
EFHD1	ENSG00000115468	NDRG2	ENSG00000165795	TRIL	ENSG00000255690
ENKUR	ENSG00000151023	NMB	ENSG00000197696	TRIM47	ENSG00000132481
F3	ENSG00000117525	NTM	ENSG00000182667	TTYH1	ENSG00000167614
FADS2	ENSG00000134824	NTRK2	ENSG00000148053	TTYH2	ENSG00000141540
FAM107A	ENSG00000168309	PBXIP1	ENSG00000163346	VAMP5	ENSG00000168899
FAM181A	ENSG00000140067	PIFO	ENSG00000173947	VCAM1	ENSG00000162692
FGF1	ENSG00000113578				

Table 2(ii): Activation-stage genes derived from glioblastomas

ALKBH2	ENSG00000189046	EXOSC9	ENSG00000123737	MYC	ENSG00000136997
ANP32B	ENSG00000136938	FBL	ENSG00000105202	NEU4	ENSG00000204099
APOD	ENSG00000189058	FEN1	ENSG00000168496	NFKBIZ	ENSG00000144802
ARC	ENSG00000198576	FOSB	ENSG00000125740	NR4A1	ENSG00000123358
ARL4A	ENSG00000122644	GINS2	ENSG00000131153	OLIG2	ENSG00000205927
ATF3	ENSG00000162772	GPATCH4	ENSG00000160818	PCNA	ENSG00000132646
BARD1	ENSG00000138376	HELLS	ENSG00000119969	PDGFRA	ENSG00000134853
BEST3	ENSG00000127325	IFRD2	ENSG00000214706	PDLIM1	ENSG00000107438
BTG2	ENSG00000159388	ITGB3BP	ENSG00000142856	PPIH	ENSG00000171960
C11orf24	ENSG00000171067	JAG1	ENSG00000101384	PPP1R15A	ENSG00000087074
CDCA7L	ENSG00000164649	JUNB	ENSG00000171223	PTBP1	ENSG00000011304
CENPH	ENSG00000153044	KLF2	ENSG00000127528	PYCR1	ENSG00000183010
CENPK	ENSG00000123219	KLF4	ENSG00000136826	RGS16	ENSG00000143333
CENPU	ENSG00000151725	LIMA1	ENSG00000050405	RPA2	ENSG00000117748
CENPW	ENSG00000203760	LYAR	ENSG00000145220	SERTAD1	ENSG00000197019
CKS2	ENSG00000123975	MAFF	ENSG00000185022	SLBP	ENSG00000163950
CLSPN	ENSG00000092853	MCM2	ENSG00000073111	TIPIN	ENSG00000075131
CSRNP1	ENSG00000144655	MCM3	ENSG00000112118	TMEM132B	ENSG00000139364
DBF4	ENSG00000006634	MCM4	ENSG00000104738	TRIB1	ENSG00000173334
DLL1	ENSG00000198719	MCM5	ENSG00000100297	TYMS	ENSG00000176890
DUSP6	ENSG00000139318	MCM6	ENSG00000076003	UHRF1	ENSG00000276043
EGR1	ENSG00000120738	METTL1	ENSG00000037897	UNG	ENSG00000076248
EGR2	ENSG00000122877	MTHFD2	ENSG00000065911	WEE1	ENSG00000166483
ERF	ENSG00000105722	MYADM	ENSG00000179820		

Table 2(iii): Differentiation-stage genes derived from glioblastomas

ACTL6B	ENSG00000077080	FNBP1L	ENSG00000137942	RAB3A	ENSG00000105649
ADD2	ENSG00000075340	GAD1	ENSG00000128683	RBFOX2	ENSG00000100320
AFAP1	ENSG00000196526	GDAP1	ENSG00000104381	REEP1	ENSG00000068615
ANK3	ENSG00000151150	GDAP1L1	ENSG00000124194	RGMB	ENSG00000174136
ANKS1B	ENSG00000185046	GNG2	ENSG00000186469	RNF165	ENSG00000141622
ARL4D	ENSG00000175906	GNG3	ENSG00000162188	ROBO2	ENSG00000185008
ASPHD1	ENSG00000174939	GPR161	ENSG00000143147	RPS6KL1	ENSG00000198208
ATL1	ENSG00000198513	HRK	ENSG00000135116	SBK1	ENSG00000188322
B4GALNT1	ENSG00000135454	JPH4	ENSG00000092051	SCN3A	ENSG00000153253
BASP1	ENSG00000176788	KALRN	ENSG00000160145	SCN3B	ENSG00000166257
BCL11A	ENSG00000119866	KIAA1549	ENSG00000122778	SEZ6	ENSG00000063015
BEND5	ENSG00000162373	KIF5A	ENSG00000155980	SEZ6L	ENSG00000100095
CCNG2	ENSG00000138764	KIF5C	ENSG00000168280	SEZ6L2	ENSG00000174938
CCSAP	ENSG00000154429	KLF12	ENSG00000118922	SH3BP5	ENSG00000131370
CDC42EP3	ENSG00000163171	KLHDC8A	ENSG00000162873	SHTN1	ENSG00000187164
CDK5R1	ENSG00000176749	MAP1B	ENSG00000131711	SNAP25	ENSG00000132639
CELF3	ENSG00000159409	MAPK10	ENSG00000109339	SOBP	ENSG00000112320
CELF4	ENSG00000101489	MEX3A	ENSG00000254726	SRRM3	ENSG00000177679
CEP170	ENSG00000143702	MLLT11	ENSG00000213190	STMN2	ENSG00000104435
CERS6	ENSG00000172292	MPPED2	ENSG00000066382	STMN4	ENSG00000015592
CHGB	ENSG00000089199	MTURN	ENSG00000180354	STXBP1	ENSG00000136854
CSRNP3	ENSG00000178662	MYT1L	ENSG00000186487	SYT1	ENSG00000067715
CXADR	ENSG00000154639	NOL4	ENSG00000101746	THSD7A	ENSG00000005108
DBN1	ENSG00000113758	NOVA2	ENSG00000104967	TMEM178B	ENSG00000261115
DCX	ENSG00000077279	NREP	ENSG00000134986	TRIM36	ENSG00000152503
DIRAS1	ENSG00000176490	PAFAH1B3	ENSG00000079462	TTC9B	ENSG00000174521
DLX2	ENSG00000115844	PARP6	ENSG00000137817	TUBB4A	ENSG00000104833
DPYSL3	ENSG00000113657	PDZD4	ENSG00000067840	UCHL1	ENSG00000154277
DPYSL5	ENSG00000157851	PKIA	ENSG00000171033	WDR47	ENSG00000085433
DUSP26	ENSG00000133878	PLXNA4	ENSG00000221866	ZBTB8A	ENSG00000160062
DYNC1I1	ENSG00000158560	POU2F2	ENSG00000028277	ZNF704	ENSG00000164684
ELAVL2	ENSG00000107105	PRKCZ	ENSG00000067606	ZNF711	ENSG00000147180
ELAVL3	ENSG00000196361	PROX1	ENSG00000117707	ZNF821	ENSG00000102984
ELAVL4	ENSG00000162374				

Methods

During the course of this thesis work, I performed extensive analysis of multi-modal biological datasets, as well as inventing and implementing the ptalign algorithm. While I have attempted to motivate and describe my analyses in sufficient detail so as to facilitate their comprehension, the inclusion of every minutae was impractical. That is not to speak of the extensive techniques and materials which were used by Oguzhan Kaya and his students to enable the underlying wetlab experiments. For an in-depth understanding of these procedures and their implementation the motivated reader is encouraged to refer to (Foerster et al., 2023), where I have elaborated all relevant computational methods. Said publication also contains Oguzhan's documentation of the experimental methods, though additional details are available in (Akçay, 2023; Bekavac, 2022; Kaya, 2023).

Source code, data files, and raw analysis notebook are, of course, available from the author upon reasonable request.

Acknowledgements

Es gibt vieles worauf man stolz sein kann, aber weniges was die eigenen kinder uebertrifft. Ich bin zwar noch kindlos; war aber selber auch mal ein kind mit stolzen eltern, Veronika und Jens. Das weis ich weil ich irgendwann das handschriftliche babytagebuch meiner mutter uebernommen habe. Ich habe nicht viel von ihr, und das buch ist auch nicht lang, aber darin stehen viele niedlichen babygeschichten, aufmerksam berichtet und liebevoll aufgefuehrt. Eine sticht besonders heraus:

```
_ _ _ _ _ _ _ _ _ _ _ _ _ _ _ _ _ _ _ _ _ _ _ _ _ _ _
|                                                     |
|                                    31.12.1995       |
|  Heute waren wir im Zoo. Leo war sehr               |
|  begeistert und nun steht sein Berufswunsch         |
|  sicher fest: Professor! [...]                      |
|                                                     |
```

Heute sind es ueber 27 jahre seit diesem zoobesuch, und ich habe diese begeisterung nie verloren! Jetzt bin ich dieser vorhersage eine grossen schritt naeher gekommen, ein schritt den ich ohne die vielen freunde, familien, und kollegen nie haette bewaeltigen koennen. Aber eine wird immer fehlen, denn Veronika starb drei monate nach diesem zoobesuch an einer gehirnblutung. Nun wollte ich hier ausnahmsweise die mehrheitliche danksagung alleine dieser erinnerung widmen. Liebe mama, ich denke nicht genug an dich, aber ich bin sehr gluecklich dass ich diesen moment meiner euphorie auch mit der erinnerung an dich und deiner liebe verknuepfen konnte.

These past five years mark the longest I've lived in one location, and it's the amazing relationships and friendships I've formed in that time that have made it the most exciting in my life. My sincere gratitude and thanks to you Ana, for your trust and guidance; for the scientific lessons but also the human ones. And to Angela, for your support in this sisyphean task. And to Oguzhan: I miss your jokes and our discussions; I couldn't have asked for a better companion on this journey. As well as Lukas, Luis, Andre, Nikhil, Perrine, Santi, Jooa, Andrea, Masha, Heike, Alena, Damian, Andres, Veronika, Sanzhar, and the other lab members, past and present, who shaped the environment, especially during the pandemic years.

And to Rosa, for your candid and unpretentious nature; and your unwavering dedication to family, both on two legs and four. To Karl-Heinz and Hans, from whom I have learned so much, but who have so much more to tell. And to Salina, Balasz, and Zeno, whom I will get to spoil. And Pablo, Jens, and Tina, who are far away but never distant.

And finally to Paul, never a dull conversation and the only one who joined my journalclub-for-fun! And Denis, a great friend and excellent motivator. And to the members of Feeders Union: I yearn for those simpler times.

and my #1, Dearest Irene, my heart of hearts, with whom I share a bond like none other.

Bibliography

Ahlmann-Eltze, C., & Huber, W. (2023). Comparison of transformations for single-cell RNA-seq data. *Nature Methods*, *20*(5), 665–672. https://doi.org/10.1038/s41592-023-01814-1

Aibar, S., González-Blas, C. B., Moerman, T., Huynh-Thu, V. A., Imrichova, H., Hulselmans, G., Rambow, F., Marine, J.-C., Geurts, P., Aerts, J., Van Den Oord, J., Atak, Z. K., Wouters, J., & Aerts, S. (2017). SCENIC: Single-cell regulatory network inference and clustering. *Nature Methods*, *14*(11), 1083–1086. https://doi.org/10.1038/nmeth.4463

Akçay, V. (2023). *SFRP1-induced methylome remodeling underlies astrocytic dormancy in glioblastoma* [Masters Thesis]. University Heidelberg.

Alcantara Llaguno, S., Chen, J., Kwon, C.-H., Jackson, E. L., Li, Y., Burns, D. K., Alvarez-Buylla, A., & Parada, L. F. (2009). Malignant Astrocytomas Originate from Neural Stem/Progenitor Cells in a Somatic Tumor Suppressor Mouse Model. *Cancer Cell*, *15*(1), 45–56. https://doi.org/10.1016/j.ccr.2008.12.006

Alcantara Llaguno, S., Sun, D., Pedraza, A. M., Vera, E., Wang, Z., Burns, D. K., & Parada, L. F. (2019). Cell-of-origin susceptibility to glioblastoma formation declines with neural lineage restriction. *Nature Neuroscience*, *22*(4), 545–555. https://doi.org/10.1038/s41593-018-0333-8

Alexandrov, L. B., Jones, P. H., Wedge, D. C., Sale, J. E., Campbell, P. J., Nik-Zainal, S., & Stratton, M. R. (2015). Clock-like mutational processes in human somatic cells. *Nature Genetics*, *47*(12), 1402–1407. https://doi.org/10.1038/ng.3441

Alpert, A., Moore, L. S., Dubovik, T., & Shen-Orr, S. S. (2018). Alignment of single-cell trajectories to compare cellular expression dynamics. *Nature Methods*, *15*(4), 267–270. https://doi.org/10.1038/nmeth.4628

Alpert, A., Nahman, O., Starosvetsky, E., Hayun, M., Curiel, T. J., Ofran, Y., & Shen-Orr, S. S. (2022). Alignment of single-cell trajectories by tuMap enables high-resolution quantitative comparison of cancer samples. *Cell Systems*, *13*(1), 71-82.e8. https://doi.org/10.1016/j.cels.2021.09.003

Altman, J., & Das, G. D. (1965). Autoradiographic and histological evidence of postnatal hippocampal neurogenesis in rats. *Journal of Comparative Neurology*, *124*(3), 319–335. https://doi.org/10.1002/cne.901240303

Altmann, C., Keller, S., & Schmidt, M. H. H. (2019). The Role of SVZ Stem Cells in Glioblastoma. *Cancers*, *11*(4), 448. https://doi.org/10.3390/cancers11040448

Amezquita, R. A., Lun, A. T. L., Becht, E., Carey, V. J., Carpp, L. N., Geistlinger, L., Marini, F., Rue-Albrecht, K., Risso, D., Soneson, C., Waldron, L., Pagès, H., Smith, M. L., Huber, W., Morgan, M., Gottardo, R., & Hicks, S. C. (2020). Orchestrating single-cell analysis with Bioconductor. *Nature Methods*, *17*(2), 137–145. https://doi.org/10.1038/s41592-019-0654-x

Anders, S., Pyl, P. T., & Huber, W. (2015). HTSeq—A Python framework to work with high-throughput sequencing data. *Bioinformatics*, *31*(2), 166–169. https://doi.org/10.1093/bioinformatics/btu638

Avila Cobos, F., Alquicira-Hernandez, J., Powell, J. E., Mestdagh, P., & De Preter, K. (2020). Benchmarking of cell type deconvolution pipelines for transcriptomics data. *Nature Communications*, *11*(1), 5650. https://doi.org/10.1038/s41467-020-19015-1

Baharudin, R., Tieng, F. Y. F., Lee, L.-H., & Ab Mutalib, N. S. (2020). Epigenetics of SFRP1: The Dual Roles in Human Cancers. *Cancers*, *12*(2), 445. https://doi.org/10.3390/cancers12020445

Barile, M., Imaz-Rosshandler, I., Inzani, I., Ghazanfar, S., Nichols, J., Marioni, J. C., Guibentif, C., & Göttgens, B. (2021). Coordinated changes in gene expression kinetics underlie both mouse and human erythroid maturation. *Genome Biology*, *22*(1), 197. https://doi.org/10.1186/s13059-021-02414-y

Basak, O., Krieger, T. G., Muraro, M. J., Wiebrands, K., Stange, D. E., Frias-Aldeguer, J., Rivron, N. C., Van De Wetering, M., Van Es, J. H., Van Oudenaarden, A., Simons, B. D., & Clevers, H. (2018). Troy+ brain stem cells cycle through quiescence and regulate their number by sensing niche occupancy. *Proceedings of the National Academy of Sciences*, *115*(4). https://doi.org/10.1073/pnas.1715911114

Bast, L., Calzolari, F., Strasser, M. K., Hasenauer, J., Theis, F. J., Ninkovic, J., & Marr, C. (2018). Increasing Neural Stem Cell Division Asymmetry and Quiescence Are Predicted to Contribute to the Age-Related Decline in Neurogenesis. *Cell Reports*, *25*(12), 3231-3240.e8. https://doi.org/10.1016/j.celrep.2018.11.088

Bekavac, M. (2022). *Dissecting Heterogeneity and Wnt-induced Quiescence in Glioblastoma* [Masters Thesis]. University Heidelberg.

Berendsen, S., Van Bodegraven, E., Seute, T., Spliet, W. G. M., Geurts, M., Hendrikse, J., Schoysman, L., Huiszoon, W. B., Varkila, M., Rouss, S., Bell, E. H., Kroonen, J., Chakravarti, A., Bours, V., Snijders, T. J., & Robe, P. A. (2019). Adverse prognosis of glioblastoma contacting the subventricular zone: Biological correlates. *PLOS ONE*, *14*(10), e0222717. https://doi.org/10.1371/journal.pone.0222717

Bhaduri, A., Andrews, M. G., Mancia Leon, W., Jung, D., Shin, D., Allen, D., Jung, D., Schmunk, G., Haeussler, M., Salma, J., Pollen, A. A., Nowakowski, T. J., & Kriegstein, A. R. (2020). Cell stress in cortical organoids impairs molecular subtype specification. *Nature*, *578*(7793), 142–148. https://doi.org/10.1038/s41586-020-1962-0

Bhaduri, A., Di Lullo, E., Jung, D., Müller, S., Crouch, E. E., Espinosa, C. S., Ozawa, T., Alvarado, B., Spatazza, J., Cadwell, C. R., Wilkins, G., Velmeshev, D., Liu, S. J., Malatesta, M., Andrews, M. G., Mostajo-Radji, M. A., Huang, E. J., Nowakowski, T. J., Lim, D. A., … Kriegstein, A. R. (2020). Outer Radial Glia-like Cancer Stem Cells Contribute to Heterogeneity of Glioblastoma. *Cell Stem Cell*, *26*(1), 48-63.e6. https://doi.org/10.1016/j.stem.2019.11.015

Bhaduri, A., Sandoval-Espinosa, C., Otero-Garcia, M., Oh, I., Yin, R., Eze, U. C., Nowakowski, T. J., & Kriegstein, A. R. (2021). An atlas of cortical arealization identifies dynamic molecular signatures. *Nature*, *598*(7879), 200–204. https://doi.org/10.1038/s41586-021-03910-8

Bian, S., Repic, M., Guo, Z., Kavirayani, A., Burkard, T., Bagley, J. A., Krauditsch, C., & Knoblich, J. A. (2018). Genetically engineered cerebral organoids model brain tumor formation. *Nature Methods*, *15*(8), 631–639. https://doi.org/10.1038/s41592-018-0070-7

Bodine, P. V. N., Stauffer, B., Ponce-de-Leon, H., Bhat, R. A., Mangine, A., Seestaller-Wehr, L. M., Moran, R. A., Billiard, J., Fukayama, S., Komm, B. S., Pitts, K., Krishnamurthy, G., Gopalsamy, A., Shi, M., Kern, J. C., Commons, T. J., Woodworth, R. P., Wilson, M. A., Welmaker, G. S., … Moore, W. J. (2009). A small molecule inhibitor of the Wnt antagonist secreted frizzled-related protein-1 stimulates bone formation. *Bone*, *44*(6), 1063–1068. https://doi.org/10.1016/j.bone.2009.02.013

Boonekamp, K. E., Heo, I., Artegiani, B., Asra, P., Van Son, G., De Ligt, J., & Clevers, H. (2021). Identification of novel human Wnt target genes using adult endodermal tissue-derived organoids. *Developmental Biology*, *474*, 37–47. https://doi.org/10.1016/j.ydbio.2021.01.009

Brennan, C. W., Verhaak, R. G. W., McKenna, A., Campos, B., Noushmehr, H., Salama, S. R., Zheng, S., Chakravarty, D., Sanborn, J. Z., Berman, S. H., Beroukhim, R., Bernard, B., Wu, C.-J., Genovese, G., Shmulevich, I., Barnholtz-Sloan, J., Zou, L., Vegesna, R., Shukla, S. A., … McLendon, R. (2013). The Somatic Genomic Landscape of Glioblastoma. *Cell*, *155*(2), 462–477. https://doi.org/10.1016/j.cell.2013.09.034

Buonfiglioli, A., & Hambardzumyan, D. (2021). Macrophages and microglia: The cerberus of glioblastoma. *Acta Neuropathologica Communications*, *9*(1), 54. https://doi.org/10.1186/s40478-021-01156-z

Caldwell, G. M., Jones, C., Gensberg, K., Jan, S., Hardy, R. G., Byrd, P., Chughtai, S., Wallis, Y., Matthews, G. M., & Morton, D. G. (2004). The Wnt Antagonist sFRP1 in Colorectal Tumorigenesis. *Cancer Research*, *64*(3), 883–888. https://doi.org/10.1158/0008-5472.CAN-03-1346

Cao, J., Spielmann, M., Qiu, X., Huang, X., Ibrahim, D. M., Hill, A. J., Zhang, F., Mundlos, S., Christiansen, L., Steemers, F. J., Trapnell, C., & Shendure, J. (2019). The single-cell transcriptional landscape of mammalian organogenesis. *Nature*, *566*(7745), 496–502. https://doi.org/10.1038/s41586-019-0969-x

Capper, D., Jones, D. T. W., Sill, M., Hovestadt, V., Schrimpf, D., Sturm, D., Koelsche, C., Sahm, F., Chavez, L., Reuss, D. E., Kratz, A., Wefers, A. K., Huang, K., Pajtler, K. W., Schweizer, L., Stichel, D., Olar, A., Engel, N. W., Lindenberg, K., … Pfister, S. M. (2018). DNA methylation-based classification of central nervous system tumours. *Nature*, *555*(7697), 469–474. https://doi.org/10.1038/nature26000

Carvajal Ibañez, D., Skabkin, M., Hooli, J., Cerrizuela, S., Göpferich, M., Jolly, A., Volk, K., Zumwinkel, M., Bertolini, M., Figlia, G., Höfer, T., Kramer, G., Anders, S., Teleman, A. A., Marciniak-Czochra, A., & Martin-Villalba, A. (2023). Interferon regulates neural stem cell function at all ages by orchestrating mTOR and cell cycle. *EMBO Molecular Medicine*, *15*(4), e16434. https://doi.org/10.15252/emmm.202216434

Castellan, M., Guarnieri, A., Fujimura, A., Zanconato, F., Battilana, G., Panciera, T., Sladitschek, H. L., Contessotto, P., Citron, A., Grilli, A., Romano, O., Bicciato, S., Fassan, M., Porcù, E., Rosato, A., Cordenonsi, M., & Piccolo, S. (2020). Single-cell analyses reveal YAP/TAZ as regulators of stemness and cell plasticity in glioblastoma. *Nature Cancer*, *2*(2), 174–188. https://doi.org/10.1038/s43018-020-00150-z

Caviness, V. S. (2003). Cell Output, Cell Cycle Duration and Neuronal Specification: A Model of Integrated Mechanisms of the Neocortical Proliferative Process. *Cerebral Cortex*, *13*(6), 592–598. https://doi.org/10.1093/cercor/13.6.592

Cebrian-Silla, A., Nascimento, M. A., Redmond, S. A., Mansky, B., Wu, D., Obernier, K., Romero Rodriguez, R., Gonzalez-Granero, S., García-Verdugo, J. M., Lim, D. A., & Álvarez-Buylla, A. (2021). Single-cell analysis of the ventricular-subventricular zone reveals signatures of dorsal and ventral adult neurogenesis. *eLife*, *10*, e67436. https://doi.org/10.7554/eLife.67436

Ceccarelli, M., Barthel, F. P., Malta, T. M., Sabedot, T. S., Salama, S. R., Murray, B. A., Morozova, O., Newton, Y., Radenbaugh, A., Pagnotta, S. M., Anjum, S., Wang, J., Manyam, G., Zoppoli, P., Ling, S., Rao, A. A., Grifford, M., Cherniack, A. D., Zhang, H., … Zmuda, E. (2016). Molecular Profiling Reveals Biologically Discrete Subsets and Pathways of Progression in Diffuse Glioma. *Cell*, *164*(3), 550–563. https://doi.org/10.1016/j.cell.2015.12.028

Cerrizuela, S., Kaya, O., Kremer, L. P. M., Sarvari, A., Ellinger, T., Straub, J., Brunken, J., Sanz-Morejón, A., Korkmaz, A., & Martín-Villalba, A. (2022). High-throughput scNMT protocol for multiomics profiling of single cells from mouse brain and pancreatic organoids. *STAR Protocols*, *3*(3), 101555. https://doi.org/10.1016/j.xpro.2022.101555

Chaligne, R., Gaiti, F., Silverbush, D., Schiffman, J. S., Weisman, H. R., Kluegel, L., Gritsch, S., Deochand, S. D., Gonzalez Castro, L. N., Richman, A. R., Klughammer, J., Biancalani, T., Muus, C., Sheridan, C., Alonso, A., Izzo, F., Park, J., Rozenblatt-Rosen, O., Regev, A., … Landau, D. A. (2021). Epigenetic encoding, heritability and plasticity of glioma transcriptional cell states. *Nature Genetics*, *53*(10), 1469–1479. https://doi.org/10.1038/s41588-021-00927-7

Chang, W., Cheng, J., Allaire, J., & Borges, B. (2024). *shiny: Web Application Framework for R*. https://github.com/rstudio/shiny

Chen, J., Li, Y., Yu, T.-S., McKay, R. M., Burns, D. K., Kernie, S. G., & Parada, L. F. (2012). A restricted cell population propagates glioblastoma growth after chemotherapy. *Nature*, *488*(7412), 522–526. https://doi.org/10.1038/nature11287

Ciani, L., & Salinas, P. C. (2005). WNTS in the vertebrate nervous system: From patterning to neuronal connectivity. *Nature Reviews Neuroscience*, *6*(5), 351–362. https://doi.org/10.1038/nrn1665

Clevers, H. (2016). Modeling Development and Disease with Organoids. *Cell*, *165*(7), 1586–1597. https://doi.org/10.1016/j.cell.2016.05.082

Cloughesy, T. F., Mochizuki, A. Y., Orpilla, J. R., Hugo, W., Lee, A. H., Davidson, T. B., Wang, A. C., Ellingson, B. M., Rytlewski, J. A., Sanders, C. M., Kawaguchi, E. S., Du, L., Li, G., Yong, W. H., Gaffey, S. C., Cohen, A. L., Mellinghoff, I. K., Lee, E. Q., Reardon, D. A., … Prins, R. M. (2019). Neoadjuvant anti-PD-1 immunotherapy promotes a survival benefit with intratumoral and systemic immune responses in recurrent glioblastoma. *Nature Medicine*, *25*(3), 477–486. https://doi.org/10.1038/s41591-018-0337-7

Colom, B., Alcolea, M. P., Piedrafita, G., Hall, M. W. J., Wabik, A., Dentro, S. C., Fowler, J. C., Herms, A., King, C., Ong, S. H., Sood, R. K., Gerstung, M., Martincorena, I., Hall, B. A., & Jones, P. H. (2020). Spatial competition shapes the dynamic mutational landscape of normal esophageal epithelium. *Nature Genetics*, *52*(6), 604–614. https://doi.org/10.1038/s41588-020-0624-3

Comba, A., Faisal, S. M., Dunn, P. J., Argento, A. E., Hollon, T. C., Al-Holou, W. N., Varela, M. L., Zamler, D. B., Quass, G. L., Apostolides, P. F., Abel, C., Brown, C. E., Kish, P. E., Kahana, A., Kleer, C. G., Motsch, S., Castro, M. G., & Lowenstein, P. R. (2022). Spatiotemporal analysis of glioma heterogeneity reveals COL1A1 as an actionable target to disrupt tumor progression. *Nature Communications*, *13*(1), 3606. https://doi.org/10.1038/s41467-022-31340-1

Conesa, A., Nueda, M. J., Ferrer, A., & Talón, M. (2006). maSigPro: A method to identify significantly differential expression profiles in time-course microarray experiments. *Bioinformatics*, *22*(9), 1096–1102. https://doi.org/10.1093/bioinformatics/btl056

Conover, J. C., & Todd, K. L. (2017). Neuronal Stem Cell Niches of the Brain. In *Biology and Engineering of Stem Cell Niches* (pp. 75–91). Elsevier. https://doi.org/10.1016/B978-0-12-802734-9.00006-8

Cooper, K. L., Sears, K. E., Uygur, A., Maier, J., Baczkowski, K.-S., Brosnahan, M., Antczak, D., Skidmore, J. A., & Tabin, C. J. (2014). Patterning and post-patterning modes of evolutionary digit loss in mammals. *Nature*, *511*(7507), 41–45. https://doi.org/10.1038/nature13496

Corbin, J. G., Nery, S., & Fishell, G. (2001). Telencephalic cells take a tangent: Non-radial migration in the mammalian forebrain. *Nature Neuroscience*, *4*(S11), 1177–1182. https://doi.org/10.1038/nn749

Couturier, C. P., Ayyadhury, S., Le, P. U., Nadaf, J., Monlong, J., Riva, G., Allache, R., Baig, S., Yan, X., Bourgey, M., Lee, C., Wang, Y. C. D., Wee Yong, V., Guiot, M.-C., Najafabadi, H., Misic, B., Antel, J., Bourque, G., Ragoussis, J., & Petrecca, K. (2020). Single-cell RNA-seq reveals that glioblastoma recapitulates a normal neurodevelopmental hierarchy. *Nature Communications*, *11*(1), 3406. https://doi.org/10.1038/s41467-020-17186-5

Dahl, E., Wiesmann, F., Woenckhaus, M., Stoehr, R., Wild, P. J., Veeck, J., Knüchel, R., Klopocki, E., Sauter, G., Simon, R., Wieland, W. F., Walter, B., Denzinger, S., Hartmann, A., & Hammerschmied, C. G. (2007). Frequent loss of SFRP1 expression in multiple human solid tumours: Association with aberrant promoter methylation in renal cell carcinoma. *Oncogene*, *26*(38), 5680–5691. https://doi.org/10.1038/sj.onc.1210345

Danciu, D.-P., Hooli, J., Martin-Villalba, A., & Marciniak-Czochra, A. (2023). Mathematics of neural stem cells: Linking data and processes. *Cells & Development*, *174*, 203849. https://doi.org/10.1016/j.cdev.2023.203849

Darmanis, S., Sloan, S. A., Croote, D., Mignardi, M., Chernikova, S., Samghababi, P., Zhang, Y., Neff, N., Kowarsky, M., Caneda, C., Li, G., Chang, S. D., Connolly, I. D., Li, Y., Barres, B. A., Gephart, M. H., & Quake, S. R. (2017). Single-Cell RNA-Seq Analysis of Infiltrating Neoplastic Cells at the Migrating Front of Human Glioblastoma. *Cell Reports*, *21*(5), 1399–1410. https://doi.org/10.1016/j.celrep.2017.10.030

Dirkse, A., Golebiewska, A., Buder, T., Nazarov, P. V., Muller, A., Poovathingal, S., Brons, N. H. C., Leite, S., Sauvageot, N., Sarkisjan, D., Seyfrid, M., Fritah, S., Stieber, D., Michelucci, A., Hertel, F., Herold-Mende, C., Azuaje, F., Skupin, A., Bjerkvig, R., … Niclou, S. P. (2019). Stem cell-associated heterogeneity in Glioblastoma results from intrinsic tumor plasticity shaped by the microenvironment. *Nature Communications*, *10*(1), 1787. https://doi.org/10.1038/s41467-019-09853-z

Do, V. H., Blažević, M., Monteagudo, P., Borozan, L., Elbassioni, K., Laue, S., Ringeling, F. R., Matijević, D., & Canzar, S. (2019). Dynamic pseudo-time warping of complex single-cell trajectories. *bioRxiv*. https://doi.org/10.1101/522672

Dobin, A., Davis, C. A., Schlesinger, F., Drenkow, J., Zaleski, C., Jha, S., Batut, P., Chaisson, M., & Gingeras, T. R. (2013). STAR: Ultrafast universal RNA-seq aligner. *Bioinformatics*, *29*(1), 15–21. https://doi.org/10.1093/bioinformatics/bts635

Doetsch, F., Caillé, I., Lim, D. A., García-Verdugo, J. M., & Alvarez-Buylla, A. (1999). Subventricular Zone Astrocytes Are Neural Stem Cells in the Adult Mammalian Brain. *Cell*, *97*(6), 703–716. https://doi.org/10.1016/S0092-8674(00)80783-7

Doetsch, F., García-Verdugo, J. M., & Alvarez-Buylla, A. (1997). Cellular Composition and Three-Dimensional Organization of the Subventricular Germinal Zone in the Adult Mammalian Brain. *The Journal of Neuroscience*, *17*(13), 5046–5061. https://doi.org/10.1523/JNEUROSCI.17-13-05046.1997

Donega, V., Van Der Geest, A. T., Sluijs, J. A., Van Dijk, R. E., Wang, C. C., Basak, O., Pasterkamp, R. J., & Hol, E. M. (2022). Single-cell profiling of human subventricular zone progenitors identifies SFRP1 as a target to re-activate progenitors. *Nature Communications*, *13*(1), 1036. https://doi.org/10.1038/s41467-022-28626-9

Dorst, M. C., Díaz-Moreno, M., Dias, D. O., Guimarães, E. L., Holl, D., Kalkitsas, J., Silberberg, G., & Göritz, C. (2021). Astrocyte-derived neurons provide excitatory input to the adult striatal circuitry. *Proceedings of the National Academy of Sciences*, *118*(33), e2104119118. https://doi.org/10.1073/pnas.2104119118

Eriksson, P. S., Perfilieva, E., Björk-Eriksson, T., Alborn, A.-M., Nordborg, C., Peterson, D. A., & Gage, F. H. (1998). Neurogenesis in the adult human hippocampus. *Nature Medicine*, *4*(11), 1313–1317. https://doi.org/10.1038/3305

Ernst, J., Nau, G. J., & Bar-Joseph, Z. (2005). Clustering short time series gene expression data. *Bioinformatics*, *21*(Suppl 1), i159–i168. https://doi.org/10.1093/bioinformatics/bti1022

Escartin, C., Galea, E., Lakatos, A., O'Callaghan, J. P., Petzold, G. C., Serrano-Pozo, A., Steinhäuser, C., Volterra, A., Carmignoto, G., Agarwal, A., Allen, N. J., Araque, A., Barbeito, L., Barzilai, A., Bergles, D. E., Bonvento, G., Butt, A. M., Chen, W.-T., Cohen-Salmon, M., … Verkhratsky, A. (2021). Reactive astrocyte nomenclature, definitions, and future directions. *Nature Neuroscience*, *24*(3), 312–325. https://doi.org/10.1038/s41593-020-00783-4

Eze, U. C., Bhaduri, A., Haeussler, M., Nowakowski, T. J., & Kriegstein, A. R. (2021). Single-cell atlas of early human brain development highlights heterogeneity of human neuroepithelial cells and early radial glia. *Nature Neuroscience*, *24*(4), 584–594. https://doi.org/10.1038/s41593-020-00794-1

Ferrer-Vaquer, A., Piliszek, A., Tian, G., Aho, R. J., Dufort, D., & Hadjantonakis, A.-K. (2010). A sensitive and bright single-cell resolution live imaging reporter of Wnt/ß-catenin signaling in the mouse. *BMC Developmental Biology*, *10*(1), 121. https://doi.org/10.1186/1471-213X-10-121

Fiorelli, R., Azim, K., Fischer, B., & Raineteau, O. (2015). Adding a spatial dimension to postnatal ventricular-subventricular zone neurogenesis. *Development*, *142*(12), 2109–2120. https://doi.org/10.1242/dev.119966

Foerster, L. C., Kaya, O., Wüst, V., Bekavac, M., Ziegler, K. C., Akcay, V., Stinchcombe, N., Gesteira Perez, N., Ma, X., Sadik, A., Le, P. U., Petrecca, K., Opitz, C., Liu, H., Wirtz, C. R., Anders, S., Goncalves, A., & Martin-Villalba, A. (2023). *Identification of astrocyte-driven pseudolineages reveals clinical stratification and therapeutic targets in Glioblastoma*. bioRxiv. https://doi.org/10.1101/2023.09.15.557713

Freundlieb, N., François, C., Tandé, D., Oertel, W. H., Hirsch, E. C., & Höglinger, G. U. (2006). Dopaminergic Substantia Nigra Neurons Project Topographically Organized to the Subventricular Zone and Stimulate Precursor Cell Proliferation in Aged Primates. *The Journal of Neuroscience*, *26*(8), 2321–2325. https://doi.org/10.1523/JNEUROSCI.4859-05.2006

Friedmann-Morvinski, D., Bushong, E. A., Ke, E., Soda, Y., Marumoto, T., Singer, O., Ellisman, M. H., & Verma, I. M. (2012). Dedifferentiation of Neurons and Astrocytes by Oncogenes Can Induce Gliomas in Mice. *Science*, *338*(6110), 1080–1084. https://doi.org/10.1126/science.1226929

Friedmann-Morvinski, D., & Verma, I. M. (2014). Dedifferentiation and reprogramming: Origins of cancer stem cells. *EMBO Reports*, *15*(3), 244–253. https://doi.org/10.1002/embr.201338254

Fuentealba, L. C., Rompani, S. B., Parraguez, J. I., Obernier, K., Romero, R., Cepko, C. L., & Alvarez-Buylla, A. (2015). Embryonic Origin of Postnatal Neural Stem Cells. *Cell*, *161*(7), 1644–1655. https://doi.org/10.1016/j.cell.2015.05.041

Furutachi, S., Miya, H., Watanabe, T., Kawai, H., Yamasaki, N., Harada, Y., Imayoshi, I., Nelson, M., Nakayama, K. I., Hirabayashi, Y., & Gotoh, Y. (2015). Slowly dividing neural progenitors are an embryonic origin of adult neural stem cells. *Nature Neuroscience*, *18*(5), 657–665. https://doi.org/10.1038/nn.3989

Futreal, P. A., Coin, L., Marshall, M., Down, T., Hubbard, T., Wooster, R., Rahman, N., & Stratton, M. R. (2004). A census of human cancer genes. *Nature Reviews Cancer*, *4*(3), 177–183. https://doi.org/10.1038/nrc1299

Gaire, J., Varholick, J. A., Rana, S., Sunshine, M. D., Doré, S., Barbazuk, W. B., Fuller, D. D., Maden, M., & Simmons, C. S. (2021). Spiny mouse (Acomys): An emerging research organism for regenerative medicine with applications beyond the skin. *Npj Regenerative Medicine*, *6*(1), 1. https://doi.org/10.1038/s41536-020-00111-1

Galli, R., Binda, E., Orfanelli, U., Cipelletti, B., Gritti, A., De Vitis, S., Fiocco, R., Foroni, C., Dimeco, F., & Vescovi, A. (2004). Isolation and Characterization of Tumorigenic, Stem-like Neural Precursors from Human Glioblastoma. *Cancer Research*, *64*(19), 7011–7021. https://doi.org/10.1158/0008-5472.CAN-04-1364

Gangoso, E., Southgate, B., Bradley, L., Rus, S., Galvez-Cancino, F., McGivern, N., Güç, E., Kapourani, C.-A., Byron, A., Ferguson, K. M., Alfazema, N., Morrison, G., Grant, V., Blin, C., Sou, I., Marques-Torrejon, M. A., Conde, L., Parrinello, S., Herrero, J., … Pollard, S. M. (2021). Glioblastomas acquire myeloid-affiliated transcriptional programs via epigenetic immunoediting to elicit immune evasion. *Cell*, *184*(9), 2454-2470.e26. https://doi.org/10.1016/j.cell.2021.03.023

Garofano, L., Migliozzi, S., Oh, Y. T., D'Angelo, F., Najac, R. D., Ko, A., Frangaj, B., Caruso, F. P., Yu, K., Yuan, J., Zhao, W., Di Stefano, A. L., Bielle, F., Jiang, T., Sims, P., Suvà, M. L., Tang, F., Su, X.-D., Ceccarelli, M., … Iavarone, A. (2021). Pathway-based classification of glioblastoma uncovers a mitochondrial subtype with therapeutic vulnerabilities. *Nature Cancer*, *2*(2), 141–156. https://doi.org/10.1038/s43018-020-00159-4

Gavish, A., Tyler, M., Greenwald, A. C., Hoefflin, R., Simkin, D., Tschernichovsky, R., Galili Darnell, N., Somech, E., Barbolin, C., Antman, T., Kovarsky, D., Barrett, T., Gonzalez Castro, L. N., Halder, D., Chanoch-Myers, R., Laffy, J., Mints, M., Wider, A., Tal, R., … Tirosh, I. (2023). Hallmarks of transcriptional intratumour heterogeneity across a thousand tumours. *Nature*, *618*(7965), 598–606. https://doi.org/10.1038/s41586-023-06130-4

Gilbert, M. R., Dignam, J. J., Armstrong, T. S., Wefel, J. S., Blumenthal, D. T., Vogelbaum, M. A., Colman, H., Chakravarti, A., Pugh, S., Won, M., Jeraj, R., Brown, P. D., Jaeckle, K. A., Schiff, D., Stieber, V. W., Brachman, D. G., Werner-Wasik, M., Tremont-Lukats, I. W., Sulman, E. P., … Mehta, M. P. (2014). A Randomized Trial of Bevacizumab for Newly Diagnosed Glioblastoma. *New England Journal of Medicine*, *370*(8), 699–708. https://doi.org/10.1056/NEJMoa1308573

Gimple, R. C., Bhargava, S., Dixit, D., & Rich, J. N. (2019). Glioblastoma stem cells: Lessons from the tumor hierarchy in a lethal cancer. *Genes & Development*, *33*(11–12), 591–609. https://doi.org/10.1101/gad.324301.119

Goh, J. J. L., Chou, N., Seow, W. Y., Ha, N., Cheng, C. P. P., Chang, Y.-C., Zhao, Z. W., & Chen, K. H. (2020). Highly specific multiplexed RNA imaging in tissues with split-FISH. *Nature Methods*, *17*(7), 689–693. https://doi.org/10.1038/s41592-020-0858-0

Goldstein, B., Takeshita, H., Mizumoto, K., & Sawa, H. (2006). Wnt Signals Can Function as Positional Cues in Establishing Cell Polarity. *Developmental Cell*, *10*(3), 391–396. https://doi.org/10.1016/j.devcel.2005.12.016

Good, Z., Sarno, J., Jager, A., Samusik, N., Aghaeepour, N., Simonds, E. F., White, L., Lacayo, N. J., Fantl, W. J., Fazio, G., Gaipa, G., Biondi, A., Tibshirani, R., Bendall, S. C., Nolan, G. P., & Davis, K. L. (2018). Single-cell developmental classification of B cell precursor acute lymphoblastic leukemia at diagnosis reveals predictors of relapse. *Nature Medicine*, *24*(4), 474–483. https://doi.org/10.1038/nm.4505

Greenwald, A. C., Darnell, N. G., Hoefflin, R., Simkin, D., Gonzalez-Castro, L. N., Mount, C., Hirsch, D., Nomura, M., Talpir, T., Kedmi, M., Goliand, I., Medici, G., Li, B., Keren-Shaul, H., Weller, M., Addadi, Y., Neidert, M. C., Suvá, M. L., & Tirosh, I. (2023). *Integrative spatial analysis reveals a multi-layered organization of glioblastoma*. bioRxiv. https://doi.org/10.1101/2023.07.06.547924

Gritti, A., Cova, L., Parati, E. A., Galli, R., & Vescovi, A. L. (1995). Basic fibroblast growth factor supports the proliferation of epidermal growth factor-generated neuronal precursor cells of the adult mouse CNS. *Neuroscience Letters*, *185*(3), 151–154. https://doi.org/10.1016/0304-3940(95)11247-T

Guder, C., Philipp, I., Lengfeld, T., Watanabe, H., Hobmayer, B., & Holstein, T. W. (2006). The Wnt code: Cnidarians signal the way. *Oncogene*, *25*(57), 7450–7460. https://doi.org/10.1038/sj.onc.1210052

Gulati, G. S., Sikandar, S. S., Wesche, D. J., Manjunath, A., Bharadwaj, A., Berger, M. J., Ilagan, F., Kuo, A. H., Hsieh, R. W., Cai, S., Zabala, M., Scheeren, F. A., Lobo, N. A., Qian, D., Yu, F. B., Dirbas, F. M., Clarke, M. F., & Newman, A. M. (2020). *Single-cell transcriptional diversity is a hallmark of developmental potential*.

Habib, S. J., Chen, B.-C., Tsai, F.-C., Anastassiadis, K., Meyer, T., Betzig, E., & Nusse, R. (2013). A Localized Wnt Signal Orients Asymmetric Stem Cell Division in Vitro. *Science*, *339*(6126), 1445–1448. https://doi.org/10.1126/science.1231077

Hagemann-Jensen, M., Ziegenhain, C., & Sandberg, R. (2022). Scalable single-cell RNA sequencing from full transcripts with Smart-seq3xpress. *Nature Biotechnology*, *40*(10), 1452–1457. https://doi.org/10.1038/s41587-022-01311-4

Haghverdi, L., Büttner, M., Wolf, F. A., Buettner, F., & Theis, F. J. (2016). Diffusion pseudotime robustly reconstructs lineage branching. *Nature Methods*, *13*(10), 845–848. https://doi.org/10.1038/nmeth.3971

Haghverdi, L., Lun, A. T. L., Morgan, M. D., & Marioni, J. C. (2018). Batch effects in single-cell RNA-sequencing data are corrected by matching mutual nearest neighbors. *Nature Biotechnology*, *36*(5), 421–427. https://doi.org/10.1038/nbt.4091

Hambardzumyan, D., & Bergers, G. (2015). Glioblastoma: Defining Tumor Niches. *Trends in Cancer*, *1*(4), 252–265. https://doi.org/10.1016/j.trecan.2015.10.009

Hanawalt, P. C., & Spivak, G. (2008). Transcription-coupled DNA repair: Two decades of progress and surprises. *Nature Reviews Molecular Cell Biology*, *9*(12), 958–970. https://doi.org/10.1038/nrm2549

Hänzelmann, S., Castelo, R., & Guinney, J. (2013). GSVA: Gene set variation analysis for microarray and RNA-Seq data. *BMC Bioinformatics*, *14*(1), 7. https://doi.org/10.1186/1471-2105-14-7

Hendriks, G., Calléja, F., Vrieling, H., Mullenders, L. H. F., Jansen, J. G., & De Wind, N. (2008). Gene transcription increases DNA damage-induced mutagenesis in mammalian stem cells. *DNA Repair*, *7*(8), 1330–1339. https://doi.org/10.1016/j.dnarep.2008.04.015

Heumos, L., Schaar, A. C., Lance, C., Litinetskaya, A., Drost, F., Zappia, L., Lücken, M. D., Strobl, D. C., Henao, J., Curion, F., Single-cell Best Practices Consortium, Aliee, H., Ansari, M., Badia-i-Mompel, P., Büttner, M., Dann, E., Dimitrov, D., Dony, L., Frishberg, A., … Theis, F. J. (2023). Best practices for single-cell analysis across modalities. *Nature Reviews Genetics*, *24*(8), 550–572. https://doi.org/10.1038/s41576-023-00586-w

Hirabayashi, Y., & Gotoh, Y. (2010). Epigenetic control of neural precursor cell fate during development. *Nature Reviews Neuroscience*, *11*(6), 377–388. https://doi.org/10.1038/nrn2810

Hoadley, K. A., Yau, C., Hinoue, T., Wolf, D. M., Lazar, A. J., Drill, E., Shen, R., Taylor, A. M., Cherniack, A. D., Thorsson, V., Akbani, R., Bowlby, R., Wong, C. K., Wiznerowicz, M., Sanchez-Vega, F., Robertson, A. G., Schneider, B. G., Lawrence, M. S., Noushmehr, H., … Mariamidze, A. (2018). Cell-of-Origin Patterns Dominate the Molecular Classification of 10,000 Tumors from 33 Types of Cancer. *Cell*, *173*(2), 291-304.e6. https://doi.org/10.1016/j.cell.2018.03.022

Holland, E. C., Li, Y., Celestino, J., Dai, C., Schaefer, L., Sawaya, R. A., & Fuller, G. N. (2000). Astrocytes Give Rise to Oligodendrogliomas and Astrocytomas after Gene Transfer of Polyoma Virus Middle T Antigen in Vivo. *The American Journal of Pathology*, *157*(3), 1031–1037. https://doi.org/10.1016/S0002-9440(10)64615-9

Holstein, T. W. (2012). The Evolution of the Wnt Pathway. *Cold Spring Harbor Perspectives in Biology*, *4*(7), a007922–a007922. https://doi.org/10.1101/cshperspect.a007922

Huang, X., Liu, J., Ketova, T., Fleming, J. T., Grover, V. K., Cooper, M. K., Litingtung, Y., & Chiang, C. (2010). Transventricular delivery of Sonic hedgehog is essential to cerebellar ventricular zone development. *Proceedings of the National Academy of Sciences*, *107*(18), 8422–8427. https://doi.org/10.1073/pnas.0911838107

Hutchins, E. J., & Bronner, M. E. (2018). Draxin acts as a molecular rheostat of canonical Wnt signaling to control cranial neural crest EMT. *Journal of Cell Biology*, *217*(10), 3683–3697. https://doi.org/10.1083/jcb.201709149

inferCNV of the Trinity CTAT Project. (2024). https://github.com/broadinstitute/inferCNV

Islam, S., Zeisel, A., Joost, S., La Manno, G., Zajac, P., Kasper, M., Lönnerberg, P., & Linnarsson, S. (2014). Quantitative single-cell RNA-seq with unique molecular identifiers. *Nature Methods*, *11*(2), 163–166. https://doi.org/10.1038/nmeth.2772

Jacob, F., Salinas, R. D., Zhang, D. Y., Nguyen, P. T. T., Schnoll, J. G., Wong, S. Z. H., Thokala, R., Sheikh, S., Saxena, D., Prokop, S., Liu, D., Qian, X., Petrov, D., Lucas, T., Chen, H. I., Dorsey, J. F., Christian, K. M., Binder, Z. A., Nasrallah, M., … Song, H. (2020). A Patient-Derived Glioblastoma Organoid Model and Biobank Recapitulates Inter- and Intra-tumoral Heterogeneity. *Cell*, *180*(1), 188-204.e22. https://doi.org/10.1016/j.cell.2019.11.036

Jacobson, M. (1977). Mapping the developing retinotectal projection in frog tadpoles by a double label autoradiographic technique. *Brain Research*, *127*(1), 55–67. https://doi.org/10.1016/0006-8993(77)90379-1

Janesick, A., Shelansky, R., Gottscho, A. D., Wagner, F., Williams, S. R., Rouault, M., Beliakoff, G., Morrison, C. A., Oliveira, M. F., Sicherman, J. T., Kohlway, A., Abousoud, J., Drennon, T. Y., Mohabbat, S. H., 10x Development Teams, & Taylor, S. E. B. (2023). High resolution mapping of the tumor microenvironment using integrated single-cell, spatial and in situ analysis. *Nature Communications*, *14*(1), 8353. https://doi.org/10.1038/s41467-023-43458-x

Jang, M.-H., Bonaguidi, M. A., Kitabatake, Y., Sun, J., Song, J., Kang, E., Jun, H., Zhong, C., Su, Y., Guo, J. U., Wang, M. X., Sailor, K. A., Kim, J.-Y., Gao, Y., Christian, K. M., Ming, G., & Song, H. (2013). Secreted Frizzled-Related Protein 3 Regulates Activity-Dependent Adult Hippocampal Neurogenesis. *Cell Stem Cell*, *12*(2), 215–223. https://doi.org/10.1016/j.stem.2012.11.021

Jékely, G. (2011). Origin and early evolution of neural circuits for the control of ciliary locomotion. *Proceedings of the Royal Society B: Biological Sciences*, *278*(1707), 914–922. https://doi.org/10.1098/rspb.2010.2027

Jékely, G. (2021). The chemical brain hypothesis for the origin of nervous systems. *Philosophical Transactions of the Royal Society B: Biological Sciences*, *376*(1821), 20190761. https://doi.org/10.1098/rstb.2019.0761

Joesting, M. S., Perrin, S., Elenbaas, B., Fawell, S. E., Rubin, J. S., Franco, O. E., Hayward, S. W., Cunha, G. R., & Marker, P. C. (2005). Identification of SFRP1 as a Candidate Mediator of Stromal-to-Epithelial Signaling in Prostate Cancer. *Cancer Research*, *65*(22), 10423–10430. https://doi.org/10.1158/0008-5472.CAN-05-0824

Johnson, K. C., Anderson, K. J., Courtois, E. T., Gujar, A. D., Barthel, F. P., Varn, F. S., Luo, D., Seignon, M., Yi, E., Kim, H., Estecio, M. R. H., Zhao, D., Tang, M., Navin, N. E., Maurya, R., Ngan, C. Y., Verburg, N., De Witt Hamer, P. C., Bulsara, K., … Verhaak, R. G. W. (2021). Single-cell multimodal glioma analyses identify epigenetic regulators of cellular plasticity and environmental stress response. *Nature Genetics*, *53*(10), 1456–1468. https://doi.org/10.1038/s41588-021-00926-8

Joksimovic, M., Yun, B. A., Kittappa, R., Anderegg, A. M., Chang, W. W., Taketo, M. M., McKay, R. D. G., & Awatramani, R. B. (2009). Wnt antagonism of Shh facilitates midbrain floor plate neurogenesis. *Nature Neuroscience*, *12*(2), 125–131. https://doi.org/10.1038/nn.2243

Jung, E., Alfonso, J., Osswald, M., Monyer, H., Wick, W., & Winkler, F. (2019). Emerging intersections between neuroscience and glioma biology. *Nature Neuroscience*, *22*(12), 1951–1960. https://doi.org/10.1038/s41593-019-0540-y

Kakugawa, S., Langton, P. F., Zebisch, M., Howell, S. A., Chang, T.-H., Liu, Y., Feizi, T., Bineva, G., O'Reilly, N., Snijders, A. P., Jones, E. Y., & Vincent, J.-P. (2015). Notum deacylates Wnt proteins to suppress signalling activity. *Nature*, *519*(7542), 187–192. https://doi.org/10.1038/nature14259

Kalamakis, G., Brüne, D., Ravichandran, S., Bolz, J., Fan, W., Ziebell, F., Stiehl, T., Catalá-Martinez, F., Kupke, J., Zhao, S., Llorens-Bobadilla, E., Bauer, K., Limpert, S., Berger, B., Christen, U., Schmezer, P., Mallm, J. P., Berninger, B., Anders, S., … Martin-Villalba, A. (2019). Quiescence Modulates Stem Cell Maintenance and Regenerative Capacity in the Aging Brain. *Cell*, *176*(6), 1407-1419.e14. https://doi.org/10.1016/j.cell.2019.01.040

Kara, R. J., Bolli, P., Karakikes, I., Matsunaga, I., Tripodi, J., Tanweer, O., Altman, P., Shachter, N. S., Nakano, A., Najfeld, V., & Chaudhry, H. W. (2012). Fetal Cells Traffic to Injured Maternal Myocardium and Undergo Cardiac Differentiation. *Circulation Research*, *110*(1), 82–93. https://doi.org/10.1161/CIRCRESAHA.111.249037

Kaya, O. (2023). *Wnt Signaling Modulates Normal and Malignant Stem Cell Activation in the Adult Brain* [PhD Thesis]. University Heidelberg.

Kikkawa, T., Casingal, C. R., Chun, S. H., Shinohara, H., Hiraoka, K., & Osumi, N. (2019). The role of Pax6 in brain development and its impact on pathogenesis of autism spectrum disorder. *Brain Research*, *1705*, 95–103. https://doi.org/10.1016/j.brainres.2018.02.041

Kirschenbaum, B., & Goldman, S. A. (1995). Brain-derived neurotrophic factor promotes the survival of neurons arising from the adult rat forebrain subependymal zone. *Proceedings of the National Academy of Sciences*, *92*(1), 210–214. https://doi.org/10.1073/pnas.92.1.210

Kishimoto, N., Shimizu, K., & Sawamoto, K. (2012). Neuronal regeneration in a zebrafish model of adult brain injury. *Disease Models & Mechanisms*, *5*(2), 200–209. https://doi.org/10.1242/dmm.007336

Kremer, L. P., Cerrizuela, S., Al Shukairi, M. E., Ellinger, T., Straub, J., Dehler, S., Korkmaz, A., Weichenhan, D., Plass, C., Anders, S., & Martin-Villalba, A. (2022). Single-cell triple-omics uncovers DNA methylation as key feature of stemness in the healthy and ischemic adult brain. *bioRxiv*. https://doi.org/10.1101/2022.07.13.499860

Kremer, L. P. M., Cerrizuela, S., Al Shukairi, M. E., Ellinger, T., Straub, J., Dehler, S., Korkmaz, A., Weichenhan, D., Plass, C., Anders, S., & Martin-Villalba, A. (2022). *Single-cell triple-omics uncovers DNA methylation as key feature of stemness in the healthy and ischemic adult brain*. bioRxiv. https://doi.org/10.1101/2022.07.13.499860

Kremer, L. P. M., Cerrizuela, S., Dehler, S., Stiehl, T., Weinmann, J., Abendroth, H., Kleber, S., Laure, A., El Andari, J., Anders, S., Marciniak-Czochra, A., Grimm, D., & Martin-Villalba, A. (2021). High throughput screening of novel AAV capsids identifies variants for transduction of adult NSCs within the subventricular zone. *Molecular Therapy - Methods & Clinical Development*, *23*, 33–50. https://doi.org/10.1016/j.omtm.2021.07.001

Kriegstein, A., & Alvarez-Buylla, A. (2009). The Glial Nature of Embryonic and Adult Neural Stem Cells. *Annual Review of Neuroscience*, *32*(1), 149–184. https://doi.org/10.1146/annurev.neuro.051508.135600

Krueger, F., & Andrews, S. R. (2011). Bismark: A flexible aligner and methylation caller for Bisulfite-Seq applications. *Bioinformatics*, *27*(11), 1571–1572. https://doi.org/10.1093/bioinformatics/btr167

La Manno, G., Soldatov, R., Zeisel, A., Braun, E., Hochgerner, H., Petukhov, V., Lidschreiber, K., Kastriti, M. E., Lönnerberg, P., Furlan, A., Fan, J., Borm, L. E., Liu, Z., Van Bruggen, D., Guo, J., He, X., Barker, R., Sundström, E., Castelo-Branco, G., … Kharchenko, P. V. (2018). RNA velocity of single cells. *Nature*, *560*(7719), 494–498. https://doi.org/10.1038/s41586-018-0414-6

Lan, X., Jörg, D. J., Cavalli, F. M. G., Richards, L. M., Nguyen, L. V., Vanner, R. J., Guilhamon, P., Lee, L., Kushida, M. M., Pellacani, D., Park, N. I., Coutinho, F. J., Whetstone, H., Selvadurai, H. J., Che, C., Luu, B., Carles, A., Moksa, M., Rastegar, N., … Dirks, P. B. (2017). Fate mapping of human glioblastoma reveals an invariant stem cell hierarchy. *Nature*, *549*(7671), 227–232. https://doi.org/10.1038/nature23666

Lancaster, M. A., & Knoblich, J. A. (2014). Generation of cerebral organoids from human pluripotent stem cells. *Nature Protocols*, *9*(10), 2329–2340. https://doi.org/10.1038/nprot.2014.158

Lande, R. (1978). Evolutionary Mechanisms of Limb Loss in Tetrapods. *Evolution*, *32*(1), 73. https://doi.org/10.2307/2407411

Larsson, I., Dalmo, E., Elgendy, R., Niklasson, M., Doroszko, M., Segerman, A., Jörnsten, R., Westermark, B., & Nelander, S. (2021). Modeling glioblastoma heterogeneity as a dynamic network of cell states. *Molecular Systems Biology*, *17*(9), e10105. https://doi.org/10.15252/msb.202010105

Lathia, J. D., Mack, S. C., Mulkearns-Hubert, E. E., Valentim, C. L. L., & Rich, J. N. (2015). *Cancer stem cells in glioblastoma*.

Lederer, A. R., Leonardi, M., Talamanca, L., Herrera, A., Droin, C., Khven, I., Carvalho, H. J. F., Valente, A., Mantes, A. D., Arabí, P. M., Pinello, L., Naef, F., & Manno, G. L. (2024). *Statistical inference with a manifold-constrained RNA velocity model uncovers cell cycle speed modulations*. bioRxiv. https://doi.org/10.1101/2024.01.18.576093

Lee, J. H., Lee, J. E., Kahng, J. Y., Kim, S. H., Park, J. S., Yoon, S. J., Um, J.-Y., Kim, W. K., Lee, J.-K., Park, J., Kim, E. H., Lee, J.-H., Lee, J.-H., Chung, W.-S., Ju, Y. S., Park, S.-H., Chang, J. H., Kang, S.-G., & Lee, J. H. (2018). Human glioblastoma arises from subventricular zone cells with low-level driver mutations. *Nature*, *560*(7717), 243–247. https://doi.org/10.1038/s41586-018-0389-3

Lee, M. S., & Sanoff, H. K. (2020). Cancer of unknown primary. *BMJ*, m4050. https://doi.org/10.1136/bmj.m4050

Lee, Y., Lee, J.-K., Ahn, S. H., Lee, J., & Nam, D.-H. (2016). WNT signaling in glioblastoma and therapeutic opportunities. *Laboratory Investigation*, *96*(2), 137–150. https://doi.org/10.1038/labinvest.2015.140

Levison, S. W., & Goldman, J. E. (1993). Both oligodendrocytes and astrocytes develop from progenitors in the subventricular zone of postnatal rat forebrain. *Neuron*, *10*(2), 201–212. https://doi.org/10.1016/0896-6273(93)90311-e

Li, C., Fleck, J. S., Martins-Costa, C., Burkard, T. R., Themann, J., Stuempflen, M., Peer, A. M., Vertesy, Á., Littleboy, J. B., Esk, C., Elling, U., Kasprian, G., Corsini, N. S., Treutlein, B., & Knoblich, J. A. (2023). Single-cell brain organoid screening identifies developmental defects in autism. *Nature*, *621*(7978), 373–380. https://doi.org/10.1038/s41586-023-06473-y

Li, L., & Clevers, H. (2010). Coexistence of Quiescent and Active Adult Stem Cells in Mammals. *Science*, *327*(5965), 542–545. https://doi.org/10.1126/science.1180794

Lim, D. A., & Alvarez-Buylla, A. (2016). The Adult Ventricular–Subventricular Zone (V-SVZ) and Olfactory Bulb (OB) Neurogenesis. *Cold Spring Harbor Perspectives in Biology*, *8*(5), a018820. https://doi.org/10.1101/cshperspect.a018820

Linkous, A., Balamatsias, D., Snuderl, M., Edwards, L., Miyaguchi, K., Milner, T., Reich, B., Cohen-Gould, L., Storaska, A., Nakayama, Y., Schenkein, E., Singhania, R., Cirigliano, S., Magdeldin, T., Lin, Y., Nanjangud, G., Chadalavada, K., Pisapia, D., Liston, C., & Fine, H. A. (2019). Modeling Patient-Derived Glioblastoma with Cerebral Organoids. *Cell Reports*, *26*(12), 3203-3211.e5. https://doi.org/10.1016/j.celrep.2019.02.063

Liu, J., Lichtenberg, T., Hoadley, K. A., Poisson, L. M., Lazar, A. J., Cherniack, A. D., Kovatich, A. J., Benz, C. C., Levine, D. A., Lee, A. V., Omberg, L., Wolf, D. M., Shriver, C. D., Thorsson, V., Hu, H., Caesar-Johnson, S. J., Demchok, J. A., Felau, I., Kasapi, M., … Mariamidze, A. (2018). An Integrated TCGA Pan-Cancer Clinical Data Resource to Drive High-Quality Survival Outcome Analytics. *Cell*, *173*(2), 400-416.e11. https://doi.org/10.1016/j.cell.2018.02.052

Liu, J., Pan, S., Hsieh, M. H., Ng, N., Sun, F., Wang, T., Kasibhatla, S., Schuller, A. G., Li, A. G., Cheng, D., Li, J., Tompkins, C., Pferdekamper, A., Steffy, A., Cheng, J., Kowal, C., Phung, V., Guo, G., Wang, Y., … Harris, J. L. (2013). Targeting Wnt-driven cancer through the inhibition of Porcupine by LGK974. *Proceedings of the National Academy of Sciences*, *110*(50), 20224–20229. https://doi.org/10.1073/pnas.1314239110

Liu, K., Gao, Z., Wu, X., Zhou, G., Zhang, W. J., Yang, X., & Liu, W. (2014). Knocking out Smad3 favors allogeneic mouse fetal skin development in adult wounds. *Wound Repair and Regeneration*, *22*(2), 265–271. https://doi.org/10.1111/wrr.12143

Liuzzi, F. J., & Lasek, R. J. (1987). Astrocytes Block Axonal Regeneration in Mammals by Activating the Physiological Stop Pathway. *Science*, *237*(4815), 642–645. https://doi.org/10.1126/science.3603044

Llorens-Bobadilla, E., Chell, J. M., Le Merre, P., Wu, Y., Zamboni, M., Bergenstråhle, J., Stenudd, M., Sopova, E., Lundeberg, J., Shupliakov, O., Carlén, M., & Frisén, J. (2020). A latent lineage potential in resident neural stem cells enables spinal cord repair. *Science*, *370*(6512), eabb8795. https://doi.org/10.1126/science.abb8795

Llorens-Bobadilla, E., Zhao, S., Baser, A., Saiz-Castro, G., Zwadlo, K., & Martin-Villalba, A. (2015). Single-Cell Transcriptomics Reveals a Population of Dormant Neural Stem Cells that Become Activated upon Brain Injury. *Cell Stem Cell*, *17*(3), 329–340. https://doi.org/10.1016/j.stem.2015.07.002

Loh, K. M., van Amerongen, R., & Nusse, R. (2016). Generating Cellular Diversity and Spatial Form: Wnt Signaling and the Evolution of Multicellular Animals. *Developmental Cell*, *38*(6), 643–655. https://doi.org/10.1016/j.devcel.2016.08.011

Lois, C., & Alvarez-Buylla, A. (1993). Proliferating subventricular zone cells in the adult mammalian forebrain can differentiate into neurons and glia. *Proceedings of the National Academy of Sciences*, *90*(5), 2074–2077. https://doi.org/10.1073/pnas.90.5.2074

Lopez-Rios, J., Esteve, P., Ruiz, J. M., & Bovolenta, P. (2008). The Netrin-related domain of Sfrp1 interacts with Wnt ligands and antagonizes their activity in the anterior neural plate. *Neural Development*, *3*(1), 19. https://doi.org/10.1186/1749-8104-3-19

Lotfollahi, M., Naghipourfar, M., Luecken, M. D., Khajavi, M., Büttner, M., Wagenstetter, M., Avsec, Ž., Gayoso, A., Yosef, N., Interlandi, M., Rybakov, S., Misharin, A. V., & Theis, F. J. (2022). Mapping single-cell data to reference atlases by transfer learning. *Nature Biotechnology*, *40*(1), 121–130. https://doi.org/10.1038/s41587-021-01001-7

Louis, D. N., Perry, A., Wesseling, P., Brat, D. J., Cree, I. A., Figarella-Branger, D., Hawkins, C., Ng, H. K., Pfister, S. M., Reifenberger, G., Soffietti, R., Von Deimling, A., & Ellison, D. W. (2021). The 2021 WHO Classification of Tumors of the Central Nervous System: A summary. *Neuro-Oncology*, *23*(8), 1231–1251. https://doi.org/10.1093/neuonc/noab106

Luecken, M. D., & Theis, F. J. (2019). Current best practices in single-cell RNA-seq analysis: A tutorial. *Molecular Systems Biology*, *15*(6), e8746. https://doi.org/10.15252/msb.20188746

Luskin, M. B. (1993). Restricted proliferation and migration of postnatally generated neurons derived from the forebrain subventricular zone. *Neuron*, *11*(1), 173–189. https://doi.org/10.1016/0896-6273(93)90281-U

Macosko, E. Z., Basu, A., Satija, R., Nemesh, J., Shekhar, K., Goldman, M., Tirosh, I., Bialas, A. R., Kamitaki, N., Martersteck, E. M., Trombetta, J. J., Weitz, D. A., Sanes, J. R., Shalek, A. K., Regev, A., & McCarroll, S. A. (2015). Highly Parallel Genome-wide Expression Profiling of Individual Cells Using Nanoliter Droplets. *Cell*, *161*(5), 1202–1214. https://doi.org/10.1016/j.cell.2015.05.002

Magnusson, J. P., Göritz, C., Tatarishvili, J., Dias, D. O., Smith, E. M. K., Lindvall, O., Kokaia, Z., & Frisén, J. (2014). A latent neurogenic program in astrocytes regulated by Notch signaling in the mouse. *Science*, *346*(6206), 237–241. https://doi.org/10.1126/science.346.6206.237

Magnusson, J. P., Zamboni, M., Santopolo, G., Mold, J. E., Barrientos-Somarribas, M., Talavera-Lopez, C., Andersson, B., & Frisén, J. (2020). Activation of a neural stem cell transcriptional program in parenchymal astrocytes. *eLife*, *9*, e59733. https://doi.org/10.7554/eLife.59733

Malatesta, P., Appolloni, I., & Calzolari, F. (2008). Radial glia and neural stem cells. *Cell and Tissue Research*, *331*(1), 165–178. https://doi.org/10.1007/s00441-007-0481-8

Marot-Lassauzaie, V., Bouman, B. J., Donaghy, F. D., Demerdash, Y., Essers, M. A. G., & Haghverdi, L. (2022). Towards reliable quantification of cell state velocities. *PLOS Computational Biology*, *18*(9), e1010031. https://doi.org/10.1371/journal.pcbi.1010031

McInnes, L., Healy, J., & Melville, J. (2020). *UMAP: Uniform Manifold Approximation and Projection for Dimension Reduction* (arXiv:1802.03426). arXiv. http://arxiv.org/abs/1802.03426

Megill, C., Martin, B., Weaver, C., Bell, S., Prins, L., Badajoz, S., McCandless, B., Pisco, A. O., Kinsella, M., Griffin, F., Kiggins, J., Haliburton, G., Mani, A., Weiden, M., Dunitz, M., Lombardo, M., Huang, T., Smith, T., Chambers, S., … Carr, A. (2021). *cellxgene: A performant, scalable exploration platform for high dimensional sparse matrices*. bioRxiv. https://doi.org/10.1101/2021.04.05.438318

Merkle, F. T., Mirzadeh, Z., & Alvarez-Buylla, A. (2007). Mosaic Organization of Neural Stem Cells in the Adult Brain. *Science*, *317*(5836), 381–384. https://doi.org/10.1126/science.1144914

Mirzadeh, Z., Merkle, F. T., Soriano-Navarro, M., Garcia-Verdugo, J. M., & Alvarez-Buylla, A. (2008). Neural Stem Cells Confer Unique Pinwheel Architecture to the Ventricular Surface in Neurogenic Regions of the Adult Brain. *Cell Stem Cell*, *3*(3), 265–278. https://doi.org/10.1016/j.stem.2008.07.004

Mizrak, D., Bayin, N. S., Yuan, J., Liu, Z., Suciu, R. M., Niphakis, M. J., Ngo, N., Lum, K. M., Cravatt, B. F., Joyner, A. L., & Sims, P. A. (2020). Single-Cell Profiling and SCOPE-Seq Reveal Lineage Dynamics of Adult Ventricular-Subventricular Zone Neurogenesis and NOTUM as a Key Regulator. *Cell Reports*, *31*(12), 107805. https://doi.org/10.1016/j.celrep.2020.107805

Mizrak, D., Levitin, H. M., Delgado, A. C., Crotet, V., Yuan, J., Chaker, Z., Silva-Vargas, V., Sims, P. A., & Doetsch, F. (2019). Single-Cell Analysis of Regional Differences in Adult V-SVZ Neural Stem Cell Lineages. *Cell Reports*, *26*(2), 394-406.e5. https://doi.org/10.1016/j.celrep.2018.12.044

Mossi Albiach, A., Janusauskas, J., Kapustová, I., Kvedaraite, E., Codeluppi, S., Munting, J. B., Borm, L. E., Kjaer Jacobsen, J., Shamikh, A., Persson, O., & Linnarsson, S. (2023). *Glioblastoma is spatially organized by neurodevelopmental programs and a glial-like wound healing response* [Preprint]. Cancer Biology. https://doi.org/10.1101/2023.09.01.555882

Nano, P. R., Fazzari, E., Azizad, D., Nguyen, C. V., Wang, S., Kan, R. L., Wick, B., Haeussler, M., & Bhaduri, A. (2023). *A Meta-Atlas of the Developing Human Cortex Identifies Modules Driving Cell Subtype Specification*. bioRxiv. https://doi.org/10.1101/2023.09.12.557406

Neftel, C., Laffy, J., Filbin, M. G., Hara, T., Shore, M. E., Rahme, G. J., Richman, A. R., Silverbush, D., Shaw, M. L., Hebert, C. M., Dewitt, J., Gritsch, S., Perez, E. M., Gonzalez Castro, L. N., Lan, X., Druck, N., Rodman, C., Dionne, D., Kaplan, A., … Suvà, M. L. (2019). An Integrative Model of Cellular States, Plasticity, and Genetics for Glioblastoma. *Cell*, *178*(4), 835-849.e21. https://doi.org/10.1016/j.cell.2019.06.024

Ng, S. B., Turner, E. H., Robertson, P. D., Flygare, S. D., Bigham, A. W., Lee, C., Shaffer, T., Wong, M., Bhattacharjee, A., Eichler, E. E., Bamshad, M., Nickerson, D. A., & Shendure, J. (2009). Targeted capture and massively parallel sequencing of 12 human exomes. *Nature*, *461*(7261), 272–276. https://doi.org/10.1038/nature08250

Ninkovic, J., Pinto, L., Petricca, S., Lepier, A., Sun, J., Rieger, M. A., Schroeder, T., Cvekl, A., Favor, J., & Götz, M. (2010). The Transcription Factor Pax6 Regulates Survival of Dopaminergic Olfactory Bulb Neurons via Crystallin αA. *Neuron*, *68*(4), 682–694. https://doi.org/10.1016/j.neuron.2010.09.030

Noctor, S. C., Flint, A. C., Weissman, T. A., Wong, W. S., Clinton, B. K., & Kriegstein, A. R. (2002). Dividing Precursor Cells of the Embryonic Cortical Ventricular Zone Have Morphological and Molecular Characteristics of Radial Glia. *The Journal of Neuroscience*, *22*(8), 3161–3173. https://doi.org/10.1523/JNEUROSCI.22-08-03161.2002

Noctor, S. C., Martínez-Cerdeño, V., & Kriegstein, A. R. (2008). Distinct behaviors of neural stem and progenitor cells underlie cortical neurogenesis. *Journal of Comparative Neurology*, *508*(1), 28–44. https://doi.org/10.1002/cne.21669

Noushmehr, H., Weisenberger, D. J., Diefes, K., Phillips, H. S., Pujara, K., Berman, B. P., Pan, F., Pelloski, C. E., Sulman, E. P., Bhat, K. P., Verhaak, R. G. W., Hoadley, K. A., Hayes, D. N., Perou, C. M., Schmidt, H. K., Ding, L., Wilson, R. K., Van Den Berg, D., Shen, H., … Aldape, K. (2010). Identification of a CpG Island Methylator Phenotype that Defines a Distinct Subgroup of Glioma. *Cancer Cell*, *17*(5), 510–522. https://doi.org/10.1016/j.ccr.2010.03.017

Obernier, K., Cebrian-Silla, A., Thomson, M., Parraguez, J. I., Anderson, R., Guinto, C., Rodas Rodriguez, J., Garcia-Verdugo, J.-M., & Alvarez-Buylla, A. (2018). Adult Neurogenesis Is Sustained by Symmetric Self-Renewal and Differentiation. *Cell Stem Cell*, *22*(2), 221-234.e8. https://doi.org/10.1016/j.stem.2018.01.003

Okonechnikov, K., Joshi, P., Sepp, M., Leiss, K., Murat, F., Sill, M., Beck, P., Chan, K. C.-H., Korshunov, A., Sahm, F., Deng, M. Y., Sturm, D., Donson, A. M., Foreman, N. K., Green, A. L., Orr, B. A., Gao, Q., Darrow, E., Hadley, J. L., … Pfister, S. M. (2021). *Mapping pediatric brain tumors to their origins in the developing cerebellum*.

Osswald, M., Jung, E., Sahm, F., Solecki, G., Venkataramani, V., Blaes, J., Weil, S., Horstmann, H., Wiestler, B., Syed, M., Huang, L., Ratliff, M., Karimian Jazi, K., Kurz, F. T., Schmenger, T., Lemke, D., Gömmel, M., Pauli, M., Liao, Y., … Winkler, F. (2015). Brain tumour cells interconnect to a functional and resistant network. *Nature*, *528*(7580), 93–98. https://doi.org/10.1038/nature16071

Ostrom, Q. T., Cioffi, G., Waite, K., Kruchko, C., & Barnholtz-Sloan, J. S. (2021). CBTRUS Statistical Report: Primary Brain and Other Central Nervous System Tumors Diagnosed in the United States in 2014–2018. *Neuro-Oncology*, *23*(Supplement_3), iii1–iii105. https://doi.org/10.1093/neuonc/noab200

Ouspenskaia, T., Matos, I., Mertz, A. F., Fiore, V. F., & Fuchs, E. (2016). WNT-SHH Antagonism Specifies and Expands Stem Cells prior to Niche Formation. *Cell*, *164*(1–2), 156–169. https://doi.org/10.1016/j.cell.2015.11.058

Paparrizos, J., & Gravano, L. (2017). Fast and Accurate Time-Series Clustering. *ACM Transactions on Database Systems*, *42*(2), 1–49. https://doi.org/10.1145/3044711

Parekh, S., Ziegenhain, C., Vieth, B., Enard, W., & Hellmann, I. (2018). zUMIs—A fast and flexible pipeline to process RNA sequencing data with UMIs. *GigaScience*, *7*(6). https://doi.org/10.1093/gigascience/giy059

Patel, A. P., Tirosh, I., Trombetta, J. J., Shalek, A. K., Gillespie, S. M., Wakimoto, H., Cahill, D. P., Nahed, B. V., Curry, W. T., Martuza, R. L., Louis, D. N., Rozenblatt-Rosen, O., Suvà, M. L., Regev, A., & Bernstein, B. E. (2014). Single-cell RNA-seq highlights intratumoral heterogeneity in primary glioblastoma. *Science*, *344*(6190), 1396–1401. https://doi.org/10.1126/science.1254257

Pedregosa, F., Varoquaux, G., Gramfort, A., Michel, V., Thirion, B., Grisel, O., Blondel, M., Prettenhofer, P., Weiss, R., Dubourg, V., Vanderplas, J., Passos, A., & Cournapeau, D. (2011). Scikit-learn: Machine Learning in Python. *MACHINE LEARNING IN PYTHON*.

Pertesi, M., Ekdahl, L., Palm, A., Johnsson, E., Järvstråt, L., Wihlborg, A.-K., & Nilsson, B. (2019). Essential genes shape cancer genomes through linear limitation of homozygous deletions. *Communications Biology*, *2*(1), 262. https://doi.org/10.1038/s42003-019-0517-0

Phillips, H. S., Kharbanda, S., Chen, R., Forrest, W. F., Soriano, R. H., Wu, T. D., Misra, A., Nigro, J. M., Colman, H., Soroceanu, L., Williams, P. M., Modrusan, Z., Feuerstein, B. G., & Aldape, K. (2006). Molecular subclasses of high-grade glioma predict prognosis, delineate a pattern of disease progression, and resemble stages in neurogenesis. *Cancer Cell*, *9*(3), 157–173. https://doi.org/10.1016/j.ccr.2006.02.019

Picelli, S., Faridani, O. R., Björklund, Å. K., Winberg, G., Sagasser, S., & Sandberg, R. (2014). Full-length RNA-seq from single cells using Smart-seq2. *Nature Protocols*, *9*(1), 171–181. https://doi.org/10.1038/nprot.2014.006

Plotly Technologies Inc. (2024). *Dash Layout*. https://dash.plotly.com/layout

Pollen, A. A., Bhaduri, A., Andrews, M. G., Nowakowski, T. J., Meyerson, O. S., Mostajo-Radji, M. A., Di Lullo, E., Alvarado, B., Bedolli, M., Dougherty, M. L., Fiddes, I. T., Kronenberg, Z. N., Shuga, J., Leyrat, A. A., West, J. A., Bershteyn, M., Lowe, C. B., Pavlovic, B. J., Salama, S. R., … Kriegstein, A. R. (2019). Establishing Cerebral Organoids as Models of Human-Specific Brain Evolution. *Cell*, *176*(4), 743-756.e17. https://doi.org/10.1016/j.cell.2019.01.017

Ponti, G., Obernier, K., & Alvarez-Buylla, A. (2013). Lineage progression from stem cells to new neurons in the adult brain ventricular-subventricular zone. *Cell Cycle*, *12*(11), 1649–1650. https://doi.org/10.4161/cc.24984

Prager, B. C., Bhargava, S., Mahadev, V., Hubert, C. G., & Rich, J. N. (2020). Glioblastoma Stem Cells: Driving Resilience through Chaos. *Trends in Cancer*, *6*(3), 223–235. https://doi.org/10.1016/j.trecan.2020.01.009

Qu, Y., Ray, P. S., Li, J., Cai, Q., Bagaria, S. P., Moran, C., Sim, M.-S., Zhang, J., Turner, R. R., Zhu, Z., Cui, X., & Liu, B. (2013). High levels of secreted frizzled-related protein 1 correlate with poor prognosis and promote tumourigenesis in gastric cancer. *European Journal of Cancer*, *49*(17), 3718–3728. https://doi.org/10.1016/j.ejca.2013.07.011

Quadrato, G., & Arlotta, P. (2017). Present and future of modeling human brain development in 3D organoids. *Current Opinion in Cell Biology*, *49*, 47–52. https://doi.org/10.1016/j.ceb.2017.11.010

Rajakulendran, N., Rowland, K. J., Selvadurai, H. J., Ahmadi, M., Park, N. I., Naumenko, S., Dolma, S., Ward, R. J., So, M., Lee, L., MacLeod, G., Pasiliao, C., Brandon, C., Clarke, I. D., Cusimano, M. D., Bernstein, M., Batada, N., Angers, S., & Dirks, P. B. (2019). Wnt and Notch signaling govern self-renewal and differentiation in a subset of human glioblastoma stem cells. *Genes & Development*, *33*(9–10), 498–510. https://doi.org/10.1101/gad.321968.118

Rao, A., Barkley, D., França, G. S., & Yanai, I. (2021). Exploring tissue architecture using spatial transcriptomics. *Nature*, *596*(7871), 211–220. https://doi.org/10.1038/s41586-021-03634-9

Raup, D. (1967). Geometric Analysis of Shell Coiling: Coiling in Ammonoids. *Journal of Paleontology*, *41*(1), 43–65.

Ravi, V. M., Will, P., Kueckelhaus, J., Sun, N., Joseph, K., Salié, H., Vollmer, L., Kuliesiute, U., Von Ehr, J., Benotmane, J. K., Neidert, N., Follo, M., Scherer, F., Goeldner, J. M., Behringer, S. P., Franco, P., Khiat, M., Zhang, J., Hofmann, U. G., … Heiland, D. H. (2022). Spatially resolved multi-omics deciphers bidirectional tumor-host interdependence in glioblastoma. *Cancer Cell*, *40*(6), 639-655.e13. https://doi.org/10.1016/j.ccell.2022.05.009

Rella, L., Fernandes Póvoa, E. E., Mars, J., Ebbing, A. L. P., Schoppink, L., Betist, M. C., & Korswagen, H. C. (2021). A switch from noncanonical to canonical Wnt signaling stops neuroblast migration through a Slt–Robo and RGA-9b/ARHGAP–dependent mechanism. *Proceedings of the National Academy of Sciences*, *118*(12), e2013239118. https://doi.org/10.1073/pnas.2013239118

Reynolds, B. A., & Weiss, S. (1992). Generation of Neurons and Astrocytes from Isolated Cells of the Adult Mammalian Central Nervous System. *Science*, *255*(5052), 1707–1710. https://doi.org/10.1126/science.1553558

Richards, L. J., Kilpatrick, T. J., & Bartlett, P. F. (1992). De novo generation of neuronal cells from the adult mouse brain. *Proceedings of the National Academy of Sciences*, *89*(18), 8591–8595. https://doi.org/10.1073/pnas.89.18.8591

Richards, L. M., Whitley, O. K. N., MacLeod, G., Cavalli, F. M. G., Coutinho, F. J., Jaramillo, J. E., Svergun, N., Riverin, M., Croucher, D. C., Kushida, M., Yu, K., Guilhamon, P., Rastegar, N., Ahmadi, M., Bhatti, J. K., Bozek, D. A., Li, N., Lee, L., Che, C., … Pugh, T. J. (2021). Gradient of Developmental and Injury Response transcriptional states defines functional vulnerabilities underpinning glioblastoma heterogeneity. *Nature Cancer*, *2*(2), 157–173. https://doi.org/10.1038/s43018-020-00154-9

Ruiz-Moreno, C., Salas, S. M., Samuelsson, E., Brandner, S., Kranendonk, M. E. G., Nilsson, M., & Stunnenberg, H. G. (2022). *Harmonized single-cell landscape, intercellular crosstalk and tumor architecture of glioblastoma*. bioRxiv. https://doi.org/10.1101/2022.08.27.505439

Sabelström, H., Quigley, D. A., Fenster, T., Foster, D. J., Fuchshuber, C. A. M., Saxena, S., Yuan, E., Li, N., Paterno, F., Phillips, J. J., James, C. D., Norling, B., Berger, M. S., & Persson, A. I. (2019). High density is a property of slow-cycling and treatment-resistant human glioblastoma cells. *Experimental Cell Research*, *378*(1), 76–86. https://doi.org/10.1016/j.yexcr.2019.03.003

Saelens, W., Cannoodt, R., Todorov, H., & Saeys, Y. (2019). A comparison of single-cell trajectory inference methods. *Nature Biotechnology*, *37*(5), 547–554. https://doi.org/10.1038/s41587-019-0071-9

Sanai, N., Alvarez-Buylla, A., & Berger, M. S. (2005). Neural Stem Cells and the Origin of Gliomas. *New England Journal of Medicine*, *353*(8), 811–822. https://doi.org/10.1056/NEJMra043666

Sanes, D. H., Reh, T. A., Harris, W. A., & Landgraf, M. (2019). *Development of the nervous system* (Fourth edition). Academic Press, an imprint of Elsevier.

Sato, T., Vries, R. G., Snippert, H. J., Van De Wetering, M., Barker, N., Stange, D. E., Van Es, J. H., Abo, A., Kujala, P., Peters, P. J., & Clevers, H. (2009). Single Lgr5 stem cells build crypt-villus structures in vitro without a mesenchymal niche. *Nature*, *459*(7244), 262–265. https://doi.org/10.1038/nature07935

Satopaa, V., Albrecht, J., Irwin, D., & Raghavan, B. (2011). Finding a "Kneedle" in a Haystack: Detecting Knee Points in System Behavior. *2011 31st International Conference on Distributed Computing Systems Workshops*, 166–171. https://doi.org/10.1109/ICDCSW.2011.20

Scherer, H. J. (1938). Structural Development in Gliomas. *The American Journal of Cancer*, *34*(3), 333–351. https://doi.org/10.1158/ajc.1938.333

Schneider, G., Schmidt-Supprian, M., Rad, R., & Saur, D. (2017). Tissue-specific tumorigenesis: Context matters. *Nature Reviews Cancer*, *17*(4), 239–253. https://doi.org/10.1038/nrc.2017.5

Schwabe, D., Formichetti, S., Junker, J. P., Falcke, M., & Rajewsky, N. (2020). The transcriptome dynamics of single cells during the cell cycle. *Molecular Systems Biology*, *16*(11), e9946. https://doi.org/10.15252/msb.20209946

Seib, D. R. M., Corsini, N. S., Ellwanger, K., Plaas, C., Mateos, A., Pitzer, C., Niehrs, C., Celikel, T., & Martin-Villalba, A. (2013). Loss of Dickkopf-1 Restores Neurogenesis in Old Age and Counteracts Cognitive Decline. *Cell Stem Cell*, *12*(2), 204–214. https://doi.org/10.1016/j.stem.2012.11.010

Serin Harmanci, A., Harmanci, A. O., & Zhou, X. (2020). CaSpER identifies and visualizes CNV events by integrative analysis of single-cell or bulk RNA-sequencing data. *Nature Communications*, *11*(1), 89. https://doi.org/10.1038/s41467-019-13779-x

Setty, M., Kiseliovas, V., Levine, J., Gayoso, A., Mazutis, L., & Pe'er, D. (2019). Characterization of cell fate probabilities in single-cell data with Palantir. *Nature Biotechnology*, *37*(4), 451–460. https://doi.org/10.1038/s41587-019-0068-4

Shi, Y., He, B., You, L., & Jablons, D. M. (2007). Roles of secreted frizzled-related proteins in cancer. *Acta Pharmacologica Sinica*, *28*(9), 1499–1504. https://doi.org/10.1111/j.1745-7254.2007.00692.x

Simpson Ragdale, H., Clements, M., Tang, W., Deltcheva, E., Andreassi, C., Lai, A. G., Chang, W. H., Pandrea, M., Andrew, I., Game, L., Uddin, I., Ellis, M., Enver, T., Riccio, A., Marguerat, S., & Parrinello, S. (2023). Injury primes mutation-bearing astrocytes for dedifferentiation in later life. *Current Biology*, *33*(6), 1082-1098.e8. https://doi.org/10.1016/j.cub.2023.02.013

Singh, S. K., Hawkins, C., Clarke, I. D., Squire, J. A., Bayani, J., Hide, T., Henkelman, R. M., Cusimano, M. D., & Dirks, P. B. (2004). Identification of human brain tumour initiating cells. *Nature*, *432*(7015), 396–401. https://doi.org/10.1038/nature03128

Smith, J. M., Burian, R., Kauffman, S., Alberch, P., Campbell, J., Goodwin, B., Lande, R., Raup, D., & Wolpert, L. (1985). Developmental Constraints and Evolution: A Perspective from the Mountain Lake Conference on Development and Evolution. *The Quarterly Review of Biology*, *60*(3), 265–287. https://doi.org/10.1086/414425

Smith, K. S., Bihannic, L., Gudenas, B. L., Haldipur, P., Tao, R., Gao, Q., Li, Y., Aldinger, K. A., Iskusnykh, I. Y., Chizhikov, V. V., Scoggins, M., Zhang, S., Edwards, A., Deng, M., Glass, I. A., Overman, L. M., Millman, J., Sjoboen, A. H., Hadley, J., … Northcott, P. A. (2022). Unified rhombic lip origins of group 3 and group 4 medulloblastoma. *Nature*, *609*(7929), 1012–1020. https://doi.org/10.1038/s41586-022-05208-9

Soneson, C., & Robinson, M. D. (2018). Bias, robustness and scalability in single-cell differential expression analysis. *Nature Methods*, *15*(4), 255–261. https://doi.org/10.1038/nmeth.4612

Song, D., & Li, J. J. (2021). PseudotimeDE: Inference of differential gene expression along cell pseudotime with well-calibrated p-values from single-cell RNA sequencing data. *Genome Biology*, *22*(1), 124. https://doi.org/10.1186/s13059-021-02341-y

Steele-Perkins, G., Plachez, C., Butz, K. G., Yang, G., Bachurski, C. J., Kinsman, S. L., Litwack, E. D., Richards, L. J., & Gronostajski, R. M. (2005). The Transcription Factor Gene *Nfib* Is Essential for both Lung Maturation and Brain Development. *Molecular and Cellular Biology*, *25*(2), 685–698. https://doi.org/10.1128/MCB.25.2.685-698.2005

Steinhart, Z., & Angers, S. (2018). Wnt signaling in development and tissue homeostasis. *Development*, *145*(11), dev146589. https://doi.org/10.1242/dev.146589

Stoeckius, M., Zheng, S., Houck-Loomis, B., Hao, S., Yeung, B. Z., Mauck, W. M., Smibert, P., & Satija, R. (2018). Cell Hashing with barcoded antibodies enables multiplexing and doublet detection for single cell genomics. *Genome Biology*, *19*(1), 224. https://doi.org/10.1186/s13059-018-1603-1

Streeter, K. A., Sunshine, M. D., Brant, J. O., Sandoval, A. G. W., Maden, M., & Fuller, D. D. (2020). Molecular and histologic outcomes following spinal cord injury in spiny mice, Acomys cahirinus. *Journal of Comparative Neurology*, *528*(9), 1535–1547. https://doi.org/10.1002/cne.24836

Stringer, C., Wang, T., Michaelos, M., & Pachitariu, M. (2021). Cellpose: A generalist algorithm for cellular segmentation. *Nature Methods*, *18*(1), 100–106. https://doi.org/10.1038/s41592-020-01018-x

Stuart, T., & Satija, R. (2019). Integrative single-cell analysis. *Nature Reviews Genetics*, *20*(5), 257–272. https://doi.org/10.1038/s41576-019-0093-7

Stupp, R., Weller, M., Belanger, K., Bogdahn, U., Ludwin, S. K., Lacombe, D., & Mirimanoff, R. O. (2005). Radiotherapy plus Concomitant and Adjuvant Temozolomide for Glioblastoma. *The New England Journal of Medicine*.

Sturm, D., Witt, H., Hovestadt, V., Khuong-Quang, D.-A., Jones, D. T. W., Konermann, C., Pfaff, E., Tönjes, M., Sill, M., Bender, S., Kool, M., Zapatka, M., Becker, N., Zucknick, M., Hielscher, T., Liu, X.-Y., Fontebasso, A. M., Ryzhova, M., Albrecht, S., … Pfister, S. M. (2012). Hotspot Mutations in H3F3A and IDH1 Define Distinct Epigenetic and Biological Subgroups of Glioblastoma. *Cancer Cell*, *22*(4), 425–437. https://doi.org/10.1016/j.ccr.2012.08.024

Subramanian, A., Tamayo, P., Mootha, V. K., Mukherjee, S., Ebert, B. L., Gillette, M. A., Paulovich, A., Pomeroy, S. L., Golub, T. R., Lander, E. S., & Mesirov, J. P. (2005). Gene set enrichment analysis: A knowledge-based approach for interpreting genome-wide expression profiles. *Proceedings of the National Academy of Sciences*, *102*(43), 15545–15550. https://doi.org/10.1073/pnas.0506580102

Sugihara, R., Kato, Y., Mori, T., & Kawahara, Y. (2022). Alignment of single-cell trajectory trees with CAPITAL. *Nature Communications*, *13*(1), 5972. https://doi.org/10.1038/s41467-022-33681-3

Suvà, M. L., & Tirosh, I. (2020). The Glioma Stem Cell Model in the Era of Single-Cell Genomics. *Cancer Cell*, *37*(5), 630–636. https://doi.org/10.1016/j.ccell.2020.04.001

Takahashi, K., & Yamanaka, S. (2006). Induction of Pluripotent Stem Cells from Mouse Embryonic and Adult Fibroblast Cultures by Defined Factors. *Cell*, *126*(4), 663–676. https://doi.org/10.1016/j.cell.2006.07.024

Tan, S. H., & Barker, N. (2018). Wnt Signaling in Adult Epithelial Stem Cells and Cancer. In *Progress in Molecular Biology and Translational Science* (Vol. 153, pp. 21–79). Elsevier. https://doi.org/10.1016/bs.pmbts.2017.11.017

The Cancer Genome Atlas Research Network. (2008). Comprehensive genomic characterization defines human glioblastoma genes and core pathways. *Nature*, *455*(7216), 1061–1068. https://doi.org/10.1038/nature07385

Tirosh, I., Venteicher, A. S., Hebert, C., Escalante, L. E., Patel, A. P., Yizhak, K., Fisher, J. M., Rodman, C., Mount, C., Filbin, M. G., Neftel, C., Desai, N., Nyman, J., Izar, B., Luo, C. C., Francis, J. M., Patel, A. A., Onozato, M. L., Riggi, N., … Suvà, M. L. (2016). Single-cell RNA-seq supports a developmental hierarchy in human oligodendroglioma. *Nature*, *539*(7628), 309–313. https://doi.org/10.1038/nature20123

Tong, C. K., Fuentealba, L. C., Shah, J. K., Lindquist, R. A., Ihrie, R. A., Guinto, C. D., Rodas-Rodriguez, J. L., & Alvarez-Buylla, A. (2015). A Dorsal SHH-Dependent Domain in the V-SVZ Produces Large Numbers of Oligodendroglial Lineage Cells in the Postnatal Brain. *Stem Cell Reports*, *5*(4), 461–470. https://doi.org/10.1016/j.stemcr.2015.08.013

Tran, H. T. N., Ang, K. S., Chevrier, M., Zhang, X., Lee, N. Y. S., Goh, M., & Chen, J. (2020). A benchmark of batch-effect correction methods for single-cell RNA sequencing data. *Genome Biology*, *21*(1), 12. https://doi.org/10.1186/s13059-019-1850-9

Tubiana, M. (1989). Tumor Cell Proliferation Kinetics and Tumor Growth Rate. *Acta Oncologica*, *28*(1), 113–121. https://doi.org/10.3109/02841868909111193

Turner, J. R. G. (1988). The Evolution of Mimicry: A Solution to the Problem of Punctuated Equilibrium. *The American Naturalist*, *131*, S42–S66.

Van Den Berge, K., Hembach, K. M., Soneson, C., Tiberi, S., Clement, L., Love, M. I., Patro, R., & Robinson, M. D. (2019). RNA Sequencing Data: Hitchhiker's Guide to Expression Analysis. *Annual Review of Biomedical Data Science*, *2*(1), 139–173. https://doi.org/10.1146/annurev-biodatasci-072018-021255

Van Galen, P., Hovestadt, V., Wadsworth Ii, M. H., Hughes, T. K., Griffin, G. K., Battaglia, S., Verga, J. A., Stephansky, J., Pastika, T. J., Lombardi Story, J., Pinkus, G. S., Pozdnyakova, O., Galinsky, I., Stone, R. M., Graubert, T. A., Shalek, A. K., Aster, J. C., Lane, A. A., & Bernstein, B. E. (2019). Single-Cell RNA-Seq Reveals AML Hierarchies Relevant to Disease Progression and Immunity. *Cell*, *176*(6), 1265-1281.e24. https://doi.org/10.1016/j.cell.2019.01.031

Van Praag, H., Schinder, A. F., Christie, B. R., Toni, N., Palmer, T. D., & Gage, F. H. (2002). Functional neurogenesis in the adult hippocampus. *Nature*, *415*(6875), 1030–1034. https://doi.org/10.1038/4151030a

Varn, F. S., Johnson, K. C., Martinek, J., Huse, J. T., Nasrallah, M. P., Wesseling, P., Cooper, L. A. D., Malta, T. M., Wade, T. E., Sabedot, T. S., Brat, D., Gould, P. V., Wöehrer, A., Aldape, K., Ismail, A., Sivajothi, S. K., Barthel, F. P., Kim, H., Kocakavuk, E., … Verhaak, R. Gw. (2022). Glioma progression is shaped by genetic evolution and microenvironment interactions. *Cell*, *185*(12), 2184-2199.e16. https://doi.org/10.1016/j.cell.2022.04.038

Veeck, J., Niederacher, D., An, H., Klopocki, E., Wiesmann, F., Betz, B., Galm, O., Camara, O., Dürst, M., Kristiansen, G., Huszka, C., Knüchel, R., & Dahl, E. (2006). Aberrant methylation of the Wnt antagonist SFRP1 in breast cancer is associated with unfavourable prognosis. *Oncogene*, *25*(24), 3479–3488. https://doi.org/10.1038/sj.onc.1209386

Velasco, S., Kedaigle, A. J., Simmons, S. K., Nash, A., Rocha, M., Quadrato, G., Paulsen, B., Nguyen, L., Adiconis, X., Regev, A., Levin, J. Z., & Arlotta, P. (2019). Individual brain organoids reproducibly form cell diversity of the human cerebral cortex. *Nature*, *570*(7762), 523–527. https://doi.org/10.1038/s41586-019-1289-x

Venteicher, A. S., Tirosh, I., Hebert, C., Yizhak, K., Neftel, C., Filbin, M. G., Hovestadt, V., Escalante, L. E., Shaw, M. L., Rodman, C., Gillespie, S. M., Dionne, D., Luo, C. C., Ravichandran, H., Mylvaganam, R., Mount, C., Onozato, M. L., Nahed, B. V., Wakimoto, H., … Suvà, M. L. (2017). Decoupling genetics, lineages, and microenvironment in IDH-mutant gliomas by single-cell RNA-seq. *Science*, *355*(6332), eaai8478. https://doi.org/10.1126/science.aai8478

Verhaak, R. G. W., Hoadley, K. A., Purdom, E., Wang, V., Qi, Y., Wilkerson, M. D., Miller, C. R., Ding, L., Golub, T., Mesirov, J. P., Alexe, G., Lawrence, M., O'Kelly, M., Tamayo, P., Weir, B. A., Gabriel, S., Winckler, W., Gupta, S., Jakkula, L., … Hayes, D. N. (2010). Integrated Genomic Analysis Identifies Clinically Relevant Subtypes of Glioblastoma Characterized by Abnormalities in PDGFRA, IDH1, EGFR, and NF1. *Cancer Cell*, *17*(1), 98–110. https://doi.org/10.1016/j.ccr.2009.12.020

Waddington, C. H. (1957). *Strategy of the Genes*. Taylor & Francis.

Wang, L., Babikir, H., Müller, S., Yagnik, G., Shamardani, K., Catalan, F., Kohanbash, G., Alvarado, B., Di Lullo, E., Kriegstein, A., Shah, S., Wadhwa, H., Chang, S. M., Phillips, J. J., Aghi, M. K., & Diaz, A. A. (2019). The Phenotypes of Proliferating Glioblastoma Cells Reside on a Single Axis of Variation. *Cancer Discovery*, *9*(12), 1708–1719. https://doi.org/10.1158/2159-8290.CD-19-0329

Wang, R., Sharma, R., Shen, X., Laughney, A. M., Funato, K., Clark, P. J., Shpokayte, M., Morgenstern, P., Navare, M., Xu, Y., Harbi, S., Masilionis, I., Nanjangud, G., Yang, Y., Duran-Rehbein, G., Hemberg, M., Pe'er, D., & Tabar, V. (2020). Adult Human Glioblastomas Harbor Radial Glia-like Cells. *Stem Cell Reports*, *14*(2), 338–350. https://doi.org/10.1016/j.stemcr.2020.01.007

Wang, S., Li, Q., Ma, P., Fang, Y., Yu, Y., Jiang, N., Miao, H., Tang, Q., Yang, Y., Xing, S., Chen, R., Yi, X., & Li, N. (2022). KRAS Mutation in Rare Tumors: A Landscape Analysis of 3453 Chinese Patients. *Frontiers in Molecular Biosciences*, *9*, 831382. https://doi.org/10.3389/fmolb.2022.831382

Wang, X., Park, J., Susztak, K., Zhang, N. R., & Li, M. (2019). Bulk tissue cell type deconvolution with multi-subject single-cell expression reference. *Nature Communications*, *10*(1), 380. https://doi.org/10.1038/s41467-018-08023-x

Wang, Z., Sun, D., Chen, Y.-J., Xie, X., Shi, Y., Tabar, V., Brennan, C. W., Bale, T. A., Jayewickreme, C. D., Laks, D. R., Alcantara Llaguno, S., & Parada, L. F. (2020). Cell Lineage-Based Stratification for Glioblastoma. *Cancer Cell*, *38*(3), 366-379.e8. https://doi.org/10.1016/j.ccell.2020.06.003

Weinreb, C., Rodriguez-Fraticelli, A., Camargo, F. D., & Klein, A. M. (2020). Lineage tracing on transcriptional landscapes links state to fate during differentiation. *Science*, *367*(6479), eaaw3381. https://doi.org/10.1126/science.aaw3381

Wilcock, A. C., Swedlow, J. R., & Storey, K. G. (2007). Mitotic spindle orientation distinguishes stem cell and terminal modes of neuron production in the early spinal cord. *Development*, *134*(10), 1943–1954. https://doi.org/10.1242/dev.002519

Wolf, F. A., Angerer, P., & Theis, F. J. (2018). SCANPY: Large-scale single-cell gene expression data analysis. *Genome Biology*, *19*(1), 15. https://doi.org/10.1186/s13059-017-1382-0

Wu, Y., Fletcher, M., Gu, Z., Wang, Q., Costa, B., Bertoni, A., Man, K.-H., Schlotter, M., Felsberg, J., Mangei, J., Barbus, M., Gaupel, A.-C., Wang, W., Weiss, T., Eils, R., Weller, M., Liu, H., Reifenberger, G., Korshunov, A., … Radlwimmer, B. (2020). Glioblastoma epigenome profiling identifies SOX10 as a master regulator of molecular tumour subtype. *Nature Communications*, *11*(1), 6434. https://doi.org/10.1038/s41467-020-20225-w

Xie, X. P., Laks, D. R., Sun, D., Ganbold, M., Wang, Z., Pedraza, A. M., Bale, T., Tabar, V., Brennan, C., Zhou, X., & Parada, L. F. (2022). Quiescent human glioblastoma cancer stem cells drive tumor initiation, expansion, and recurrence following chemotherapy. *Developmental Cell*, *57*(1), 32-46.e8. https://doi.org/10.1016/j.devcel.2021.12.007

Yamashita, T., Ninomiya, M., Hernandez Acosta, P., Garcia-Verdugo, J. M., Sunabori, T., Sakaguchi, M., Adachi, K., Kojima, T., Hirota, Y., Kawase, T., Araki, N., Abe, K., Okano, H., & Sawamoto, K. (2006). Subventricular Zone-Derived Neuroblasts Migrate and Differentiate into Mature Neurons in the Post-Stroke Adult Striatum. *Journal of Neuroscience*, *26*(24), 6627–6636. https://doi.org/10.1523/JNEUROSCI.0149-06.2006

Yu, J., Xie, Y., Li, M., Zhou, F., Zhong, Z., Liu, Y., Wang, F., & Qi, J. (2019). Association between SFRP promoter hypermethylation and different types of cancer: A systematic review and meta-analysis. *Oncology Letters*. https://doi.org/10.3892/ol.2019.10709

Zheng, G. X. Y., Terry, J. M., Belgrader, P., Ryvkin, P., Bent, Z. W., Wilson, R., Ziraldo, S. B., Wheeler, T. D., McDermott, G. P., Zhu, J., Gregory, M. T., Shuga, J., Montesclaros, L., Underwood, J. G., Masquelier, D. A., Nishimura, S. Y., Schnall-Levin, M., Wyatt, P. W., Hindson, C. M., … Bielas, J. H. (2017). Massively parallel digital transcriptional profiling of single cells. *Nature Communications*, *8*(1), 14049. https://doi.org/10.1038/ncomms14049

Zhong, S., Ding, W., Sun, L., Lu, Y., Dong, H., Fan, X., Liu, Z., Chen, R., Zhang, S., Ma, Q., Tang, F., Wu, Q., & Wang, X. (2020). Decoding the development of the human hippocampus. *Nature*, *577*(7791), 531–536. https://doi.org/10.1038/s41586-019-1917-5

Zhu, L.-L., Wu, L.-Y., Yew, D. T., & Fan, M. (2005). Effects of Hypoxia on the Proliferation and Differentiation of NSCs. *Molecular Neurobiology*, *31*(1–3), 231–242. https://doi.org/10.1385/MN:31:1-3:231

Zywitza, V., Misios, A., Bunatyan, L., Willnow, T. E., & Rajewsky, N. (2018). Single-Cell Transcriptomics Characterizes Cell Types in the Subventricular Zone and Uncovers Molecular Defects Impairing Adult Neurogenesis. *Cell Reports*, *25*(9), 2457-2469.e8. https://doi.org/10.1016/j.celrep.2018.11.003